

PNNL-32770

FAST-1.1: A Computer Code for Thermal-Mechanical Nuclear Fuel Analysis under Steady-state and Transients

Developed under NQA-1-2017

April 2022

KJ Geelhood, PNNL
L Kyriazidis, NRC
JJ Whitman, NRC

DV Colameco, PNNL
CE Goodson, PNNL

WG Luscher, PNNL
J Corson, NRC



Prepared for the U.S. Nuclear Regulatory Commission
Office of Nuclear Regulatory Research
Under contract DE-AC05-76RL01830
Interagency Agreement 31310019N0001
Task Order Number: 31310019F0047

DISCLAIMER

This report was prepared as an account of work sponsored by an agency of the United States Government. Neither the United States Government nor any agency thereof, nor Battelle Memorial Institute, nor any of their employees, makes **any warranty, express or implied, or assumes any legal liability or responsibility for the accuracy, completeness, or usefulness of any information, apparatus, product, or process disclosed, or represents that its use would not infringe privately owned rights.** Reference herein to any specific commercial product, process, or service by trade name, trademark, manufacturer, or otherwise does not necessarily constitute or imply its endorsement, recommendation, or favoring by the United States Government or any agency thereof, or Battelle Memorial Institute. The views and opinions of authors expressed herein do not necessarily state or reflect those of the United States Government or any agency thereof.

PACIFIC NORTHWEST NATIONAL LABORATORY
operated by
BATTELLE
for the
UNITED STATES DEPARTMENT OF ENERGY
under Contract DE-AC05-76RL01830

Printed in the United States of America

**Available to DOE and DOE contractors from the
Office of Scientific and Technical Information,
P.O. Box 62, Oak Ridge, TN 37831-0062;
ph: (865) 576-8401
fax: (865) 576-5728
email: reports@adonis.osti.gov**

**Available to the public from the National Technical Information Service
5301 Shawnee Rd., Alexandria, VA 22312
ph: (800) 553-NTIS (6847)
email: orders@ntis.gov <<https://www.ntis.gov/about>>
Online ordering: <http://www.ntis.gov>**

FAST-1.1: A Computer Code for Thermal-Mechanical Nuclear Fuel Analysis under Steady-state and Transients

Developed under NQA-1-2017

April 2022

KJ Geelhood, PNNL	DV Colameco, PNNL
WG Luscher, PNNL	L Kyriazidis, NRC
CE Goodson, PNNL	J Corson, NRC
JJ Whitman, NRC	

Prepared for the U.S. Nuclear Regulatory Commission
Office of Nuclear Regulatory Research
Under Contract DE-AC05-76RL01830
Interagency Agreement 31310019N0001
Task Order Number: 31310019F0047

Pacific Northwest National Laboratory
Richland, Washington 99352

Project Summary and Document Characteristics

Project Name	FAST Fuel Performance Code Development and Assessment
Project No.	77701 Task 3130019F0047
Product Management Office No. / Organization	PM053 / Nuclear Science and Legacy Waste

Approvals

Role	Name	Signature	Date
Project Manager	Tara O'Neill		
Lead Software Developer	Ken Geelhood		
Code Custodian	David Colameco		

Revision History

Revision	Date	Comments
0	April 2022	Initial Release

Abstract

Fuel Analysis under Steady-state and Transients (FAST) is the U.S. Nuclear Regulatory Commission (NRC)'s computer code that calculates the steady-state and transient response of nuclear reactor fuel rods during long-term in-reactor burnup, anticipated operational occurrences (AOOs), design basis accidents (DBAs), and dry storage conditions. The code calculates the temperature, pressure, and deformation of a fuel rod as functions of time-dependent fuel rod power and coolant boundary conditions. The phenomena modeled by the code include:

- heat conduction through the fuel and other materials
- heat transfer from the cladding-to-coolant
- cladding elastic and plastic deformation, including creep
- fuel-cladding mechanical interaction
- fission gas release from the fuel
- rod internal pressure and void volume
- cladding oxidation

The code contains necessary material and coolant properties, as well as clad-to-coolant heat-transfer correlations, for normal operation through postulated accidents and AOOs for today's U.S.-based light water reactor (LWR) fuel designs. FAST-1.1 also contains preliminary materials and models for new LWR fuel concepts, such as accident tolerant fuel (ATF), and non-LWR fuel concepts such as metallic fuels for sodium fast reactors (SFRs). FAST has been developed for use on Windows and Linux operating systems.

This document describes FAST-1.1 and is one of a series of documents on the code; the other documents detail the material properties used by FAST as well as its integral assessment to experiments and commercial data.

This page intentionally blank.

Foreword

Computer codes related to fuel performance have played an important role in the work of the U.S. Nuclear Regulatory Commission (NRC) since the agency's inception in 1975. Formal requirements for fuel performance analysis appear in several of the agency's regulatory guides and regulations, including those related to emergency core cooling system evaluation models, as set forth in Appendix K to Title 10, Part 50, of the *Code of Federal Regulations* (10 CFR Part 50), "Domestic Licensing of Production and Utilization Facilities."

This document describes an update to the initial version of the NRC's fuel performance code, FAST (Fuel Analysis under Steady-state and Transients) Version-1.1. FAST is a merger of the NRC's previous steady-state fuel performance code FRAPCON-4.0 and transient fuel performance code FRAPTRAN-2.0. This code provides the ability to accurately calculate the long-term burnup response of a single light water reactor (LWR) fuel rod, as well as various operational transients and hypothetical accidents, accomplishing a key objective of the NRC's reactor safety research program. The FAST code serves as an independent audit tool used in the NRC's review of industry fuel performance codes and industry analyses that demonstrate a given fuel design application meeting specified acceptable design limits in U.S. NRC Standard Review Plan (SRP) Section 4.2 [NRC, 2007].

This version of FAST is built off the foundation of FRAPCON-4.0 with the addition of the transient conduction solution, new clad-to-coolant heat transfer models, a more detailed coolant enthalpy rise model, high temperature cladding oxidation, new cladding deformation (ballooning) and failure models, transient internal gas flow, an updated fission gas release model, and new material properties to scope out new fuel and cladding materials under consideration in the U.S. nuclear industry.

This page intentionally blank.

Executive Summary

The nuclear fuel performance code, FAST, has been co-developed by the U.S. Nuclear Regulatory Commission and Pacific Northwest National Laboratory (PNNL) as a confirmatory tool designed to calculate the steady-state and transient fuel behavior at high burnup (up to rod-average burnup of 62 GWD/MTU, depending on application). The code is an evolution of the former PNNL developed codes FRAPCON and FRAPTRAN, which were used to calculate the steady-state and transient response of LWR fuel rods, respectively. This document is Volume 1 of a three volume series of reports that describes the current version of FAST. Volume 1 contains:

1. Code limitations and structure;
2. Fuel performance model summaries; and
3. Code input instructions and features to aid the user.

Volume 2 [Geelhood et al., 2022c] provides a code assessment based on comparisons of code predictions to integral performance data up to high burnup. Volume 3 [Geelhood et al., 2022a] provides a description and assessment of the material models used by FAST's material library, MatLib.

The FAST code is designed to perform steady-state and transient fuel rod calculations. The code uses a single-channel coolant enthalpy rise model. The code uses a finite difference heat conduction model, which uses a variable mesh spacing in the fuel material to accommodate for the power peaking at the pellet edge that occurs in high-burnup fuel.

FAST has been validated for boiling water reactors (BWRs), pressurized reactors (PWRs), and heavy water reactors (HWRs). The fuels that have been validated are uranium dioxide (UO_2), mixed oxide fuel (MOX), urania-gadolinia ($\text{UO}_2\text{-Gd}_2\text{O}_3$), and UO_2 with zirconium diboride (ZrB_2) coatings. The cladding types that have been validated are Zircaloy-2, Zircaloy-4, M5^{®1}, ZIRLO^{®2}, and Optimized ZIRLO^{™,3}. FAST-1.1 can predict fuel and cladding temperature, rod internal pressure, fission gas release, cladding axial and hoop strain, and cladding corrosion and hydriding. The code uses an updated version of the MATPRO material properties package [Hagrman et al., 1981] as described in a separate material properties handbook [Geelhood et al., 2022a] that has been updated for high burnup conditions and advanced cladding alloys.

¹M5[®] is a registered trademark of Framatome.

²ZIRLO[®] is a registered trademark of Westinghouse Electric Company LLC

³Optimized ZIRLO[™] is a trademark of Westinghouse Electric Company LLC.

This page intentionally blank.

Acronyms and Abbreviations

ANS	American Nuclear Society
AOO	anticipated operating occurrence
ATF	accident tolerant fuel
ATWS	anticipated transient without SCRAM
BOL	beginning of life
BWR	boiling water reactor
CHF	critical heat flux
DBA	design basis accident
DNB	departure from nucleate boiling
ECI	Exterior Communications Interface
ECR	equivalent cladding reacted
EOL	end of life
EPMA	electron probe microanalysis
ERI	Energy Research, Inc.
FAST	Fuel Analysis under Steady-State and Transients
FEA	finite element analysis
FGR	fission gas release
HBU	high burnup
HWR	heavy water reactor
ID	inner diameter
IFBA	integral fuel burnable absorber
JSON	JavaScript Object Notation
LBLOCA	large break loss-of-coolant accident
LOCA	loss-of-coolant accident
LWR	light water reactor
MCNP	Monte Carlo N-Particle
MLI	mean linear intercept
MOX	mixed oxide fuel
NRC	U.S. Nuclear Regulatory Commission
OD	outer diameter
ORNL	Oak Ridge National Laboratory
PCMI	pellet-cladding mechanical interaction
PCT	peak cladding temperature
PNNL	Pacific Northwest National Laboratory
PWR	pressurized water reactor
RIA	reactivity-initiated accident
RXA	re-crystallized annealed
SBLOCA	small break loss-of-coolant accident
SFR	sodium fast reactor

SNAP	Symbolic Nuclear Analysis Package
SRA	stress relief annealed
SRP	standard review plan
STP	standard temperature and pressure
TD	theoretical density
XRF	X-ray fluorescence

Contents

Abstract	v
Foreword	vii
Executive Summary	ix
Acronyms and Abbreviations	xi
Contents	xiii
Figures	xix
Tables	xxiii
1.0 Introduction	1
1.1 Objective of the FAST Code	1
1.2 Limitations of FAST-1.1	2
1.3 Report Outline and Relation to Other Reports	3
2.0 General Modeling Description	7
2.1 Solution Scheme	7
2.1.1 Steady-State	7
2.1.2 Transient	8
2.2 Coupling of Thermal and Mechanical Models	11
2.2.1 Steady-State	11
2.2.2 Transient	11
2.3 Mesh Layout	13
2.3.1 Cylindrical Geometry	13
2.3.2 Thermal Mesh	13
2.3.3 Void Volume Mesh	17
2.3.4 Fission Gas Release Mesh	19
2.4 Plenum Thermal Response	20
2.4.1 Plenum Temperature Equations	20

2.4.2	Heat Conduction Coefficients	24
2.4.3	Stored Energy	29
2.5	Fuel Rod Mechanical Response	30
2.5.1	The FRACAS-1 Model	30
2.5.2	Cladding Ballooning Model	65
2.6	Rod Internal Pressure and Fission Gas Release	70
2.6.1	Fuel Rod Internal Gas Pressure	71
2.6.2	Fuel Rod Void Volume	74
2.6.3	Gas Production	77
2.6.4	Steady-State Gas Release	78
2.6.5	Transient Gas Release	93
2.6.6	Nitrogen Release	94
2.6.7	Helium Production and Release	95
2.6.8	Metallic Fuel Fission Gas Release Model	98
2.7	Corrosion and Hydrogen Pickup	99
2.7.1	LWR Waterside Corrosion Models	99
2.7.2	Hydrogen Pickup Fraction	102
2.7.3	High-Temperature Corrosion	103
2.8	Transient Options	105
2.9	Heat Conduction and Temperature Solution	105
2.9.1	One-Dimensional Radial Steady-State Heat Conduction	105
2.9.2	One-Dimensional Radial Transient Heat Conduction	106
2.10	Cladding Failure Models	109
2.10.1	Low-Temperature PCMI Cladding Failure Model	110
2.10.2	High-Temperature Cladding Ballooning Failure Model	111
2.11	Coolant Conditions	111
3.0	Calculations of Cladding Surface Temperature	115

3.1	Heat Conduction Equation	115
4.0	Coolant Model and Heat Transfer Correlations	119
4.1	Coolant Enthalpy Model	119
4.2	Water Heat Transfer and Critical Heat Flux Correlations	123
4.2.1	Summary	123
4.2.2	Void Fraction	124
4.2.3	Heat Transfer Coefficient Correlations	124
4.2.4	Critical Heat Flux Correlations	143
4.2.5	Influence of Rod Bowing on Critical Heat Flux	157
4.3	Sodium	158
4.3.1	Heat Transfer Coefficient Correlations	158
4.4	Helium	159
4.4.1	Heat Transfer Coefficient Correlations	159
5.0	External Code Interfaces	161
5.1	Communication Interfaces	161
5.1.1	File-based JSON Interface	161
5.1.2	Exterior Communications Interface (ECI)	162
5.1.3	FAST Driving External Codes	162
5.2	FAST/EPIC Interface	162
5.2.1	Methodology for Single Rod Analysis	163
5.2.2	FAST-to-EPIC File	163
5.2.3	EPIC-to-FAST File	165
5.3	FAST/TRACE Interface	165
5.4	Output File for FAST-to-TRACE Data Transfer	166
5.4.1	File Variables	166
5.4.2	File Units	167

5.4.3	File Header	167
5.4.4	File Time-Dependent Data	168
6.0	References	171
Appendix A	Running the Code	A.1
A.1	Windows-Based OS	A.1
A.2	Linux-Based OS	A.1
A.3	Using SNAP	A.2
Appendix B	Input Instructions for the FAST-1.1 Code	B.1
B.1	File and Comment Structure	B.1
B.2	frpcn block	B.4
B.3	frpcon Block	B.5
B.4	geometry block	B.10
B.5	material block	B.12
B.6	transient Block	B.17
B.7	boundary Block	B.20
B.8	spentfuel Block	B.25
B.9	refabrication block	B.27
B.10	uncertainty Block	B.29
B.11	developer Block	B.30
B.12	lua Block	B.32
Appendix C	Output and Plotting Capabilities	C.1
C.1	Output File	C.1
C.2	Plot File	C.2
C.3	FRAPlot	C.3
C.4	AptPlot	C.11
Appendix D	Numerical Solution of the Plenum Energy Equations	D.1

Appendix E	Overriding Material Properties With Lua Scripts	E.1
E.1	Basic Operation	E.1
E.2	Advanced Features	E.1

This page intentionally blank.

Figures

2-1	Simplified FAST steady-state flowchart	7
2-2	Flowchart of FAST transient (Part 1)	9
2-3	Flowchart of FAST transient (Part 2)	9
2-4	Flowchart of FAST transient (Part 3)	10
2-5	Order of FAST solution schemes	12
2-6	Schematic of fuel rod materials and node placement	14
2-7	Axial and radial discretization of user-defined fuel rod geometry	17
2-8	Layout of user-defined inputs for fuel pellet dish and chamfer	18
2-9	A schematic of the impact of dishes and chamfers on void volume	19
2-10	Energy flow in plenum model – energy exchange mechanisms	20
2-11	Energy flow in plenum model – spring model with two nodes	20
2-12	Cladding nodalization	21
2-13	Geometrical relationship between the cladding and spring	26
2-14	Typical isothermal stress-strain curve	32
2-15	Schematic of the method of successive elastic solutions	36
2-16	Cladding creep as a function of time and hoop stress for 630 °F and $\phi = 1 \times 10^{18}$ n/m ² -s for SRA Zircaloy	41
2-17	Cladding creep as a function of time and hoop stress for 630 °F and $\phi = 1 \times 10^{18}$ n/m ² -s for RXA Zircaloy	41
2-18	Fuel rod geometry and coordinates	45
2-19	Calculation of effective stress σ_e from $d\varepsilon_P$	48
2-20	Idealized stress-strain behavior	53
2-21	Computing stress	55
2-22	Predicted vs. measured yield stress from the PNNL database ($293\text{ K} \leq T \leq 755\text{ K}$, $0 \leq \Phi \leq 14 \times 10^{25}$ n/m ² , $0 \leq H_{ex} \leq 850$ ppm)	60
2-23	Interpellet void volume	63
2-24	Power and burnup dependence of the FAST-1.1 relocation model with the FRAPCON- 3.4 model shown for reference	65

2-25	Description of the BALON2 model	66
2-26	True hoop stress at burst used in FAST-1.1's implementation of BALON2	67
2-27	Engineering burst stress data and FAST predictions for low heating rates	68
2-28	Engineering burst stress data and FAST predictions for high heating rates	69
2-29	Permanent burst strain data and FAST predictions for low temperature ramp rates (between 2 and 10 °C/s)	69
2-30	Permanent burst strain data and FAST predictions for high temperature ramp rates (greater than 20 °C/s)	70
2-31	Internal pressure distribution with the transient gas flow model	73
2-32	Hagen number versus width of fuel-cladding gap	74
2-33	Modeling of the pellet high burnup rim structure	85
2-34	FAST metallic fuel FGR model and available data	99
2-35	Description of geometry terms in finite difference equations for 1-D radial heat con- duction	107
2-36	Predicted minus measured uniform elongation from irradiated samples from the PNNL database as a function of excess hydrogen ($293\text{ K} \leq T \leq 795\text{ K}$ and $0 \leq \Phi \leq$ $14.0 \times 10^{25}\text{ n/m}^2$)	111
2-37	Relation of surface heat flux to surface temperature	112
4-1	Description of geometry terms in coolant enthalpy model	120
4-2	Illustration of FAST's forced convection heat transfer regimes for full boiling curve . .	125
5-1	FAST-EPIC calculational scheme	163
A.1	Running FAST using the Windows Command Prompt	A.1
A.2	Running FAST using the Linux Command Line (OS=Ubuntu 16)	A.2
B.1	Sample comment and file input structure for FAST input file	B.3
C.1	Summary of output file layout	C.1
C.2	FRAPLot's tabs containing plottable data	C.4
C.3	Units selection	C.4
C.4	"Load Plot File" selection	C.5
C.5	"Load Plot File" pop-up window	C.5

C.6	View of Listboxes once Plot File is loaded into Memory	C.6
C.7	Examples of “Data” plot using British units	C.6
C.8	Examples of “Data” plot using SI units (continued)	C.7
C.9	Nodal plot using burnup for x-axis	C.8
C.10	Axial Plot with “Fix Max Extents” and “User-specified Time for Axial Plot”	C.9
C.11	Example of a 2D Data plot	C.10
C.12	Example of a Gas Data plot	C.11
C.13	How to load FAST plot file in AptPlot (a)	C.12
C.14	How to load FAST plot file in AptPlot (b)	C.12
C.15	Available data channels for the FAST plug-in in AptPlot	C.13
C.16	Examples of fuel centerline temperature measurements using AptPlot’s (a) time- dependent and (b) axial graphs.	C.14

This page intentionally blank.

Tables

1-1	Roadmap to documentation of models and properties used in NRC’s fuel performance code FAST	4
2-1	Input variables defining radial geometry dimensions used in thermal mesh	14
2-2	Input variables defining number of radial material boundaries	15
2-3	Input variables defining number of axial material boundaries and geometry	16
2-4	Variables used to define dish and chamfer geometry	18
2-5	Nomenclature for plenum thermal model	22
2-6	Summary of FRACAS-I governing equations	35
2-7	Parameters for FAST-1.1 creep equation for SRA and RXA cladding	39
2-8	Void volumes	72
2-9	Decay constants and precursor coefficients for short-lived noble gases and iodines with half-life < 6 h	91
2-10	Decay constants and precursor coefficients for long-lived noble gases and iodines with 6 h < half-life < 60 d	91
2-11	Decay constants for gases with half-life > 60 d	93
2-12	Fitting parameters for helium in MOX	96
2-13	Enthalpy and transition thicknesses under PWR conditions [Garzarolli et al., 1982]	100
2-14	Hydrogen pickup fraction under PWR conditions [Geelhood and Beyer, 2011]	102
2-15	Constants for Cathcart-Pawel and Baker-Just models	104
2-16	Recommended time steps for various transients	105
2-17	Water heat transfer mode selection and correlation	113
4-1	Coolant quality and temperature criteria	123
4-2	Groeneveld fitting constants	137
4-3	Range of conditions for EPRI-1 CHF correlation	143
4-4	Optimized constants for EPRI-1 CHF correlation	145
4-5	Range of conditions for Bowring’s CHF correlation	147
4-6	Range of conditions for MacBeth’s CHF correlation	150

4-7	Range of conditions for MacBeth’s 6-coefficient correlation	152
4-8	Coefficients for MacBeth’s 6-coefficient model for a given reference pressure (psia) .	152
4-9	Range of conditions for MacBeth’s 12-coefficient model	153
4-10	Coefficients for MacBeth’s 12-coefficient model for a given reference pressure (psia)	153
5-1	Codes linked with FAST	161
5-2	FAST-to-EPIC file input definitions	164
5-3	geometryDefinition options	164
5-4	powerDefinition options	164
5-5	meshDefinition options	164
5-6	materialDefinition options	165
5-7	stateDefinition options	165
5-8	EPIC-to-FAST file input definitions	165
5-9	Variables ^(a) written in MAKECHAN file	167
5-10	File case-specific information	167
5-11	File variables written in MAKECHAN file	168
5-12	Time-dependent information format	169
B.1	Available input and output files in FAST-1.1	B.2
B.2	Available namelist input blocks	B.3
B.3	frpcn input block	B.4
B.4	frpcon input block	B.5
B.5	geometry input block	B.10
B.6	material Input Block	B.12
B.7	transient input block	B.17
B.8	boundary input block	B.20
B.9	spentfuel input block	B.25
B.10	refabrication input block	B.27
B.11	uncertainty input block	B.29

B.12	developer input block	B.30
B.13	lua input block	B.32
C.1	Available parameters in plot file	C.3

This page intentionally blank.

1.0 Introduction

1.1 Objective of the FAST Code

The ability to accurately calculate the performance of light water reactor (LWR) fuel rods under long-term burnup conditions is a major objective of the reactor safety research program being conducted by the U.S. Nuclear Regulatory Commission (NRC). To achieve this objective, the NRC has sponsored an extensive program of analytical computer code development, as well as both in-pile and out-of-pile experiments to benchmark and assess the analytical code capabilities. The computer code, FRAPCON-3, was originally developed to calculate the long-term burnup response of a single fuel rod. This report describes FAST-1.1, the second release of this code.

FAST (Fuel Analysis under Steady-State and Transients) is an analytical tool that calculates the thermal-mechanical behavior of nuclear fuel when given power and boundary conditions. There are two conditions that are commonly referred to as “steady-state” and “transient”. For the term “steady-state” to apply (i.e., time-independent), changes must be sufficiently slow. This includes situations such as long periods at constant power and slow power ramps that are typical of normal power reactor operations. “Transient” means rapid power and/or boundary condition changes (time-dependent) such as an anticipated operating occurrence (AOO), reactivity-initiated accident (RIA), or loss-of-coolant accident (LOCA) events. FAST-1.1 may be used for AOO transients while FRAPTRAN-2.0 initialized with FRAPCON-4.0 should still be used to model RIA and LOCA events. The code calculates the variation with time of all significant fuel rod variables, including fuel and cladding temperatures, cladding hoop strain, cladding oxidation, hydriding, fuel irradiation swelling, fuel densification, fission gas release (FGR), and rod internal gas pressure.

FAST uses fuel, cladding, and gas material properties from MatLib [Geelhood et al., 2022a] that have been recently updated to include burnup-dependent properties and properties for advanced fuel, cladding, and coolants. The only material properties not included in the updated MatLib document are FGR, cladding corrosion, and cladding hydrogen pickup, and these properties are described in this document. The material properties in FRAPCON-3 are contained in modular subroutines that define material properties for temperatures ranging from room temperature to temperatures above melting and for rod-average burnup levels between 0 and 62 GWd/MTU. Each subroutine defines only a single material property. For example, FAST contains subroutines defining fuel thermal conductivity as a function of fuel temperature, fuel density, and burnup; fuel thermal expansion as a function of fuel temperature; and the cladding stress-strain relation as a function of cladding temperature, strain rate, cold work, hydride content, and fast neutron fluence.

The predecessors of FAST are the FRAPCON-4.0 [Geelhood et al., 2015b] and FRAPTRAN-2.0 [Geelhood et al., 2015a] codes.

FAST-1.0 took a major step toward code simplification by removing extra input parameters and model selection features that cannot easily be measured and have a large impact on results. Also, reasonable default values were set for some parameters. The only model options available to the user are in the selection of the mechanical model and in the selection of the FGR model.

For the mechanical model, the user may select the FRACAS-I model (finite difference model) or the FEA (finite element analysis) model. The FRACAS-I model is recommended by Pacific Northwest National Laboratory (PNNL) and is the default selection. The FEA model is useful for modeling

cladding axial strain in cases where there is slip between the fuel and cladding. The details of the FEA model are described elsewhere [Knuutila, 2006]. This document is posted on the FAST code users' group website <https://fast.labworks.org>. Only the FRACAS-1 mechanical model will be described in this document.

For the FGR model, the user can select the Massih model, one of the American Nuclear Society (ANS) 5.4 models (ANS-1982 or ANS-2011), or the FRAPFGR model. The Massih model is recommended and is the default model. The ANS-5.4 1982 model is useful for calculating the release of short-lived radioactive gas nuclides and has been shown to provide very conservative release values [ANS, 1982]. The ANS-5.4 2011 model also calculates the short-lived radioactive gas nuclides but is non-conservative with respect to total FGR as it does not include any long-lived nuclides (such as Kr or Xe) [ANS, 2011]. The FRAPFGR model is useful for determining the distribution of fission gases within the fuel pellet (grain boundary vs. retained within grains). The Massih and FRAPFGR models will be described in this document.

FAST-1.1 includes fuel models for uranium dioxide (UO₂), mixed oxide fuel (MOX), integral fuel burnable absorber (IFBA) and gadolinia doped fuel (UO₂-Gd₂O₃), and cladding models for Zircaloy-2, Zircaloy-4, M5, ZIRLO, and Optimized ZIRLO. For scoping studies, FAST has been updated with properties for accident tolerant fuel (ATF) candidate claddings (FeCrAl and HT-9) and cladding coatings (Cr and CrN) as well as metallic fuels (U-Pu-Zr). Other code improvements include an Excel-based input generator, an Excel-based plot routine, and the ability to bias model predictions for uncertainty analyses.

1.2 Limitations of FAST-1.1

The FAST-1.1 code has inherent limitations. The major limitations are as follows:

1. The code is limited to modeling fuel consisting of UO₂, UO₂-(<10 wt% PuO₂) (MOX), and UO₂-(<10 wt% Gd₂O₃) (UO₂-Gd₂O₃) pellets in zirconium alloy cladding with a gas gap under LWR and heavy water reactor (HWR) conditions from standard temperature and pressure (STP) up to pressurized water reactor (PWR) operating conditions. Some additional fuel, cladding, and coolant materials are available [Geelhood et al., 2022a] but have not been validated and additional model changes may be required to accommodate them.
2. The code has been validated up to a rod-average burnup of 62 GWd/MTU, although the code should give reasonable predictions for burnup beyond this level for some parameters. Also, the code is not validated beyond the fuel or cladding melting temperature. If melting of the fuel or the cladding occurs, the code will stop.
3. The thermal models of the code are based on 1-D radial heat flow. This assumption is valid for modeling a typical fuel rod (i.e., with a large length-to-diameter ratio). Similarly, the FGR models are based on steady-state and slow power ramp data and do not reflect release rates expected for rapid power changes. Therefore, under normal operation analysis, time steps should be no less than 0.1 day but no greater than 50 days. When modeling transients or power ramps, the FGR model will not allow for re-resolution of the gases.

4. Only small cladding deformations (<5% hoop strain) are meaningfully calculated. All of the thermal and mechanics modeling assumes an axisymmetric fuel rod with no axial constraints. These assumptions are reasonable for modeling an LWR fuel rod.
5. The code's ability to predict cladding strains resulting from pellet-cladding mechanical interaction (PCMI) has been assessed against power ramp data. FAST has been found to slightly overpredict cladding strain up to a burnup of about 65 GWd/MTU. The limited high burnup data suggests that FAST may underpredict the cladding strain during power ramps at very high burnup (i.e., > 65 GWd/MTU) for hold times greater than 30 minutes.

1.3 Report Outline and Relation to Other Reports

The full documentation of this fuel performance code is described in three documents. The code structure and behavioral models are described in the Code Description (this document). Sections 2.0 and 3.0 of this report deal with the modeling concepts and the code description, respectively. Instructions for creating an input file are discussed in Appendix A. The reader is cautioned that although the thermal and mechanical models are described separately, they actually are highly interrelated. Section 2.2 is included to outline these interrelationships.

This report does not present an assessment of the code performance with respect to in-reactor data. Critical comparisons with experimental data from well-characterized, instrumented test rods are presented in Volume 2 of this series of reports [Geelhood et al., 2022c].

The basic fuel, cladding, fill gas, and coolant material properties used in FAST-1.1 are described in the third volume of this series of reports [Geelhood et al., 2022a]. Table 1-1 shows where each specific material property and model used in the NRC fuel performance codes are documented.

Table 1-1. Roadmap to documentation of models and properties used in NRC's fuel performance code FAST

Model/Property	FAST-1.1^(a)
Fuel thermal conductivity	MatLib Document
Fuel thermal expansion	MatLib Document
Fuel melting temperature	MatLib Document
Fuel specific heat	MatLib Document
Fuel enthalpy	MatLib Document
Fuel emissivity	MatLib Document
Fuel densification	MatLib Document
Fuel swelling – solid	MatLib Document
Fuel swelling – gaseous	MatLib Document
Fission gas release	FAST-1.1 Code Description
Fuel relocation	FAST-1.1 Code Description
Fuel grain growth	FAST-1.1 Code Description
High burnup rim model	FAST-1.1 Code Description
Nitrogen release	FAST-1.1 Code Description
Helium release	FAST-1.1 Code Description
Radial power profile	FAST-1.1 Code Description
Stored energy	FAST-1.1 Code Description
Decay heat model	FAST-1.1 Code Description
Fuel and cladding temperature solution	FAST-1.1 Code Description
Cladding thermal conductivity	MatLib Document
Cladding thermal expansion	MatLib Document
Cladding Young's modulus	MatLib Document
Cladding creep model	MatLib Document
Cladding specific heat	MatLib Document
Cladding emissivity	MatLib Document
Cladding axial growth	MatLib Document
Cladding Meyer hardness	MatLib Document
Cladding annealing	FAST-1.1 Code Description
Cladding yield stress, ultimate stress, and plastic deformation	FAST-1.1 Code Description
Cladding failure criteria	FAST-1.1 Code Description
Cladding waterside corrosion	FAST-1.1 Code Description
Cladding hydrogen pickup	FAST-1.1 Code Description
Cladding high temperature oxidation	FAST-1.1 Code Description
Cladding ballooning model	FAST-1.1 Code Description

Table 1-1. Roadmap to documentation of models and properties used in NRC's fuel performance code FAST (continued)

Model/Property	FAST-1.1^(a)
Cladding mechanical deformation	FAST-1.1 Code Description
Oxide thermal conductivity	MatLib Document
Crud thermal conductivity	MatLib Document
Gas conductivity	MatLib Document
Gap conductance	FAST-1.1 Code Description
Plenum gas temperature	FAST-1.1 Code Description
Rod internal pressure	FAST-1.1 Code Description
Coolant temperature and heat transfer coefficients	FAST-1.1 Code Description
Not Developed at PNNL	
Water-cooled, water-moderated energy reactor fuel and cladding models	NUREG/IA-0164
Cladding finite element analysis model	VTT-R-11337-06

^(a) MatLib Document [[Geelhood et al., 2022a](#)]

FAST-1.1 Code Description (this document) [[Geelhood et al., 2022b](#)]

NUREG/IA-0164 [[Shestopalov et al., 1999](#)]

VTT-R-11337-06 [[Knuutila, 2006](#)]

This page intentionally blank.

2.0 General Modeling Description

2.1 Solution Scheme

FAST-1.1 has two solution schemes for solving the conduction equation in order to obtain the temperature profile; one is for the steady-state (time-independent) solution and the other is for the transient (time-dependent) solution.

2.1.1 Steady-State

FAST code iteratively calculates the interrelated effects of fuel and cladding temperature, rod internal gas pressure, fuel and cladding deformation, release of fission product gases, fuel swelling and densification, cladding thermal expansion and irradiation-induced growth, cladding corrosion and hydriding, and crud deposition for a given buildup rate as functions of time and fuel-rod-specific power.

The calculation procedure is illustrated in Figure 2-1, with a simplified flowchart of FAST. The calculation begins by processing input data. Next, the initial fuel rod state is determined through a self-initialization calculation. Time is advanced according to the input-specified time-step size, a steady-state solution is performed, and the new fuel rod state is determined. The new fuel rod state provides the initial state conditions for the next time step. The calculations are cycled in this manner for the user-specified number of time steps.

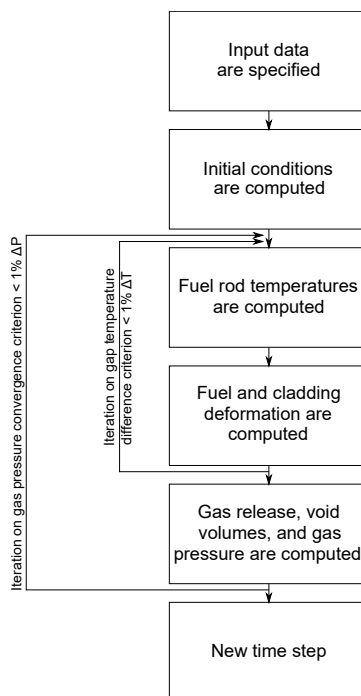


Figure 2-1. Simplified FAST steady-state flowchart

The solution for each time step consists of:

1. Calculating the temperature of the fuel and the cladding
2. Calculating fuel and cladding deformation
3. Calculating the fission product generation and release, void volume, and fuel rod internal gas pressure

Each calculation is made in a separate subcode. As shown in Figure 2-1, the fuel rod response for each time step is determined by repeated cycling through two nested loops of iterative calculations until the fuel-cladding gap temperature difference and internal gas pressure converge.

For the FRACAS-I mechanical model [Bohn, 1977], the fuel temperature and deformation are alternately calculated in the inner loop. On the first cycle through this loop for each time step, the gap conductance is computed using the fuel-cladding gap size from the previous time step. Then the fuel rod temperature distribution is computed. This temperature distribution feeds the deformation calculation by influencing the fuel and cladding thermal expansions and the cladding stress-strain relation. An updated fuel-cladding gap size is calculated and used in the gap conductance calculation on the next cycle through the inner loop. The cyclic process through the inner loop is repeated until two successive cycles calculate essentially the same temperature distribution.

The outer loop of calculations is cycled in a manner similar to that of the inner loop, but with the amount of internal gas being determined during each iteration. The calculation alternates between the fuel rod void volume-gas pressure calculation and the fuel rod temperature-deformation calculation. On the first cycle through the outer loop for each time step, the gas pressure from the previous time step is used. For each cycle through the outer loop, the number of gas moles is calculated and the updated gas pressure is computed and fed back to the deformation and temperature calculations (the inner loop). The calculations are cycled until two successive cycles calculate essentially the same gas pressure, and then a new power-time step is begun.

2.1.2 Transient

The transient solution to the conduction equation is similar to the steady-state solution described above in Section 2.1.1 with the addition of the time-dependent terms (density, specific heat, and time). The code iteratively calculates the interrelated effects of fuel and cladding temperature, fuel rod plenum temperature, fuel and cladding deformation, and rod internal gas pressure. Charts of the overall flow of the computations are shown in Figures 2-2 through 2-4. The input requirements and initialization procedure are shown in Figure 2-2; the temperature, mechanical response, and pressure calculations are shown in Figure 2-3; and the cladding oxidation, local cladding ballooning, and FGR calculations are shown in Figure 2-4.

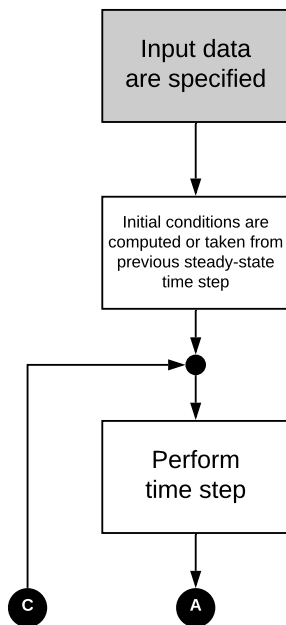


Figure 2-2. Flowchart of FAST transient (Part 1)

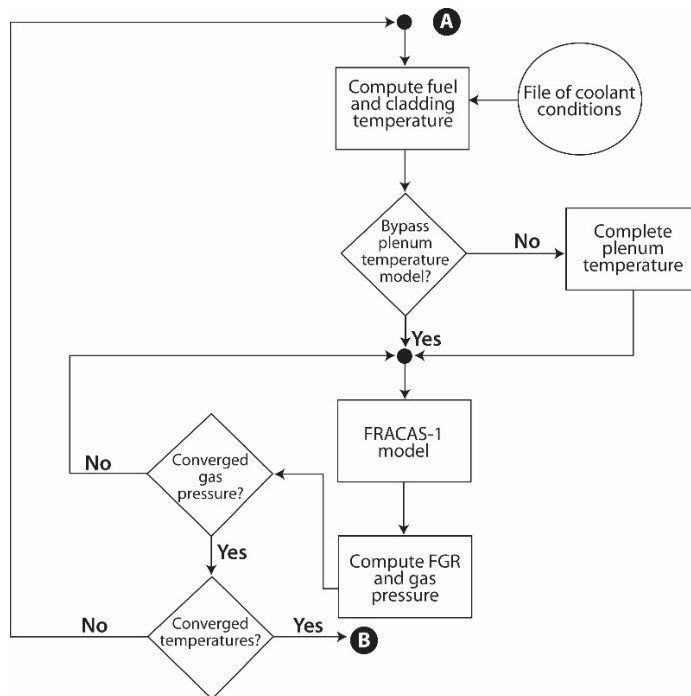


Figure 2-3. Flowchart of FAST transient (Part 2)

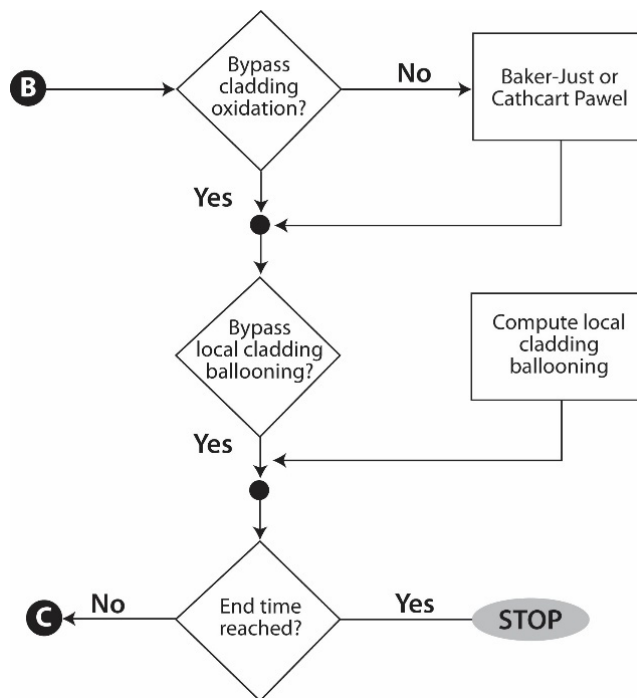


Figure 2-4. Flowchart of FAST transient (Part 3)

As shown in Figure 2-3, the temperature, mechanical response, and internal gas pressure calculations are performed iteratively so that all significant interactions are taken into account. For example, the deformation of the cladding affects the fuel rod internal gas pressure because the internal volume of the rod is changed. The deformation of the cladding also affects the temperature of the fuel and cladding because the flow of heat from the fuel to the cladding is dependent on the fuel-cladding gap width and interface pressure when the gap is closed.

These and all other interactions are accounted for by repeatedly cycling through two nested loops of calculations until convergence is achieved. In the outside loop, the fuel rod temperature and mechanical response are alternately calculated. On the first cycle through this loop, the gap conductance is calculated using the fuel-cladding gap size from the previous time step.

Then the fuel rod temperature distribution is calculated. This temperature distribution then feeds into the mechanical response calculations and influences such variables as the fuel and cladding thermal expansions and the cladding stress-strain relation. A new fuel-cladding gap is calculated which is used in the gap conductance calculation on the next cycle of calculations. The calculations are cycled until two successive cycles compute the same temperature distribution within the convergence criteria.

The inner loop of calculations, shown in Figure 2-3, is cycled in a manner similar to that used for the outer loop, but with the internal gas pressure being the variable determined by iteration. The fuel rod mechanical response and gas pressure are alternately determined. The temperature distribution remains the same during the inner loop of calculations. On the first cycle through this loop, the mechanical response is calculated using the previous time step gas pressure. Variables that influence the gas pressure solution, such as fuel-cladding gap width and plenum volume,

are calculated. Then the gas pressure calculation is made and an updated cladding internal gas pressure is fed back to the mechanical response calculations. The calculations are cycled until two successive cycles result in the same gas pressure within the convergence criteria.

After the two loops of calculations have converged, cladding oxidation, local cladding ballooning, and FGR are calculated. These calculations are performed only once per time step.

2.2 Coupling of Thermal and Mechanical Models

2.2.1 Steady-State

The close coupling of the thermal modeling and mechanical modeling is the result of the existence of the fuel-cladding gap. As the fuel temperature increases, the extreme stresses resulting from the large temperature gradients in the fuel cause the fuel to crack and relocate. Cracks can be circumferential or radial, but are predominantly radial. Void space, which is originally in the fuel-cladding gap, is relocated into the fuel as fragments of fuel move outwardly into the fuel-cladding gap.

As the fuel becomes hotter, the fuel expands, filling some of the voids within the fuel. However, asperities do not align exactly, thereby causing the fuel diameter to appear larger and the fuel to interact with the cladding at a lower power than that expected due to normal expansion (or contraction) mechanisms, including thermal expansion, swelling, and densification. FRACAS-I has been modified to allow 50% of the original fuel surface relocation to be recovered due to fuel swelling before hard contact is established between the fuel and the cladding.

The modeling of the cracked and relocated fuel, both thermally and mechanically, requires accounting for changed fuel-cladding gap size (and hence gap conductance) and the changed fuel pellet diameter as the fuel interacts with the cladding. The fuel surface relocation provides a new fuel-cladding gap size for calculating gap conductance and mechanical interactions. Also considered is the shift of voids from the fuel-cladding gap into cracks in the fuel pellet (and the resultant pressure change due to higher temperature in the cracks) and the feedback into the mechanics and thermal calculations.

FRACAS-I uses the relocated fuel-cladding gap size for the thermal calculations and makes partial use of the fuel surface relocation in the mechanics calculation (i.e., when 50% of the relocation is recovered, the code assumes the pellet to be a rigid structure, and, therefore, hard contact is assumed between the fuel and cladding).

2.2.2 Transient

The order of the general models in FAST is shown in Figure 2-5. The solution for the fuel rod variables begins with the calculation of the temperatures of the fuel and cladding. The temperature of the gases in the fuel rod is then calculated. Next, the stresses and strains in the fuel and cladding are calculated. The pressure of the gas inside the fuel rod is then calculated, including predicting the FGR. This sequence of calculations is cycled until essentially the same temperature distribution (i.e., within specified convergence criteria) is calculated for two successive cycles. Finally, the cladding oxidation and clad ballooning are calculated. Time is then incrementally advanced, and

the complete sequence of calculations is then repeated to obtain the values of the fuel rod variables at the advanced time.

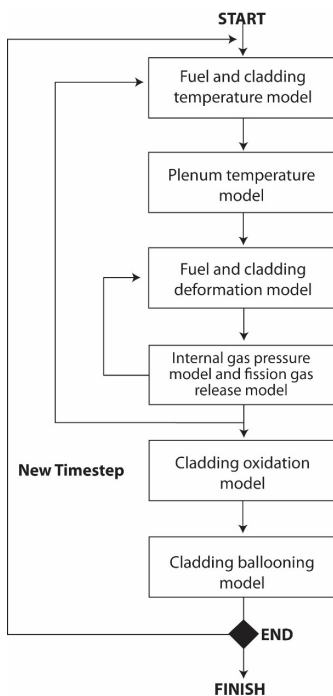


Figure 2-5. Order of FAST solution schemes

The models interact in several ways. The temperature of the fuel, which is calculated by the thermal model, is dependent on the width of the fuel-cladding gap and fuel-cladding interfacial pressure, which is calculated by the deformation model. The diameter of the fuel pellet is dependent on the temperature distribution in the fuel pellet. The mechanical properties of the cladding vary significantly with temperature. The internal gas pressure varies with the temperature of the fuel rod gases, the strains of the fuel and cladding, and any FGR predicted. The stresses and strains in the cladding are dependent on the internal gas pressure. In addition, there is a burnup dependence to the initial value of numerous variables necessary for calculating the transient response of a fuel rod.

The model interactions are taken into account by iterative calculations. The variables calculated in one model are treated as independent variables by the other models. For example, the fuel-cladding gap size, which is calculated by the deformation model, is treated as an independent variable by the thermal model. On the first iteration of a new time step, the thermal model assumes the fuel-cladding gap size is equal to the value calculated by the deformation model on the last iteration of the previous time step. On the i^{th} iteration, the thermal model assumes the fuel-cladding gap size is equal to the value calculated by the deformation model in the $(i - 1)^{th}$ iteration.

The sequence of the iterative computations is shown in Figure 2-5. Two nested loops of calculations are repeatedly cycled until convergence occurs. In the inside loop, the deformation and gas pressure models are repeatedly cycled until two successive cycles calculate gas pressure within the convergence criteria. Convergence usually occurs within two cycles. In the outside loop, the

fuel and cladding thermal model, plenum gas thermal model, and the inner loop are repeatedly cycled until the fuel rod temperature distribution is calculated within the convergence criteria. Convergence usually occurs within two or three cycles. After the computations of the outer loop have converged, the cladding oxidation and ballooning are calculated, and a new time step is taken.

The convergences of both the inner and the outer calculational loops are accelerated by use of the method of Newton. In the inner loop, the deformation model for the $(i + 1)^{th}$ iteration is given the predicted gas pressure for the $(i + 1)^{th}$ iteration. The gas pressure is predicted by the method of Newton and is based on the gas pressures calculated in the $(i - 1)^{th}$ and i^{th} iterations. The gas pressure is predicted by:

$$P_p^{i+1} = \frac{\left(P_c^{i-1} - \frac{P_c^i - P_c^{i-1}}{P_p^i - P_p^{i-1}} P_p^{i-1} \right)}{\left(1 - \frac{P_c^i - P_c^{i-1}}{P_p^i - P_p^{i-1}} \right)} \quad (2-1)$$

Where,

P_p^x = Gas pressure predicted for the $(x)^{th}$ iteration

P_c^x = Gas pressure calculated for the $(x)^{th}$ iteration

The convergence of the outer loop is accelerated in a manner similar to that of the inner loop, but with the fuel-cladding gap conductance as the predicted variable instead of the gas pressure.

2.3 Mesh Layout

2.3.1 Cylindrical Geometry

The default geometry modeled by FAST is an axi-symmetric (2-D (r, z)) solid right cylinder. The mesh is generated internally by FAST during code initialization, determined by the number of mesh points and geometry, which are defined in the input file. There are three meshes that are generated by the code for calculating different values:

- Thermal mesh: Calculates the thermal and mechanical solutions
- Fission gas mesh: Calculates the fission gas diffusion and release
- Void volume mesh: Calculates the void volume and rod internal pressure

2.3.2 Thermal Mesh

The thermal mesh is composed of several different layers of materials, including fuel, gas, cladding, coating, oxide and crud layers, as shown in Figure 2-6.

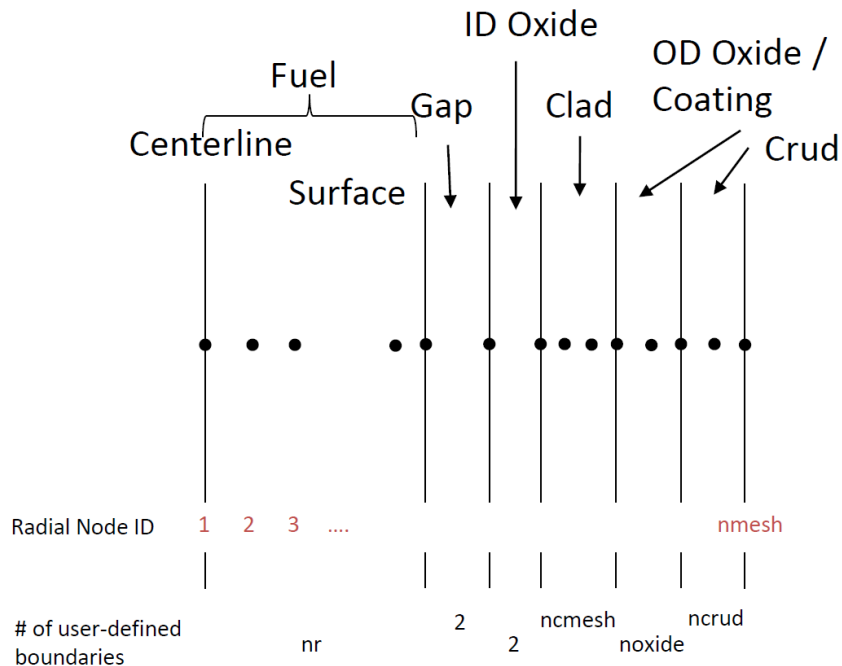


Figure 2-6. Schematic of fuel rod materials and node placement

The input variables that define the dimensions of each material are shown in Table 2-1. Not all materials are allowed as inputs (e.g., oxide thicknesses) due to these initially being non-existent during fabrication and forming once in reactor. The code initially establishes these as small meshes (1×10^{-9} m) with the same properties as the base cladding material until the layer forms.

Table 2-1. Input variables defining radial geometry dimensions used in thermal mesh

Variable	Description
rc	Fuel inner radius
thkgap	Gas-gap thickness
thkcoatid	Cladding ID oxide coating thickness
thkcld	Cladding thickness
dco	Cladding Outer Diameter
thkcoat	Cladding OD oxide coating thickness
crdt	Crud thickness

The `frpcn` block in the input file contains the variables used to define the number of radial boundaries for each material region. The default number of boundaries for each material are reproduced in Table 2-2. A minimum of two boundaries (left and right) are required to model each material.

Table 2-2. Input variables defining number of radial material boundaries

Variable	Material Boundary	Default Value
nr	Fuel	17
–	Gas-gap	2
–	Cladding ID Oxide	2
nlayersid	Cladding ID Coating	1
ncmesh	Cladding	1
nlayers	Cladding OD Coating	1
noxide	Cladding OD Oxide	1
ncrud	Crud	1

The total number of radial nodes in the conduction solution is defined as the sum of all radial nodes in the fuel, gap, ID oxide, cladding, OD oxide, and crud layers, as shown in Equation 2-2.

$$N_{Nodes} = N_{Fuel} + N_{Gap} + N_{ID-Oxide} + N_{ID-Coating} + N_{Clad} + N_{OD-Coating} + N_{OD-Oxide} + N_{Crud} \quad (2-2)$$

Due to adjoining material boundaries, the number of boundaries for each material is reduced by 1 (except for the fuel, as it is considered as the starting boundary and has an independently defined left and right boundary). Substituting in the user-defined values,

$$N_{Nodes} = nr + (2 - 1) + (2 - 1) + (ncmesh - 1) + (noxide - 1) + (ncrud - 1) \quad (2-3)$$

By default (assuming no coating layers present),

$$N_{Nodes} = 17 + 1 + 1 + 1 + 1 + 1 = 2 \quad (2-4)$$

Where N_{Nodes} is the same as the variable n_{mesh} (used internally by FAST) shown in Figure 2-6.

The placement of the fuel radial nodes ($r_{f,i}$) is shown in Equation 2-5. More boundaries are placed at the pellet outer edge than in the center of the pellet to capture the effects of edge power peaking with high burnup fuel.

$$r_{f,i} = \left(1 - \left[\frac{i-1}{nr-1} \right]^3 \right) (r_p - r_c) + r_c \quad (2-5)$$

Where,

$r_{f,i}$ = Location of fuel radial node i

r_p = Fuel pellet radius, m

r_c = Fuel central hole (if exists) radius, m

r_p = Number of radial boundaries in the fuel (see nr in Table 2-2)

nr = Number of radial fuel boundaries

The placement of the remaining boundaries assumes an equal radial distance spacing. For example, the spacing of each cladding mesh is calculated as:

$$r_{clad,i} = \frac{r_{clad_outer} - r_{clad_inner}}{ncmesh - 1} \quad (2-6)$$

Resulting in each cladding node placement:

$$r_{clad,i} = r_{clad,i-1} + r_{clad,i} \quad (2-7)$$

Note: This radial mesh placement is repeated for each axial node. However, there is the ability for the user to specify different dimensions at each axial node (see Appendix B.4).

The placement of each axial boundary can be either equally-spaced (default) or defined lengths. The variables related to the axial mesh formation are shown in Table 2-3.

Table 2-3. Input variables defining number of axial material boundaries and geometry

Variable	Boundary	Default Value
na	Axial mesh placement	9
Variable	Description	–
totl	Fuel column axial length	–
deltaz	Length of each axial node	–
cp1	Plenum axial length	–

If equally-spaced axial lengths are used, the length of each axial node (Δz_i) is calculated using Equations 2-8 and 2-9.

$$\text{Fuel: } \Delta z_{i,i=1,na} = \frac{totl}{na} \quad (2-8)$$

$$\text{Plenum: } \Delta z_{na+1} = cp1 \quad (2-9)$$

If variable axial spacing is used, the length of each axial node is specified in the input file and calculated using Equations 2-10 and 2-11.

$$\text{Fuel: } \Delta z_{i,i=1,na} = \text{deltaz}(i) \tag{2-10}$$

$$\text{Plenum: } \Delta z_{na+1} = \text{cpl} \tag{2-11}$$

Note: $\sum_{i=1}^{na} \text{deltaz}(i) = \text{totl}$

A schematic of the discretization is shown in Figure 2-7.

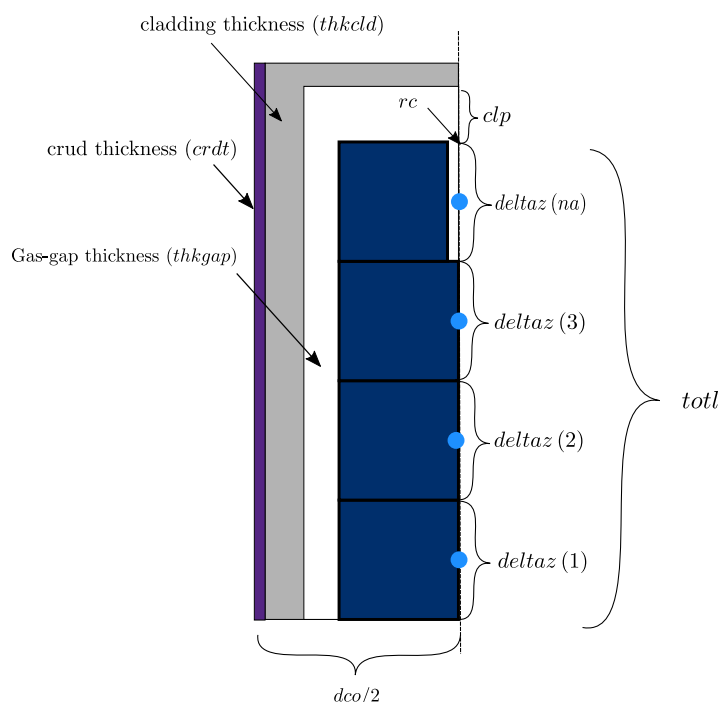


Figure 2-7. Axial and radial discretization of user-defined fuel rod geometry

2.3.3 Void Volume Mesh

The mesh that is used for void volume calculations is discretized similar to the thermal mesh, except that the void volume mesh is focused only on the fuel and gas-gap (i.e., areas where voids are present) and accounts for the presence of dish and chamfers on the fuel pellet. The radial locations are defined the same as Equation 2-5. The difference is in the height of each radial node, accounting for the presence of the dish/chamfer. A schematic of a dish and chamfer is shown in Figure 2-8, and a description of the input geometry terms is shown in Table 2-4.

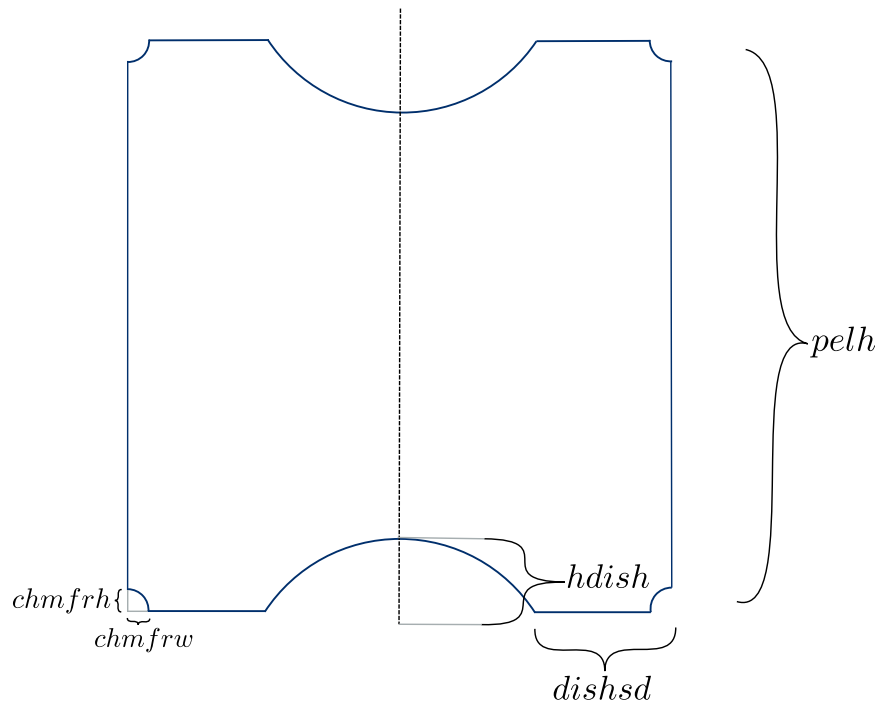


Figure 2-8. Layout of user-defined inputs for fuel pellet dish and chamfer

Table 2-4. Variables used to define dish and chamfer geometry

Variable	Description
hdish	Height (depth) of pellet dish, assumed to be a spherical indentation
dishsd	Pellet end-dish shoulder width (outer radius of pellet - radius of dish)
chmfrh	Chamfer height
chmfrw	Chamfer width

A schematic of the fuel pellet when no dishes or chamfers are present is shown in Figure 2-9.

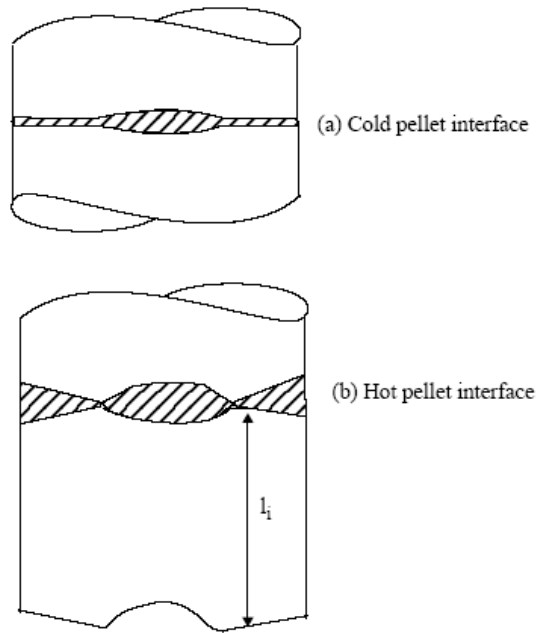


Figure 2-9. A schematic of the impact of dishes and chamfers on void volume

2.3.4 Fission Gas Release Mesh

The FGR calculation typically requires a finer level of discretization on the fuel pellet than the thermal mesh (Note: there is no mesh on any other materials). The mesh is generated with equal area rings (A_{fgr}) using Equation 2-12. The user-defined input for the number of radial rings is $ngasr$, compared to the number of radial boundaries, nr , in the thermal mesh. Note that the number of radial boundaries is equal to the number of rings + 1, so the number of boundaries used in the FGR mesh is $ngasr + 1$.

$$A_{fgr,i} = \frac{\pi (r_p^2 - r_c^2)}{ngasr} \tag{2-12}$$

By using equal area rings, the radius of each ring is calculated using Equation 2-13. Rather than the radius be taken at the boundary (i.e., starting at r_c and ending at r_p), the radius is calculated as the area-average radius of each radial ring.

$$r_{i+1} = \sqrt{r_i^2 + \frac{A_{fgr,i}}{2\pi}} \tag{2-13}$$

The fission gas mesh uses temperatures and radial power distribution from the thermal mesh by performing interpolation based on radial location.

2.4 Plenum Thermal Response

2.4.1 Plenum Temperature Equations

The plenum thermal model calculates the energy exchange between the plenum gas and structural components, which consists of the hold-down spring, end fuel pellet, and cladding. Energy exchange between the gas and structural components occurs by natural convection, conduction, and radiation. A schematic of these energy exchange mechanisms is shown in Figure 2-10.

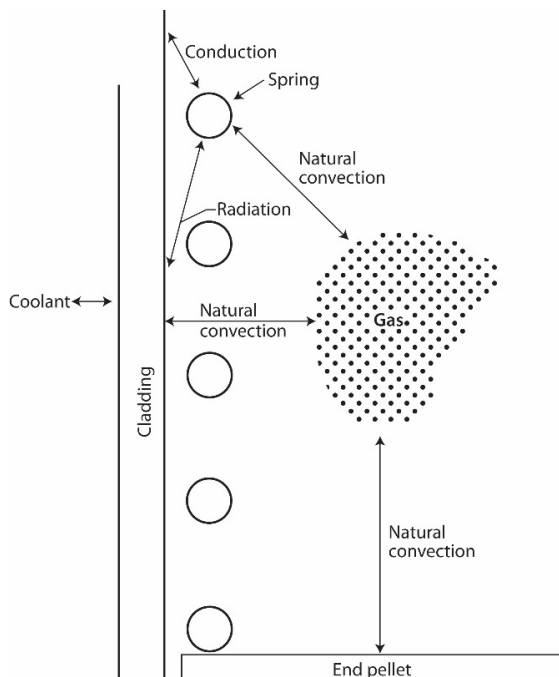


Figure 2-10. Energy flow in plenum model – energy exchange mechanisms

The spring is modeled by two nodes of equal mass (a center node and a surface node) as shown in Figure 2-11.

R_{ss} = radius of spring

$$R_{sc} = \frac{R_{ss}}{\sqrt{2}}$$

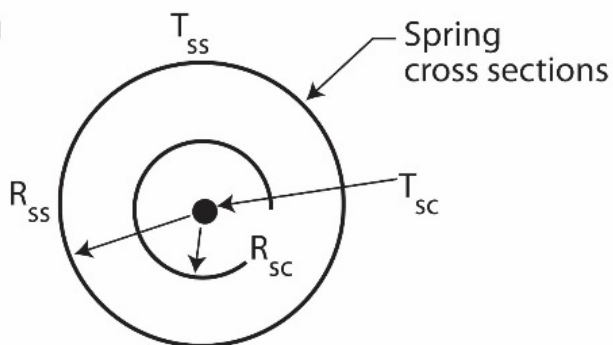


Figure 2-11. Energy flow in plenum model – spring model with two nodes

The cladding is modeled by three nodes (two surface nodes and one center node) as shown in Figure 2-12. The center node has twice the mass of the surface nodes. This nodalization scheme results in a set of six energy equations from which the plenum thermal response can be calculated.

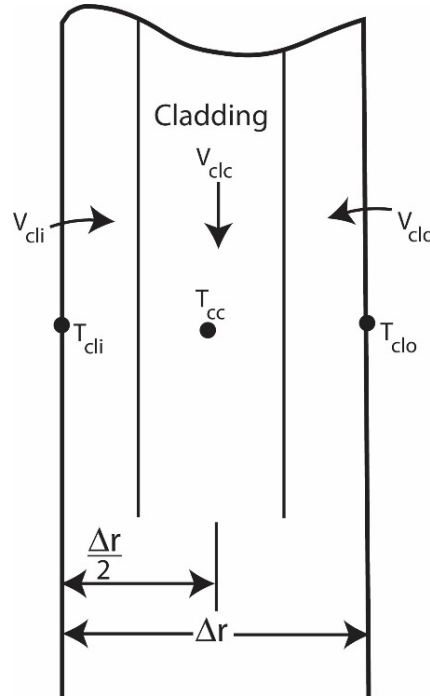


Figure 2-12. Cladding nodalization

The transient energy equations for the gas, spring, and cladding are as follows (the nomenclature used in the equations is defined in Table 2-5):

1. Plenum gas

$$V_g \rho_g C_g \frac{\partial T_g}{\partial t} = A_{ep} h_{ep} (T_{ep} - T_g) + A_{cl} h_{cl} (T_{cli} - T_g) + A_{SS} h_S (T_{SS} - T_g) \quad (2-14)$$

2. Spring center node

$$V_{sc} \rho_s C_s \frac{\partial T_{SS}}{\partial t} = \bar{q} V_{sc} + \frac{A_{SC} k_S (T_{SS} - T_{SC})}{R_{SS}} \quad (2-15)$$

3. Spring surface node

$$V_{ss} C_s \rho_s \frac{\partial T_{SS}}{\partial t} = \bar{q} V_{ss} + A_{SC} k_S (T_{SC} - T_{SS}) + A_{SS} h_{rads} (T_{cli} - T_{SS}) + A_{SS} h_S (T_g - T_{SS}) + A_{SS} h_{cons} (T_{cli} - T_{SS}) \quad (2-16)$$

where h_{cons} is the conductance between the spring and cladding. The conductance is used only when a stagnant gas condition exists; that is, when the natural convection heat transfer coefficient for the spring (h_s) is zero.

4. Cladding interior node

$$V_{cli}\rho_{cl}C_{cl}\frac{\partial T_{cli}}{\partial t} = \bar{q}V_{cli} + A_{cl}h_{radc}(T_{SS} - T_{cli}) + A_{cl}h_{cl}(T_g - T_{cli}) + A_{cl}h_{conc}(T_{SS} - T_{cli}) + \frac{A_{cl}k_{cl}}{\frac{r}{2}}(T_{clc} - T_{cli}) \quad (2-17)$$

5. Cladding central node

$$V_{clc}\rho_{cl}C_{cl}\frac{\partial T_{clc}}{\partial t} = \bar{q}V_{clc} + \frac{A_{cl}k_{cl}}{\frac{r}{2}}(T_{cli} - T_{clc}) + \frac{A_{cl}k_{cl}}{\frac{r}{2}}(T_{clo} - T_{clc}) \quad (2-18)$$

6. Cladding exterior node

$$T_{clo} = T_{cool} \quad (2-19)$$

Table 2-5. Nomenclature for plenum thermal model

Variable	Description
Quantities	
A	Surface area
C	Heat capacitance
$DIAC$	Diameter of the spring coil
$DIAS$	Diameter of the spring wire
$\bar{F}_{1 \rightarrow 2}$	Gray body shape from body 1 to body 2
$F_{1 \rightarrow 2}$	View factor from body 1 to body 2
Gr	Grashof number
h	Surface heat transfer to coolant
I	Gamma flux
ID	Inside diameter of the cladding
k	Thermal conductivity
L	Length
OD	Outside diameter of the cladding
Pr	Prandtl number
q	Energy
\bar{q}''	Surface heat flux

Table 2-5. Nomenclature for plenum thermal model (continued)

Variable	Description
\bar{q}'''	Volumetric heat generation
R	Radius
ΔR	Thickness of the cladding
T	Temperature
V	Volume
σ	Stefan-Boltzman constant
C_g	Heat capacitance of gas
ρ	Density
Σ_γ	Absorption coefficient
ε	Emissivity
δ	Spring to cladding spacing = $\frac{ID-DIAC}{2}$
t	Time
Subscripts	
cl	Cladding
clc	Cladding center node
cli	Cladding interior node
clo	Cladding outside node
$cool$	Coolant
$conc, cons$	Conduction between the spring and cladding
$conv$	Convective heat transfer to coolant
ep	End pellet
g	Gas
p	Plenum
sc	Spring center node
ss	Spring surface node
s	Spring
$rads, radc$	Radiation heat transfer between the spring and the cladding
$m, m + 1$	Old and new time step

For steady-state analysis, the time derivatives of temperature on the left side of Equations 2-14

through 2-18 are set equal to zero and the temperature distribution in the spring and cladding is assumed to be uniform.

To obtain a set of algebraic equations, Equations 2-14 through 2-19 are written in the Crank-Nicolson implicit finite difference form [Crank and Nicolson, 1974]. This formulation results in a set of six equations and six unknowns. The details of the finite difference formulation of Equations 2-14 through 2-19 and the logic of the plenum temperature model are given in Appendix D.

2.4.2 Heat Conduction Coefficients

Heat transfer between the plenum gas and the structural components occurs by natural convection, conduction, and radiation. The required heat transfer coefficients for these three modes are described in the following section.

2.4.2.1 Natural Convection Heat Transfer Coefficients

Energy exchange by natural convection occurs between the plenum gas and the top of the fuel pellet stack, the spring, and the cladding. Heat transfer coefficients h_{ep} , h_s , and h_{cl} , in the equations above, model this energy exchange. To calculate these heat transfer coefficients, the top of the fuel stack is assumed to be a flat plate, the spring is assumed to be a horizontal cylinder, and the cladding is assumed to be a vertical surface. Both laminar and turbulent natural convection are assumed to occur. Correlations for the heat transfer coefficients for these types of heat transfer are obtained from [Kreith, 1964] and [McAdams, 1954].

The flat plate natural convection coefficients used for the end pellet surface heat transfer are given below, using the nomenclature from Table 2-5.

1. For laminar conditions on a heated surface:

$$h_{ep} = 0.54k_g \frac{(GrPr)^{0.25}}{ID} \quad (2-20)$$

2. For turbulent conditions (Grashof Number, $Gr > 2.0 \times 10^7$), on a heated surface:

$$h_{ep} = 0.14k_g \frac{(GrPr)^{0.33}}{ID} \quad (2-21)$$

3. For laminar conditions on a cooled surface:

$$h_{ep} = 0.27k_g \frac{(GrPr)^{0.25}}{ID} \quad (2-22)$$

The following natural convection coefficients for horizontal cylinders are used for the film coefficient for the spring.

1. For laminar conditions:

$$h_s = 0.53k_g \frac{(GrPr)^{0.25}}{DIAS} \quad (2-23)$$

2. For turbulent conditions ($1.0 \times 10^9 \leq Gr \leq 1.0 \times 10^{12}$):

$$h_s = 0.18 (T_g - T_{SS})^{0.33} \quad (2-24)$$

The vertical surface natural convection coefficients used for the cladding interior surface are given below.

1. For laminar conditions:

$$h_{cl} = 0.55k_g \frac{(GrPr)^{0.25}}{L_p} \quad (2-25)$$

2. For turbulent conditions ($Gr > 1 \times 10^9$):

$$h_{cl} = 0.021k_g \frac{(GrPr)^{0.4}}{L_p} \quad (2-26)$$

These natural convection correlations were derived for flat plates, horizontal cylinders, and vertical surfaces in an infinite gas volume. Heat transfer coefficients calculated using these correlations are expected to be higher than those actually existing within the confined space of the plenum. Until additional plenum temperature experimental data are available, these coefficients are believed to provide an acceptable estimate of the true value.

2.4.2.2 Conduction Heat Transfer Coefficients

Conduction of energy between the spring and cladding is represented by the heat transfer coefficients h_{cons} and h_{conc} in Equations 2-16 and 2-17. These coefficients are both calculated when stagnant gas conditions exist. The conduction coefficients are calculated based on the spring and cladding geometries shown in Figure 2-13 and the following assumptions:

- The cladding and spring surface temperatures are uniform.
- Energy is conducted only in the direction perpendicular to the cladding wall (heat flow is one-dimensional).

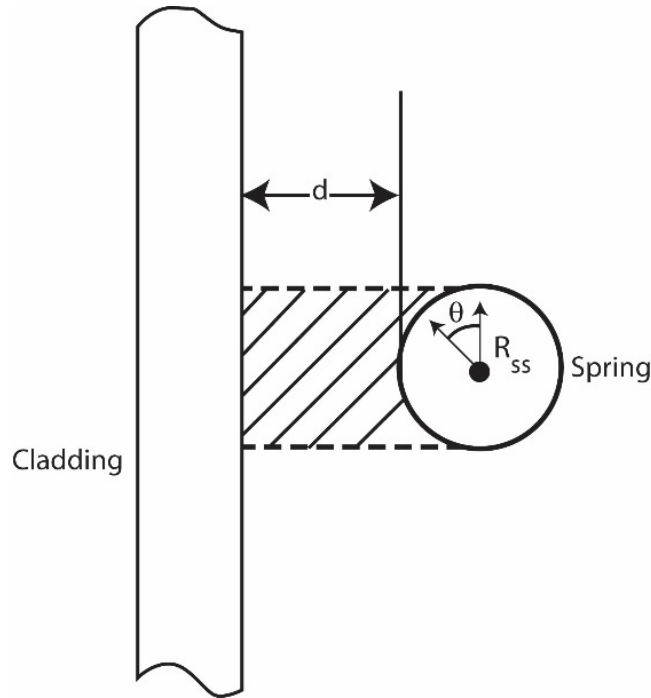


Figure 2-13. Geometrical relationship between the cladding and spring

Based on these assumptions, and the geometry given in Figure 2-13, the energy (q) conducted from an elemental surface area of the spring ($L_S R_S d\theta$) to the cladding is:

$$dq = \frac{k_g (T_{SS} - T_{cli}) (L_S R_S \sin \theta d\theta)}{d + R_S - R_S \sin \theta} \quad (2-27)$$

Where,

θ = Azimuthal coordinate

By integration of Equation 2-27 over the surface area of the spring facing the cladding, the total flow of energy is given by:

$$q = \frac{k_g A_{SS}}{\pi} (T_{SS} - T_{cli}) \left\{ -\frac{\pi}{2R_S} + \frac{2}{R_S} \left[\frac{1}{(\delta + 2R_S)^2} + \left(\frac{\tan \frac{\theta}{2} - \frac{R_S}{\delta + 2R_S}}{1 - \frac{R_S^2}{(\delta + 2R_S)^2}} \right) \right] \right\} \Bigg|_{\theta=0}^{\theta=\frac{\pi}{2}} \quad (2-28)$$

The two conduction heat transfer coefficients, h_{cons} and h_{conc} , are calculated by Equations 2-29 and 2-30.

$$h_{cons} = \frac{q (T_{SS} - T_{cli})}{A_{SS}} \quad (2-29)$$

$$h_{conc} = h_{cons} \frac{A_{SS}}{A_{cl}} \quad (2-30)$$

When natural convection heat transfer exists (h_{cl} or h_s greater than 0.0), energy is assumed to flow to the gas from the spring and then from the gas to the cladding wall, or vice versa. Under these conditions, h_{cons} and h_{conc} are set equal to zero. Therefore, h_{cons} and h_{conc} are used only when the temperature is uniform throughout the plenum. Future plenum data or analytical analysis may indicate that natural convection flow between the spring and cladding does not exist, in which case non-zero conduction coefficients should be used at all times.

2.4.2.3 Radiation Heat Transfer Coefficients

Transport of energy by radiation between the spring and cladding is included in the plenum model by use of the heat transfer coefficients h_{rads} and h_{radc} in Equations 2-16 and 2-17. These coefficients are derived from the radiant energy exchange equation for two gray bodies in thermal equilibrium as follows [Kreith, 1964]:

$$q_{1 \rightarrow 2} = A_1 \bar{F}_{1 \rightarrow 2} \sigma (T_1^4 - T_2^4) \quad (2-31)$$

Where,

$q_{1 \rightarrow 2}$ = Net rate of heat flow by radiation between bodies 1 and 2

The gray body factor, $\bar{F}_{1 \rightarrow 2}$, is related to the geometrical view factor, $F_{1 \rightarrow 2}$, from body 1 to body 2 by:

$$A_1 \bar{F}_{1 \rightarrow 2} = \frac{1}{\frac{1 - \varepsilon_1}{A_1 \varepsilon_1} + \frac{1}{A_1 F_{1 \rightarrow 2}} + \frac{1 - \varepsilon_2}{A_2 \varepsilon_2}} \quad (2-32)$$

Using Equations 2-31 and 2-32 and approximating the geometric view factor from the cladding to the spring, F_{cl-s} , by:

$$F_{cl-s} = \frac{A_{SS}}{2A_{cl}} + \frac{(2A_{cl} - A_{SS}) A_{SS}}{4A_{cl}^2} \quad (2-33)$$

The net radiation energy exchange between the cladding and spring may be written as:

$$q_{cl-s} = A_{cl} \bar{F}_{cl-s} (T_{cl}^4 - T_{SS}^4) \quad (2-34)$$

The radiation heat transfer coefficients, h_{radc} and h_{rads} , are calculated by Equations 2-35 and 2-36.

$$h_{radc} = \frac{q_{cl-s} (T_{cli} - T_{SS})}{A_{cl}} \quad (2-35)$$

$$h_{rads} = h_{radc} \frac{A_{cl}}{A_{SS}} \quad (2-36)$$

2.4.2.4 Gamma Heating of the Spring and Cladding

The volumetric power generation term, q , used in Equation 2-15 through 2-18, represents the gamma radiation heating of the spring and cladding. A simple relationship is used to calculate q . The relationship used is derived from the gamma flux attenuation equation:

$$-dI(x) = \Sigma_{\gamma} I(x) dx \quad (2-37)$$

Where,

$I(x)$ = Gamma flux

Σ_{γ} = Gamma ray absorption coefficient

x = Spatial dimension of solid on which the gamma radiation is incident

Because the cladding and spring are thin in cross section, the gamma ray flux can be assumed constant throughout the volume. Of the gamma flux, I , incident on the spring and cladding, the portion absorbed, I , can be described by:

$$-I = \Sigma_{\gamma} I \bar{x} \quad (2-38)$$

Where,

\bar{x} = Thickness of the spring or cladding

Therefore, the volumetric gamma ray absorption rate is given by:

$$-\frac{I}{\bar{x}} = \Sigma_{\gamma} I \quad (2-39)$$

Equation 2-39 can also represent gamma volumetric energy deposition by letting I represent the energy flux associated with the gamma radiation. Approximately 10% of the energy released by the fission of uranium is in the form of high energy gamma radiation. Therefore, the gamma energy flux leaving the fuel rod would be approximately equal to 10% of the thermal flux. The gamma energy flux throughout the reactor can then be estimated by:

$$I = 0.10\bar{q}_{rod} \quad (2-40)$$

Where,

\bar{q}_{rod} = Average fuel rod power, kW/m

For zirconium, Σ_{γ} is approximately 36.1 1/m. Therefore, the gamma energy deposition rate is given by Equation 2-41. This is an estimate of the gamma heating rate for the spring and cladding.

$$-\frac{I}{x} = \bar{q} = 3.61\bar{q}_{rod} \quad (2-41)$$

2.4.3 Stored Energy

The stored energy in the fuel rod is calculated separately for the fuel and the cladding, by summing the energy of each pellet or cladding ring calculated at the ring temperature. The expression for stored energy is shown in Equation 2-42.

$$E_s = \frac{\sum_{i=1}^I m_i \int_{T_{ref}}^{T_i} C_p(T) dT}{m} \quad (2-42)$$

Where,

E_s = Stored energy, J/kg

m_i = Mass of ring segment i , kg

T_i = Temperature of ring segment i , K

T_{ref} = Reference temperature for stored energy, K

$C_p(T)$ = Specific heat evaluated at temperature T , J/kg-K

m = Total mass of the axial node, kg

I = Number of annular rings

The stored energy is calculated for each axial node. By default, the reference temperature (T_{ref}) is taken at STP conditions (298 K or 77 °F); however, this can be changed using the input file.

2.5 Fuel Rod Mechanical Response

An accurate calculation of fuel and cladding deformation is necessary in any fuel rod response analysis because the heat transfer coefficient across the fuel-cladding gap is a function of both the effective fuel-cladding gap size and the fuel-cladding interfacial pressure. In addition, an accurate calculation of stresses in the cladding is needed to accurately calculate the strain and the onset of cladding failure (and subsequent release of fission products). This section describes the default mechanical model, FRACAS-I. The optional cladding FEA model is described elsewhere [Knuutila, 2006].

2.5.1 The FRACAS-1 Model

The FRACAS-I model is available for the calculation of the small displacement deformation of the fuel and cladding. The simplified model, FRACAS-I, neglects the stress-induced deformation of the fuel, and is called the “rigid pellet model.”

In analyzing the deformation of fuel rods, two physical situations are envisioned. The first situation occurs when the fuel and cladding are not in contact. Here the problem of a cylindrical shell (the cladding) with specified internal and external pressures and a specified cladding temperature distribution must be solved. This situation is called the “open gap” regime.

The second situation envisioned is when the fuel (considerably hotter than the cladding) has expanded so as to be in contact with the cladding. Further heating (thermal expansion) of the fuel “drives” the cladding outward. This situation is called the “closed gap” regime. In addition, this closed gap can occur due to fuel swelling, relocation, and the creep of the cladding onto the fuel due to a high coolant pressure.

The deformation analysis in FAST consists of a small deformation analysis that includes stresses, strains, and displacements in the fuel and cladding for the entire fuel rod. This analysis assumes that the cladding retains its cylindrical shape during deformation, and includes the effects of the following:

- Fuel thermal expansion, swelling, densification, and relocation
- Cladding thermal expansion, creep, and plasticity
- Fission gas and external coolant pressures

As part of the small displacement analysis, the applicable local deformation regime (open gap or closed gap) is determined. Finally, an analysis is performed to determine cladding stresses and strains.

In Section 2.5.1.1, the general theory of plastic analysis is outlined and the method of solution used in the FRACAS-I model is presented. This method of solution is used in the rigid pellet model. In Section 2.5.1.2, the equations for the rigid pellet model are described.

2.5.1.1 General Theory and Method of Solution

The general theory of plastic analysis and the method of solution are used in the rigid pellet model.

General Considerations in Elastic-Plastic Analysis

Problems involving elastic-plastic deformation and multiaxial stress states involve aspects that do not require consideration in a uniaxial problem. In the following discussion, an attempt is made to briefly outline the structure of incremental plasticity and to outline the method of successive substitutions (also called the method of successive elastic solutions) [Mendelson, 1968], which has been used successfully in treating multiaxial elastic-plastic problems. The method can be used for any problem for which a solution based on elasticity can be obtained. This method is used in the rigid pellet model.

In a problem involving only uniaxial stress, σ_1 , the strain, ε_1 , is related to the stress by an experimentally determined stress-strain curve as shown in Figure 2-14 (including the elastic strains and plastic strains, but without thermal expansion strains) so Hooke's law is taken as:

$$\varepsilon_1 = \frac{\sigma_1}{E} + \varepsilon_1^P + \int \alpha dT \quad (2-43)$$

Where,

ε_1 = Total strain, m/m

σ_1 = Uniaxial stress, MPa

E = Modulus of elasticity, MPa

ε_1^P = Plastic strain, m/m

α = Thermal expansion coefficient, K^{-1}

T = Temperature, K

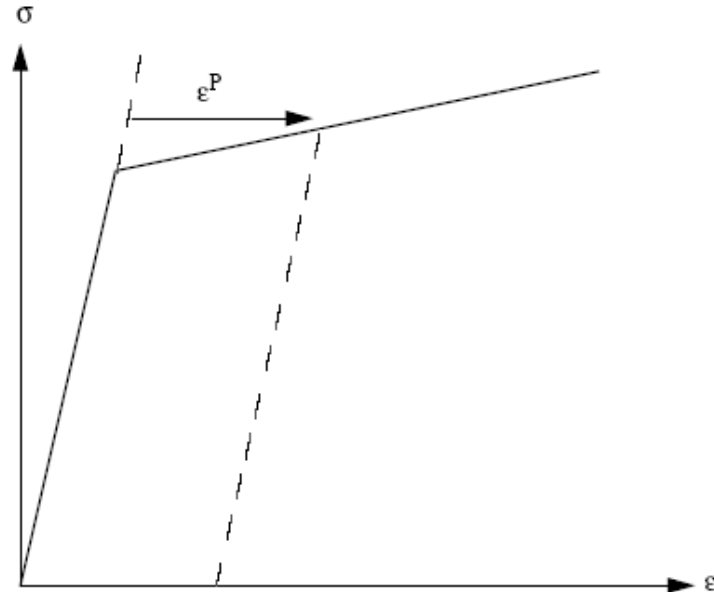


Figure 2-14. Typical isothermal stress-strain curve

The onset of yielding occurs at the yield stress, which can be determined directly from Figure 2-14. Given a load (stress) history, the resulting deformation can be determined in a simple manner. The increase of yield stress with work-hardening is easily computed directly from Figure 2-14.

In a problem involving multiaxial states of stress, as with a fuel rod, the situation is not as clear. In such a problem, a method of relating the onset of plastic deformation to the results of a uniaxial test is required, and further, when plastic deformation occurs, some means is needed for determining how much plastic deformation has occurred and how that deformation is distributed among the individual components of strain. These two complications are taken into account by use of the so-called “yield function” and “flow rule,” respectively.

A wealth of experimental evidence exists on the onset of yielding in a multiaxial stress state. Most of this evidence supports the von Mises yield criterion, which asserts that yielding occurs when the stress state is such that:

$$\sigma_y^2 = \frac{1}{2} \left[(\sigma_1 - \sigma_2)^2 + (\sigma_2 - \sigma_3)^2 + (\sigma_3 - \sigma_1)^2 \right] \quad (2-44)$$

Where,

σ_i = Principle stresses in direction i , $i = 1, 2, 3$

σ_y = Yield stress as determined in a uniaxial stress-strain test

The square root of the left side of Equation 2-44 is referred to as the “effective stress,” σ_e , and this effective stress is one commonly used type of yield function.

To determine how the yield stress changes with permanent deformation, the yield stress is hypothesized to be a function of the equivalent plastic strain, ε^p . An increment of equivalent plastic strain is determined at each load step, and ε^p is defined as the sum of all increments incurred, as shown in Equation 2-45.

$$\varepsilon^p = \sum d\varepsilon^p \quad (2-45)$$

Each increment of effective plastic strain is related to the individual plastic strain components by:

$$d\varepsilon^p = \frac{\sqrt{2}}{3} \sqrt{(\varepsilon_1^p - d\varepsilon_2^p)^2 + (d\varepsilon_2^p - d\varepsilon_3^p)^2 + (d\varepsilon_3^p - d\varepsilon_1^p)^2} \quad (2-46)$$

Where,

$d\varepsilon_i^p$ = Plastic strain components in principle coordinates

Experimental results indicate that at pressures on the order of the yield stress, plastic deformation occurs with no change in volume, which implies that:

$$d\varepsilon_1^p + d\varepsilon_2^p + d\varepsilon_3^p = 0 \quad (2-47)$$

Therefore, in a uniaxial test with $\sigma_1 = \sigma$, $\sigma_2 = \sigma_3 = 0$, the plastic strain increments are:

$$d\varepsilon_2^p = d\varepsilon_3^p = -\frac{1}{2}d\varepsilon_1^p \quad (2-48)$$

Therefore, in a uniaxial test, Equations 2-44 and 2-46 reduce to:

$$\sigma = \sigma_y \quad (2-49)$$

$$d\varepsilon^p = d\varepsilon_1^p \quad (2-50)$$

Thus, when the assumption is made that the yield stress is a function of the total effective plastic strain (called the “strain-hardening hypothesis”), the functional relationship between yield stress and plastic strain can be taken directly from a uniaxial stress-strain curve by virtue of Equations 2-49 and 2-50.

The relationship between the magnitudes of the plastic strain increments and the effective plastic strain increment is provided by the Prandtl-Reuss flow rule:

$$d\varepsilon_i^p + \frac{3}{2} \frac{d\varepsilon_1^p}{\sigma_e} S_i, \quad i = 1, 2, 3 \quad (2-51)$$

Where,

S_i = Deviatoric stress components (in principal coordinates)

Furthermore, the deviatoric stress components, S_i , are defined by:

$$S_i = \sigma_i - \frac{1}{3} (\sigma_1 + \sigma_2 + \sigma_3), \quad i = 1, 2, 3 \quad (2-52)$$

Equation 2-51 embodies the fundamental observation of plastic deformation; that is, plastic strain increments are proportional to the deviatoric stresses. The constant of proportionality is determined by the choice of the yield function. Direct substitution shows that Equations 2-44, 2-46, 2-51, and 2-52 are consistent with one another.

Once the plastic strain increments have been determined for a given load step, the total strains are determined from a generalized form of Hooke's law given by:

$$\varepsilon_1 = \frac{1}{E} (\sigma_1 - \nu (\sigma_2 + \sigma_3)) + \varepsilon_1^p + d\varepsilon_1^p + \int \alpha_1 dt \quad (2-53a)$$

$$\varepsilon_2 = \frac{1}{E} (\sigma_2 - \nu (\sigma_1 + \sigma_3)) + \varepsilon_2^p + d\varepsilon_2^p + \int \alpha_2 dt \quad (2-53b)$$

$$\varepsilon_3 = \frac{1}{E} (\sigma_3 - \nu (\sigma_2 + \sigma_1)) + \varepsilon_3^p + d\varepsilon_3^p + \int \alpha_3 dt \quad (2-53c)$$

Where,

ε_i^p = Total plastic strain components at the end of the previous load increment

E = Modulus of elasticity [Geelhood et al., 2022a]

ν = Poisson's ratio [Geelhood et al., 2022a]

The remaining continuum field equations of equilibrium, strain displacement, and strain compatibility are unchanged. The complete set of governing equations is presented in Table 2-6, written in terms of rectangular Cartesian coordinates and employing the usual indicial notation in which a repeated Latin index implies summation (index notation). This set of equations is augmented by an experimentally determined uniaxial stress-strain relation.

Table 2-6. Summary of FRACAS-I governing equations

Parameter	Governing Equation
Equilibrium	$\sigma_{ji,j} + \rho f_i = 0$
Stress strain	$\varepsilon_{ij} = \frac{1+\nu}{E} \sigma_{ij} - \delta_{ij} \left(\frac{\nu}{E} - \int \alpha dT \right) + \varepsilon_{ij}^p + d\varepsilon_{ij}^p$
Compatibility	$\varepsilon_{ij,kl} + \varepsilon_{kl,ij} - \varepsilon_{ik,jl} - \varepsilon_{jl,ik} = 0$
Definitions used in plasticity	$\sigma_e \triangleq \sqrt{\frac{3}{2} S_{ij} S_{ij}}$ $S_{ij} \triangleq \sigma_{ij} - \frac{1}{3} \sigma_{kk}$
Prandtl-Reuss flow rule	$d\varepsilon_{ij}^p = \frac{3}{2} \frac{d\varepsilon^p}{\sigma_e} S_{ij}$

Where,

σ = Stress tensor

ρ = Mass density

f_i = Components of body force per unit mass

The Method of Solution

When the problem under consideration is statically determinate so that stresses can be found from equilibrium conditions alone, the resulting plastic deformation can be determined directly. However, when the problem is statically indeterminate and the stresses and deformation must be found simultaneously, the full set of plasticity equations proves to be quite formidable, even in the case of simple loadings and geometries.

One numerical procedure which has been used with considerable success is the method of successive substitutions. This method can be applied to any problem for which an elastic solution can be obtained, either in closed form or numerically. A full discussion of this technique, including a number of technologically useful examples, is contained in [Knuutila, 2006].

Briefly, the method involves dividing the loading path into small increments. For example, in the present application, the loads are external pressure, temperature, and either internal pressure or a prescribed displacement of the inside surface of the cladding. These loads all vary during the operating history of the fuel rod. For each new increment of the loading, the solution to all the plasticity equations listed in Table 2-6 is obtained as follows.

First, an initial estimate of the plastic strain increments, $d\varepsilon_{ij}^p$, is made. Based on these values, the equations of equilibrium, Hooke’s law, and strain-displacement and so obtained, the deviatoric stresses, S_{ij} , may be computed. This “pseudo-elastic” solution represents one path in the computational scheme.

Independently, through use of the assumed $d\varepsilon_{ij}^p$ values, the increment of effective plastic strain, $d\varepsilon^p$, may be computed. From this result and the stress-strain curve, a value of the effective stress, σ_e , is obtained from Equation 2-44.

Finally, a new estimate of the plastic strain increments is obtained from the Prandtl-Reuss flow rule:

$$d\varepsilon_{ij}^p = \frac{3}{2} \frac{d\varepsilon^p}{\sigma_e} S_{ij} \tag{2-54}$$

The entire process is continued until the $d\varepsilon_{ij}^p$ converges. A schematic of the iteration scheme is shown in Figure 2-15.

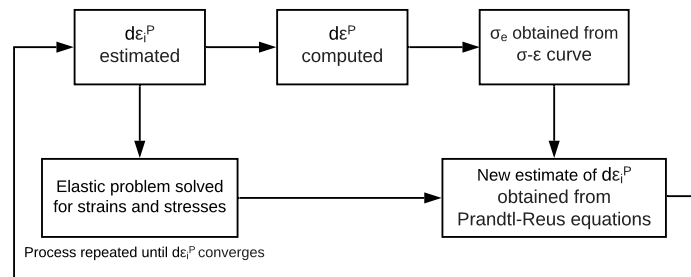


Figure 2-15. Schematic of the method of successive elastic solutions

The mechanism by which improved estimates of $d\varepsilon_{ij}^p$ are obtained results from the fact that the effective stress obtained from $d\varepsilon^p$ and the stress-strain curve will not be equal to the effective stress that would be obtained with the stresses from the elastic solution. The effective stresses will only agree when convergence is obtained.

The question of convergence is one that cannot, in general, be answered *a priori*. However, convergence can be shown to be obtained for sufficiently small load increments. Experience has shown that this technique is suitable for both steady-state and transient fuel rod analyses.

Extension to Creep

The method of solution described for the time-independent plasticity calculations can also be used for time-dependent creep calculations. In this context, the term “creep” refers to any time-dependent constant volume permanent deformation. Creep is a stress-driven process and is usually highly dependent on temperature. The only change required to extend the method of successive elastic solutions to allow consideration of creep is to rewrite the Prandtl-Reuss flow rule, Equation 2-51, as:

$$d\varepsilon_1^c = 1.5 \frac{\dot{\varepsilon} \Delta t}{\sigma_e} S_1 + \frac{\dot{V}^c \Delta t}{9} \frac{(\sigma_1 + \sigma_2 + \sigma_3)}{\sigma_m} \tag{2-55a}$$

$$d\varepsilon_2^c = 1.5 \frac{\dot{\varepsilon} \Delta t}{\sigma_e} S_2 + \frac{\dot{V}^c \Delta t}{9} \frac{(\sigma_1 + \sigma_2 + \sigma_3)}{\sigma_m} \tag{2-55b}$$

$$d\varepsilon_3^c = 1.5 \frac{\dot{\varepsilon} \Delta t}{\sigma_e} S_3 + \frac{\dot{V}^c \Delta t}{9} \frac{(\sigma_1 + \sigma_2 + \sigma_3)}{\sigma_m} \tag{2-55c}$$

Where,

σ_m = Mean stress

The first term on the right-hand side of each of these equations (Equation 2-55) computes the constant volume creep, whereas the second term in each equation computes the permanent change in volume. To use this form of the flow rule, two additional material property correlations must be available. The first is a correlation for constant volume creep, ε^c (taken in a uniaxial test), as a function of stress, time, temperature, and neutron flux, namely:

$$\varepsilon^c = f(\sigma, T, t, \phi) \quad (2-56)$$

Where,

σ = Uniaxial stress, MPa

T = Temperature, K

t = Time, s

ϕ = Neutron flux, n/m²-s

In the FRACAS-I model, the strain hardening hypothesis is assumed, which implies that the strain correlation can be differentiated with respect to time and solved for creep strain rate in the form:

$$\dot{\varepsilon} = h(\sigma, \varepsilon^c, t, T, \phi) \quad (2-57)$$

which is no longer an explicit function of time. The function h is contained in subroutine CREPR, and is described as follows.

A model described by Limbäck and Andersson [Limbäck and Andersson, 1996] of ABB Atom and AB Sandvik Steel, respectively, was selected for cladding irradiation creep in FAST. This model uses a thermal creep model described by [Matsuo, 1987] and an empirical irradiation creep rate with tuned model parameters that were fit to the data set given by [Franklin et al., 1983]. The Limbäck model was further modified by PNNL to use effective stress rather than hoop stress as an input so that the principal stresses could be included and account for the difference in creep behavior during tensile and compressive creep. Several of the fitting coefficients from the Limbäck paper were consequently changed to accommodate this change based on comparisons to several data sets [Franklin et al., 1983] [Soniak et al., 2002] [Gilbon et al., 2000] [Sontheimer and Nissen, 1994]. In addition, a temperature-dependent term was added to the formula for irradiation creep strain rate. This was done because creep data were used with temperature greater than the temperature of the data given by Franklin, and these data along with the Franklin data showed a dependence on temperature. This model has different parameters for stress relief annealed (SRA) and re-crystallized annealed (RXA) cladding types, and provides reasonable creep strains in the

LWR range of temperature and cladding hoop stresses that compare well to data. This model is described below.

The steady-state thermal and irradiation creep rates are given by:

$$\dot{\epsilon}_{th} = A \frac{E}{T} \left(\sinh \frac{a_i \sigma_{eff}}{E} \right)^n \exp \left(\frac{-Q}{RT} \right) \quad (2-58a)$$

$$E = 1.148 \times 10^5 - 59.9 \cdot T \quad (2-58b)$$

$$a_i = 650 \left[1 - 0.56 \left(1 - \exp \left(-1.4 \times 10^{-27} \Phi^{1.3} \right) \right) \right] \quad (2-58c)$$

$$\dot{\epsilon}_{irr} = c_0 \phi^{c_1} \sigma_{eff}^{c_2} f(T) \quad (2-59)$$

Where,

$\dot{\epsilon}_{th}, \dot{\epsilon}_{irr}$ = Thermal and irradiation strain rate, respectively, m/m-hr

A = Constant (see Table 2-7)

E = Young's modulus, MPa

T = Temperature, K

a_i = Fluence term (parameters changed from original Limbäck equation [[Limbäck and Andersson, 1996](#)])

Φ = Fast neutron fluence, n/m²

σ_{eff} = Effective stress, MPa

n = Stress exponent (see Table 2-7)

Q = Activation energy, 201000 J/mol

R = Universal gas constant, 8.314 J/mol-K

c_0 = Constant (see Table 2-7)

ϕ = Fast neutron flux, n/m²-s

c_1 = Flux exponent, 0.85

c_2 = Stress exponent, 1.0

$f(T)$ = Temperature term (see Table 2-7)

A number of variables for the thermal and irradiation strain rates are dependent on the cladding cold work (refer to [Geelhood et al., 2022a]):

Table 2-7. Parameters for FAST-1.1 creep equation for SRA and RXA cladding

Parameter	Values for SRA	Values for RXA	Units
A	1.08×10^9	5.47×10^8	K/MPa-hr
n	2.0	3.5	unitless
c_0	4.0985×10^{-24}	1.87473×10^{-24}	$(n/m^2-s)^{-c_1} MPa^{-c_2}$
$f(T)$ for $T \leq 570$ K	0.7283	0.7994	unitless
$f(T)$ for $570 \text{ K} < T < 625$ K	$-7.0237 + 0.0136 T$	$-3.18562 + 6.99132 \times 10^{-3} T$	unitless
$f(T)$ for $T \geq 625$ K	1.4763	1.1840	unitless

These rates are added together, so:

$$\dot{\epsilon}_{th+irr} = \dot{\epsilon}_{th} + \dot{\epsilon}_{irr} \tag{2-60}$$

The saturated primary hoop strain is given by:

$$\epsilon_p^s = 0.0216 \dot{\epsilon}_{th+irr}^{0.109} (2 - \tanh(35500 \epsilon_{th+irr}))^{-2.05} \tag{2-61}$$

The total thermal strain is given by:

$$\epsilon_H = \epsilon_p^s \left(1 - \exp\left(-52\sqrt{\dot{\epsilon}_{th+irr}t}\right) \right) + \dot{\epsilon}_{th+irr}t \tag{2-62}$$

In FAST, strain rate is used. Taking the derivative with respect to time of the expression above gives:

$$\dot{\epsilon}_H = \frac{26\epsilon_p^s \sqrt{\dot{\epsilon}_{th+irr}}}{\sqrt{t}} \exp\left(-52\sqrt{\dot{\epsilon}_{th+irr}t}\right) + \dot{\epsilon}_{th+irr} \tag{2-63}$$

The first term in Equation 2-63 represents the primary creep. It has been observed that following significant changes in stress or stress reversals, the primary creep is best related to the change in effective stress and the direction of the change in hoop stress [Geelhood, 2013]. In FAST, the first term in Equation 2-63 is calculated based on the time since the last significant stress change (> 5 MPa) using the change in effective stress and in the direction of the change in hoop stress.

The effective stress in the cladding is found using the principal stresses at the mid-wall radius using the thick wall formula as shown in Equations 2-64 to 2-66.

$$\sigma_r = \frac{P_i r_i^2 - P_o r_o^2 + \frac{r_i^2 r_o^2 (P_o - P_i)}{r^2}}{r_o^2 - r_i^2} \quad (2-64)$$

$$\sigma_t = \frac{P_i r_i^2 - P_o r_o^2 - \frac{r_i^2 r_o^2 (P_o - P_i)}{r^2}}{r_o^2 - r_i^2} \quad (2-65)$$

$$\sigma_l = \frac{P_i r_i^2 - P_o r_o^2}{r_o^2 - r_i^2} \quad (2-66)$$

Where,

σ_r = Radial stress, MPa

σ_t = Tangential stress, MPa

σ_l = Longitudinal stress, MPa

P_i = Inner pressure, MPa

P_o = Outer pressure, MPa

r_i = Inner radius, cm

r_o = Outer radius, cm

r = Radius within tube, cm

The effective stress, σ_{eff} , is then given by:

$$\sigma_{eff} = \sqrt{\frac{1}{2} \left((\sigma_l - \sigma_t)^2 + (\sigma_t - \sigma_r)^2 + (\sigma_r - \sigma_l)^2 \right)} \quad (2-67)$$

The correlations above are developed for SRA and RXA Zircaloy-4 and Zircaloy-2. For M5, the correlation for RXA Zircaloy is used. For ZIRLO and Optimized ZIRLO, the correlation for SRA Zircaloy reduced by a factor of 0.8 is used [Sabol et al., 1994].

A plot of the resulting creep is shown as a function of time and effective stress for representative flux and temperature values in Figures 2-16 and 2-17.

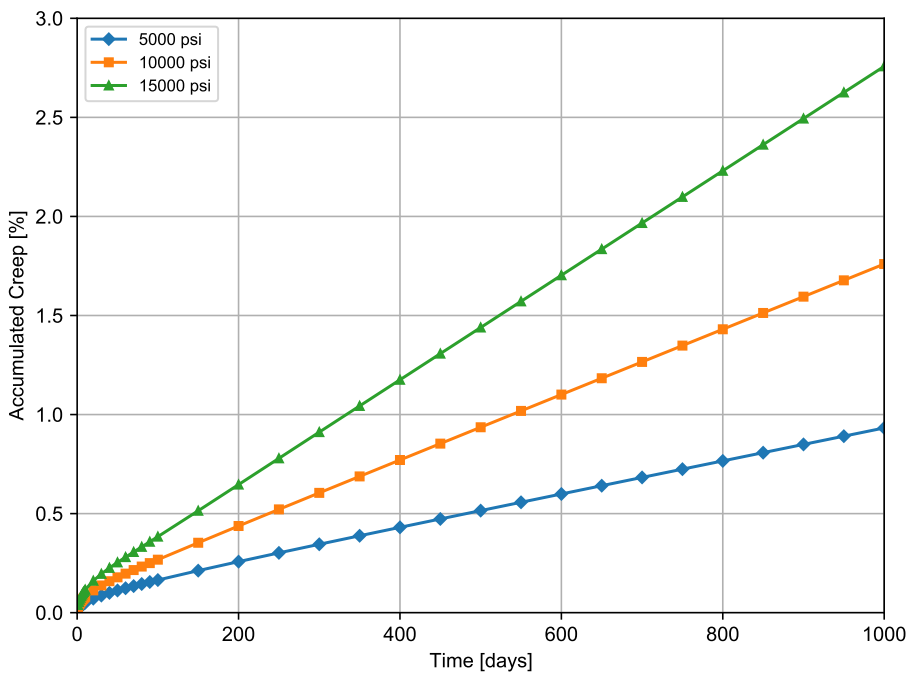


Figure 2-16. Cladding creep as a function of time and hoop stress for 630 °F and $\phi = 1 \times 10^{18} \text{ n/m}^2\text{-s}$ for SRA Zircaloy

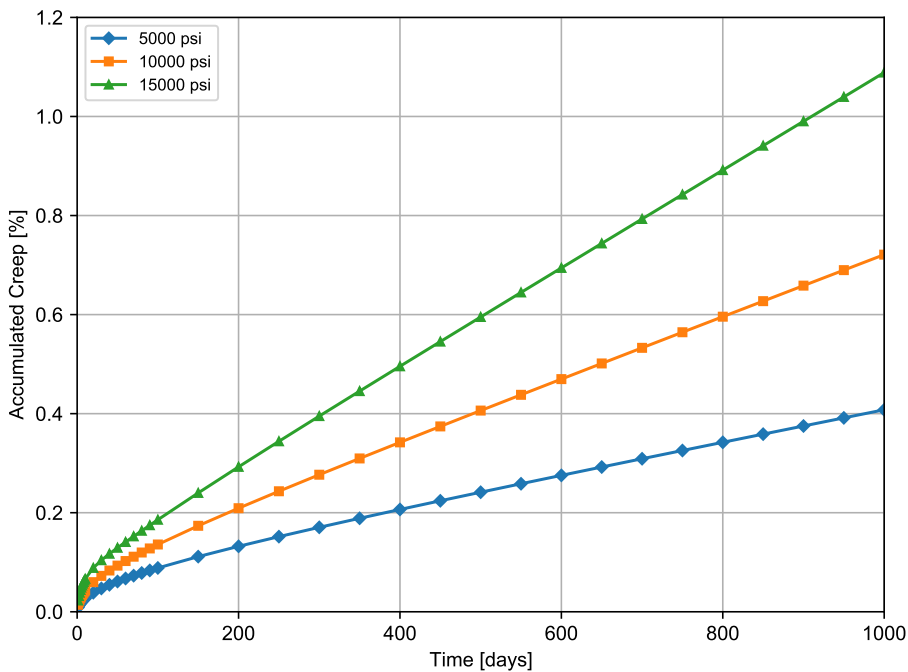


Figure 2-17. Cladding creep as a function of time and hoop stress for 630 °F and $\phi = 1 \times 10^{18} \text{ n/m}^2\text{-s}$ for RXA Zircaloy

The second additional correlation required is a relationship between the rate of permanent volu-

metric strain and the applied loads; that is:

$$\dot{V}^c = g(\sigma_m, T, t, V_{avail}) \quad (2-68)$$

Where,

$\sigma_m = (\sigma_1 + \sigma_2 + \sigma_3)/3 =$ Mean stress, MPa

$T =$ Temperature, K

$t =$ Time, s

$V_{avail} =$ Measure of maximum permanent volumetric change possible

The permanent volumetric strain increment dV_c is related to the creep increments by the equation:

$$dV^c = d\varepsilon_1^c + d\varepsilon_2^c + d\varepsilon_3^c \quad (2-69)$$

As previously noted, the FRACAS-I model is the default model available for analyzing the small deformation of the fuel and cladding. The model considers the fuel pellets to be essentially rigid and to deform due to thermal expansion, swelling, and densification only. Thus, in the rigid pellet model, the displacement of the fuel is calculated independently of the deformation of the cladding. This rigid pellet analysis is performed with the FRACAS-I subcode.

2.5.1.2 Rigid Pellet Cladding Deformation Model

FRACAS-I consists of a cladding deformation model and a fuel deformation model. If the fuel-cladding gap is closed, the fuel deformation model will apply a driving force to the cladding deformation model. The cladding deformation model, however, never influences the fuel deformation model.

The cladding deformation model in FRACAS-I is based on the following assumptions:

- Incremental theory of plasticity
- Prandtl-Reuss flow rule
- Isotropic work-hardening
- Thick wall cladding (thick wall approximation formula is used to calculate stress at midwall)
- If fuel and cladding are in contact, no axial slippage occurs at fuel cladding interface
- Bending strains and stresses in cladding are negligible
- Axisymmetric loading and deformation of cladding

The fuel deformation model in FRACAS-I is based on the following assumptions:

- Thermal expansion, swelling, and densification are the only sources for fuel deformation
- No resistance to expansion of fuel
- No creep deformation of fuel
- Isotropic fuel properties

The cladding and fuel deformation models in FRACAS-I are described below.

Cladding Deformation Model

The rigid pellet cladding deformation subcode (FRACAS-I) consists of four sets of models, each used independently.

Deformation and stresses in the cladding in the open gap regime are computed using a model which considers a thick wall cylindrical shell with specified internal and external pressures and a prescribed uniform temperature.

Calculations for the closed gap regime are made using a model which considers a cylindrical shell with prescribed external pressure and a prescribed radial displacement of the cladding inside surface. The prescribed displacement is obtained from the fuel expansion models (including swelling) described later in this section. Further, since no slippage is assumed when the fuel and cladding are in contact, the axial expansion of the fuel is transmitted directly to the cladding, and hence, the change in axial strain in the shell is also prescribed.

The decision whether the fuel-cladding gap is open or closed is made by considering the relative movement of the cladding inside surface and the fuel outside surface. At the completion of the FRACAS-I analysis, either a new fuel-cladding gap size or a new fuel-cladding interfacial pressure and the elastic-plastic cladding stresses and strains are obtained.

Two additional models are used to compute changes in yield stress with work-hardening, given a uniaxial stress-strain curve. This stress-strain curve is obtained from the updated MATPRO properties. The first model computes the effective total strain and new effective plastic strain, given a value of effective stress and the effective plastic strain at the end of the last loading increment. The second model computes the effective stress, given an increment of plastic strain and the effective plastic strain at the end of the last loading increment. Depending on the work-hardened value of yield stress, loading can be either elastic or plastic, and unloading is constrained to occur elastically. (Isotropic work-hardening is assumed in these calculations.) These four sets of models are described below.

The determination of whether or not the fuel is in contact with the cladding is made by comparing the radial displacement (delta change) of the fuel surface (u_r^{fuel}) with the radial displacement (delta change) that would occur in the cladding (u_r^{clad}) due to the prescribed external (coolant) pressure and the prescribed internal (fission and fill gas) pressure. The free radial displacement of the

cladding is obtained using Equation 2-53. The following expression is used to determine if fuel-cladding contact has occurred:

$$u_r^{fuel} \geq u_r^{clad} + \delta \quad (2-70)$$

Where,

δ = As-fabricated fuel-cladding gap size, m

If Equation 2-70 is satisfied, the fuel is in contact with the cladding. The loading history enters into this decision by virtue of the permanent plastic cladding strains which are applied to the as-fabricated geometry. These plastic strains, and total effective plastic strain, ϵ^P , are retained for use in subsequent calculations.

If the fuel and cladding displacements are such that Equation 2-70 is not satisfied, the fuel-cladding gap has not closed during the current step and the solution obtained by the open gap solution is appropriate. The current value of the fuel-cladding gap size is then computed and is used in the temperature calculations. The plastic strain values may be changed in the solution if additional plastic straining has occurred.

If Equation 2-70 is satisfied, however, fuel and cladding contact has occurred during the current loading increment. At the contact interface, radial continuity requires that:

$$u_r^{clad} = u_r^{fuel} - \delta \quad (2-71)$$

while in the axial direction the assumption is made that no slippage occurs between the fuel and the cladding. This state is referred to as “lockup.”

Note that only the additional strain which occurs in the fuel after lockup has occurred is transferred to the cladding. Thus, if $\epsilon_{z,0}^{clad}$ is the axial strain in the cladding just prior to contact, and $\epsilon_{z,0}^{fuel}$ is the corresponding axial strain in the fuel, then the no-slippage condition in the axial direction becomes:

$$\epsilon_z^{clad} - \epsilon_{z,0}^{clad} = \epsilon_z^{fuel} - \epsilon_{z,0}^{fuel} \quad (2-72)$$

The values of the “prestrains”, $\epsilon_{z,0}^{fuel}$ and $\epsilon_{z,0}^{clad}$, are set equal to the values of the strains that existed in the fuel and cladding at the time of fuel-cladding gap closure and are stored and used in the cladding sequence of calculations. The values are updated at the end of any load increment during which the fuel-cladding gap is closed.

After u_r^{clad} and ϵ_z^{clad} have been computed, they are used in a calculation which considers a cylindrical shell with prescribed axial strain, external pressure, and prescribed radial displacement of the inside surface. After the solution is obtained, a value of the fuel-cladding interfacial pressure is computed along with new plastic strains and stresses.

The open gap modeling considers a cylindrical shell loaded by both internal and external pressures. Axisymmetric loading and deformation are assumed. Loading is also restricted to being uniform in the axial direction and no bending is considered. The geometry and coordinates are shown in Figure 2-18. The displacements of the midplane of the shell are u and w in the radial and axial directions, respectively.

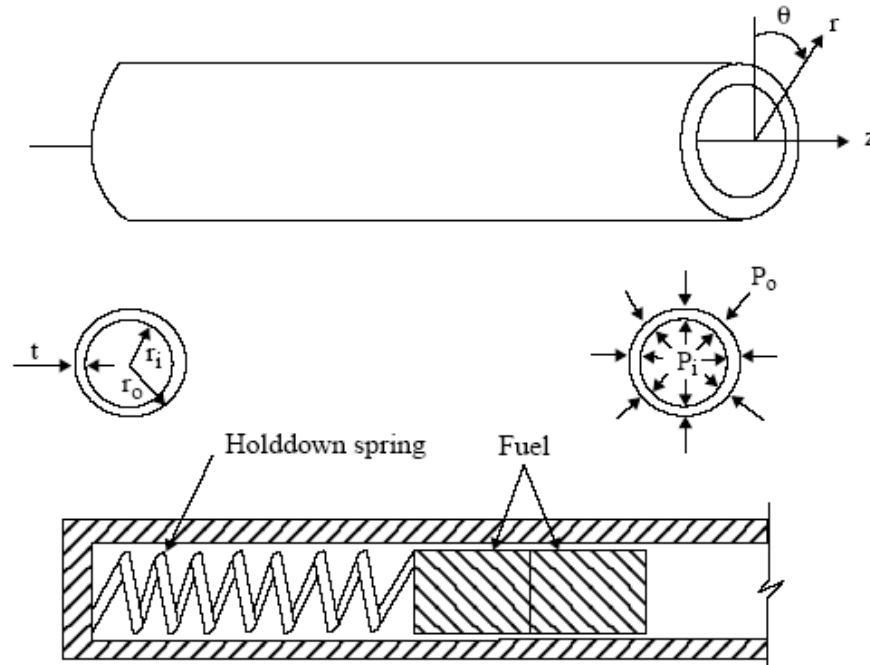


Figure 2-18. Fuel rod geometry and coordinates

For this case, the equilibrium equations are identically satisfied by the thick wall approximation below.

$$\sigma_{\theta} = \frac{r_i P_i - r_o P_o}{t} \quad (2-73)$$

$$\sigma_z = \frac{r_i^2 P_i - r_o^2 P_o}{r_o^2 - r_i^2} \quad (2-74)$$

Where,

σ_{θ} = Hoop stress, MPa

σ_z = Axial stress, MPa

r_i = Inside radius of cladding, m

r_o = Outside radius of cladding, m

P_i = Fuel rod internal gas pressure, MPa

P_o = Coolant pressure, MPa

t = Cladding thickness, m

For membrane shell theory, the strains are related to the midplane displacements by:

$$\varepsilon_\theta = \frac{u}{\bar{r}} \quad (2-75)$$

$$\varepsilon_z = \frac{\partial w}{\partial z} \quad (2-76)$$

Where,

\bar{r} = Radius of the midplane

Strain across the thickness of the shell is allowed. In shell theory, since the radial stress can be neglected, and since the hoop stress, σ_θ , and axial stress, σ_z , are uniform across the thickness when bending is not considered, the radial strain is due only to the Poisson effect and is uniform across the thickness. (Normally, radial strains are not considered in a shell theory, but plastic radial strains must be included when plastic deformations are considered.)

The stress-strain relations are written in incremental form as:

$$\varepsilon_\theta = \frac{1}{E} (\sigma_\theta - \nu\sigma_z) + \varepsilon_\theta^P + d\varepsilon_\theta^P + \int_{T_0}^T \alpha_\theta dT \quad (2-77)$$

$$\varepsilon_z = \frac{1}{E} (\sigma_z - \nu\sigma_\theta) + \varepsilon_z^P + d\varepsilon_z^P + \int_{T_0}^T \alpha_z dT \quad (2-78)$$

$$\varepsilon_r = -\frac{\nu}{E} (\sigma_\theta - \nu\sigma_z) + \varepsilon_r^P + d\varepsilon_r^P + \int_{T_0}^T \alpha_r dT \quad (2-79)$$

Where,

t_o = Strain-free reference temperature, K

α = Coefficient of thermal expansion

t = Current average cladding temperature, K

E = Modulus of elasticity

ν = Poisson's ratio

The terms ε_{θ}^P , ε_z^P , and ε_r^P are the plastic strains at the end of the last load increment, and $d\varepsilon_{\theta}^P$, $d\varepsilon_z^P$, and $d\varepsilon_r^P$ are the additional plastic strain increments which occur due to the new load increment.

The magnitude of the additional plastic strain increments is determined by the effective stress and the Prandtl-Reuss flow rule, expressed as:

$$\sigma_e = \frac{1}{\sqrt{2}} \left[(\sigma_{\theta} - \sigma_z)^2 + (\sigma_z)^2 + (\sigma_{\theta})^2 \right]^{\frac{1}{2}} \quad (2-80)$$

$$d\varepsilon_i^P = \frac{3}{2} \frac{d\varepsilon^P}{\sigma_e} S_i \quad \text{for } i = r, \theta, z \quad (2-81)$$

$$S_i = \sigma_i - \frac{1}{3} (\sigma_{\theta} + \sigma_z) \quad \text{for } i = r, \theta, z \quad (2-82)$$

The solution of the open gap case proceeds as follows. At the end of the last load increment the plastic strain components, ε_{θ}^P , ε_z^P and ε_r^P are known. Also the total effective plastic strain, ε^P , is known.

The loading is now incremented with the prescribed values of P_i , P_o , and T . The new stresses can be determined from Equation 2-73 and Equation 2-74, and a new value of effective stress is obtained from Equation 2-80.

The increment of effective plastic strain, $d\varepsilon^P$, which results from the current increment of loading, can now be determined from the uniaxial stress-strain curve at the new value of σ_e , as shown in Figure 2-19. (The new elastic loading curve depends on the value of ε_{old}^P .)

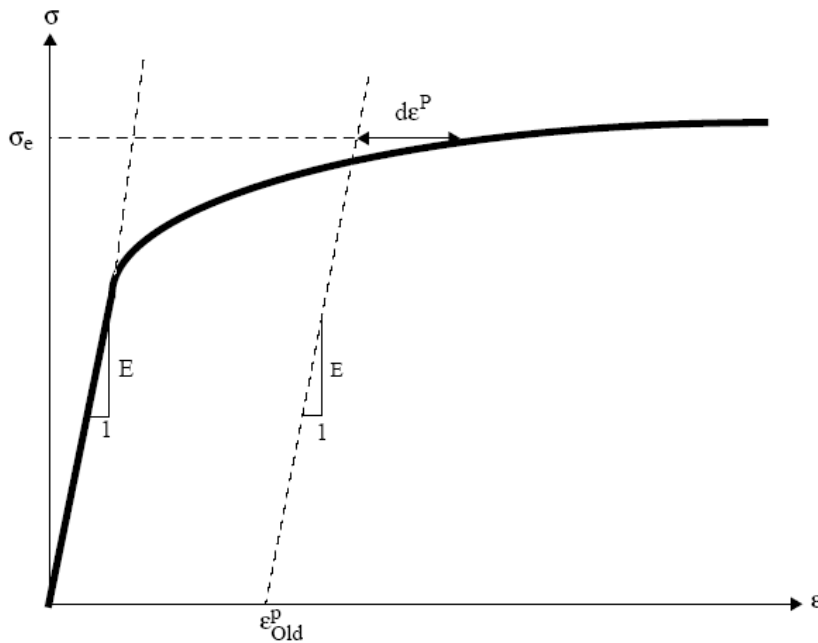


Figure 2-19. Calculation of effective stress σ_e from $d\epsilon^P$

Once $d\epsilon^P$ is determined, the individual plastic strain components are found from Equation 2-81, and the total strain components are obtained from Equations 2-77 through 2-79.

The displacement of the inside surface of the shell must be determined so that a new fuel-cladding gap width can be computed. The radial displacement of the inside surface is given by:

$$u(r_i) = \bar{r}\epsilon\theta - \frac{t}{2}\epsilon r \tag{2-83}$$

where the first term is the radial displacement of the midplane (from Equation 2-75) and ϵ_r is the uniform strain across the cladding thickness, t .

The cladding thickness is computed by the equation:

$$t = (1 + \epsilon_r) t_o \tag{2-84}$$

Where,

t_o = As-fabricated, unstressed thickness

The final step performed is to add the plastic strain increments to the previous plastic strain values; that is:

$$(\varepsilon_{\theta}^P)_{new} = (\varepsilon_{\theta}^P)_{old} + d\varepsilon_{\theta}^P \quad (2-85a)$$

$$(\varepsilon_z^P)_{new} = (\varepsilon_z^P)_{old} + d\varepsilon_z^P \quad (2-85b)$$

$$(\varepsilon_r^P)_{new} = (\varepsilon_r^P)_{old} + d\varepsilon_r^P \quad (2-85c)$$

$$(\varepsilon^P)_{new} = (\varepsilon^P)_{old} + d\varepsilon_r^P \quad (2-85d)$$

These values are used for the next load increment.

Thus, all the stresses and strains can be computed directly, since in this case the stresses are determinate. In the case of the fuel-driven cladding displacement, the stresses depend on the displacement, and such a straightforward solution is not possible.

The closed gap modeling considers the problem of a cylindrical shell for which the radial displacement of the inside surface and axial strain are prescribed. Here the stresses cannot be computed directly since the pressure at the inside surface (the fuel-cladding interfacial pressure) must be determined as part of the solution.

As in the open gap modeling, the displacement at the inside surface is given by:

$$u(r_i) = u - \frac{t}{2}\varepsilon_r \quad (2-86)$$

Where,

u = radial displacement of the midplane

From Equation 2-75, $u = r\varepsilon_{\theta}$ and:

$$u(r_i) = \bar{r}\varepsilon_{\theta} - \frac{t}{2}\varepsilon_r \quad (2-87)$$

Thus, prescribing the displacement of the inside surface of the shell is equivalent to a constraining relation between ε_{θ} and ε_r . As before, Hooke's law is taken in the form:

$$\varepsilon_{\theta} = \frac{1}{E} (\sigma_{\theta} - \nu\sigma_z) + \varepsilon_z^P + d\varepsilon_z^P + \int_{T_0}^T \alpha_z dT \quad (2-88)$$

$$\varepsilon_z = \frac{1}{E} (\sigma_z - \nu \sigma_\theta) + \varepsilon_z^P + d\varepsilon_z^P + \int_{T_0}^T \alpha_z dT \quad (2-89)$$

$$\varepsilon_r = -\frac{\nu}{E} (\sigma_\theta - \sigma_z) + \varepsilon_r^P + d\varepsilon_r^P + \int_{T_0}^T \alpha_r dT \quad (2-90)$$

Use of Equations 2-87 and 2-90 in Equation 2-88 results in a relation between the stresses σ_θ and σ_z , and the prescribed displacement $u(r_i)$:

$$\begin{aligned} \frac{u(r_i)}{\bar{r}} + \frac{1}{2} \frac{1}{2\bar{r}} \left[\varepsilon_r^P + d\varepsilon_r^P + \int_{T_0}^T \alpha dT \right] - \left[\varepsilon_\theta^P + d\varepsilon_\theta^P + \int_{T_0}^T \alpha dT \right] = \\ \frac{1}{E} \left[\left(1 + \frac{\nu t}{2\bar{r}} \right) \sigma_\theta + \nu \left(\frac{t}{2\bar{r}} - 1 \right) \sigma_z \right] \end{aligned} \quad (2-91)$$

Equations 2-89 and 2-91 are now a pair of simultaneous algebraic equations for the stresses σ_θ and σ_z , which may be written as:

$$\begin{bmatrix} A_{11} & A_{12} \\ A_{21} & A_{22} \end{bmatrix} \begin{bmatrix} \sigma_\theta \\ \sigma_z \end{bmatrix} = \begin{bmatrix} B_1 \\ B_2 \end{bmatrix} \quad (2-92)$$

Where,

$$A_{11} = 1 + \frac{\nu t}{2\bar{r}}$$

$$A_{12} = \nu \left(\frac{t}{2\bar{r}} - 1 \right)$$

$$A_{21} = -\nu$$

$$A_{22} = 1$$

$$B_1 = \left(E \frac{u(r_i)}{\bar{r}} + \frac{Et}{4\bar{r}} \left[\varepsilon_r^P + d\varepsilon_r^P + \int_{T_0}^T \alpha dT \right] \right) - E \left[\varepsilon_\theta^P + d\varepsilon_\theta^P + \int_{T_0}^T \alpha dT \right]$$

$$B_2 = E \left(\varepsilon_z - E\varepsilon_z^P + d\varepsilon_z^P + \int_{T_0}^T \alpha dT \right)$$

Then the stresses can be written explicitly as:

$$\sigma_\theta = \frac{B_1 A_{22} - B_2 A_{12}}{A_{11} A_{22} - A_{12} A_{21}} \quad (2-93)$$

$$\sigma_z = \frac{B_2 A_{11} - B_1 A_{12}}{A_{11} A_{22} - A_{12} A_{21}} \quad (2-94)$$

These equations relate the stresses to $u(r_i)$ and ε_z , which are prescribed, and to $d\varepsilon_\theta^P$, $d\varepsilon_z^P$, and $d\varepsilon_r^P$, which are to be determined. The remaining equations which must be satisfied are:

$$\sigma_e = \frac{1}{\sqrt{2}} [(\sigma_\theta - \sigma_z)^2 + (\sigma_z)^2 + (\sigma_\theta)^2]^{\frac{1}{2}} \quad (2-95)$$

$$d\varepsilon^P = \frac{\sqrt{2}}{3} [(d\varepsilon_r^P - d\varepsilon_\theta^P)^2 + (d\varepsilon_\theta^P - d\varepsilon_z^P)^2 + (d\varepsilon_z^P - d\varepsilon_r^P)^2]^{\frac{1}{2}} \quad (2-96)$$

and the Prandtl-Reuss flow equations (defined in Equation 2-81):

$$d\varepsilon_\theta^P = \frac{3}{2} \frac{d\varepsilon^P}{\sigma_e} \left[\sigma_\theta - \frac{1}{3}(\sigma_\theta + \sigma_z) \right] \quad (2-97)$$

$$d\varepsilon_z^P = \frac{3}{2} \frac{d\varepsilon^P}{\sigma_e} \left[\sigma_z - \frac{1}{3}(\sigma_\theta + \sigma_z) \right] \quad (2-98)$$

$$d\varepsilon_r^P = -d\varepsilon_\theta^P - d\varepsilon_z^P \quad (2-99)$$

The effective stress, σ_e , and the plastic strain increment, $d\varepsilon^P$, must, of course, be related by the uniaxial stress-strain law. Equations 2-93 through 2-99 must be simultaneously satisfied for each loading increment.

As discussed in Section 2.5.1.1, a straightforward numerical solution to these equations can be obtained using the method of successive elastic solutions. By this method, arbitrary values are initially assumed for the increments of plastic strain, and Equations 2-93 through 2-99 are used to obtain improved estimates of the plastic strain components. The following steps are performed for each increment of load:

1. Values of $d\varepsilon_\theta^P$, $d\varepsilon_z^P$, and $d\varepsilon_r^P$ are assumed. Then, $d\varepsilon^P$ is computed from Equation 2-96 and the effective stress is obtained from the stress-strain curve at the value of $d\varepsilon^P$.
2. From Hooke's law, still using the assumed plastic strain increments and the prescribed values of $u(r_i)$ and ε_z , values for the stresses can be obtained from Equations 2-93 and 2-94.
3. New values for $d\varepsilon_\theta^P$, $d\varepsilon_z^P$, and $d\varepsilon_r^P$ are now computed from the Prandtl-Reuss relations:

$$d\varepsilon_i^P = \frac{3}{2} \frac{d\varepsilon^P}{\sigma_e} \left[\sigma_i - \frac{1}{3}(\sigma_\theta + \sigma_z) \right] \text{ for } i = r, \theta, z \quad (2-100)$$

4. The old and new values of $d\varepsilon_\theta^p$, $d\varepsilon_z^p$, and $d\varepsilon_r^p$ are compared and the process continued until convergence is obtained.
5. Once convergence has been obtained, the fuel-cladding interfacial pressure is computed from the following thick wall approximation equation:

$$P_{int} = \frac{t\sigma_\theta + r_o P_o}{r_i} \quad (2-101)$$

When Steps 1 through 5 have been accomplished, the solution is complete, provided that the fuel-cladding interface pressure is not less than the local gas pressure.

However, due to unequal amounts of plastic straining in the hoop and axial directions upon unloading, the fuel-cladding interfacial pressure as obtained in step 5 is often less than the gas pressure even though the fuel-cladding gap has not opened. When this situation occurs, the frictional “locking” (which is assumed to constrain the cladding axial deformation to equal the fuel axial deformation) no longer exists. The axial strain and stress adjust themselves so that the fuel-cladding interfacial pressure equals the gas pressure, at which point the axial strain is again “locked.” Thus, upon further unloading, the axial strain and the hoop and axial stresses continually readjust themselves to maintain the fuel-cladding interfacial pressure equal to the gas pressure until the fuel-cladding gap opens. Since the unloading occurs elastically, a solution for this portion of the fuel-cladding interaction problem can be obtained directly as discussed below.

Since the external pressure and the fuel-cladding interfacial pressure are known, the hoop stress is obtained from Equation 2-101 as:

$$\sigma_\theta = \frac{r_i P_{int} - r_o P_o}{t} \quad (2-102)$$

From Equation 2-87, the following expression can be written:

$$\varepsilon_\theta = \frac{u_r^{fuel} - \delta + \frac{t}{2}\varepsilon}{\bar{r}} \quad (2-103)$$

Substitution of ε_θ and ε_r , as given by Equations 2-88 and 2-90, into Equation 2-103 results in an explicit equation for σ_z :

$$\nu r_i \sigma_z = \left(r + \nu \frac{t}{2} \right) \sigma_\theta + rE \left(\int \alpha dT + d\varepsilon_\theta^p \right) - \frac{t}{2} E \left(\int \alpha dT + d\varepsilon_r^p \right) - Eu(r_i) \quad (2-104)$$

in which σ_θ is known from Equation 2-102. With σ_z and σ_θ known, the strains may be computed from Hooke’s law, Equations 2-88 through 2-90. This set of equations is automatically invoked whenever P_{int} is computed to be less than the local gas pressure.

As in the open gap modeling, the last step is to set the plastic strain components and total effective strain equal to their new values by adding in the computed increments $d\varepsilon_i^p$ and $d\varepsilon^p$.

The stress-strain modeling is used to relate stress and plastic strain, taking into consideration the direction of loading and the previous plastic deformation. A typical stress-strain curve is shown in Figure 2-20. This curve presents the results of a uniaxial stress-strain experiment and may be interpreted beyond initial yield as the focus of work-hardened yield stresses. The equation of the curve is provided by the updated MATPRO properties at each temperature given in Section 2.5.1.3.

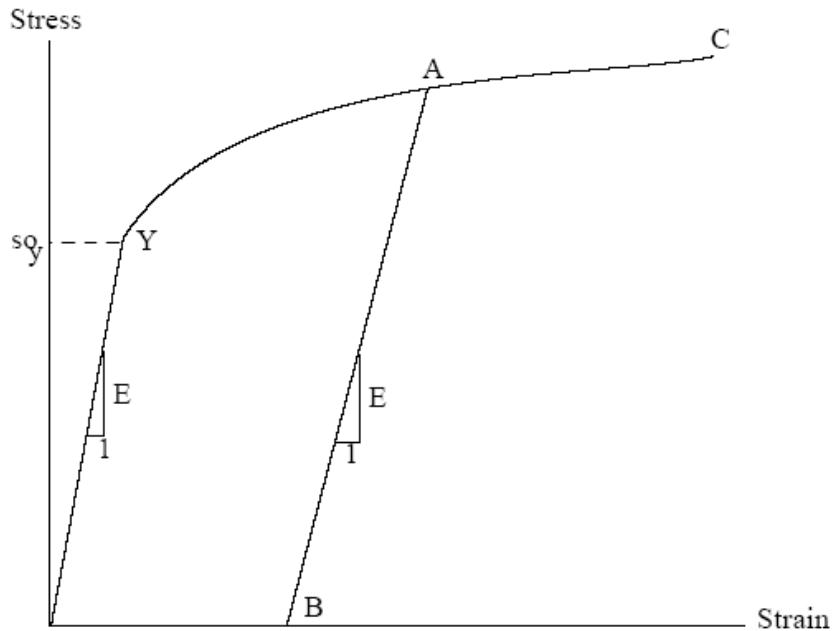


Figure 2-20. Idealized stress-strain behavior

To use this information, the usual idealization of the mechanical behavior of metals is made. Thus, linear elastic behavior is assumed until a sharply defined yield stress is reached, after which plastic (irrecoverable) deformation occurs. Unloading from a stress state beyond the initial yield stress, σ_y^o , is assumed to occur along a straight line having the elastic modulus for its slope. When the (uniaxial) stress is removed completely, a residual plastic strain remains, and this completely determines the subsequent yield stress. That is, when the specimen is loaded again, loading will occur along line BA in Figure 2-20 and no additional deformation will occur until point A is again reached. Point A is the subsequent yield stress. If $\sigma = f(\epsilon)$ is the equation of the plastic portion of the stress-strain curve (YAC), then for a given value of plastic strain, the subsequent yield stress is found by simultaneously solving the pair of equations.

$$\sigma = f(\epsilon) \tag{2-105a}$$

$$\sigma = E(\epsilon - \epsilon^P) \tag{2-105b}$$

Which may be written as:

$$\sigma = f\left(\frac{\sigma}{E} + \varepsilon^P\right) \quad (2-106)$$

This nonlinear equation may be solved efficiently by using an iteration scheme:

$$\sigma^{m+1} = f\left(\frac{\sigma^m}{E} + \varepsilon^P\right) \text{ for } m = 0, 1, 2, \dots \quad (2-107)$$

The initial iterate, σ^m , is arbitrary, and without loss of generality, is taken as 34.5 MPa. For any monotonically, increasing stress-plastic strain relation, the iteration scheme in Equation 2-107 will converge uniformly and absolutely.

The computations of the stress-strain modeling are described below. The first computes strain as a function of plastic strain, temperature, and stress. The second computes stress as a function of plastic strain, temperature, and plastic strain increments.

Values of plastic strain, ε^P , temperature, and stress are used as follows:

1. For a given temperature, $\sigma = f(\varepsilon)$ is obtained from the updated MATPRO properties given in Section 2.5.1.3.
2. The yield stress σ_y for given ε^P is obtained from Equation 2-107.
3. For a given value of stress, σ ,

- if $\sigma \leq \sigma_y$

$$\begin{aligned} \varepsilon &= \frac{\sigma}{E} + \varepsilon^P \\ \varepsilon_{new}^P &= \varepsilon_{old}^P \end{aligned} \quad (2-108)$$

- if $\sigma > \sigma_y$

$$\begin{aligned} \varepsilon &= f(\sigma) \\ \varepsilon_{new}^P &= \varepsilon - \frac{\sigma}{E} \\ d\varepsilon^P &= \varepsilon_{new}^P - \varepsilon_{old}^P \end{aligned} \quad (2-109)$$

Where E is computed using the correlation in the material properties handbook [Luscher and Geelhood, 2014].

Values of plastic strain, ε^P , temperature, and plastic strain increment, $d\varepsilon^P$, are used as follows:

1. For a given temperature, $\sigma = f(\varepsilon)$ is obtained from the updated MATPRO properties given in Section 2.5.1.3.
2. The yield stress σ_y for given ε^P is obtained from Equation 2-107.
3. Given $d\varepsilon^P$: see Equation 2-110 and Figure 2-21.

$$\varepsilon_{new}^P = \varepsilon_{old}^P + d\varepsilon^P \tag{2-110}$$

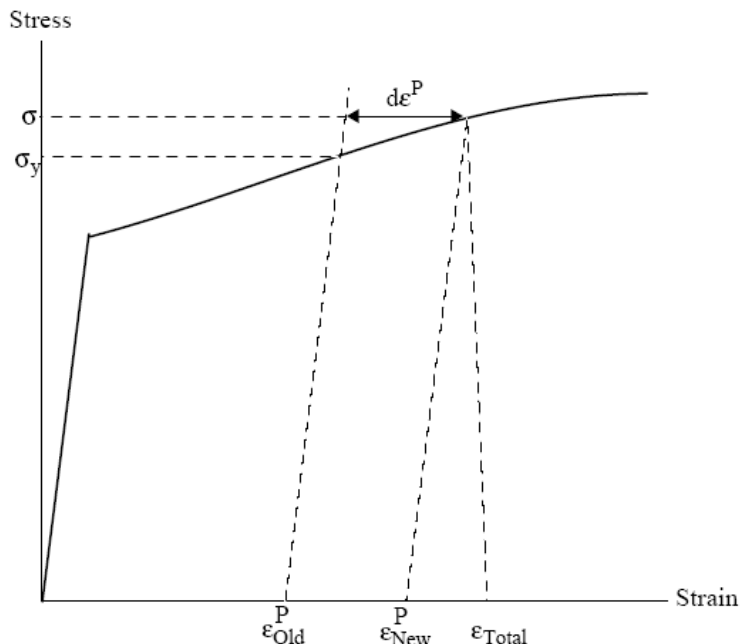


Figure 2-21. Computing stress

Since $d\varepsilon^P > 0$, the new value of stress and strain must lie on the plastic portion of the stress-strain curve $\sigma = f(\varepsilon)$. So, σ and ε are obtained by performing a simultaneous solution, as before.

2.5.1.3 Updated MATPRO Cladding Mechanical Properties Models

The mechanical properties of fuel rod Zircaloy cladding are known to change with irradiation because of damage induced from the fast neutron fluence. The changes are similar to cold-working the material because dislocation tangles are created that tend to both strengthen and harden the cladding while decreasing the ductility. In addition to the fast fluence effects, the presence of excess hydrogen in the form of hydrides in the Zircaloy may also affect the mechanical properties.

Three MATPRO models have been modified to account for the high fast neutron fluence levels, temperature, and strain rate. Those models are a) the strength coefficient in CKMN, b) the strain hardening exponent in CKMN, and c) the strain rate exponent in CKMN.

Strength Coefficient, K

The strength coefficient, K , has been modified from MATPRO and is a function of temperature, fast neutron fluence, cold work, and alloy composition. The strength coefficient has not been found to be a function of hydrogen concentration. The fluence dependency, $K(\Phi)$, has been modified from MATPRO to better fit the high burnup data. The models for the strength coefficients of Zircaloy-2 and Zircaloy-4 are given below.

$$K = \frac{K(T) \cdot (1 + K(CW) + K(\Phi))}{K(Zry)} \quad (2-111)$$

Where,

$$K(T) = \begin{cases} 1.17628 \times 10^9 + 4.54859 \times 10^5 \cdot T - 3.28185 \times 10^3 \cdot T^2, & T < 750 \text{ K} \\ 2.522488 \times 10^6 \exp\left(\frac{2.850027 \times 10^6}{T^2}\right), & 750 \text{ K} < T < 1090 \text{ K} \\ 1.841376039 \times 10^8 - 1.434544 \times 10^5 \cdot T, & 1090 \text{ K} < T < 1255 \text{ K} \\ 4.330 \times 10^7 - 6.685 \times 10^4 \cdot T + 3.7579 \times 10^1 \cdot T^2 - 7.33 \times 10^{-3} \cdot T^3, & 1255 \text{ K} < T < 2100 \text{ K} \end{cases} \quad (2-112)$$

$$K(CW) = 0.546CW \quad (2-113)$$

$$K(\Phi) = \begin{cases} (0.1464 + 1.464 \times 10^{-25}\Phi)f(CW, T), & \Phi < 0.1 \times 10^{25} \text{ n/m}^2 \\ 2.928 \times 10^{-26}\Phi, & 0.1 \times 10^{25} \text{ n/m}^2 < \Phi < 2 \times 10^{25} \text{ n/m}^2 \\ 0.53236 + 2.6618 \times 10^{-27}\Phi, & 2 \times 10^{25} \text{ n/m}^2 < \Phi < 12 \times 10^{25} \text{ n/m}^2 \end{cases} \quad (2-114)$$

$$f(CW, T) = 2.25 \exp(-20CW) \min \left[1, \exp\left(\frac{T - 550}{10}\right) \right] + 1 \quad (2-115)$$

Where,

$K(Zry) = 1.305$ for Zircaloy-2; 1 for Zircaloy-4

T = Temperature, K

CW = Cold work (valid from 0 to 0.75), unitless

Φ = Fast neutron fluence, n/m^2 ($E > 1 \text{ MeV}$)

The effective cold work and fast neutron fluence used to calculate the strength coefficient, K , can be reduced by annealing if the time and/or temperature are high enough. FAST uses the MATPRO model, CANEAL, to calculate the effective cold work and fast neutron fluence at each time step using the following equations.

$$CW_i = CW_{i-1} \exp \left[-1.504 (1.504(1 + 2.2 \times 10^{-25} \Phi_{i-1}) t \exp \left(\frac{-2.33 \times 10^{18}}{T^6} \right)) \right] \quad (2-116)$$

$$\Phi_i = \frac{1 \times 10^{20}}{2.49 \times 10^{-6} t \exp \left(\frac{-5.35 \times 10^{23}}{T^8} \right) + \frac{10^{20}}{\Phi_{i-1}}} \quad (2-117)$$

Where,

CW_{i-1} , and CW_i = Effective cold work for strength coefficient at the start and end of the time step, respectively, unitless

Φ_i , and Φ_{i-1} = Effective fast neutron fluence for strength coefficient at the start and end of the time step, respectively, n/m²

t = Time step size, s

T = Cladding temperature, K

Strain-Hardening Exponent, n

The strain-hardening exponent, n , has been modified from MATPRO to better fit the high burnup data and is a function of temperature, fast neutron fluence, and alloy composition. The strain hardening exponent has not been found to be a function of hydrogen concentration. The models for the strain hardening exponents of Zircaloy-2 and Zircaloy-4 are given below.

$$n = \frac{n(T)n(\Phi)}{n(Zry)} \quad (2-118)$$

Where,

$$n(T) = \begin{cases} 0.11405, & T < 419.4 \text{ K} \\ -9.490 \times 10^{-2} + 1.165 \times 10^{-3}T & 419.4 \text{ K} < T < 1099.0772 \text{ K} \\ -1.992 \times 10^{-6}T^2 + 9.588 \times 10^{-10}T^3, & \\ -0.22655119 + 2.5 \times 10^{-4}T, & 1099.0772 \text{ K} < T < 1600 \text{ K} \\ 0.17344880, & T > 1600 \text{ K} \end{cases} \quad (2-119)$$

$$n(\Phi) = \begin{cases} 1.321 + 0.48 \times 10^{-25}\Phi, & \Phi < 0.1 \times 10^{25} \text{ n/m}^2 \\ 1.369 + 0.096 \times 10^{-25}\Phi, & 0.1 \times 10^{25} \text{ n/m}^2 < \Phi < 2 \times 10^{25} \text{ n/m}^2 \\ 1.5435 + 0.008727 \times 10^{-25}\Phi, & 2 \times 10^{25} \text{ n/m}^2 < \Phi < 7.5 \times 10^{25} \text{ n/m}^2 \\ 1.608953, & \Phi > 7.5 \times 10^{25} \text{ n/m}^2 \end{cases} \quad (2-120)$$

and,

$n(Zry) = 1.0$ for Zircaloy-4; 1.6 for Zircaloy-2

T = Temperature, K

Φ = Fast neutron fluence ($E > 1$ MeV), n/m^2

The effective fast neutron fluence used to calculate the strain-hardening exponent, n , can be reduced by annealing if the time or temperature, or both, are high enough. FAST uses the MATPRO model, CANEAL, to calculate the effective fast neutron fluence at each time step using the following equation.

$$\Phi = \frac{1 \times 10^{20}}{2.49 \times 10^{-6} t \exp\left(\frac{-5.35 \times 10^{23}}{T^8}\right) + \frac{1 \times 10^{20}}{\Phi_{i-1}}} \quad (2-121)$$

Where,

Φ_i , and Φ_{i-1} = Effective fast neutron fluence for strain hardening exponent at the start and end of the time step, respectively, n/m^2

t = Time step size, s

T = Cladding temperature, K

Strain Rate Exponent

The strain rate exponent, m , has been modified from MATPRO to better fit the high burnup data and is given by a function of temperature only as described in the equation below.

$$m = \begin{cases} 0.015, & T < 750 \text{ K} \\ 7.458 \times 10^{-4} T - 0.544338, & 750 \text{ K} < T < 800 \text{ K} \\ 3.24124 \times 10^{-4} T - 0.20701, & T > 800 \text{ K} \end{cases} \quad (2-122)$$

Where,

m = Strain rate exponent

T = Temperature, K

The impact of the strain rate exponent on yield stress is to increase the yield strength with increasing strain rate, but the effect is not large. For example, increasing the strain rate from $1 \times 10^{-4} \text{ s}^{-1}$ to 1.0 s^{-1} will increase the yield strength by about 15% .

Assembled Model

Tensile strength, yield strength, and strain are calculated using the same relationships in MATPRO's CMLIMIT subroutine with slight modifications. The true ultimate strength is calculated using:

$$\sigma = K \left(\frac{\dot{\epsilon}}{1 \times 10^{-3}} \right)^m \epsilon_{p+e}^n \quad (2-123)$$

Where,

σ = True ultimate strength, MPa

K = Strength coefficient, MPa

$\dot{\epsilon}$ = Strain rate, unitless

m = Strain rate sensitivity constant from MATPRO, unitless

ϵ_{p+e} = True strain at maximum load, unitless

n = Strain hardening exponent, unitless

This is a change in the original MATPRO model in that the true strain at maximum load in the original model was set equal to the strain hardening exponent. This change was made to better fit the ultimate tensile strength data.

The CMLIMIT subroutine equations predicting true yield strength and true strain at yield remain unchanged.

This model is applicable over the following ranges with an uncertainty (standard deviation) on yield and tensile strength of approximately 17% relative.

- Cladding temperature: 560 to 700 K
- Oxide corrosion thickness: 0 to 100 μm
- Excess hydrogen level: 0 to 650 ppm
- Strain rate: 1×10^{-4} to 1×10^{-5} 1/s
- Fast neutron fluence: 0 to 12×10^{25} n/m²
- Zircaloy: cold work and stress relieved

A plot of predicted vs. measured yield stress is shown in Figure 2-22. Further data comparisons are shown in [Geelhood et al., 2008].

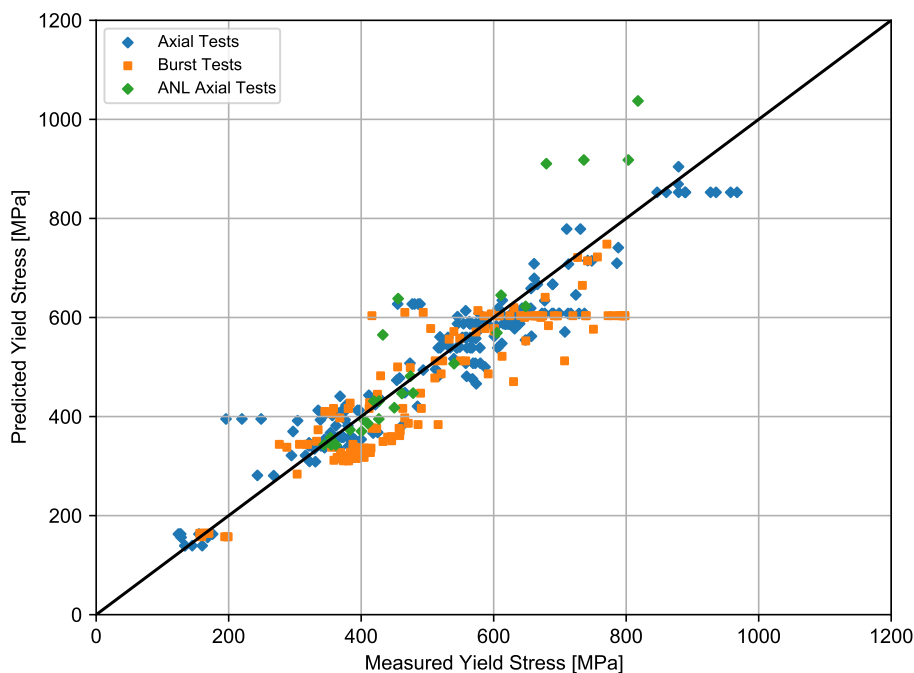


Figure 2-22. Predicted vs. measured yield stress from the PNNL database ($293 \text{ K} \leq T \leq 755 \text{ K}$, $0 \leq \Phi \leq 14 \times 10^{25} \text{ n/m}^2$, $0 \leq H_{ex} \leq 850 \text{ ppm}$)

Rigid Pellet Fuel Deformation in FRACAS-I

This section describes the analytical models used to compute fuel deformation in FRACAS-I. Models are available to calculate length change and fuel radial displacement. Relocation is also considered in FRACAS-I and is also discussed in this section. The effect of relocation is included in the thermal response; however, no hard contact between the fuel and cladding (and therefore no mechanical interaction) is allowed until the other fuel expansion components (swelling and thermal expansion) recover 50% of the original relocated pellet radius. Therefore, the rigid pellet for mechanical analyses, and that also controls contact conductance, includes 50% of the original relocated pellet radius as well as the other pellet expansion components.

The assumptions made with respect to fuel deformation in FRACAS-I are that no pellet deformation is induced by fuel-cladding contact stress or thermal stress and that free-ring thermal expansion applies. Each individual fuel ring is assumed to expand without restraint from any other ring, and the total expansion is the sum of the individual expansions.

Radial Deformation

By default, radial deformation of the pellet due to thermal expansion, irradiation swelling, and densification is calculated with a free-ring expansion model. The governing equation for this model is:

$$R_H = \sum_{i=1}^N \Delta r_i \left[1 + \alpha_{T_i} (T_i - T_{ref}) + \varepsilon_i^s + \varepsilon_i^d \right] \quad (2-124)$$

Where,

R_H = Hot-pellet radius, m

α_{T_i} = Coefficient of thermal expansion of the i^{th} radial temperature, 1/K

T_i = Average temperature of i^{th} radial ring, K

T_{ref} = Reference temperature, K

r_i = Width of i^{th} radial ring, m

N = Number of annular rings unitless

ε_i^s = Swelling strain (positive)

ε_i^d = Densification strain (negative)

The fuel densification and solid fuel swelling models are briefly discussed. The densification asymptotically approaches the (input) ultimate density change, typically over a local (node-average) burnup of approximately 5 GWd/MTU. Solid fuel swelling is considered only as the athermal swelling associated with solid fission product accumulation. It is linear with local (node-average) burnup, and starts following a burnup of 6 GWd/MTU (delayed for swelling into as-fabricated porosity). It then accumulates per time step at a rate equal to 0.062 volume%/GWd/MTU up to 80 GWd/MTU and 0.086 volume%/GWd/MTU beyond 80 GWd/MTU [[Luscher and Geelhood, 2014](#)].

A gaseous swelling model is included in FAST. The model is based on data from Mogensen [[Mogensen et al., 1985](#)] and was developed after ramp test results suggested gaseous swelling may influence permanent cladding hoop strain in high burnup rods. The linear strain is given as a function of temperature over the ranges given in the following equations. These models are phased in between 40 and 50 GWd/MTU by applying a factor that varies linearly between 0 and 1 at 40 and 50 GWd/MTU, respectively.

$$\frac{\Delta l}{l} = \begin{cases} 4.55 \times 10^{-5} T - 4.7 \times 10^{-2}, & 960^\circ\text{C} < T < 1370^\circ\text{C} \\ -4.05 \times 10^{-5} + 7.40 \times 10^{-2}, & 1370^\circ\text{C} < T < 1832^\circ\text{C} \end{cases} \quad (2-125)$$

An alternative thermal expansion model is included in FAST and can be activated by setting `nthermex = 1` in the user input file. This model uses the thermal expansion strain to calculate a displacement in the circumferential direction and then calculate the change in radius that would result from the change in circumference. The change in radius is calculated at each point along the fuel radius, and the maximum value of the change is determined:

$$u_{\theta,\max} = \max[\alpha_{T_i} (T_i - T_{ref}) r_i] \quad (2-126)$$

Where,

$u_{\theta,\max}$ = Maximum change in radius due to circumferential expansion, m

α_{T_i} = Coefficient of thermal expansion of the i^{th} radial temperature, 1/K

T_i = Average temperature of i^{th} radial ring, K

T_{ref} = Reference temperature, K

r_i = As-fabricated pellet radius at i^{th} radial ring, m

The sum of the displacements due to radial thermal expansion is then added to this maximum value for the area beyond the radius of maximum radius change, $r_{\theta,\max}$. Including swelling and densification strain, the hot pellet radius calculated using the alternative thermal expansion model becomes:

$$R_H = R_{asfab} + u_{\theta,\max} + \sum_{i=r_{\theta,\max}}^N [\Delta r_i \alpha_{T_i} (T_i - T_{ref})] + \sum_{i=1}^N \Delta r_i [\varepsilon_i^s + \varepsilon_i^d] \quad (2-127)$$

For $n_{thermex} = 1$, FAST compares the results of Equation 2-124 to Equation 2-127 and sets the hot pellet radius equal to whichever value is greater. For most cases (parabolic temperature distributions) Equation 2-124 provides the maximum value for the displacement of the outer edge of the fuel. However, when a temperature profile is edge peaked, as in a RIA shortly after the power pulse, Equation 2-127 gives a larger value for R_H than Equation 2-124. Assessment of cladding permanent hoop strain following an RIA suggests that the hoop strain is best predicted when the second option ($n_{thermex} = 1$) is used. This option is recommended for RIA cases.

Axial Deformation

Axial deformation of the total fuel stack takes into account the thermal, densification, and swelling strains at each axial node. The calculation proceeds differently for flat-ended versus dished-pellets as described below.

For flat-ended pellets, the volume-averaged ring axial deformation is calculated for each axial node, and these are summed to find the total stack deformation assuming isotropic behavior. The ring deformations account for thermal, densification, and swelling strains specific to each ring.

For dished pellets, the axial deformation of the “maximum ring” (the ring with the maximum deformed length) per node is found, and these “maximum ring” deformations are summed to find the total deformation. Typically, the “maximum ring” is the innermost ring on the dish shoulder because the deformation of the rings within the dish does not fill the dish volume, as illustrated in Figure 2-23.

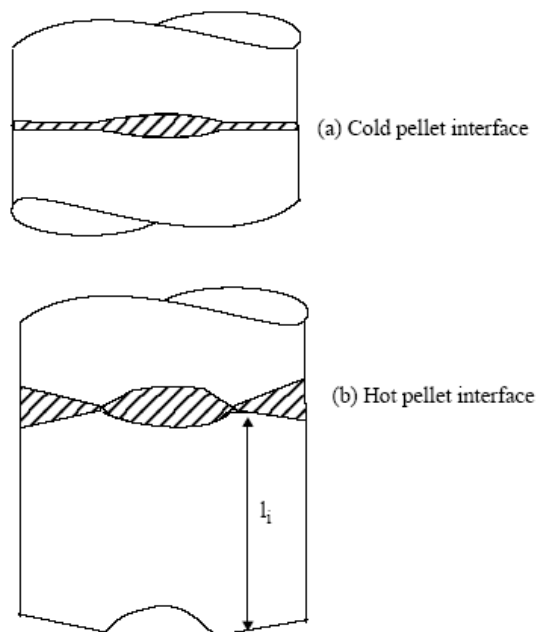


Figure 2-23. Interpellet void volume

Fuel Relocation

Fuel pellet center temperatures measured at beginning of life (BOL) in instrumented test rods have repeatedly been found to be lower than values predicted by thermal performance computer programs when the predicted fuel-cladding gap in operation is calculated based only on fuel and cladding thermal expansion [Lanning, 1982]. It has long been concluded, based on microscopic examination of fuel cross sections [Galbraith, 1973] [Cunningham and Beyer, 1984], that fuel pellet cracking promotes an outward relocation of the pellet fragments that causes additional gap closure. This process begins at BOL and quickly reaches equilibrium. [Oguma, 1983] characterized this approach to equilibrium based on his analysis of BOL test rod elongation data from Halden instrumented test assemblies.

The fuel pellet cracking that promotes relocation is predominantly radial; however, some circumferential components to these crack patterns exist, and these components could alter the fuel thermal conductivity. Thus, cracking and relocation will to some degree increase the thermal resistance in the pellet while reducing the thermal resistance of the pellet-cladding gap by reducing its effective size. The relocation model implicitly includes any crack effects on heat transfer because the model is based on fuel centerline temperature data.

The best estimate pellet relocation model developed for GT2R2 [Cunningham and Beyer, 1984], has been altered for use in FAST in conjunction with the FRACAS-I mechanical model. This model is based on the model developed for FRAPCON-3.5. The gap closure at beginning of life was fit to the first ramp to power data. Due to the excellent centerline temperature predictions throughout life, the FRAPCON-3.4 pellet relocation model beyond 5 GWd/MTU was retained. Data from IFA-677.1 which contained very stable pellets that exhibited little to no densification was available

showing stack elongation (which is proportional to fuel temperature) as a function of power for ramps to power at 0.1, 0.6, 4, and 5 GWd/MTU [Thérache, 2005]. These data demonstrated that the increase in relocation from 0 to 5 GWd/MTU appears to follow a logarithmic trend. Therefore, a logarithmic function was adopted to model the relocation between 0 and 5 GWd/MTU.

The gap closure due to relocation as a fraction of the as-fabricated pellet-cladding gap is given by:

$$\frac{\Delta G}{G} = \begin{cases} 0.055, & Bu \leq 0.0937 \text{ GWd/MTU} \\ 0.055, + \min [reloc, reloc (0.5795 + 2447 \ln (Bu))] & Bu > 0.0937 \text{ GWd/MTU} \end{cases} \quad (2-128)$$

Where,

$\Delta G/G$ = Fraction of as fabricated gap closure due to pellet relocation, unitless

P = Local power, kW/ft

Bu = Local burnup, GWd/MTU

and,

$$reloc = \begin{cases} 0.345, & P > 20 \text{ kW/ft} \\ 0.45 + \frac{P - 20}{200}, & 20 \text{ kW/ft} \leq P \leq 40 \text{ kW/ft} \\ 0.445, & P > 40 \text{ kW/ft} \end{cases} \quad (2-129)$$

A plot of this model as a function of burnup and LHGR is shown in Figure 2-24. Also shown for reference is the relocation model from FRAPCON-3.4.

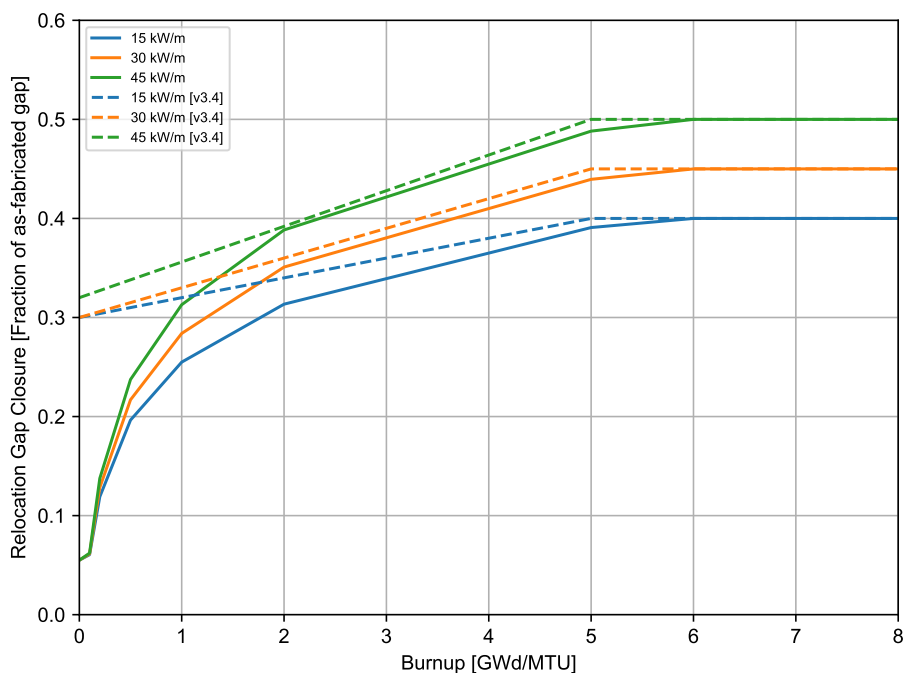


Figure 2-24. Power and burnup dependence of the FAST-1.1 relocation model with the FRAPCON-3.4 model shown for reference

The fuel-cladding gap size used in the thermal and internal pressure calculations includes the fuel relocation, while the fuel-cladding gap size used in the mechanical calculations allows for 50% of the relocation to be recovered before cladding stress-strain is driven by the fuel.

2.5.2 Cladding Ballooning Model

After the cladding deformation has been calculated by FRACAS-I, a check is made to determine whether or not the cladding ballooning model should be used. The check consists of comparing the cladding effective plastic strain, which is part of the calculated deformation, with the cladding instability strain given by MATPRO [Hagrman et al., 1981]. If the cladding effective plastic strain is greater than the cladding instability strain, the ballooning model, BALON2, is used to calculate the localized, non-uniform straining of the cladding. Refer to [Hagrman et al., 1981] for the details of the BALON2 model. Once the instability strain is reached in one node, no further strain is calculated by FRACAS-I for any nodes. The BALON2 model divides the ballooning node into 12 radial and 12 axial subnodes as seen in Figure 2-25. For the node that has reached the instability strain, the radial average hoop, axial, and radial strains at the axial subnode with the maximum hoop strain calculated by BALON2 is used as the hoop, axial, and radial strains for the ballooning node.

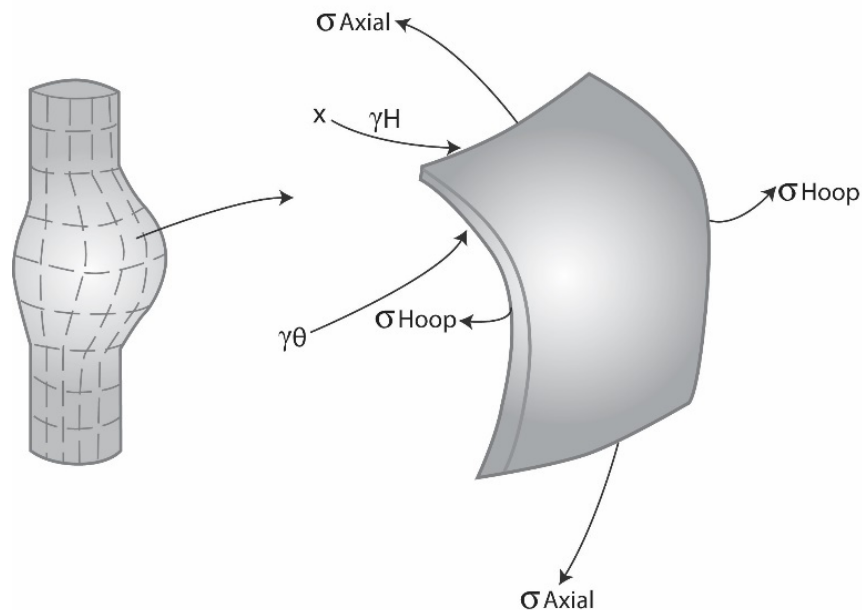


Figure 2-25. Description of the BALON2 model

BALON2 calculates the extent and shape of the localized large cladding deformation that occurs between the time that the cladding effective strain exceeds the instability strain and the time of cladding rupture. The cladding is assumed to consist of a network of membrane elements subjected to a pressure difference between the inside surface and the outside surface, as shown in Figure 2-25. The equations for the model are derived from the thin shell membrane equilibrium equation and geometric constraints. In addition, the model calculates the temperature rise of the cladding due to heat transfer across the fuel-cladding gap. The fuel surface is assumed to have a non-uniform temperature. The model accounts for the extra cooling the cladding receives as it bulges outwardly.

The BALON2 model predicts failure in the ballooning node when the cladding true hoop stress exceeds an empirical limit that is a function of temperature. This correlation is shown in Figure 2-26. Although the data shown in the figure are all from Zircaloy, this model is used in FAST-1.1 for Zircaloy-2, Zircaloy-4, ZIRLO, Optimized ZIRLO, and M5.

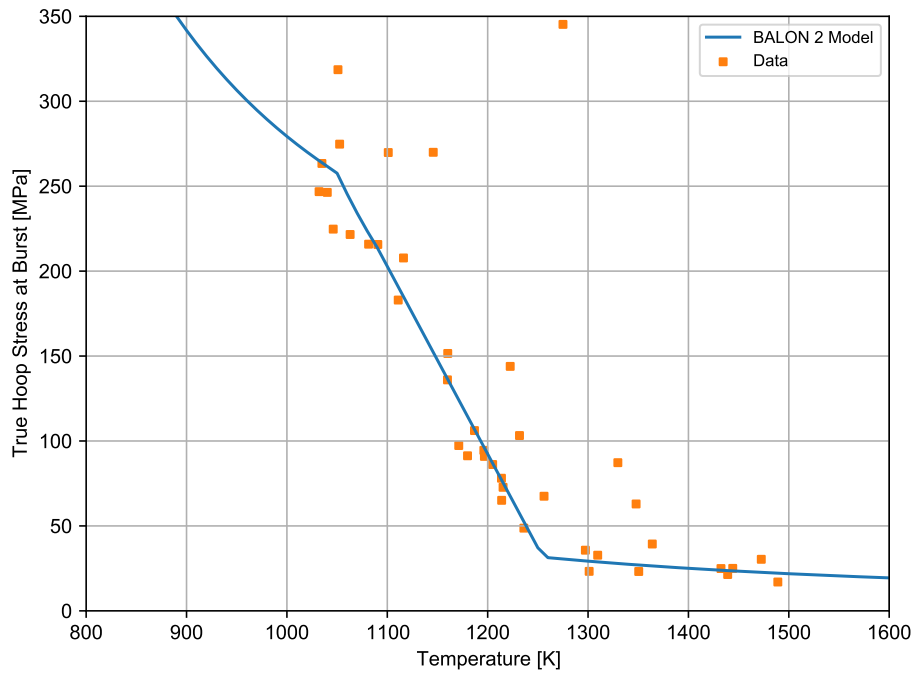


Figure 2-26. True hoop stress at burst used in FAST-1.1's implementation of BALON2

Using this limit, FAST predicts failure well when compared to measured engineering burst stress at various temperature levels. However, in some cases the calculated failure strain is very large. To avoid this, a second empirical strain limit was added such that FAST will predict failure in the ballooning node when the true hoop stress exceeds the stress limit in BALON2, or when the predicted cladding permanent hoop strain exceeds the FAST strain limit. The FAST strain limit is provided in Equations 2-130 through 2-132.

- For $940 \text{ K} \leq T < 1200 \text{ K}$:

$$\begin{aligned} \varepsilon_{fail} = & 1.58797 \times 10^{-9}T^4 - 6.692798 \times 10^{-6}T^3 \\ & + 1.053049 \times 10^{-2}T^2 - 7.331051T + 1906.22 \end{aligned} \quad (2-130)$$

- For $1200 \text{ K} \leq T < 1700 \text{ K}$:

$$\varepsilon_{fail} = -1.67939 \times 10^{-8}T^3 + 6.23050 \times 10^{-5}T^2 - 7.360497 \times 10^{-2}T + 28.1199 \quad (2-131)$$

- For $T \geq 1700 \text{ K}$:

$$\varepsilon_{fail} = 0.544589 \quad (2-132)$$

Where,

ε_{fail} = Plastic strain at failure, m/m

T = Cladding temperature, K

With these two limits in place, FAST predictions agree with both cladding failure stress and strain data. The predictions also agree with or bound the previously published curves from NUREG-0630 [Powers and Meyer, 1980]. These comparisons are shown in Figures 2-27 through 2-30 for different temperature ramp rates.

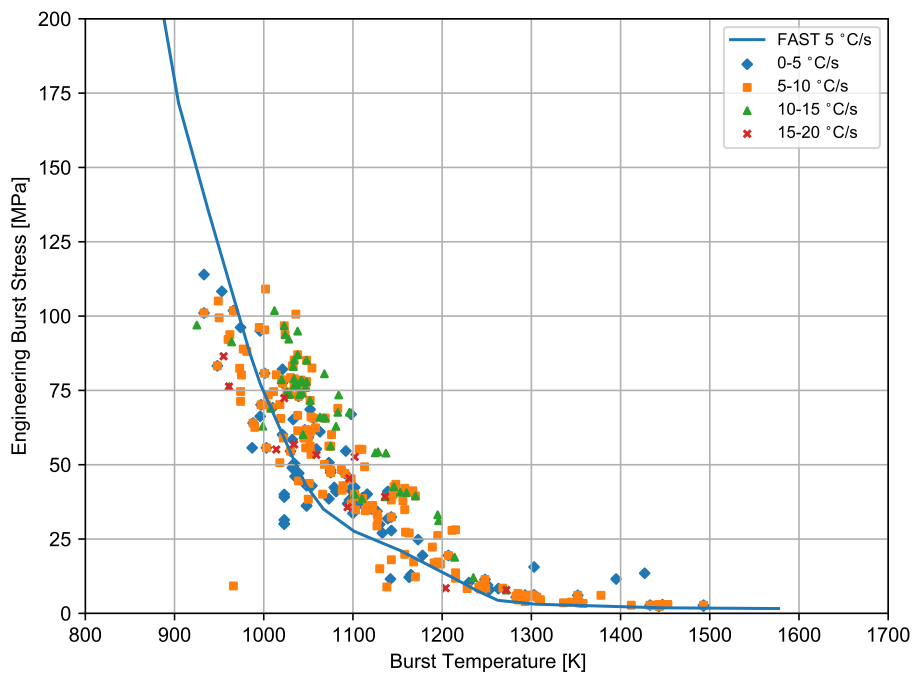


Figure 2-27. Engineering burst stress data and FAST predictions for low heating rates

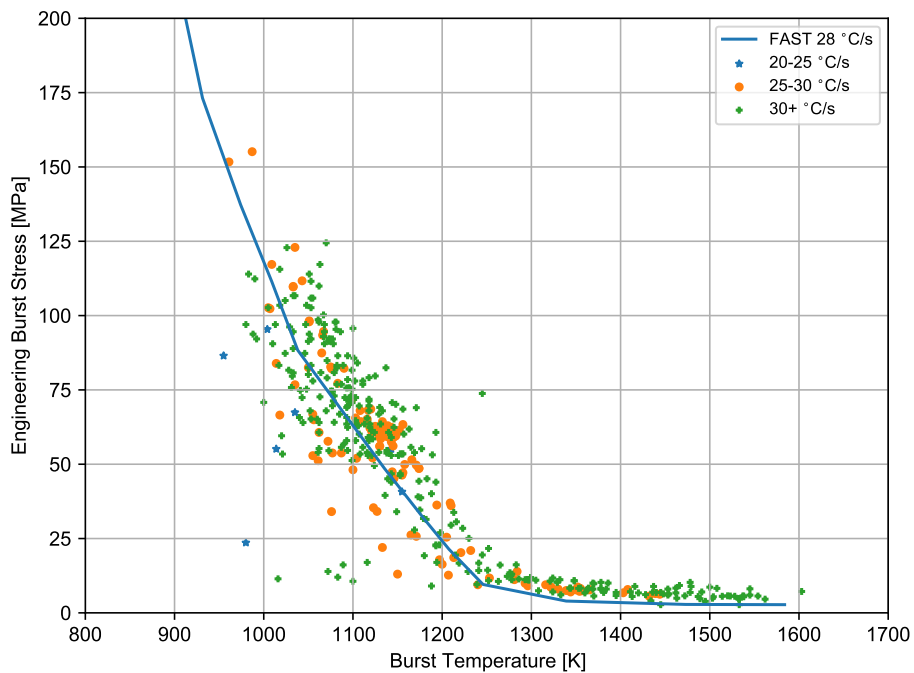


Figure 2-28. Engineering burst stress data and FAST predictions for high heating rates

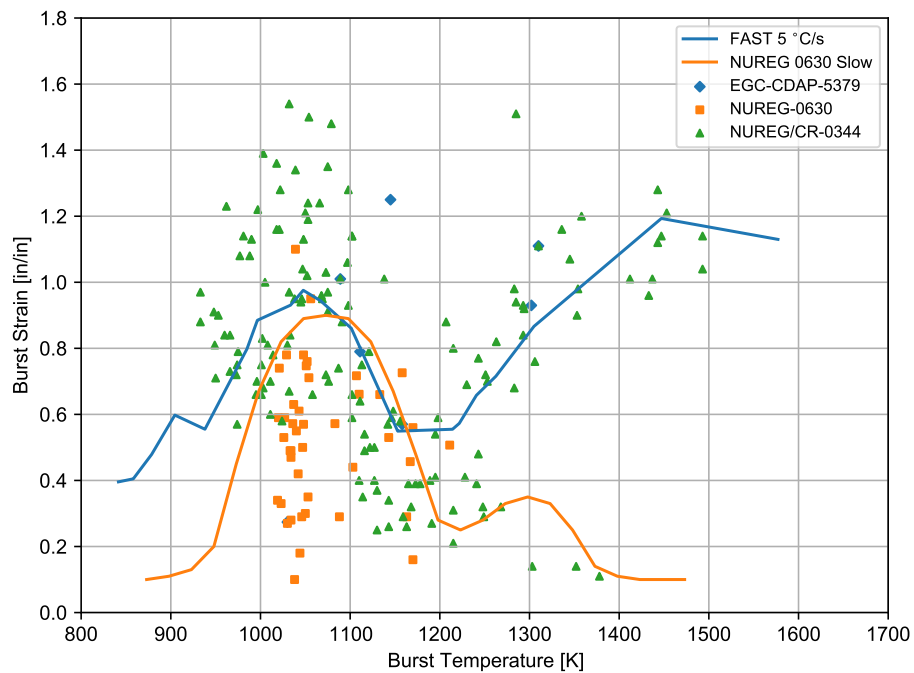


Figure 2-29. Permanent burst strain data and FAST predictions for low temperature ramp rates (between 2 and 10 °C/s)

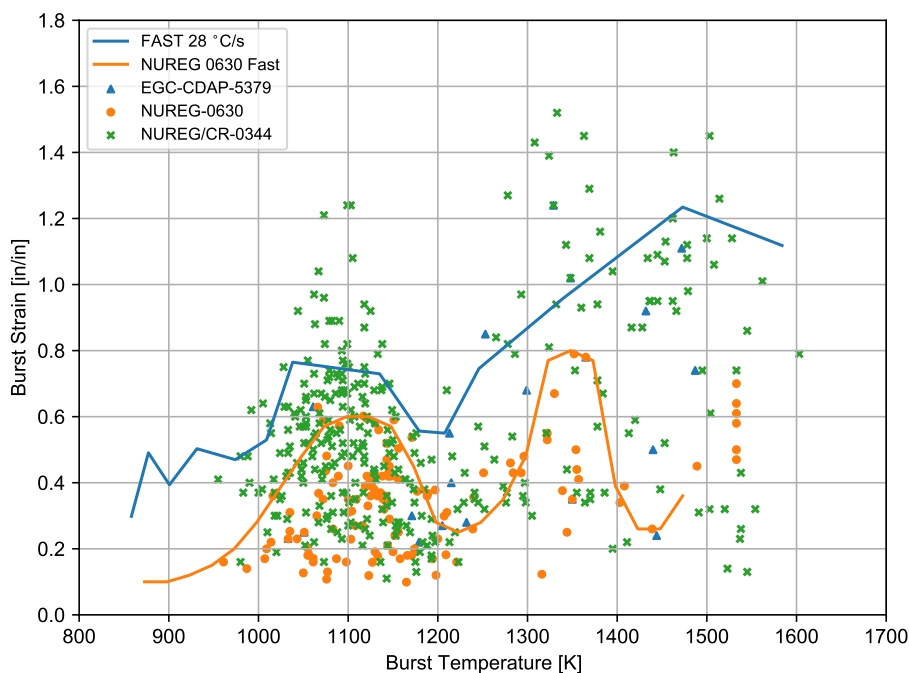


Figure 2-30. Permanent burst strain data and FAST predictions for high temperature ramp rates (greater than 20 °C/s)

2.6 Rod Internal Pressure and Fission Gas Release

The pressure of the gas in the fuel rod must be known in order to calculate the deformation of the cladding and the transfer of heat across the fuel-cladding gap. The pressure is a function of the gas temperature, composition, void volume, and quantity of gas. Because the temperature is spatially non-uniform, the fuel rod must be divided into several smaller volumes so that the temperature in each small volume can be assumed to be uniform. In particular, the fuel rod is divided into a plenum volume and several fuel-cladding gap and fuel void volumes. The temperature of each volume is given by the thermal models described in Section 2.4, the size of the volume by the deformation models described in Section 2.5, and the quantity of gases by the FGR models.

The internal gas pressure can be calculated either by a static pressure model (which assumes that all volumes inside the fuel rod equilibrate in pressure instantaneously) or by a transient pressure model which takes into account the viscous flow of the gas in the fuel rod. The static pressure model is the default model. The transient model is an input option. Unless the fuel-cladding gap is small ($\leq 25 \mu\text{m}$), the static and transient models give identical results.

The static fuel rod internal gas pressure model is based on the following assumptions:

1. Perfect gas law holds ($PV = NRT$)
2. Gas pressure is constant throughout the fuel rod
3. Gas in the fuel cracks is at the average fuel temperature

The transient fuel rod internal gas pressure model is based on the following assumptions:

1. Perfect gas law holds ($PV = NRT$)
2. Gas flow past the fuel column is a quasi-steady process
3. Gas flow is compressible and laminar
4. Gas flow past the fuel column can be analyzed as Poiseuille flow (that is, by force balance only)
5. Gas expansion in the plenum and ballooning zone is an isothermal process
6. The entire fuel-cladding gap can be represented as one volume containing gas at a uniform pressure
7. The flow distance is equal to the distance from the plenum to the centroid of the fuel-cladding gap
8. The minimum cross-sectional area of flow is equivalent to an annulus with inner radius equal to that of the fuel pellet radius and a radial thickness of 25 μm

2.6.1 Fuel Rod Internal Gas Pressure

2.6.1.1 Static Gas Pressure

Fuel rod internal gas pressure is calculated from the application of the perfect gas law to a multiple volume region. The volumes accounted for in FAST-1.1 include the hot plenum volume(s), gap, annulus, crack, dish, porosity, roughness, and pellet-pellet interface volumes specific to each node. Thus, the equation for rod internal pressure is:

$$P = \frac{MR}{\frac{V_{pu}}{T_{pu}} + \frac{V_{pl}}{T_{pl}} + \frac{V_{pext}}{T_{pext}} + \sum_{n=1}^N \left[\frac{V_g}{T_g} + \frac{V_{ch}}{T_{ch}} + \frac{V_{cr}}{T_{cr}} + \frac{V_{dsh}}{T_{dsh}} + \frac{V_{por}}{T_{por}} + \frac{V_{rfc}}{T_{rfc}} + \frac{V_i}{T_i} \right]} \quad (2-133)$$

Where,

P = Rod internal pressure, Pa

M = Total number of moles of gas

R = Universal gas constant, 8.314 J/mol-K

N = Number of axial nodes into which fuel rod is divided for numerical solution

n = Axial node number

V = Volume, m^3

T = Temperature, K

The following void volumes are accounted for in the pressure solution:

Table 2-8. Void volumes

Symbol	Location	Temperature Description
p_u	Upper plenum	As described in Section 2.6.2.1, dependent on the upper cladding and fuel temperatures
p_l	Lower plenum	Lower plenum, dependent on inlet coolant and bottom fuel temperatures
p_{ext}	External plenum	External plenum, temperature supplied by the user
g	Gap	Average of the fuel surface and cladding ID temperatures
ch	Central hole	Nodal fuel centerline temperature
cr	Fuel cracks	Average of fuel surface and temperature at the restructured fuel radius
dsh	Fuel dish	Fuel volume average temperature
$cham$	Fuel chamfer	Fuel volume average temperature
por	Fuel open-porosity	Fuel volume average temperature
r_{fc}	Fuel and clad surface roughness	Temperature at fuel surface and cladding ID
i	Interface volumes	Average between fuel volume average and surface temperature

Note: In the FAST-1.1 output file, a table appears that presents the fractions of total volume represented by the plenum, gap, cracks, dishes, annulus, open porosity, and roughness, and the rod-averaged temperatures associated with these various volume-fractions. These are not the node-specific values that appear in the above equation, but are the results of the sum of each axial node for each volume.

The gas pressure calculation, therefore, requires information on the gas inventory, void volumes, and the void temperatures, which is provided by the following supportive models.

2.6.1.2 Transient Internal Gas Flow

Transient flow of gas between the plenum and fuel-cladding gap is calculated by the Poiseuille equation for viscous flow along an annulus according to Equation 2-134. Assumptions inherent in the equation are ideal gas, laminar flow, and density based on linear average pressure:

$$\dot{m} = \frac{\pi (P_P^2 - P_S^2)}{R\mu \sum_{i=I_s}^{I_p} \frac{l_i T_i H}{D_g D_h^3}} \quad (2-134)$$

Where,

\dot{m} = Mass flow rate, g-moles/s

μ = Gas viscosity at temperature T_a , N-s/m²

T_a = Volume-averaged temperature of gas in gas (fuel-cladding) gap, K

T_i = Gas temperature at node i , K

l_i = Axial length of node i , m

I_P = Number of top axial node

I_s = Number of axial node closest to centroid of gas gap (see Figure 2-31)

H = Hagen number (see Equation 2-135)

P_P = Fuel rod plenum gas pressure, N/m²

P_S = Fuel-cladding gap gas pressure, N/m²

R = Universal gas constant, 8.314 J/mol-K

D_g = Mean diameter of fuel-cladding gap, m

D_h = Hydraulic diameter of fuel-cladding gap = $2t_{gi}$ for a small gap, m

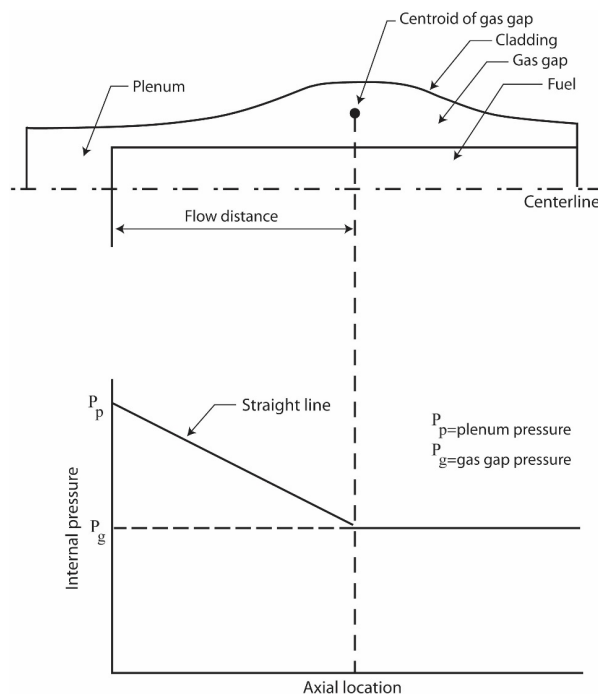


Figure 2-31. Internal pressure distribution with the transient gas flow model

The Hagen number is calculated by:

$$H = 22 + \frac{0.24558}{2t_{gi} - 7.874 \times 10^{-4}} \quad (2-135)$$

Where,

t_{gi} = Fuel-cladding radial gap thickness at node i , in

A plot of the relation between Hagen number and gap width given by Equation 2-135 is shown in Figure 2-32. For gaps smaller than 25 μm , the function is cut off at a Hagen value of 1177. To calculate the fuel-cladding gap pressure, a modified form of Equation 2-133 is used. The plenum term is deleted and the moles of gas in the fuel-cladding gap is substituted in place of the moles of gas in the fuel rod.

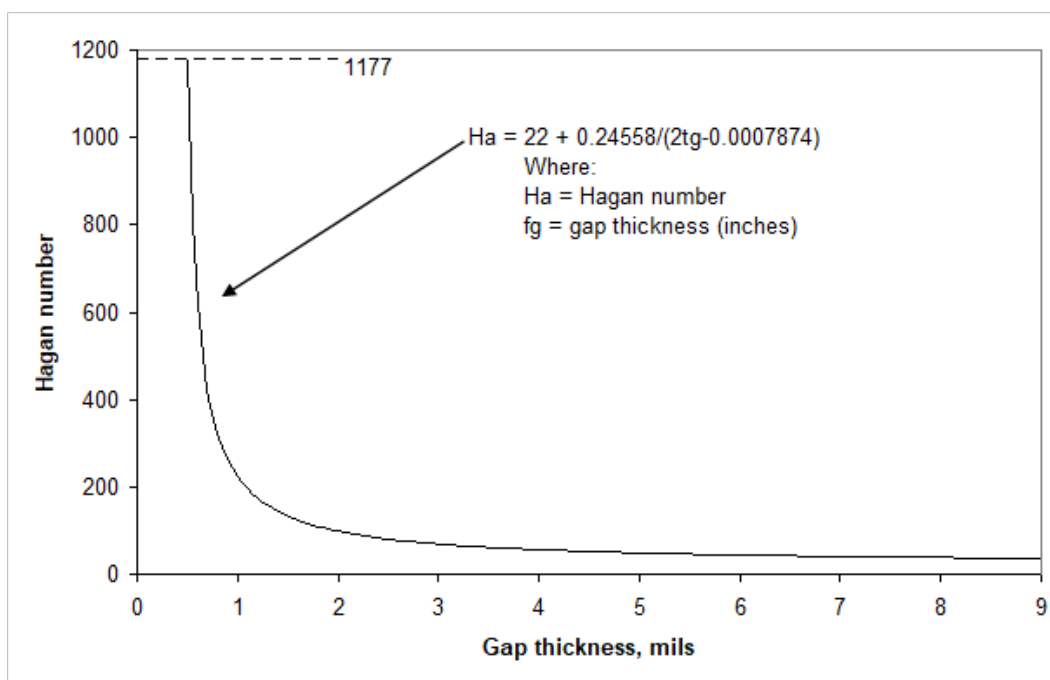


Figure 2-32. Hagen number versus width of fuel-cladding gap

2.6.2 Fuel Rod Void Volume

Void volumes computed by FAST-1.1 include the plenum(s), pellet dishes and chamfers, the fuel-cladding gap, the fuel cracks, the fuel open porosity, pellet-pellet interface, the fuel and cladding surface roughness volumes, and (if it exists) the fuel central hole volume. These void volumes are calculated as indicated below.

2.6.2.1 Plenum Volume

The plenum volume is calculated from geometry considerations and irradiation induced effects on both the fuel and cladding. In FAST, there are three different plenum volumes that are calculated

by the code:

1. Upper plenum
2. Lower plenum
3. External plenum

In the upper plenum, the cladding undergoes elastic/plastic deformation, creep, thermal expansion, and the formation of crud/oxide layers. In addition, the upper plenum accounts for the dimensional changes along the entire fuel rod stack including those of both the fuel (swelling/densification, thermal expansion, etc.) and the cladding. The axial effects of both the fuel and cladding deformation are accounted for in determining the reduction (or possibly expansion) of the plenum free volume. In addition, the volume of the hold-down spring is considered, as well as changes in the spring geometry due to thermal expansion.

In the lower plenum, the same effects are accounted for as the upper plenum except for the changes in fuel and cladding geometry along the fuel stack impacting the plenum volume. It is assumed that the fuel sits on top of the lower plenum and can not reduce the plenum length.

The external plenum is supplied with its own void volume that does not change as a function of time. In addition, the temperature of the external plenum is also supplied (as a function time). An external plenum is commonly used when analyzing test specimens that have void volume outside of the heated zone.

2.6.2.2 Pellet Dish and Chamfer Volumes

The volume between pellets is calculated and included as part of the overall volume in the internal gas pressure model. The inter-pellet volume is calculated at each time step based on hot-pellet geometries. Figure 2-23 shows 1) a cold-pellet interface configuration for the case where the pellets are dished and 2) an exaggerated hot-pellet interface configuration. The void volume available for internal fill gas is defined by the cross-hatched areas (a and b in Figure 2-23). The dish volume is that portion of the hot inter-pellet volume that is within the dishes, excluding the volume of any central hole. The chamfer volume is included in the portion of the hot inter-pellet volume that is outside the dishes.

2.6.2.3 Fuel-Cladding Gap Volume

The fuel-cladding gap volume is calculated by considering the area between two concentric cylinders. The outer cylinder is assumed to have a diameter equal to the diameter of the cladding inside surface based on plastic deformation. The inside cylinder is assumed to have a diameter equal to the diameter of the relocated fuel pellets.

2.6.2.4 Fuel Crack Volume

As the fuel expands, extensive cracking occurs due to the high thermally induced stresses, resulting in a relocated fuel surface. The crack volume is computed in Equation 2-136.

$$V_c = V_g - V_{eg} - V_{tx} \quad (2-136)$$

Where,

V_c = Fuel crack volume per unit length, m²

V_g = Volume per unit length within the thermally expanded cladding, m²

V_{eg} = Fuel volume per unit length defined by expanded radial nodes, including the thermal expansion swelling, and densification, m²

V_{tx} = Computed fuel-cladding gap volume per unit length based on the relocated fuel surface, m²

2.6.2.5 Open Porosity Volume

A portion of the initial fabrication porosity is open to free gas flow, which is given by the following expressions:

$$V_{por} = \begin{cases} 2.77 \times 10^{-4} - 3.8181G_{den} \\ \quad - 1.43 \times 10^{-8}G_{den}^2 + 2.497 \times 10^{-10}G_{den}^3, & G_{den} \leq 91.25 \\ 1.97 \times 10^{-8} (94.0 - G_{den}), & 91.25 < G_{den} < 94.0 \\ 0.0, & G_{den} \geq 94.0 \end{cases} \quad (2-137)$$

Where,

V_{por} = Porosity volume per unit length, m²

$G_{den} = DEN - 1.25$

DEN = Fuel density, %TD

Note: It should be noted that most commercially fabricated fuel today has little open porosity.

2.6.2.6 Pellet-Pellet Interface Volume

The pellet-pellet interface volume is calculated as the difference between the hot inter-pellet volume and the dish volume.

2.6.2.7 Surface Roughness Volume

The roughness of the surface of the fuel and cladding results in a small void volume accounted for by:

$$V_{rough} = \frac{\pi \left(r_p^2 - (r_p - rough_p)^2 \right) + \pi \left((r_c + rough_c)^2 - r_c^2 \right)}{V/L} \quad (2-138)$$

Where,

V_{rough} = Fraction of pellet volume in roughness

r_p = Outer radius of pellet, m

r_c = Inner radius of cladding, m

$rough_p$ = Fuel surface roughness, m

$rough_c$ = Cladding surface roughness, m

V = Volume of pellet stack, m³

L = Length of fuel stack, m

The gas pressure response resulting from the above models feeds back into the mechanical and temperature response models in the iteration scheme.

2.6.2.8 Central Hole Volume

The central hole volume is calculated by considering the area of the central hole (if present), the length of the axial node, and the length of the central hole.

2.6.3 Gas Production

Given production rates for the major fission-produced diffusing gases, the burnup-dependent total fission gas generated at axial elevation z is calculated by Equation 2-139.

$$GPT(z) = \frac{Bu(z)VF(z)}{100A_v} (PR_{He} + PR_{Kr} + PR_{Xe}) \quad (2-139)$$

Where,

$GPT(z)$ = Total fission gas produced at Elevation z , moles

$Bu(z)$ = Burnup at elevation z , fission/cm³

$VF(z)$ = Fuel volume, cm³

A_v = Avogadro's number

PR = Fission gas production rate, atoms/100-fissions

To obtain a burnup in fission/cm³, FAST converts the user supplied rod power, assuming it is all recoverable energy from fission, at 200 MeV/fission and converts power using 1.60218×10^{-13} W-s/MeV.

All the fission gas produced, however, is not released. A portion is trapped in the fuel and a portion is released to the fuel-cladding gap volume. Only the released portion is used to calculate the rod internal gas pressure. The gas release fraction is calculated as discussed in the following sections.

In addition to fission gas production, also present is the as-fabricated content of gases in the fuel matrix as a result of fabrication. The gases modeled by FAST include nitrogen and water, and the initial fraction, relative to the fuel, is defined by the user. These gases, once released, contribute to the overall pressure inside the rod and gap gas mixture content, but do not contribute to the calculated FGR.

2.6.4 Steady-State Gas Release

There are two types of steady-state FGR models present in FAST: long-lived stable gas production models which calculate the gas released to the plenum and therefore impact the gap gas mixture, and radioactive gas release models which can be used to predict the release to birth ratios of short and long-lived radioactive isotopes. There are four FGR model options, two of which are for long-lived stable isotopes and two are for radioactive gases. The two long-lived stable modes are the modified Forsberg and Massih model [Forsberg and Massih, 1985], modified at PNNL; and the FRAPFGR model developed at PNNL. The two radioactive gas models are the ANS-5.4 (1982) [ANS, 1982] and the more recent ANS-5.4 (2011) [ANS, 2011]. All four of these release models are based on earlier formulations for diffusion from a sphere by Booth [Booth, 1957] and are discussed below.

The Massih model is recommended and is set as the default model. The ANS-5.4 models are useful for calculating the release of short-lived radioactive gas nuclides, but are known to provide very conservative values for release. To compensate for this, the ANS-5.4 models were implemented to only calculate the radioactive gases and do not feed them back into the gap gas mixture. When these models are used, the Massih model is used to calculate the stable gas release. The FRAPFGR model provides a better estimate of the distribution of fission gases within the pellet than the Massih model and is therefore useful when also using the transient burst release model, such as for RIAs. However, neither the ANS-5.4 model nor the FRAPFGR model predicts stable FGR as well as the Massih model does, thus it is recommended that the Massih model be used for best-estimate calculation of stable FGR.

In addition to FGR (krypton, xenon and helium), FAST also calculates the release of nitrogen. The nitrogen is released from the fuel lattice, where it is trapped during the fuel fabrication process. The nitrogen release is described further in Section 2.6.6.

2.6.4.1 Modified Forsberg-Massih Model

The original Forsberg-Massih model begins with a solution of the gas diffusion equation for constant production and properties in a spherical grain:

$$\frac{\partial C}{\partial t} = D(t) \Delta_r C(r, t) + \beta(t) \quad (2-140)$$

Where,

C = Gas concentration

β = Gas production

$$\Delta_r = \frac{d^2}{dr^2} + \frac{2}{r} \left(\frac{d}{dr} \right)$$

D = Diffusion constant

t = Time

With boundary conditions,

$$C(r, 0) = 0$$

$$C(a, t) = 0$$

Forsberg and Massih attempt to solve the equation for the case where there is re-solution of gas on the grain surface, which changes the outer boundary condition to:

$$C(a, t) = \frac{b(t) \lambda N(t)}{2D} \quad (2-141)$$

Where,

N = Surface gas concentration

λ = Resolution layer depth

a = Hypothetical grain radius

b = Resolution rate

They make use of a four-term approximation to the integration kernel, K , where:

$$\int_0^a 4\pi r^2 C(r, t) dr = \int_0^\tau K(\tau - \tau_0) \beta_e(\tau_0) d\tau_0 \quad (2-142)$$

and

$$\beta_e = \frac{\beta}{D} \quad (2-143a)$$

$$\tau = Dt \tag{2-143b}$$

$$K = \frac{8a^3}{\pi} \sum_{n=1}^{\infty} \frac{e^{\left(\frac{-n^2\pi^2\tau}{a^2}\right)}}{n^2} \tag{2-143c}$$

Low-Temperature Fission Gas Release Model at High Burnup

The modified Forsberg-Masih model is used to calculate FGR unless the low-temperature FGR model predicts a higher value for FGR. The low-temperature FGR model is defined as:

$$F = 7 \times 10^{-5} Bu + C \tag{2-144}$$

Where,

F = Fission gas release fraction, unitless

Bu = Local burnup, GWd/MTU

and,

$$C = \begin{cases} 0, & Bu \leq 40 \text{ GWd/MTU} \\ 0.01 \frac{Bu - 40}{10}, & Bu > 40 \text{ GWd/MTU and } F \leq 0.05 \end{cases}$$

Grain Boundary Accumulation and Re-Solution

The final solution for a given time step, without re-resolution and with constant production rate during the step, can be written as:

$$\Delta G_n = f_n G_n(\tau_1) + A_n \int_{\tau_1}^{\tau_2} e^{\frac{-B_n(\tau_2 - \tau_0)}{a^2}} q(\tau_0) d\tau_0 \tag{2-145}$$

$$\Delta G = \sum_{n=1}^4 \Delta G_n \tag{2-146}$$

Where,

ΔG = Change in gas concentration in fuel grain

$$\Delta G_B = \sum f_n G_n(\tau_1) + A_n \int_{\tau_1}^{\tau_2} f(\tau_2 - \tau_0) q(\tau_0) d\tau_0 \quad (2-147)$$

Where,

ΔG_B = Change in gas concentration on grain boundaries

$$f_n = \exp \left[\frac{-B_n(\tau_2 - \tau_0)}{a^2} \right] - 1 \quad (2-148)$$

and,

f_n = Fission gas production fraction remaining in the grain from the previous time step

Where q is determined from:

$$a^2 q \left[- \sum_{n=1}^4 \left(\frac{f_n A_n}{B_n} \right) + f(\Delta\tau) \right] = \beta \Delta t \quad (2-149)$$

With the following relationship:

$$f(\Delta\tau) = \int_{\tau_1}^{\tau_2} f(\tau_2 - \tau_0) d\tau = \begin{cases} \frac{6}{\sqrt{\pi}} \sqrt{\frac{\tau_2 - \tau_0}{a^2}} - 3 \frac{\tau_2 - \tau_0}{a^2}, & \tau < 0.1 \\ 1 - \frac{6}{\pi^2} \exp \left[-\pi^2 \frac{(\tau_2 - \tau_0)}{a^2} \right], & \tau \geq 0.1 \end{cases} \quad (2-150)$$

Where,

A_n, B_n = Constants given by Massih

$$K_2 = \frac{a}{3} - \frac{K}{4\pi a^2}$$

$$K_3 = \frac{3}{a} K_2$$

$$1 + K_3 = \sum_{n=1}^4 A_n \exp \left(-\frac{B_n \tau}{a^2} \right)$$

In modifying the original model, it was chosen to introduce re-resolution by defining the partition of the gas arriving at the boundary each time step as follows:

$$\Delta \text{Resolved Gas} = \Delta G_B \frac{F}{1+F} \quad (2-151)$$

The calculated increase in grain boundary gas is then reduced by:

$$\Delta G_B = \frac{\Delta G_B}{1+F} \quad (2-152a)$$

$$F = M \left[\frac{1.84 \times 10^{-14} r_{grn}}{3D} \right] \quad (2-152b)$$

and

M = An empirical multiplier on the term in brackets that is the original Massih equation for the resolution rate = 300

r_{grn} = Grain radius, m

D = Diffusion constant, m²/s

Note: Although F is unitless in Massih's derivation, it does not represent the fraction of retained gas.

Diffusion Constant

The diffusion constant (D) in the original Forsberg-Massih model is defined over three temperature ranges, as follows:

$$D = \begin{cases} 1.51 \times 10^{-17} \exp\left(\frac{-9508}{T}\right), & T < 1381 \text{ K} \\ 2.14 \times 10^{-13} \exp\left(\frac{-22884}{T}\right), & 1381 \text{ K} \leq T \leq 1650 \text{ K} \\ 1.09 \times 10^{-17} \exp\left(\frac{-6614}{\min(T, 1850)}\right), & T > 1650 \text{ K} \end{cases} \quad (2-153)$$

In principle, typically only the mid-range diffusion constant from Equation 2-153 is generally used. The activation energy term is ($\frac{Q}{R} = 22884(1.15)$). If the modified constant is less than the low-range Massih diffusion constant, the latter is used.

A burnup enhancement factor multiplies the mid-range diffusion constant and has the form shown in Equation 2-154:

$$\text{burnup factor} = 100^{\left(\frac{Bu-21}{40}\right)} \quad (2-154)$$

Where

Bu = burnup, GWd/MTU

The enhancement factor has a maximum value of 20000. A factor of 12 is applied to the burnup-enhanced diffusion constant as a final step.

Gas Release

The gas is accumulated at the grain boundary until a saturation concentration is achieved, at which time the grain boundary gas is released. The saturation area density of gas is given by:

$$N_s = \left[\frac{4rF(\theta)V_c}{3K_B T \sin^2(\theta)} \right] \left(\frac{2\gamma}{r} + P_{ext} \right) \quad (2-155)$$

Where,

N_s = Saturation concentration, atoms/m²

θ = Dihedral half-angle, 50°

K_B = Boltzman constant

γ = Surface tension, 0.6 J/m²

V_c = Critical area coverage fraction, 0.25 unitless

r = Bubble radius, 0.5 μ m

P_{ext} = External pressure on bubbles, gas pressure Pa

and,

$$F(\theta) = 1 - 1.5 \cos(\theta) + 0.5 \cos^3(\theta) \quad (2-156)$$

The final modification to the original model was to release both the grain boundary and the resolved gas whenever the saturation condition is achieved and the grain boundary gas is released.

To summarize, optimized parameters have been applied based on comparisons to selected steady-state and transient data:

- The activation energy $\frac{Q}{R} = 1.15(22884) = 26317$ (High temperature diffusion).
- The resolution parameter = 1.84×10^{-14} .
- Burnup enhancement factor on diffusion constant = $100^{\frac{(Bu-21)}{40}}$.
- Multiplier on the diffusion constant (applied after all other modifications) = 12.0

2.6.4.2 FRAPFGR Model

The FRAPFGR model was developed at PNNL to initialize the transient release model in FRAP-TRAN (now incorporated into FAST) that is used to calculate FGR during fast transients such as a RIA. Because of this, it is important that the FRAPFGR model predict not only the steady-state gas release, but also the amount of gas that remains within the grains and the amount of gas that is currently residing on the grain boundaries for each axial and radial node. The grain boundary gas is released during a fast transient due to cracking along the grain boundaries. To do this, gas release data as well as electron probe microanalysis (EPMA) and X-ray fluorescence (XRF) data have been used to validate that the model can accurately predict these parameters.

The basic layout of the FRAPFGR model is similar to the modified Massih model with the following differences.

Grain Growth Model

The FRAPFGR model accepts an input grain size that can be specified in the input. The default value for this is 10 μm using the mean linear intercept (MLI) method. The FRAPFGR model uses a grain growth model proposed by [Khorushii et al., 1999] given by:

$$\frac{da}{dt} = K \left(\frac{1}{a} - \frac{1}{a_{\max}} - \frac{1}{a_{ir}} \right) \quad (2-157)$$

Where,

$$\frac{da}{dt} = \text{Grain radius growth rate, } \mu\text{m/h}$$

$$K = 5.24 \times 10^7 \exp\left(\frac{-32100}{T}\right)$$

$$T = \text{Temperature, K}$$

$$a = \text{Grain size, } \mu\text{m}$$

$$a_{\max} = 2.23 \times 10^3 \left(\frac{-7620}{T}\right)$$

$$a_{ir} = \left[\frac{50}{\dot{F}} \times \frac{1400}{T} \right] 326.5 \exp\left(\frac{-5620}{T}\right)$$

$$\dot{F} = \text{Fission rate, MW/tU}$$

Equation 2-157 is solved by dividing the current time step into 1 hour time steps and solving assuming constant rates within each sub-step.

High Burnup Rim Thickness and Porosity

The high burnup rim that is observed in the outer edge of high burnup pellets can be characterized in terms of sub-micron grains and high porosity. These two items are modeled in the FRAPFGR

model. The size of the high burnup rim has been measured by optical microscopy [Manzel and Walker, 2002] and is modeled using the equation:

$$t_{rim} = 1.439 \times 10^{-6} Bu^{4.427} \tag{2-158}$$

Where,

t_{rim} = Thickness of high burnup rim, μm

Bu = Pellet average burnup, GWd/MTU

Figure 2-33 shows how the high burnup structure is modeled in FRAPFGR. The calculated value of t_{rim} sets a thickness on the pellet surface that is entirely restructured grains. The grain size (MLI) for these grains is set at $0.15 \mu\text{m}$. The next region, which has a width also set by t_{rim} , is composed of a mixture of restructured grains and non-restructured grains. The fraction of restructured grains decreases linearly to zero across this thickness of this region. If the temperature in a given axial node is greater than $1000 \text{ }^\circ\text{C}$ then no restructured grains are assumed to form.

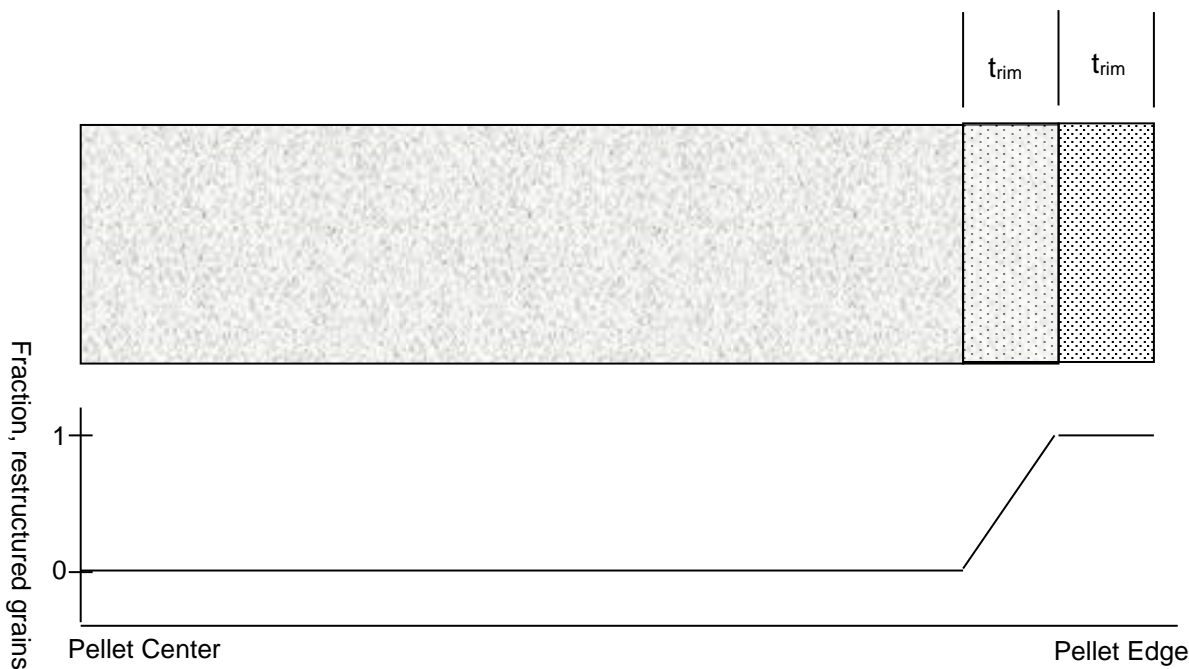


Figure 2-33. Modeling of the pellet high burnup rim structure

In addition to the restructured grains, there is also a porosity increase within the high burnup rim. The porosity is modeled based on a fit to observations on high burnup fuel [Spino et al., 1996] [Une et al., 2001] [Manzel and Walker, 2000]. This model is given by:

$$P = \begin{cases} 0, & Bu < 57 \text{ GWd/MTU} \\ 11.283, \ln(Bu) - 45.621 & Bu \geq 57 \text{ GWd/MTU} \end{cases} \quad (2-159)$$

Where,

P = Porosity increase in high burnup rim structure, fraction of fuel TD

Bu = Local radial node burnup, GWd/MTU

This porosity is subtracted off the input theoretical density, which is used to calculate the production in each radial node. Therefore, as the porosity in the rim increases, the power production in the outer radial nodes is slightly decreased due to increase porosity.

Diffusion Constant

The diffusion constant used in FRAPFGR is given by Equation 2-160.

$$D(T) = \begin{cases} 1.51 \times 10^{-17} \exp\left(-\frac{9508}{\max(T, 675)}\right), & T < 1381 \text{ K} \\ 2.14 \times 10^{-13} \exp\left(-\frac{22884}{T}\right), & 1381 \text{ K} \leq T < 1650 \text{ K} \\ 7.14433 \times 10^{-10} \exp\left(-\frac{34879}{\min(T, 1850)}\right), & 1650 \text{ K} \leq T \end{cases} \quad (2-160)$$

Where,

D = Diffusion constant, m²/s

T = Temperature, K

For non-restructured grains, Equation 2-161 is used, up to a maximum adjustment of 49.81. For restructure grains, there is no burnup adjustment.

$$D(T, Bu) = D(T) \left(10^{\frac{\max((Bu-21), 0)}{40}} + 10 \times \frac{\min(Bu, 12)}{12} \right) \quad (2-161)$$

Where,

$D(T, Bu)$ = Diffusion constant adjusted for burnup, m²/s

$D(T)$ = Temperature dependent diffusion constant given by Equation 2-160, m²/s

Bu = Local radial node burnup, GWd/MTU

The diffusion constant is also modified for the effects of low power using an error function as shown in Equation 2-162.

$$D(T, Bu, P) = \frac{D(T, Bu)}{2.5 - 1.5 \operatorname{erf}(P - 3)} \quad (2-162)$$

Where,

$D(T, Bu, P)$ = Diffusion constant adjusted for burnup and power, m²/s

$D(T, Bu)$ = Diffusion constant adjusted for burnup given by Equation 2-161, m²/s

P = Local radial node power, kW/ft

Gas Release

Gas release calculations are performed separately for restructured grains and non-restructured grains. For those nodes that contain both restructured and non-restructured grains, the releases from each are combined based on the relative amount of each type of grain.

For the restructured grains, it is assumed that, because the grains are so small, all the gas produced in the grain will diffuse out to the grain boundary. Therefore, the only gas that will remain in these grains at the end of the time step is the gas that is re-solved back into the grains.

The gas re-solved back into the grain is given by the resolution factor from Massih [Forsberg and Massih, 1985]. The gas that is in the grain for a given time step, i , is given by:

$$GG_i = GB_{i-1} \frac{f}{1 + f} \quad (2-163)$$

Where,

GG_i = Gas in grains, moles/m³

GB_i = Gas on grain boundaries, moles/m³

$$f = \frac{1.84 \times 10^{-14} a}{3D} \quad (2-164)$$

Where,

a = Grain radius, 0.075×10^{-6} m (for restructured grains)

D = Diffusion constant, m²/s

For the non-restructured grains, the same formulas as those in Massih are used to calculate diffusion from the grains except that the release is reduced to account for resolution during the calculation of release. The following terms are changed as follows:

From Equation 2-147, the following term is changed:

$$\sum f_n G_n (\tau_1) \rightarrow \frac{\sum f_n G_n (\tau_1)}{\text{resolterm}} \quad (2-165)$$

From Equation 2-149, the following term is changed:

$$\left[-\sum_{n=1}^4 \left(\frac{f_n A_n}{B_n} \right) + f(\tau) \right] \rightarrow \frac{\left[-\sum_{n=1}^4 \left(\frac{f_n A_n}{B_n} \right) + (\Delta\tau) \right]}{\text{resolterm}} \quad (2-166)$$

Where,

T = Temperature, K

and,

$$\text{resolterm} = \max \begin{cases} 0.14009 \exp(0.00282T), & T < 1528.77 \text{ K} \\ 22.976 - 0.0082T, & T \leq 1528.77 \text{ K} \end{cases} \quad (2-167)$$

In order for gas to be released from the grain boundaries, the saturation concentration must be reached. The saturation concentration is given by:

$$g_s = \frac{3N_s}{2a} \quad (2-168)$$

Where,

g_s = Grain boundary saturation concentration, mol/m³

N_s = Saturation area density given in Equation 2-155, mol/m²

a = Grain radius, m

When the grain boundary gas concentration for a given radial node exceeds the saturation value for the first time, all the gas on the grain boundary except 65% of the saturation value is released. From then on for that radial node, any gas above 65% of the saturation values is released.

As discussed, for radial nodes that contain some restructured grains and some non-restructured grains, the released gas is calculated as:

$$\Delta rel_{tot} = \Delta rel_1 (restructure^2) + \Delta rel_2 (1 - restructure^2) \quad (2-169)$$

Where,

Δrel_{tot} = Total release from a radial node, mol/m³

Δrel_1 = Release from restructured grains in a radial node, mol/m³

Δrel_2 = Release from non-restructured grains in a radial node, mol/m³

restructure = Fraction of restructured grains in radial node, unitless

As with the Massih model, an athermal release term of 1% for every 10 GWd/MTU beyond 40 GWd/MTU is added on if the predicted release is less than 5% to account for the observed gas release from rods with very low power at high burnup.

2.6.4.3 ANS-5.4 (1982) Gas Release Model

The ANS-5.4 [ANS, 1982] fractional FGR is calculated as a function of time and radial fuel temperature and axial burnup. The fuel is divided into radial and axial nodes according to the old 1982 ANS standard. A user requirement is that the time step sizes be such that the burnup increments do not exceed 2 GWd/MTU.

The modeling is divided into two main sections, one for release of stable isotopes and the other for release of short-lived isotopes. There are high- and low-temperature models for both the stable and radioactive fission products. The release is calculated using both the high-temperature and the low-temperature models, and the larger release value is used. Time steps should not exceed 50 d.

The ANS-5.4 FGR model [ANS, 1982] is incorporated as specified by the standard and will not be described in more detail in this document. The 1982 model is not an approved standard and provides a very conservative prediction of release in FAST, while the revised 2011 model [ANS, 2011] provides a less conservative prediction even at the 95/95 upper bound. The 1982 model is retained in FAST for compliance with various regulations.

2.6.4.4 ANS-5.4 (2011) Gas Release Model

The new ANS-5.4 standard was approved in 2011 and provides a methodology for determining the radioactive releases from fuel rods, and to determine radiological consequences of postulated accidents. The model is based on the assumption that no significant power transient will occur, such as RIAs. This model includes volatile and gaseous fission products of primary importance such as krypton, xenon, iodine, and cesium. The largest contributor to the equivalent dose to individuals is generally ¹³¹I, which is included in the model. The radioactive gaseous and volatile fission products are divided into three categories:

1. Short-lived radioactive nuclides with a half-life < 6 h

2. Long-lived radioactive nuclides with $6 \text{ h} < \text{half-life} < 60 \text{ d}$
3. Stable radioactive nuclides with $\text{half-life} > 60 \text{ d}$

This distinction is particularly important when considering diffusion processes that proceed slowly as compared to the decay time for the nuclides under consideration. The model presented in the ANS 5.4 2011 standard is applicable to short lived nuclides; a further distinction is applied in the standard for nuclides with a half-life smaller than 6 h, and nuclides with half-lives greater than 6 h but smaller than 60 d.

The first incarnation of the ANS-5.4 standard was first implemented in 1982 and it was originally based on the Booth diffusion model. The model coefficients were determined from the measured release data for xenon and krypton. Because of the lack of data for ^{131}I , the diffusion coefficient for this nuclide was assumed to be a factor of 7 higher than the one used for xenon and krypton. However, in the last twenty-five years, fuel experiments in test reactors have been performed and measured data have been used to validate the standard at higher burnups. Based on this data it was also concluded that the prediction for ^{131}I was overly conservative.

The FGR model from ANS 5.4 2011 [ANS, 2011] implements the model described in the standard and it calculates the release-to-birth ratio (R/B), or the so-called “gap release” for short-lived and long-lived nuclides, as defined by the standard. The short-lived and long-lived nuclides considered by the model are listed in Tables 2-9 and Table 2-10, respectively, together with their precursor coefficients and decay constants for radioactive nuclides. The nuclides are categorized as short lived if their half-life is less than 6 h, while they are considered long lived, if their half-life is greater than 6 h but less than 60 d.

Table 2-9. Decay constants and precursor coefficients for short-lived noble gases and iodines with half-life < 6 h

Nuclide	Precursor Coefficient (α)	Decay Constant
^{135m}Xe	23.5	7.55×10^{-4}
^{137}Xe	1.07	3.02×10^{-3}
^{138}Xe	1.00	8.19×10^{-4}
^{139}Xe	1.00	1.75×10^{-2}
^{85m}Kr	1.31	4.30×10^{-5}
^{87}Kr	1.25	1.52×10^{-4}
^{88}Kr	1.03	6.78×10^{-5}
^{89}Kr	1.21	3.35×10^{-3}
^{90}Kr	1.11	2.15×10^{-2}
$^{132}\text{I}^{(a)}$	137.0	8.44×10^{-5}
^{134}I	4.4	2.20×10^{-4}

As recommended by the standard, it should be noted that although ^{132}I is considered a short-lived isotope, it is modeled using the long-lived correlation due to the long decay time of ^{132}Te (3.2 d).

Table 2-10. Decay constants and precursor coefficients for long-lived noble gases and iodines with $6 \text{ h} < \text{half-life} < 60 \text{ d}$

Nuclide	Precursor Coefficient (α)	Decay Constant
^{131m}Xe	1.00	6.730×10^{-7}
^{133}Xe	1.25	1.527×10^{-6}
^{135}Xe	1.85	2.107×10^{-5}
^{131}I	1.00	9.973×10^{-7}
^{133}I	1.21	9.217×10^{-6}
^{135}I	1.00	2.864×10^{-5}

The release-to-birth ratios for short- and long-lived isotopes are defined in Equations 2-170 and 2-171, respectively.

$$\left(\frac{R}{B}\right)_{i,m} = \left(\frac{S}{V}\right)_{i,m} \sqrt{\frac{\alpha_{\text{nuclide}} D_{i,m}}{\lambda_{\text{nuclide}}}} \quad (2-170)$$

$$\left(\frac{R}{B}\right)_{i,nuclide} = F_{nuclide} \left(\frac{S}{V}\right)_{i,m} \sqrt{\frac{\alpha_{(Kr-85m)} D_{i,m}}{\lambda_{(Kr-85m)}}} \quad (2-171)$$

Where,

$\frac{R}{B}$ = Release-to-birth ratio

$\frac{S}{V}$ = Surface-to-volume ratio, 1/cm

$\alpha_{i,m}$ = Precursor coefficient

$\lambda_{i,m}$ = Decay constant, 1/s

D = Diffusion coefficient, cm²/s

$F_{nuclide}$ = Nuclide scaling factor

The nuclide scaling factor ($F_{nuclide}$) is calculated using Equation 2-172.

$$F_{nuclide} = \left(\frac{\alpha_{nuclide} \lambda_{(Kr-85m)}}{\lambda_{nuclide} \alpha_{(Kr-85m)}}\right)^{0.25} \quad (2-172)$$

The diffusion coefficient (D) is calculated using Equation 2-173.

$$D = 7.6 \times 10^{-7} \exp\left(\frac{-35000.0}{T}\right) + 1.41 \times 10^{-18} \sqrt{F} \exp\left(\frac{-13800.0}{T}\right) + 2.0 \times 10^{-30} F \quad (2-173)$$

Where,

F = Fission rate, fissions/cm³-s

T = Local fuel temperature, K

The surface-to-volume ratio ($\frac{S}{V}$) is dependent on the temperature at which bubbles become interlinked to grain boundaries. The linkage temperature (T_{link}) is dependent on the pellet average burnup at the local axial node. The linkage temperature is calculated using Equation 2-174 and the corresponding surface-to-volume ratio is calculated using Equation 2-175.

$$T_{link} = \begin{cases} 5000.0, & Bu \leq 0.01 \text{ MWd/kgU} \\ \frac{9800.0}{\ln(176.0Bu)} + 273.15, & 0.01 \text{ MWd/kgU} < Bu \leq 18.2 \text{ MWd/kgU} \\ 1434.0 - 12.85Bu + 273.15, & Bu > 18.2 \text{ MWd/kgU} \end{cases} \quad (2-174)$$

$$\frac{S}{V} = \begin{cases} 120.0, & T \leq T_{link} \\ 650.0, & T > T_{link} \end{cases} \quad (2-175)$$

Where,

T_{link} = Linkage temperature, K

T = Local fuel temperature, K

Bu = Pellet average burnup, MWd/kgU

In addition to short- and long-lived, there are also “stable” radioactive isotopes as defined by the standard that are calculated based on the stable krypton release. In FAST, the stable krypton release is calculated using the Massih model, with the assumption that all the Kr release predicted by the Massih model is ^{85}Kr . The 2011 standard also recommends to multiply the diffusion coefficient of ^{85}Kr by a factor of 2 to calculate the Cs release. As recommended in [Beyer and Clifford, 2011], due to the approximation that release is proportional to the square root of the diffusion coefficient, the calculated value for ^{85}Kr release is multiplied by $(\sqrt{2})$ to obtain the release for ^{134}Cs and ^{137}Cs . The stable radioactive isotopes and their half-lives are shown in Table 2-11.

Table 2-11. Decay constants for gases with half-life > 60 d

Nuclide	Half-Life (y)
^{85}Kr	10.76
^{134}Cs	2.07
^{137}Cs	30.10

General notes when using the ANS-2011 Model:

- The ANS-2011 standard requires at least 11 axial meshes in order to accurately predict the FGR.
- The ANS-2011 standard recommends multiplying the best estimate predictions of short and long-lived radioisotopes by a factor of 5.0 to obtain upper tolerance gap inventories. FAST provides the best estimate predictions only.

2.6.5 Transient Gas Release

The transient release of fission gas is highly dependent on the location of the gas in the fuel pellet, both radially, and in each radial node the location (in the grains versus on the grain boundaries) of the gas. Because of this, the transient gas release model in FAST-1.1 may only be used if initialized with the FRAPFGR model. This model has been developed specifically to predict the location of

fission gas within the pellets. This transient release model is a burst release (not diffusion release) model as described below:

- All grain boundary gas for a given radial node is released when the temperature exceeds 2000 °F (1093 °C).
- All gas in the restructured grains (matrix) of the high burnup structure for a given radial node is released when the temperature exceeds 3300 °F (1816 °C).
- 5% of the gas in the un-restructured grains (matrix) for a given radial node is released when the temperature exceeds 3300 °F (1816 °C).

This release model was developed to predict the measured release data from RIA experimental tests in CABRI and NSRR. (See data comparisons in [[Luscher and Geelhood, 2014](#)]).

2.6.6 Nitrogen Release

The release of nitrogen initially present in fuel material from fabrication occurs as a result of a diffusion transport mechanism. The release of nitrogen affects the rod internal pressure and the gas conductivity. The model proposed by [[Booth, 1957](#)] is used, given the following: assumptions:

- The initial concentration of diffusing substance, C , is uniform throughout a sphere of radius, a .
- Transport of material does not occur from the external phase (gaseous nitrogen) back into the initial carrier medium.

The governing equation is:

$$r \frac{\partial C}{\partial t} = D \left(\frac{\partial^2}{\partial r^2} (Cr) \right) \quad (2-176)$$

Where,

r = Radial location, m

C = Concentration of diffusing substance

t = Time, s

D = Diffusion coefficient, m²/s

With the following boundary conditions:

$$C = \begin{cases} 0, & \text{at } r = a \\ C, & \text{at } t = 0 \end{cases} \quad (2-177)$$

By applying a series solution method, the fractional release of the diffusing substance (nitrogen) can be approximated based on the value of B :

$$B = \pi^2 \frac{D_{N_2}}{a^2} t \quad (2-178)$$

Where,

$\frac{D_{N_2}}{a^2}$ = Temperature-dependent diffusion coefficient for nitrogen divided by the effective diffusion radius squared 1/s (Equation 2-180)

t = Time from the start of diffusion, s

The fraction of nitrogen released (F_{N_2}) as of time (t) is shown in Equation 2-179:

$$F_{N_2} = \begin{cases} 6\sqrt{\left[\frac{D_{N_2}}{a^2} \frac{t}{\pi}\right]} - 3\frac{D_{N_2}}{a^2} t, & B \leq 1 \\ 1 - \frac{6e^{-B}}{\pi^2}, & B > 1 \end{cases} \quad (2-179)$$

From the experimental data of [Ferrari, 1963] and [Ferrari, 1964]:

$$\frac{D_{N_2}}{a^2} = 1.73 \exp\left(\frac{33400}{1.9869T}\right) \quad (2-180)$$

Where,

T = Temperature, K

2.6.7 Helium Production and Release

2.6.7.1 Steady-state Production

Helium is produced at different rates in UO₂ and MOX. The release of helium affects the rod internal pressure and the gas conductivity.

For UO₂, helium production is given by:

$$He_{prod} = 1.297 \times 10^{-18} Q \times t \times SA \times PR \quad (2-181)$$

Where,

He_{prod} = Helium produced for a given axial node, mol

Q = Surface heat flux, W/m²

t = Time, s

SA = Axial node surface area, m²

PR = Fission gas production rate, atoms/100-fissions

For MOX, a formula has been developed as a function of Pu concentration (Pu) and burnup (Bu , in GWd/MTU):

$$He_{prod} = (A_1Pu + A_2) Bu^2 + (B_1Pu + B_2) Bu \tag{2-182}$$

Table 2-12 shows the fitting parameters that should be used for reactor-grade plutonium and weapons-grade plutonium.

Table 2-12. Fitting parameters for helium in MOX

Parameter	Reactor-Grade Plutonium	Weapons-Grade Plutonium
A_1	1.5350×10^{-4}	-2.4360×10^{-4}
A_2	2.1490×10^{-3}	3.6059×10^{-3}
B_1	-2.9080×10^{-3}	3.3790×10^{-3}
B_2	9.7223×10^{-2}	5.3658×10^{-2}

The above equations calculate the amount of helium produced as a function of time. In order to calculate the helium released to the void volume, an approach similar to the approach for nitrogen release is used. By applying a series solution method, the fractional release of the diffusing substance (helium) can be approximated based on the value of B :

$$B = \pi^2 \frac{D_{He} t}{a^2} \tag{2-183}$$

Where,

$\frac{D_{He}}{a^2}$ = Temperature dependent diffusion coefficient for helium divided by the effective diffusion radius squared, 1/s

t = Time from the start of diffusion, s

If $t \leq \frac{1}{\pi^2 \frac{D_{He}}{a^2}}$ then the fraction of helium released, F_{He} , as of time, t , equals

$$F_{He} = 4 \sqrt{\left[\frac{D_{He} t}{a^2} \frac{1}{\pi} \right]} - \frac{3D_{He} t}{2a^2} \quad (2-184)$$

If this fraction is greater than 0.57, then, when $B < 1$, the fraction of helium released as a function of time, t , equals

$$F_{He} = 1 + \frac{0.607927e^{-B} - 0.653644}{B} \quad (2-185)$$

and, when $B > 1$,

$$F_{He} = 1 \quad (2-186)$$

When $t > \frac{1}{\pi^2 \frac{D_{He}}{a^2}}$, the fraction of helium released is equal to that shown in Equations 2-185 and 2-186. The diffusion coefficient of helium divided by the effective radius squared is shown in Equation 2-187.

$$\frac{D_{He}}{a^2} = \begin{cases} 0.452847 \times 10^{-10}, & T \leq 873 \text{ K} \\ 0.28 \times 10^{-5} \exp\left(\frac{4.0 \times 10^4}{1.986} \left(\frac{1}{1673} - \frac{1}{T}\right)\right) & T > 873 \text{ K} \end{cases} \quad (2-187)$$

2.6.7.2 Integral Fuel Burnable Absorber Production

Some fuel designs use a thin layer of ZrB₂ applied to the surface of the pellets to act as an IFBA. The use of such coatings produces a large amount of helium. The following empirical correlation was fit to results from Monte Carlo N-Particle (MCNP), a neutron transport code, for helium production from IFBA liners.

$$He_{prod} = -(A_1 IFBA + A_2) B10^2 + (B_1 IFBA + B_2) B10 \quad (2-188)$$

Where,

He_{prod} = Helium production, atoms He/cm³-s

IFBA = Percent of fuel rods in a core containing IFBA liners, % (valid only between 10 and 50%)

B10 = ¹⁰B enrichment, % (valid from 0 to 90%)

$A_1 = 6.23309 \times 10^{-9}$

$$A_2 = 7.02006 \times 10^{-7}$$

$$B_1 = -1.35675 \times 10^{-7}$$

$$B_2 = 3.1506 \times 10^{-4}$$

It can be seen from Equation 2-188 that the helium production rate is a function of the number of IFBA rods in a core and the ^{10}B enrichment. Helium is produced as the ^{10}B burns out until there is no more ^{10}B in the liner. The rate of ^{10}B depletion is equal to the helium production rate. The depletion of ^{10}B is calculated in the code and the remaining ^{10}B enrichment, B_{10} in Equation 2-188, at the end of the time step is used to calculate the helium production for the next time step. It is assumed in the code that all helium produced in the ZrB_2 coatings is released directly to the rod-free volume.

2.6.8 Metallic Fuel Fission Gas Release Model

FAST was primarily developed for oxide fuel but the capability to model metallic fuel has also been included. Most of the changes are reflected in the use of material properties for metallic fuel and are described in MatLib [Geelhood et al., 2022a]; however, the mechanisms that drive fission gas release behavior are profoundly different for metal fuel than for oxide fuel. In general, the diffusivity of fission gas in metal is much greater than in oxide which leads to the situation where the majority of the fission gas produced in the pellets or slugs is released to the rod void volume. For this reason, metallic fuel is often designed with a large plenum region to accommodate this gas.

There has been considerably less focus on understanding the mechanisms of FGR in metallic fuel than in oxide fuel. So, in FAST, the FGR model for metallic fuel is simply an empirical fit to measured released fraction as a function of burnup. Current data indicates that this approach will result in reasonable predictions of FGR.

The model included in FAST is described by:

$$FGR = \begin{cases} 0, & burnup \leq 0.8 \text{ at\%} \\ \frac{1}{0.000727} \ln\left(\frac{burnup - 0.8}{0.0345}\right), & 0.8 \text{ at\%} < burnup \leq 7.4 \text{ at\%} \\ 0.722, & burnup > 7.4 \text{ at\%} \end{cases} \quad (2-189)$$

Where,

FGR = fission gas release, fraction

$burnup$ = burnup, at% (Note: 1 GWd/MTU = 0.1066 at%)

Based on the spread of the data, a relative standard error of 6.7% has been calculated for this model. The FGR model, available data from U-10Zr, U-8Pu-10Zr, and U-19Pu-10Zr fuel [Pahl et al., 1992], and 2σ bounds are shown in Figure 2-34.

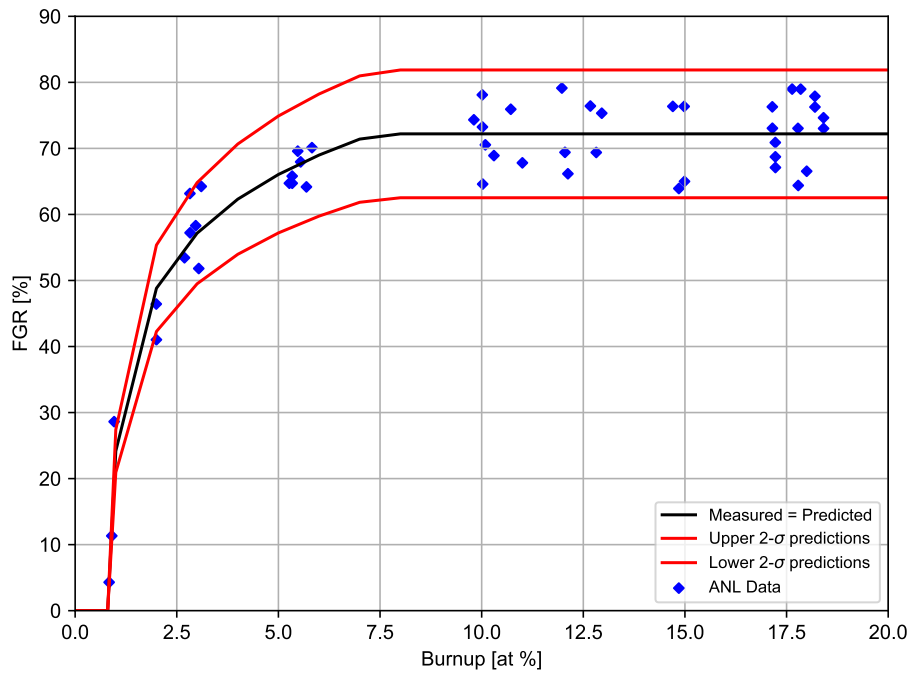


Figure 2-34. FAST metallic fuel FGR model and available data

2.7 Corrosion and Hydrogen Pickup

There are two types of corrosion models in FAST-1.1: corrosion under normal LWR operating conditions and under high temperature steam-oxidation.

2.7.1 LWR Waterside Corrosion Models

2.7.1.1 PWR Conditions

For Zircaloy-4 under PWR conditions, a cubic rate law for corrosion-layer thickness as a function of time is applied until a transition thickness is attained [Garzarolli et al., 1982]:

$$\frac{ds}{dt} = \frac{A}{s^2} \exp\left(-\frac{Q_1}{RT_1}\right) \quad (2-190)$$

In FAST-1.1, this equation is integrated without regard to the feedback between oxide layer thickness and oxide metal interface temperature to obtain:

$$s_{i+1} = \left(3A \exp\left(-\frac{Q_1}{RT_1}\right) (t_{i+1} - t_i) + s_i^3\right)^{\frac{1}{3}} \quad (2-191)$$

Where,

$i, i + 1$ = Refers to beginning (i) and end ($i + 1$) of current time step

s = Oxide thickness, μm

$A = 6.3 \times 10^9 \mu\text{m}^3/\text{day}$

Q_1 = Activation energy (see Table 2-13)

$R = 1.98 \text{ cal/mol-K}$

T_1 = Metal-oxide interface temperature, K

t = Time, days

Table 2-13. Enthalpy and transition thicknesses under PWR conditions [Garzarolli et al., 1982]

Cladding Type	Q_1 cal/mol	Q_2 cal/mol	Transition Thickness μm
Zircaloy-4	32289	27354	2
M5	27446	29816	7
ZIRLO	32289	27080	2
Optimized ZIRLO	32289	27354	2

After the transition thickness is attained, a flux-dependent linear rate law is applied, with the rate constant being an Arrhenius function of oxide-metal interface temperature:

$$\frac{ds}{dt} = \left(C_0 + U (M\phi)^P \right) \exp \left(-\frac{Q_2}{RT_1} \right) \quad (2-192)$$

Because there is significant feedback between oxide-layer thickness and oxide-metal interface temperature, the oxide thickness is converted to weight gain, and the approximate integral solution from [Garzarolli et al., 1982] is used. This solution has the form:

$$\Delta w_{i+1} = \Delta w_i + \frac{RT_0^2 \lambda}{\gamma Q_2 q''} \ln \left[1 - \frac{\gamma Q_2 q''}{RT_0^2 \lambda} k_0 \exp \left(\frac{-Q_2}{RT_0} + \frac{\gamma Q_2 q'' \Delta w_i}{RT_0^2 \lambda} \right) (t_{i+1} - t_i) \right]^{-1} \quad (2-193)$$

Weight gain can be converted to thickness using the following formula:

$$s = \frac{\Delta w \gamma}{100} \quad (2-194)$$

Where,

$i, i + 1$ = Refers to beginning (i) and end ($i + 1$) of current time step

s = Oxide thickness, m

Δw = Weight gain, g/cm²

R = Universal gas constant, 1.98 cal/mol-K

T_0 = Oxide-to-water interface temperature, K

λ = Oxide thermal conductivity, W/cm-K

γ = 0.6789 cm³/g

Q_2 = See Table 2-13

q'' = Heat flux, W/cm²

$k_0 = 11863 + 3.5 \times 10^4 (1.91 \times 10^{-15} \phi)^{0.24}$

ϕ = Fast neutron flux ($E > 1$ MeV), n/cm²/s

t = Time, days

Above the transition thickness, if the oxide thickness is less than 80 μm then use $2\Delta w_i$ in Equation 2-194 and then divide the second term of Equation 2-193 by 2 as shown in Equation 2-195.

$$\Delta w_{i+1} = \Delta w_i + \frac{RT_0^2 \lambda}{2\gamma Q_2 q''} \ln \left[1 - \frac{\gamma Q_2 q''}{RT_0^2 \lambda} k_0 \exp \left(\frac{-Q_2}{RT_0} + \frac{\gamma Q_2 q'' 2\Delta w_i}{RT_0^2 \lambda} \right) (t_{i+1} - t_i) \right]^{-1} \quad (2-195)$$

2.7.1.2 BWR Conditions

For Zircaloy-2 under BWR conditions, a flux-dependent linear rate law is applied, with the rate constant being an Arrhenius function of oxide-metal interface temperature:

$$\frac{ds}{dt} = K \exp \left(-\frac{Q}{RT_1} \right) \left[1 + Cq'' \exp \left(\frac{Q}{RT_1} \right) \right] \quad (2-196)$$

Because there is significant feedback between oxide-layer thickness and oxide-metal interface temperature, the oxide thickness is converted to weight gain (as shown in Equation 2-194), and the approximate integral solution from [Garzarolli et al., 1982] is used. This solution has the form

$$\Delta w_{i+1} = \Delta w_i + \frac{RT_0^2 \lambda}{\gamma Q q''} \ln \left[1 - \frac{\gamma Q q''}{RT_0^2 \lambda} k \exp \left(\frac{-Q}{RT_0} + \frac{\gamma Q q'' \Delta w_i}{RT_0^2 \lambda} \right) (t_{i+1} - t_i) \right]^{-1} + Ck (t_{i+1} - t_i) q'' \quad (2-197)$$

Where,

$i, i + 1$ = Refers to beginning (i) and end ($i + 1$) of current time step

s = Oxide thickness, m

Δw = Weight gain, g/cm²

R = Universal gas constant, 1.98 cal/mol-K

T_0 = Oxide-to-water interface temperature, K

λ = Oxide thermal conductivity, W/cm-K

γ = 0.6789 cm³/g

Q = Activation energy, 27350 cal/mol

q'' = Heat flux, W/cm²

k = 11800 g/cm²-day

Φ = Fast neutron flux ($E > 1$ MeV), n/cm²-s

C = 2.5×10^{-16} m²/W

t = Time, days

To achieve numerical stability, the rate equation is integrated across each time step and applied to calculated corrosion layer increments per time step, which are accumulated to calculate cumulative layer thickness as a function of axial position (axial node) along the fuel rod.

2.7.2 Hydrogen Pickup Fraction

The fraction of the hydrogen liberated by the metal-water corrosion reaction that is absorbed locally by the cladding is called the pickup fraction. For PWR conditions, a constant hydrogen pickup fraction has been found to be applicable. Table 2-14 lists the hydrogen pickup fraction for the claddings available in FAST.

Table 2-14. Hydrogen pickup fraction under PWR conditions [Geelhood and Beyer, 2011]

Cladding Type	Pickup Fraction
Zircaloy-4	0.15
M5	0.10
ZIRLO	0.175
Optimized ZIRLO	0.175

For BWR conditions, a constant hydrogen pickup fraction does not fit the observed hydrogen concentration data. Therefore, FAST-1.1 uses a burnup-dependent hydrogen concentration model

[Geelhood and Beyer, 2008]. For Zircaloy-2 prior to 1998 (when the vendors did not have tight control over concentration and second-phase precipitate particle size), Equation 2-198 is used.

$$H_{conc} = \begin{cases} 47.8 \exp\left(-\frac{1.3}{1 + Bu}\right) + 0.316Bu & Bu < 50 \text{ GWd/MTU} \\ 28.9 + \exp(0.117(Bu - 20)) & Bu \geq 50 \text{ GWd/MTU} \end{cases} \quad (2-198)$$

For modern Zircaloy-2 since 1998 (when the vendors have had tight control over concentration and second phase precipitate particle size), Equation 2-199 is used.

$$H_{conc} = 22.8 + \exp(0.117(Bu - 20)) \quad (2-199)$$

Where,

H_{conc} = Hydrogen concentration, ppm

Bu = Local burnup, GWd/MTU

2.7.3 High-Temperature Corrosion

In FAST, the initial oxide thickness from in-reactor behavior is calculated using the previously described correlations, or input to the code. During a reduced-cooling, high-temperature transient, such as LOCA, the cladding temperature can become very hot relative to steady-state operations. Under these circumstances, a large corrosion layer could form in a matter of seconds to minutes. This corrosion layer both erodes the structural thickness of the cladding and produces excess energy term resulting from the exothermic Zirconium-Water reaction. FAST contains two high-temperature corrosion models, the Cathcart-Pawel model [Cathcart et al., 1977] and the Baker-Just model [Baker and Just, 1962], that are selected using the input variable `modmw`. In addition, the option exists to not model high-temperature corrosion. Guidance on model selection is given in the input instructions shown in Appendix B.

The Cathcart-Pawel (default) model is activated in FAST-1.1 when the cladding temperature exceeds 1073 K (800 °C). The Baker-Just model is activated in FAST-1.1 when the cladding temperature exceeds 1000 K (727 °C). These models are described below.

Both the Cathcart-Pawel and Baker-Just models are of the following form:

$$\frac{dK}{dt} = \frac{1}{K} A \exp\left(\frac{-B}{RT}\right) \quad (2-200)$$

Where,

K = Oxide thickness, m

t = Time, s

T = Temperature, K

A, B, R = Constants (see Table 2-15)

This equation can be integrated and rearranged to the following form:

$$K_2 = \sqrt{K_1^2 + 2A \exp\left(\frac{-B}{RT}\right) \Delta t} \tag{2-201}$$

Where,

K_1 = Oxide thickness at beginning of time step, m

K_2 = Oxide thickness at end of time step, m

Table 2-15 shows the parameters that are used for the Cathcart-Pawel and Baker-Just models.

Table 2-15. Constants for Cathcart-Pawel and Baker-Just models

Constant	Cathcart-Pawel	Baker-Just
A	$1.126 \times 10^{-6} \text{ m}^2/\text{s}$	$9.415 \times 10^{-5} \text{ m}^2/\text{s}$
B	$1.502 \times 10^5 \text{ J/mol}$	$4.550 \times 10^4 \text{ cal/mol}$
R	8.314 J/mol-K	1.987 cal/mol-K

For the Cathcart-Pawel model, the user can specify that the weight gain be calculated assuming perfect stoichiometry of the oxide, or by assuming a stoichiometric gradient `iStoicGrad`. It can be seen from Equation 2-200 that the rate of oxidation is inversely proportional to the oxide layer thickness. In FAST there are two ways of treating the initial oxide thickness layer that are selected using the input variable `ProtectiveOxide`. If `ProtectiveOxide = .TRUE.`, the initial oxide from steady state is included with the high temperature oxidation, so the rate of oxidation for a previously oxidized rod is lower than for a rod with no oxide. If `ProtectiveOxide = .FALSE.`, the initial oxide from steady-state is not included with the high-temperature oxidation, so the rate of oxidation for a previously oxidized rod is the same as the rate for a rod with no oxide.

FAST calculates the oxidation of the outer rod surface and, if the inner cladding surface is in contact with steam (i.e., the rod has burst), the oxidation of the inner rod surface. From these ID and OD oxide layer thicknesses, FAST calculates the oxygen-stabilized alpha layer, the oxygen uptake, the metal water reactor energy, and equivalent cladding reacted (ECR). For the stress calculations, FAST reduces the wall thickness based on the thinning from the oxide layer growth. No strength is attributed to the oxide layer. FAST-1.1 includes an option to calculate ID oxidation regardless of rupture above a specified burnup `BuOxide`.

2.8 Transient Options

The development of FAST was focused around the merger of the transient capabilities from FRAP-TRAN-2.0 coupled with the steady-state capabilities of FRAPCON-4.0. A set of “transient” input options allow the user to control the time-dependent thermal/mechanical code solution and transient fuel rod models. These options are described in Section B.6. The transient code solution control is based on the problem time step size (and code output intervals) and convergence criteria. The recommended time step size to be used is outlined in Table 2-16.

Table 2-16. Recommended time steps for various transients

Transient/Accident	Period of Transient/Accident	Time Step s
Steady-state equilibrium	–	0.0 ^(a)
Large break loss-of-coolant accident (LBLOCA)	Blowdown	0.2
LBLOCA	Reflood	0.5
Small break loss-of-coolant accident (SBLOCA)	Prior to SCRAM	0.2
SBLOCA	Adiabatic heatup	2.0
SBLOCA	Quenching	0.5
RIA	During power pulse	1.0×10^{-5}
Anticipated transient without SCRAM (ATWS)	–	0.2

^(a) Will default to using the steady-state solution.

The model options in the `transient` input block define the high temperature cladding oxidation model, the high temperature cladding deformation (ballooning) model, and the time step size control.

2.9 Heat Conduction and Temperature Solution

Once values for the heat generation, gap conductance, and cladding surface temperature have been obtained, the complete temperature distribution in the fuel and cladding is obtained by applying the law for heat conduction in solids in one dimension.

2.9.1 One-Dimensional Radial Steady-State Heat Conduction

$$\int_S k(\bar{x}, T) \bar{\nabla} T d\bar{s} = \int_V S(\bar{x}) dV \quad (2-202)$$

Where,

T = Temperature, K

\bar{x} = Spatial coordinate, m

S = Heat source, W/m³

k = Thermal conductivity, W/m-K

2.9.2 One-Dimensional Radial Transient Heat Conduction

Heat conduction in the radial direction in both the fuel and cladding is described by Equation 2-203.

$$\int_V \rho(\bar{x}, T) c_p(\bar{x}, T) \frac{\partial T}{\partial t} dV = \int_S k(\bar{x}, T) \bar{\nabla} T d\bar{s} + \int_V S(\bar{x}) dV \quad (2-203)$$

Where,

T = Temperature, K

\bar{x} = Spatial coordinate, m

t = Time, s

S = Heat source, W/m³

c_p = Specific heat, J/kg-K

ρ = Density, kg/m³

k = Thermal conductivity, W/m-K

The first integral calculates the enthalpy change of an arbitrary infinitesimal volume, V , of material, the second the heat transfer through the surface, S , of the volume, and the third the heat generation within the volume. The parameters c_p and k are temperature dependent. The fuel thermal conductivity is also burnup dependent. The following boundary conditions in Equations 2-204 and 2-205 are used with Equation 2-203:

$$\left. \frac{\partial T}{\partial t} \right|_{r=0} = 0 \quad (2-204)$$

$$T \Big|_{r=0} = T_s \quad (2-205)$$

Where,

r = Radial position, m

r_0 = Outer radius of fuel, m

T_s = Fuel rod outer surface temperature, K

Equation 2-203 is numerically solved by using an implicit finite difference approximation. The solution method is taken from the HEAT-1 code [Wagner, 1963]. The solution method accounts for temperature- and time-dependent thermal properties; transient spatially varying heat generation; and melting and freezing of the fuel and cladding.

With Figure 2-35 as a reference for geometry terms, the finite difference approximation for heat conduction is shown in Equation 2-206.

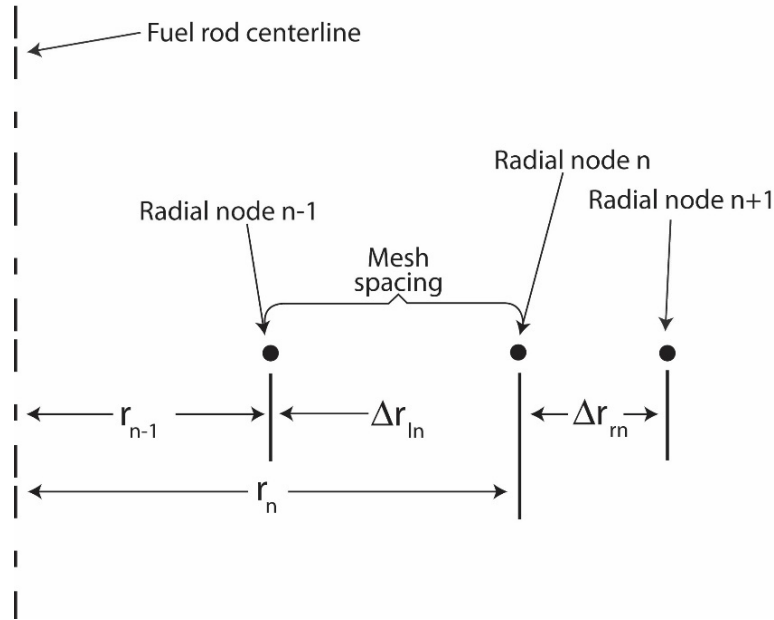


Figure 2-35. Description of geometry terms in finite difference equations for 1-D radial heat conduction

$$\frac{(T_n^{m+1} + T_n^m) (c_{ln}h_{ln}^V + c_{rn}h_{rn}^V)}{\Delta t} = - \left(T_n^{m+\frac{1}{2}} - T_{n-1}^{m+\frac{1}{2}} \right) k_{ln}h_{ln}^S + \left(T_{n+1}^{m+\frac{1}{2}} - T_n^{m+\frac{1}{2}} \right) k_{rn}h_{rn}^S + Q_{ln}h_{ln}^V + Q_{rn}h_{rn}^V \quad (2-206)$$

Where,

T_n^{m+1} = Temperature at radial node n and time point $m + 1$, K

$T_n^{m+\frac{1}{2}}$ = $0.5(T_n^m + T_n^{m+1})$

t = Time step, s

c_{ln} = Volumetric heat capacity on left side of node n , J/m³-K

c_{rn} = Volumetric heat capacity on right side of node n , J/m³-K

k_{ln} = Thermal conductivity at left side of node n , W/m-K

k_{rn} = Thermal conductivity at right side of node n , W/m-K

h_{ln}^V = Volume weight of mesh spacing on left side of radial node n , m² = $\pi r_{ln} (r_n - \frac{r_{ln}}{4})$

h_{rn}^V = Volume weight on right side of node n = $\pi r_{rn} (r_n + \frac{r_{rn}}{4})$, m²

h_{ln}^S = Surface weight on left side of node n $\frac{2\pi}{r_{ln}} (r_n - \frac{r_{ln}}{2})$

Q_{ln} = Heat generation per unit volume for mesh spacing on left side of radial node n , W/m³

Q_{rn} = Heat generation per unit volume for mesh spacing on right side of radial node n , W/m³

If a phase change from solid to liquid or liquid to solid occurs at radial node n , Equation 2-206 is modified as shown in Equation 2-207 to account for the storage or release of the heat of fusion while the temperature remains equal to the melting temperature.

$$\rho H (h_{ln}^V + h_{rn}^V) \frac{d\alpha_n^{m+\frac{1}{2}}}{dt} = - \left(T_L - T_{n-1}^{m+\frac{1}{2}} \right) k_{ln} h_{ln}^S + \left(T_{n+1}^{m+\frac{1}{2}} - T_L \right) k_{rn} h_{rn}^S + Q_{ln}^{m+\frac{1}{2}} h_{ln}^V + Q_{rn}^{m+\frac{1}{2}} h_{rn}^V \quad (2-207)$$

Where,

$\frac{d\alpha_n^{m+\frac{1}{2}}}{dt}$ = Rate of change of volume fraction of material melted in the two half-mesh spaces on either side of radial node n during the midpoint of the time step, s⁻¹

H = Heat of fusion of the material, J/kg

T_L = Melting temperature of the material, K

The phase change from solid to liquid is complete when:

$$\sum_{m=M_1}^{M_2} \frac{d\alpha_n^{m+\frac{1}{2}}}{dt} t^m = 1 \quad (2-208)$$

Where,

M_1 = Number of time step at which melting started

M_2 = Number of time step at which melting ends

t^m = Size of m^{th} time step, s

The finite difference approximations at each radial node are combined together to form one tri-diagonal matrix equation. The equation has the form:

$$\begin{bmatrix} b_1 & c_1 & 0 & 0 & \dots & 0 \\ a_2 & b_2 & c_2 & 0 & \dots & 0 \\ 0 & a_3 & b_3 & c_3 & \dots & 0 \\ \vdots & \dots & \ddots & \ddots & \ddots & \vdots \\ \vdots & \dots & 0 & a_{N-1} & b_{N-1} & c_{N-1} \\ 0 & \dots & \vdots & 0 & a_N & b_N \end{bmatrix} \begin{bmatrix} T_1^{m+1} \\ T_2^{m+1} \\ T_3^{m+1} \\ \vdots \\ T_{N-1}^{m+1} \\ T_N^{m+1} \end{bmatrix} = \begin{bmatrix} d_1 \\ d_2 \\ d_3 \\ \vdots \\ d_{N-1} \\ d_N \end{bmatrix} \quad (2-209)$$

Equation 2-209 is solved by Gaussian elimination for the radial node temperatures. Because the off-diagonal elements are negative and the sum of the diagonal elements is greater than the sum of the off-diagonal elements, little roundoff error occurs as a result of using Gaussian elimination. When the forward reduction step of Gaussian elimination has been applied, the last equation in the transformed equation is:

$$AT_N^{m+1} + B = q_N^{m+1} \quad (2-210)$$

Where,

T_N^{m+1} = Cladding surface temperature, K

q_N^{m+1} = Cladding surface heat flux, W/m²

A, B = Coefficients that are defined in Section 3.1

Equation 2-210 is combined with the correlation for convective heat transfer to solve for the cladding surface temperature, as previously shown in Figure 2-35.

The description of the calculations for the temperature distribution in the fuel and cladding is complete at this point. The calculation of the temperature of the gas in the fuel rod plenum is then needed to complete the solution for the fuel rod temperature distribution. This calculation is performed by a separate model and is described in Section 2.4.

2.10 Cladding Failure Models

FAST has two principle models that are used to predict when cladding failure happens. The first failure model is applicable mainly to RIA events where deformation is due to PCMI (fuel expansion into the cladding) and the temperature of the cladding is relatively low (<700 K). The second failure model is applicable mainly to LOCA events, but may also be experienced under certain RIAs,

where deformation is due to a high pressure difference across the cladding (high internal gas pressure with low external rod pressure) coupled with high cladding temperature (<700 K). In either case, when the code predicts cladding failure, the internal gas is assumed to become steam and the cladding inner surface will oxidize for axial nodes 1.5 in above and below the failed node.

2.10.1 Low-Temperature PCMI Cladding Failure Model

At low temperature, where PCMI is the driving force for cladding deformation, a model based on uniform plastic elongation from irradiated cladding [Geelhood et al., 2008] is used as the failure criteria. This model is a function of temperature and hydrogen concentration and is described below.

$$UE = \begin{cases} \min(UE_0, UE_{Hex}), & H_{ex} < 650 \text{ ppm} \\ 5\%, & H_{ex} \geq 650 \text{ ppm} \end{cases} \quad (2-211)$$

Where,

UE = Uniform plastic elongation, %

$UE_0 = 2.2\%$

and,

$$UE_{Hex} = \begin{cases} UE_0, & H_{ex} = 0 \text{ ppm} \\ AH_{ex}^{-p}, & H_{ex} > 0 \text{ ppm} \end{cases} \quad (2-212)$$

$$A = \begin{cases} 1211e^{-0.00927T}, & T < 700 \text{ K} \\ 1.840803, & T \geq 700 \text{ K} \end{cases} \quad (2-213)$$

$$p = \begin{cases} 1.355231 - 0.001783T, & T < 700 \text{ K} \\ 0.107131, & T \geq 700 \text{ K} \end{cases} \quad (2-214)$$

$$H_{ex} = \max(0, H_{Tot} - H_{Sol}) \quad (2-215)$$

$$H_{Sol} = 1.2 \times 10^5 \exp\left(\frac{-8550}{1.985887T}\right) \quad (2-216)$$

Where,

H_{Tot} = Total hydrogen in cladding, ppm

T = Temperature, K

If the predicted plastic hoop stress for any axial node exceeds the model prediction of uniform elongation based on the hydrogen concentration and average cladding temperature at that axial node, the code assumes the cladding has failed at that node. The cladding average temperature is taken as the average of each of the cladding radial node temperatures. A plot of predicted minus measured uniform plastic elongation data provided in Figure 2-36 as a function of excess hydrogen (H_{ex}) demonstrates that the uniform elongation model provides a reasonable fit as a function of excess hydrogen level (hydrogen above the solubility limit) in the cladding.

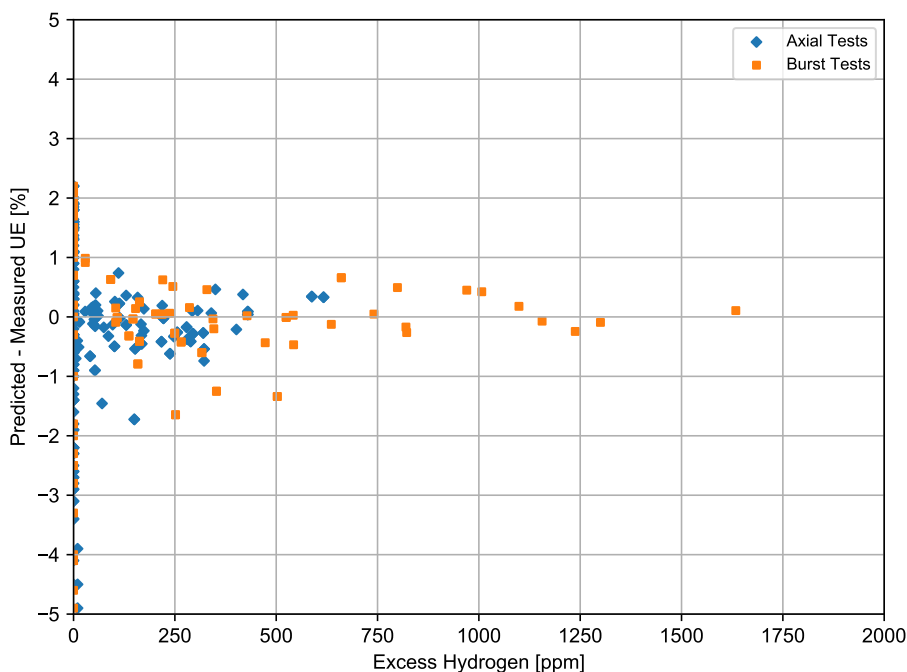


Figure 2-36. Predicted minus measured uniform elongation from irradiated samples from the PNNL database as a function of excess hydrogen ($293\text{ K} \leq T \leq 795\text{ K}$ and $0 \leq \Phi \leq 14.0 \times 10^{25}\text{ n/m}^2$)

Further comparisons to the uniform elongation data are provided in [Geelhood et al., 2008]. It is noted that this failure model was not adjusted to fit RIA data and does a good job predicting failure and non-failure in RIA tests [Luscher and Geelhood, 2014].

2.10.2 High-Temperature Cladding Ballooning Failure Model

In the case of a LOCA, the cladding can fail by ballooning and burst. The BALON2 model is used to model the ballooning in the cladding. FAST contains empirical stress and strain limits that it uses to predict when cladding failure will occur. These limits are discussed in detail in Section 2.5.2.

2.11 Coolant Conditions

If the user chooses to model the coolant as water, the fuel rod cooling model calculates the amount of heat transfer from the fuel rod to the surrounding coolant. The model calculates the heat transfer

coefficient, surface heat flux, and temperature at the cladding surface. These variables are determined by the simultaneous solution of two independent equations for cladding surface heat flux and surface temperature.

One of the equations is the appropriate correlation for convective heat transfer from the fuel rod surface. This correlation relates surface heat flux to surface temperature and coolant conditions. Different correlations are required for different heat transfer modes, such as nucleate or film boiling. The relation of the surface heat flux to the surface temperature for the various heat transfer modes is shown in Figure 2-37.

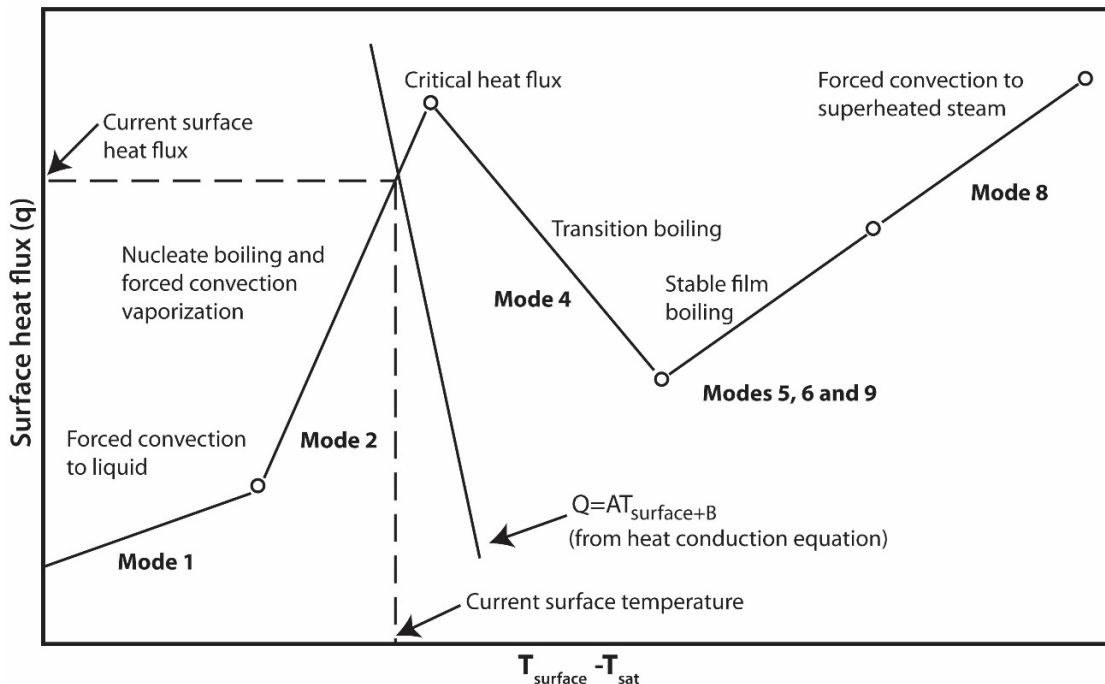


Figure 2-37. Relation of surface heat flux to surface temperature

Logic for selecting the appropriate mode and the correlations available for each mode are shown in Table 2-17. The correlations are described in Section 4.0.

Table 2-17. Water heat transfer mode selection and correlation

Heat Transfer Mode	Range ^(a)	Default Correlation ^(b)	Optional Heat Transfer Correlation(s)
Forced convection to subcooled liquid (Mode 1)	$T_w < T_{sat}$ $Q_2 < Q_1 < Q_{crit}$	Dittus-Boelter [Dittus and Boelter, 1930] for turbulent flow; constant $Nu = 7.86$ for laminar flow [Sparrow et al., 1961]	–
Subcooled nucleate boiling (Mode 2)	$Q_1 < Q_2 < Q_{crit}$ $T_b > T_{sat}$ $T_w > T_{sat}$	Jens-Lottes [Jens and Lottes, 1951]	Chen [Chen, 1963] Thom [Thom et al., 1965]
Saturated nucleate boiling (Mode 3)	$Q_1 < Q_2 < Q_{crit}$ $T_b = T_{sat}$ $T_w > T_{sat}$	Jens-Lottes [Jens and Lottes, 1951]	Chen [Chen, 1963] Thom [Thom et al., 1965]
Post-critical heat flux (CHF) transition boiling (Mode 4)	$Q_2 > Q_{crit}$ $Q_4 > Q_5$ $G > 200000$	Modified Tong-Young [Tong and Young, 1974]	Bjornard-Griffith [Bjornard and Griffith, 1977] Modified Condie-Bengston [INEL, 1978]
Post-CHF film boiling (Mode 5)	$Q_2 > Q_{crit}$ $Q_5 > Q_4$ $Q_5 > Q_6$ $G > 200000$	Groeneveld 5.9 [Groeneveld, 1973] [Groeneveld, 1978] [Groeneveld and Delorme, 1976]	Bishop-Sandberg-Tong [Bishop et al., 1965] Groeneveld-Delorme [Groeneveld and Delorme, 1976]
Post-CHF boiling for low-flow conditions (Mode 7)	$Q_2 > Q_{crit}$ $Q_6 > Q_5$ $G < 200000$	Bromley [Bromley, 1949]	–
Forced convection to superheated steam (Mode 8)	$X > 1$	Dittus-Boelter [Dittus and Boelter, 1930]	–

^(a) The symbols used are:

- Q_i = Surface flux in the i^{th} heat transfer mode
- X = Coolant Quality
- Q_{crit} = Critical heat flux
- G = Mass flux, lbm/hr-ft²)
- T_w = Cladding surface temperature
- P = Coolant Pressure, psia
- T_{sat} = Saturation temperature of coolant
- T_{bulk} = Local bulk temperature of coolant

^(b) Parameter limits describing the range of the heat transfer apply to the default correlation for each mode. The correlation to be used is specified in the input.

The second independent equation containing surface temperature and surface heat flux as the only unknown variables is derived from the finite difference equation for heat conduction at the mesh bordering the fuel rod surface. A typical plot of this equation during the nucleate boiling mode of heat transfer is also shown in Figure 2-37. The intersection of the plot of this equation

and that of the heat transfer correlations determines the surface heat flux and temperature. The derivation of this equation and the simultaneous solution for surface temperature and surface heat flux are described in Section 3.1. Neither of the two equations solved simultaneously contains past iteration values so that numerical instabilities at the onset of nucleate boiling are avoided. A separate set of heat transfer correlations is used to calculate fuel rod cooling during the reflooding portion of a LOCA. During this period, liquid cooling water is injected into the lower plenum and the liquid level gradually rises over time to cover the fuel rods. This complex heat transfer process is modeled by a set of empirical relations derived from experiments performed in the FLECHT facility [Cadek et al., 1972]. A description of these models is presented in Section 4.2.3.

The user specifies the inlet condition at the bottom of the fuel rod. The enthalpy rise across the height of the coolant channel is initially calculated based on the known surface heat flux from the previous timestep. The values obtained from the bottom and top of the coolant channel (axial nodes $j - 1$ and j) are averaged together to obtain a “cell-centered” average coolant condition used as the boundary condition in the conduction solution.

3.0 Calculations of Cladding Surface Temperature

3.1 Heat Conduction Equation

The numerical solution of the heat conduction (Equation 2-203) requires solving a set of tri-diagonal equations. This set of equations is shown as follows:

$$\begin{bmatrix} b_1 & c_1 & 0 & 0 & \dots & 0 \\ a_2 & b_2 & c_2 & 0 & \dots & 0 \\ 0 & a_3 & b_3 & c_3 & \dots & 0 \\ \vdots & \dots & \ddots & \ddots & \ddots & \vdots \\ \vdots & \dots & 0 & a_{N-1} & b_{N-1} & c_{N-1} \\ 0 & \dots & \vdots & 0 & a_N & b_N \end{bmatrix} \begin{bmatrix} T_1^{m+1} \\ T_2^{m+1} \\ T_3^{m+1} \\ \vdots \\ \vdots \\ T_{N-1}^{m+1} \\ T_N^{m+1} \end{bmatrix} = \begin{bmatrix} d_1 \\ d_2 \\ d_3 \\ \vdots \\ \vdots \\ d_{N-1} \\ d_N \end{bmatrix} \quad (3-1)$$

Where,

a_n, b_n, c_n, d_n = Terms of the heat conduction equation in finite difference form at the n^{th} mesh point

T_N^{m+1} = Temperature at n^{th} mesh point at time step $m + 1$

N = Number of mesh point at outer surface

The mesh point temperatures are solved by the Gaussian elimination method.

$$T_N^{m+1} = \frac{d_n - a_n F_{n-1}}{b_n - a_n E_{n-1}} \quad (3-2)$$

$$T_j^{m+1} = -E_j T_{j+1}^{m+1} + F_j \quad (3-3)$$

Where,

$$E_1 = \frac{c_1}{b_1} \quad (3-4a)$$

$$F_1 = \frac{d_1}{b_1} \quad (3-4b)$$

and,

$$E_j = \frac{c_j}{b_j - a_j E_{j-1}} \quad \text{for } j = 1, 2, 3, \dots, n - 1 \quad (3-5a)$$

$$F_j = \frac{d_j - a_j F_{j-1}}{b_j - a_j E_{j-1}} \quad \text{for } j = 1, 2, 3, \dots, n-1 \quad (3-5b)$$

The coefficients a_n , b_n , and d_n in Equation 3-2 are derived from the energy balance equation for the half mesh interval bordering the outside surface. The continuous form of the energy balance equation for this half mesh interval is:

$$\rho C_p V \frac{\partial T}{\partial t} = -A_{n-\frac{1}{2}} K \left. \frac{\partial T}{\partial r} \right|_{r=r_n-\frac{r}{2}}^{-\theta A_n + qV} \quad (3-6)$$

Where all the terms in Equation 3-6 are defined below.

The finite difference form of Equation 3-6 is:

$$\underbrace{\frac{-0.5A_{n-\frac{1}{2}}K}{\Delta r}}_{a_n} T_n^{m+1} + \left[\underbrace{\frac{\rho C_p \Delta V}{\Delta t} + \frac{0.5A_{n-\frac{1}{2}}K}{\Delta r}}_{b_n} T_n^{m+1} \right] \underbrace{\frac{\rho C_p \Delta V}{\Delta r} T_n^m \frac{-0.5A_{n-\frac{1}{2}}K}{\Delta r} (T_n^m - T_{n-1}^m) - 0.5A_n (\theta^m + \theta^{m+1}) + q^{m+\frac{1}{2}} \Delta V}_{d_n} \quad (3-7)$$

The complete expressions for coefficients a_n , b_n , and d_n are then:

$$a_n = \frac{-0.5A_{n-\frac{1}{2}}K}{r} \quad (3-8a)$$

$$b_n = \frac{\rho C_p V}{t} + \frac{0.5A_{n-\frac{1}{2}}K}{r} \quad (3-8b)$$

$$d_n = \frac{\rho C_p V}{r} T_n^m \frac{-0.5A_{n-\frac{1}{2}}K}{r} (T_n^m - T_{n-1}^m) - 0.5A_n (\theta^m + \theta^{m+1}) + q^{m+\frac{1}{2}} V \quad (3-8c)$$

$$A_{n-\frac{1}{2}} = 2\pi \left(r_n - \frac{r}{2} \right) \quad (3-8d)$$

$$A_n = 2\pi r_n \quad (3-8e)$$

$$V = \pi \left(r_n r - \frac{r^2}{4} \right) \quad (3-8f)$$

Where,

K = Thermal conductivity of material in half mesh interval bordering the surface, W/m-K

C_p = Specific heat of material in half mesh interval bordering the surface, J/kg-K

ρ = Density of material in half mesh interval bordering the surface, kg/m³

r_n = Radius to outside surface

r = Width of mesh interval bordering outside surface, m

t = Time step, s

θ^m = Surface heat flux at m^{th} time step, W/m²

T_n^m = Surface temperature at m^{th} time step, K

$q^{m-\frac{1}{2}}$ = Heat generation rate in half mesh interval bordering outside surface (heat generation caused by cladding oxidation), W/m³

Because the coefficients a_n , b_n , d_n , E_{n-1} and F_{n-1} in Equation 3-2 do not contain temperature, the equation can be written as follows:

$$A_q T_n^{m+1} + B_q = \theta^{m+1} \quad (3-9)$$

Where,

$$A_1 = \frac{-(b_n - a_n E_{n-1})}{0.5 A_n} \quad (3-10)$$

$$B_1 = - \left[\frac{0.5 \theta^m A_n + a_n F_{n-1} - \frac{\rho C_p}{t} V T_n^m - a_n (T_n^m - T_{n-1}^m) - q^{m-\frac{1}{2}} V}{0.5 A_n} \right] \quad (3-11)$$

As shown in Equation 3-2, the coefficients E_{n-1} and F_{n-1} are evaluated by forward reduction of Equation 3-1. Therefore, Equation 3-9 contains only T_n^{m+1} and θ^{m+1} as unknown quantities.

Empirically derived clad-to-coolant heat transfer correlations are available from which the surface heat flux due to convection can be calculated in terms of surface temperature, geometric parameters, and flow conditions. Also, the equation for radiation heat transfer from a surface to surrounding water is known. Thus, the total surface heat flux can be expressed by the equation:

$$\theta^{m+1} = f_i (C, G, T_n^{m+1}) + \sigma F_A F_E \left[(T_n^{m+1})^4 - T_w^4 \right] \quad (3-12)$$

Where,

θ^{m+1} = Surface heat flux at time step $m + 1$

$f_i ()$ = Function specifying rate at which heat is transferred from surface by convection heat transfer during heat transfer mode i (These functions are defined in Section 4.2.3)

i = Number identification of convective heat transfer mode (nucleate boiling, film boiling, etc.)

C = Set of parameters describing coolant conditions

G = Set of parameters describing geometry

σ = Stefan-Boltzmann constant

F_A = Configuration factor for radiation heat transfer

F_E = Emissivity factor for radiation heat transfer

T_w = Bulk temperature of water surrounding fuel rod surface

Equations 3-9 and 3-12 are two independent equations with unknowns T_n^{m+1} and θ^{m+1} . Simultaneous solution of the two equations yields the new surface temperature T_n^{m+1} .

4.0 Coolant Model and Heat Transfer Correlations

The coolant enthalpy rise model and clad-to-coolant heat transfer correlations are described in this section. The heat transfer correlations supply one of the equations required for calculation of the fuel rod surface temperature, as discussed in Section 2.11. Also described is the calculation of the coolant void fraction for water. The available coolants are:

- Water (default)
- Sodium
- Helium

The following inputs are used to calculate the coolant temperature, pressure and heat transfer coefficient as a function of time and location:

- Inlet temperature
- Inlet mass flux
- Inlet pressure

It is allowed to bypass the coolant model entirely but still use the built-in clad-to-coolant heat transfer coefficients based on the coolant type. Instructions on how to use this option are provided in Section B.7.

4.1 Coolant Enthalpy Model

The coolant enthalpy is calculated by a one-dimensional transient fluid flow model [Meyer and Williams, 1962] as shown in Figure 4-1. The model is given as input information the coolant enthalpy and mass flux at the bottom of the fuel rods and the elevation averaged coolant pressure. The input information can vary with time. The model also receives the FAST-calculated cladding surface heat flux. The heat flux can vary with time and elevation. The coolant enthalpy model then calculates the coolant enthalpy, which varies with time and elevation.

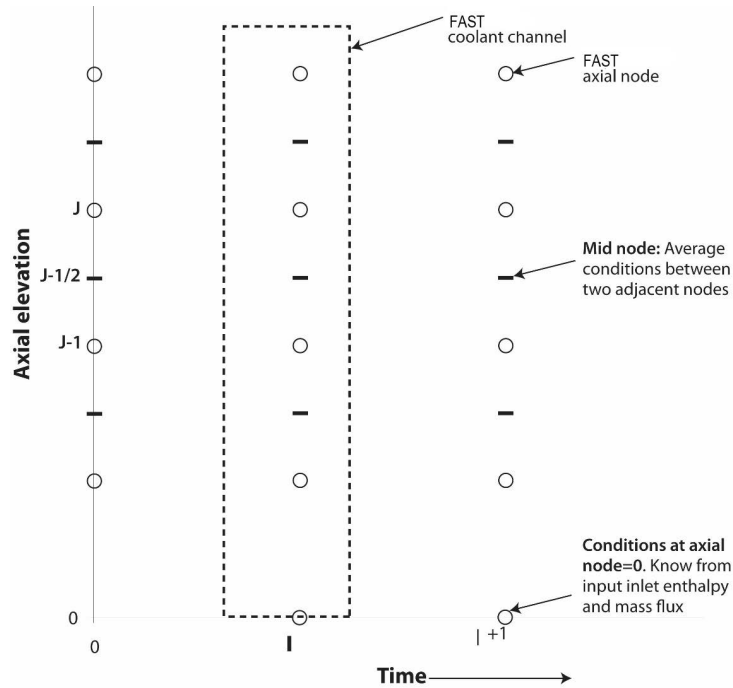


Figure 4-1. Description of geometry terms in coolant enthalpy model

The model includes an energy conservation equation and a mass conservation equation. The coolant pressure is assumed to be spatially uniform and to change slowly with time so that the spatial and transient pressure terms are omitted from the energy equation. Thus, sonic effects are ignored. The model assumes homogeneous two-phase flow and a flow channel with a constant cross-sectional area.

The energy and mass conservation equations are:

$$\rho \frac{\partial H}{\partial t} + G \frac{\partial H}{\partial z} = \frac{1}{L} (\varphi + rq) \tag{4-1}$$

$$\frac{\partial \rho}{\partial t} + \frac{\partial G}{\partial z} = 0 \tag{4-2}$$

Where,

ρ = Coolant density, kg/m³

G = Coolant mass flux, kg/m²-s

H = Coolant enthalpy, J/kg

$\frac{1}{L} (\varphi + rq)$ = Volumetric heat addition to coolant, J/m³-s

L = Flow area per unit transfer surface area per unit axial length, m

φ = Surface heat flux, J/m²-s

q = Heat generation rate/area, J/m²-s

r = Fraction of heat generated directly in the coolant by neutrons and gamma rays

t = Time, s

z = Axial elevation, m

Assuming constant pressure, coolant conditions are considered a function of enthalpy only so that:

$$\rho = \rho(H) \text{ and } \frac{\partial \rho}{\partial t} = \frac{\partial H}{\partial t} \frac{\partial \rho}{\partial H} \quad (4-3)$$

where density (ρ) is evaluated at a reference pressure. By combining Equations 4-1, 4-2, and 4-3, a relation can be established between the axial mass flux distribution and axial enthalpy distribution:

$$\frac{\partial G}{\partial z} = -\frac{\partial \rho}{\partial t} = -\frac{\partial H}{\partial t} \frac{\partial \rho}{\partial H} = -\frac{1}{\rho} \frac{\partial \rho}{\partial H} \left[\frac{1}{L} (\varphi + rq) - G \frac{\partial H}{\partial z} \right] \quad (4-4)$$

The numerical solution for the local coolant enthalpy is given by the finite difference form of Equation 4-3 with forward difference in time and averaged between spatial nodes. The equation is:

$$H_j^{l+1} = H_{j-1}^l - \left(H_{j-1}^{l+1} - H_j^l \right) \frac{1 - \alpha_{j-\frac{1}{2}}^l}{1 + \alpha_{j-\frac{1}{2}}^l} + \frac{2t^{l+1} Q_{j-\frac{1}{2}}^l}{\rho_{j-\frac{1}{2}}^l \left(1 + \alpha_{j-\frac{1}{2}}^l \right)} \quad (4-5)$$

Where,

$$\alpha_{j-\frac{1}{2}}^l = \frac{G_{j-\frac{1}{2}}^{l+1} t^l}{\rho_{j-\frac{1}{2}}^l z_j}$$

$$\rho_{j-\frac{1}{2}}^l = \frac{1}{2} \left(\rho_j^l + \rho_{j-1}^l \right)$$

$$G_{j-\frac{1}{2}}^{l+1} = \frac{1}{2} \left(G_j^{l+1} + G_{j-1}^{l+1} \right)$$

$$Q_{j-\frac{1}{2}}^l = \frac{1}{2L} \left(\varphi_j^l + \varphi_{j-1}^l \right) + \frac{1}{2L} \left(r q_j^l + r q_{j-1}^l \right)$$

$$z_j = z_j - z_{j-1}$$

$$t^l = t^l - t^{l-1}$$

j = FAST axial node number (see Figure 4-1)

l = Time step number

The numerical solution for the mass flux at the midpoint between axial nodes j and $j - 1$ at the new time step is given by the finite difference form of Equation 4-4. The equation is:

$$G_j^{l+1} = G_{j-1}^{l+1} \frac{2 + A_{j-\frac{1}{2}}}{2 - A_{j-\frac{1}{2}}} + \frac{2 \left(\frac{1}{\rho_{j-\frac{1}{2}}^l} \left(\frac{\partial \rho}{\partial H} \right)_{j-\frac{1}{2}} Q_{j-\frac{1}{2}} z_j \right)}{A_{j-\frac{1}{2}} - 2} \quad (4-6)$$

Where,

$$A_{j-\frac{1}{2}} = H \frac{1}{\rho_{j-\frac{1}{2}}^l} \left(\frac{\partial \rho}{\partial H} \right)_{j-\frac{1}{2}} \quad (4-7a)$$

$$\left(\frac{\partial \rho}{\partial H} \right)_{j-\frac{1}{2}} = \frac{\rho_j^l - \rho_{j-1}^l}{H_j^l - H_{j-1}^l} \quad (4-7b)$$

$$H = H_j^l - H_{j-1}^l \quad (4-7c)$$

G_j^{l+1} is calculated using Equation 4-6 before H_j^{l+1} is calculated with Equation 4-5. After the coolant enthalpy at the new time step has been calculated, the coolant density at the new time step is determined from the equation of state for water.

In summary, coolant inlet enthalpy and mass flux are input to define conditions at node zero. The mass fluxes for the remaining nodes are calculated from Equation 4-6 using values for heat flux, enthalpy, and density calculated in the previous time step or iteration. The enthalpy is then updated using Equation 4-5, and a corresponding density is calculated from the fluid property relationships. Using the fluid conditions in the heat transfer correlations, a new heat flux is calculated, and the process is repeated.

If the time step is less than the minimum time for a drop of coolant to pass between any two axial nodes, the solution scheme is stable. This criterion is given by the equation:

$$t^l \leq \left[\frac{z_j}{v_{j+\frac{1}{2}}^l} \right]_{\min} \quad (4-8)$$

Where,

$v_{j+\frac{1}{2}}^l$ is the velocity of coolant at midpoint between axial nodes j and $j + 1$ m/s

The water quality and temperature are computed based on the local coolant enthalpy by the equations shown in Table 4-1.

Table 4-1. Coolant quality and temperature criteria

Phase	Criteria	Temperature/Enthalpy
Sub-cooled Liquid	$h_i(z) < h_f(P)$	$X_i(z) = 0$ $T_i(z) = \theta(h_i(z), P)$
Saturated	$h_f(P) \leq h_i(z) \leq h_g(P)$	$X_i(z) = \frac{h_i(z) - h_f(P)}{h_g(P) - h_f(P)}$ $T_i(z) = T_s(P)$
Superheated Vapor	$h_i(z) > h_g(P)$	$X_i(z) = 1$ $T_i(z) = \theta(h_i(z), P)$

Where,

$X_i(z)$ = Quality of coolant in flow channel i at distance z from flow inlet, dimensionless

$T_i(z)$ = Temperature of coolant in flow channel i at distance z from flow inlet, K

P = Coolant pressure, Pa

$h_f(P)$ = Enthalpy of saturated liquid, J/kg

$h_g(P)$ = Enthalpy of saturated gas, J/kg

$T_s(P)$ = Saturation temperature, K

$\theta(h_i, P)$ = Function calculating coolant temperature, K

The functions defining h_f , h_g , $\theta(h, P)$, and T_s are supplied by the `st_h2xt` water properties package.

4.2 Water Heat Transfer and Critical Heat Flux Correlations

4.2.1 Summary

The correlations for heat transfer coefficient and CHF have been selected based on their applicability to the range of conditions that are expected to be encountered in analyses with FAST. Because the code is used for analysis of the response of a single fuel rod to postulated operational transients and design basis accidents, and to model fuel performance experiments, heat transfer models have been selected that are applicable to a wide range of relatively severe thermal-hydraulic conditions, particularly in the post-CHF regimes. The available correlations for determining the transition from nucleate boiling to film boiling (i.e., the CHF or departure from nucleate boiling (DNB)) are described in Section 4.2.4.

The heat transfer correlations in FAST cover the full range of the boiling curve, from single-phase forced convection to subcooled liquid through nucleate boiling to the critical heat flux point, on into transition and film boiling in the post-CHF heat transfer regimes, and finally to single-phase forced convection to superheated steam. The available heat transfer correlations for each regime are described in Section 4.2.3.

4.2.2 Void Fraction

The void fraction of the coolant is calculated by Equation 4-9:

$$\alpha = \frac{XV_g}{|(1-X)V_f\gamma| + XV_g} \quad (4-9)$$

Where,

α = Void fraction, unitless

X = Coolant quality, unitless

V_f = Specific volume of saturated liquid, m³/kg

V_g = Specific volume of saturated gas, m³/kg

γ = Slip velocity ratio (assumed to always be 1.0; homogeneous flow)

4.2.3 Heat Transfer Coefficient Correlations

Heat transfer correlations are empirical models developed to quantify the rate of energy exchange between a solid surface and a fluid flowing over it. Heat transfer correlations are expressed as a coefficient relating the surface heat flux to the temperature difference between the surface and the fluid:

$$q'' = h(T_{wall} - T_{fluid}) \quad (4-10)$$

Where,

q'' = Surface heat flux, W/m²

T_{wall} = Wall surface temperature, K

T_{fluid} = Fluid temperature, K

h = Heat transfer coefficient, W/m²-K

This relationship is a constitutive model based on empirical observation, not an expression of a law of nature. It is a convenient simplification of an extensive array of physical phenomena that influence the rate of heat transfer from a surface, which can include the thermodynamic properties of the flowing fluid, the fluid dynamic forces in the boundary layer, the effects of phase change (for boiling flow), and the geometry of the heated surface. There is no generic formulation for a heat transfer coefficient correlation that satisfies the above relationship for all conditions. Specific formulations for any particular application must be derived from experimental data.

For forced convection heat transfer, the general behavior of this relationship can be broadly divided into five regions, or modes, which are differentiated by the basic heat transfer behavior within each region. These are single-phase forced convection to liquid (Mode 1), nucleate boiling (Mode 2 for subcooled boiling and Mode 3 for saturated boiling), post-CHF transition boiling (Mode 4), post-CHF film boiling 2 (Mode 5), and single-phase forced convection to vapor (Mode 8). Figure 4-2 illustrates the relationship between wall superheat and heat flux for the full range of regimes, and shows the typical shape of the boiling curve from single-phase liquid to single-phase vapor convection.

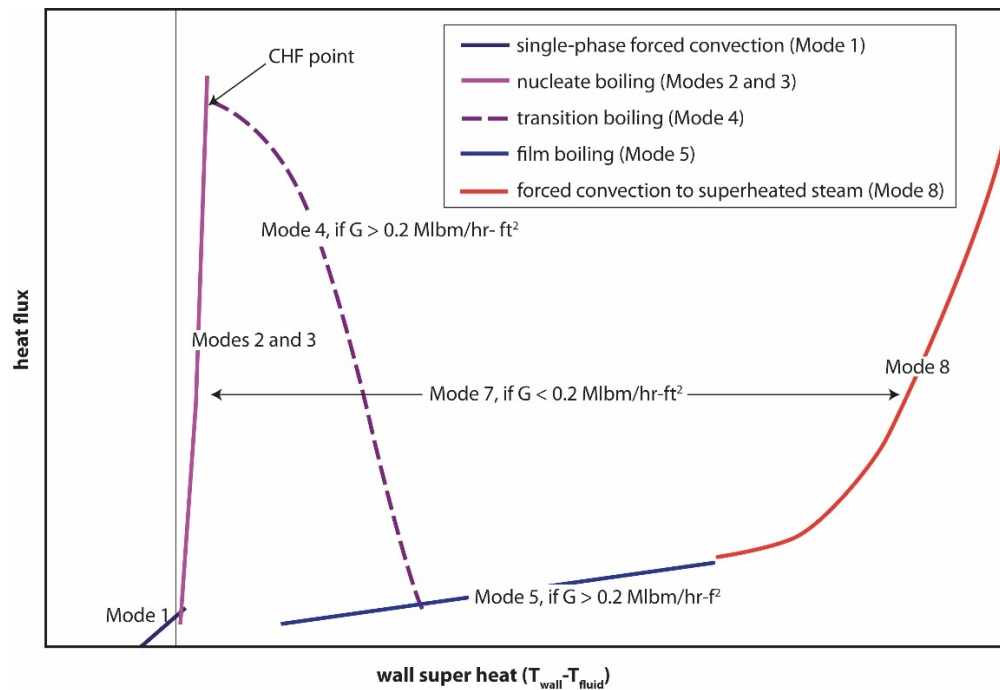


Figure 4-2. Illustration of FAST's forced convection heat transfer regimes for full boiling curve

Additional Modes are defined in FAST to cover the full range of flow conditions that can be encountered in severe transients, which do not always remain in the forced convection heat transfer regime. These are:

- Mode 7: low flow conditions, $< 2 \times 10^6$ lbm/hr-ft² (2700 kg/s-m²)
- Mode 10: stagnant fluid conditions, 2.0 lbm/hr-ft² (0.0027 kg/s-m²). In this regime, the heat transfer coefficient is set to a constant minimum value of 5.0 Btu/hr-ft²-°F (28.4 W/m²-K).
- Mode 11: adiabatic conditions, (i.e., no heat transfer from the rod surface), in which the heat transfer coefficient is set to zero.

4.2.3.1 Mode 1: Single-Phase Convection to Subcooled Liquid

For turbulent flow ($Re > 2000$), [Dittus and Boelter, 1930] heat transfer correlation is used, so that:

$$h_{turbulent} = 0.023 \left(\frac{k}{D_e} \right) Re^{0.8} Pr^{0.4} \quad (4-11)$$

Where,

$h_{turbulent}$ = Heat transfer coefficient for turbulent flow, W/m²-K

k = Thermal conductivity of the fluid, W/m-K

D_e = Hydraulic diameter of flow channel, m

Re = Reynolds number of the flow (for characteristic length D_e), unitless

Pr = Prandtl number of the fluid, unitless

For laminar flow ($Re < 2000$), the heat transfer coefficient is defined with a constant Nusselt number (Nu) of 7.86, from [Sparrow et al., 1961] such that:

$$h_{laminar} = 7.86 \left(\frac{k}{D_e} \right) \quad (4-12)$$

The local heat transfer coefficient (h) for single-phase convection to subcooled liquid is defined as:

$$h = \max(h_{turbulent}, h_{laminar}) \quad (4-13)$$

4.2.3.2 Modes 2 and 3: Subcooled and Saturated Nucleate Boiling

Jens-Lottes Correlation

The Jens-Lottes correlation [Jens and Lottes, 1951] is the default in the code for nucleate boiling. The general form of the correlation is:

$$\frac{q''_{NB}}{1 \times 10^6} = \frac{e^{\frac{-4Pressure}{6.2 \times 10^6}}}{25^4} (T_s - T_{sat})^4 \quad (4-14)$$

Where,

q''_{NB} = Nucleate boiling heat flux, Btu/hr-ft²

$Pressure$ = Coolant pressure, Pa

T_s = Local rod surface temperature, °F

T_{sat} = Fluid saturation temperature, °F

The heat transfer coefficient (h_{NB}) is solved by re-writing Equation 4-14. Converted to SI units, the correlation is implemented as shown in Equation 4-15.

$$h_{NB} = JLCoeff \frac{\left[(T_s - T_{sat}) \exp\left(\frac{Pressure}{6.2 \times 10^6}\right) \right]^4}{T_s - T_b} \quad (4-15)$$

Where,

h_{NB} = Nucleate boiling heat transfer coefficient, W/m²-K

T_s = Local rod surface temperature, K

T_{sat} = Fluid saturation temperature, K

T_b = Bulk fluid temperature, K

$Pressure$ = Coolant pressure, Pa

$JLCoeff$ = Jens-Lotte Coefficient = $3.15248 \times \left(\frac{9}{5}\right)^4 \times \frac{1 \times 10^6}{60^4} \approx 2.553509$

Thom Correlation

The Thom correlation [Thom et al., 1965] is an alternative option for subcooled nucleate boiling that can be selected by user input. This correlation defines the local heat transfer coefficient as the sum of a nucleate boiling component and a single-phase convection component, such that:

$$h = h_{NB} + h_{spl} \quad (4-16)$$

Where,

h_{NB} = Nucleate boiling heat transfer coefficient, W/m²-K

h_{spl} = Single-phase convection coefficient from Equation 4-13, W/m²-K

The nucleate boiling heat transfer coefficient (h_{NB}) is evaluated using the relationship:

$$h_{NB} = \frac{\left(\frac{\exp\left(\frac{P}{8.7 \times 10^6}\right)}{22.65} (T_s - T_{sat}) \right)^2}{T_s - T_b} \times 10^6 \quad (4-17)$$

Where,

P = Pressure, Pa

T_s = Local rod surface temperature, K

T_{sat} = Fluid saturation temperature, K

T_b = Bulk fluid temperature, K

Chen Correlation

The Chen correlation is an alternative option for subcooled nucleate boiling [Chen, 1963]. This correlation has a similar structure to the Thom correlation, in that it treats heat transfer in subcooled nucleate boiling as a linear combination of a nucleate boiling term and a single-phase convection component. The general form of the Chen correlation is:

$$h = \frac{(q''_{NB} + q''_{FC})}{T_s - T_b} \quad (4-18)$$

Where,

q''_{NB} = Nucleate boiling heat flux, W/m²

q''_{FC} = Single-phase forced convection heat flux, W/m²

T_s = Local rod surface temperature, K

T_b = Bulk fluid temperature, K

The forced convection heat flux (q''_{FC}) is evaluated as:

$$q''_{FC} = h_{FC} (T_s - T_b) \quad (4-19)$$

Where,

h_{FC} = Forced convection heat transfer coefficient, W/m²-K

T_s = Local rod surface temperature, K

T_b = Bulk fluid temperature, K

For subcooled nucleate boiling (Mode 2), the correlation for the forced convection heat transfer coefficient (h_{FC}) is the Dittus-Boelter correlation from Equation 4-11. For saturated nucleate boiling (Mode 3), the heat transfer coefficient is modified by the Reynold's number factor, (F), and instead uses the two-phase Reynold's number, ($Re_{2\phi}$):

$$h_{FC} = 0.023 \left(\frac{k_f}{D_e} \right) Re_{2\phi}^{0.8} Pr^{0.4} F \quad (4-20)$$

The two-phase Reynolds number used in Equation 4-20 modifies the liquid Reynold's number by being defined in terms of the equilibrium quality of the flow, such that:

$$Re_{2\phi} = (1 - x) Re = \frac{(1 - x) GD_e}{\mu_f} \quad (4-21)$$

Where,

x = Equilibrium quality, unitless

G = Mass velocity of fluid, kg/m²s

D_e = Hydraulic diameter of flow channel, m

μ_f = Saturated liquid viscosity, kg/m-s

The equilibrium quality (x) is a unitless number calculated by:

$$x = \frac{h - h_f}{h_{fg}} \quad (4-22)$$

Where,

h = Local fluid enthalpy, J/kg

h_f = Saturated liquid enthalpy, J/kg

h_{fg} = Latent heat of vaporization, J/kg

The Reynold's number factor (F) accounts for the enhanced flow and turbulence due to the presence of the vapor as a function of the inverse Martinelli Factor. The Martinelli factor (X_{tt}) is a function of the quality, density and viscosity of the liquid and vapor phases.

$$F = \begin{cases} 1, & \frac{1}{X_{tt}} \leq 0.1 \\ 2.35 \left(0.213 + \frac{1}{X_{tt}} \right), & \frac{1}{X_{tt}} > 0.1 \end{cases} \quad (4-23)$$

$$\frac{1}{X_{tt}} = \left(\frac{x}{1-x} \right)^{0.9} \left(\frac{\rho_f}{\rho_g} \right)^{0.5} \left(\frac{\mu_g}{\mu_f} \right)^{0.1} \quad (4-24)$$

Where,

X_{tt} = Martinelli Factor

x = Equilibrium quality, unitless

ρ_f = Saturated liquid density, kg/m³

ρ_g = Saturated vapor density, kg/m³

μ_f = Saturated liquid viscosity, kg/m-s

μ_g = Saturated vapor viscosity, kg/m-s

The nucleate boiling heat flux is evaluated as:

$$q''_{NB} = h_{NB} (T_s - T_{sat}) \quad (4-25)$$

Where,

q''_{NB} = Nucleate boiling heat flux, W/m²

h_{NB} = Nucleate boiling heat transfer coefficient, W/m²-K

T_s = Local rod surface temperature, K

T_{sat} = Fluid saturation temperature, K

and

$$h_{NB} = 1.22 \times 10^{-3} \left[\frac{k_f^{0.79} C_{p_f}^{0.45} \rho_f^{0.49}}{\sigma^{0.5} \mu_f^{0.29} h_{fg}^{0.24} \rho_g^{0.24}} \right] (T_s - T_{sat})^{0.24} (P_{sat_{T_s}} - P_{sat})^{0.75} S \quad (4-26)$$

Where,

S = Two-phase suppression factor

k_f = Saturated liquid thermal conductivity, W/m-K

C_{p_f} = Saturated liquid specific heat, J/kg-K

ρ_f = Saturated liquid density, kg/m³

ρ_g = Saturated vapor density, kg/m³

σ = Surface tension, N/m

μ_f = Saturated liquid viscosity, kg/m-s

h_{fg} = Latent heat of vaporization, J/kg

T_s = Local rod surface temperature, K

T_{sat} = Fluid saturation temperature, K

$P_{sat_{T_s}}$ = Saturation pressure corresponding to rod surface temperature T_s , Pa

P_{sat} = Saturation pressure at bulk coolant temperature, Pa

In this formulation, the local fluid properties (thermal conductivity (k), Prandtl number (Pr), and the viscosity (μ) used in the Reynolds number (Re)) are evaluated at the bulk fluid temperature (T_b).

The two-phase suppression factor (S), which appears in the nucleate boiling heat flux term for both subcooled and saturated boiling heat transfer, is a function of a modified two-phase Reynolds number (Re_{TP}).

$$S = \frac{1}{1 + 2.53 \times 10^{-6} Re_{TP}^{1.17}} \quad (4-27)$$

The modified two-phase Reynolds number is defined as:

$$Re_{TP} = \frac{Re_f F^{1.25}}{1 \times 10^4} \quad (4-28)$$

Where,

Re_f = Reynolds number of homogeneous fluid = $\frac{GD_e}{\mu_f}$

G = Mass velocity of fluid, kg/m²-s

D_e = Hydraulic diameter of flow channel, m

μ_f = Saturated liquid viscosity, kg/m-s

4.2.3.3 Mode 4 Post-CHF: Transition Boiling

Modified Tong-Young

The modified Tong-Young correlation [Tong and Young, 1974] is the default heat transfer correlation for the transition boiling region (Mode 4). This correlation evaluates the transition boiling heat flux in terms of the CHF and the film boiling heat flux, using the relationship:

$$q''_{TB} = C_1 (q''_{CHF} - q''_{FB}) \quad (4-29)$$

Where,

q''_{TB} = Transition boiling heat flux, Btu/hr-ft²

q''_{CHF} = CHF, Btu/hr-ft²

q''_{FB} = Film boiling heat flux, Btu/hr-ft²

C_1 = Empirically derived formula relating heat flux to fluid conditions and wall superheat, unitless

The C_1 multiplicative term has the form:

$$C_1 = \exp \left[-0.012x^{\frac{2}{3}} \left(\frac{GD_e h_{fg}}{4q''_{Total}} \right) (0.01\Delta T_f)^{(1.0+0.0016\Delta T_f)} \right] \quad (4-30)$$

Where,

x = Equilibrium quality, unitless

G = Homogeneous mass velocity of fluid, lbm/hr-ft²

D_e = Hydraulic diameter of flow channel, ft

h_{fg} = Latent heat of vaporization, Btu/lbm

q''_{Total} = Total surface heat flux, Btu/hr-ft² = $q''_{TB} + q''_{FB}$

ΔT_f = Wall superheat, °F, = $T_s - T_{sat}$

T_s = Local rod surface temperature, °F

T_{sat} = Saturation temperature, °F

Bjornard-Griffith Correlation

The Bjornard-Griffith correlation [Bjornard and Griffith, 1977] can be selected by user input for transition boiling heat transfer. This correlation evaluates the transition boiling heat flux as a simple interpolation between the CHF and the heat flux at the minimum film boiling temperature for the local thermal-hydraulic conditions. The formulation is specified as:

$$q''_{TB} = \delta q''_{CHF} + (1 - \delta) q''_{MFB} \quad (4-31)$$

Where,

q''_{TB} = Transition boiling heat flux, Btu/hr-ft²

q''_{CHF} = CHF, Btu/hr-ft²

q''_{MFB} = Heat flux at the minimum film boiling temperature, Btu/hr-ft²

δ = Interpolation factor, unitless

The interpolation factor (δ) for this correlation is defined as:

$$\delta = \left[\frac{T_s - T_{MFB}}{T_{CHF} - T_{MFB}} \right]^2 \quad (4-32)$$

Where,

T_s = Local rod surface temperature, °F

T_{CHF} = CHF temperature, °F

T_{MFB} = Minimum film boiling temperature, °F

The minimum film boiling temperature (T_{MFB}) is calculated from the Iloeje correlation [Iloeje et al., 1989] as:

$$T_{MFB} = T_{sat} + 0.29\Delta T_{BER} (1.0 - 0.295x^{2.45}) (1.0 + 0.36G^{0.49}) \quad (4-33)$$

Where,

T_{sat} = Saturation temperature, °F

ΔT_{BER} = Wall superheat at minimum film boiling temperature, °F

x = Equilibrium quality, unitless

G = Mass velocity of fluid, lbm/hr-ft²

The wall superheat at the minimum film boiling temperature is calculated from the Berenson correlation as:

$$\Delta T_{BER} = 0.127 \left(\frac{\rho_{vf} h_{fg}}{k_{vf}} \right) \left(\frac{g(\rho_f - \rho_g)}{\rho_f + \rho_g} \right)^{\frac{2}{3}} \left(\left(\frac{g_c}{g} \right) \frac{\sigma}{\rho_f - \rho_g} \right)^{\frac{1}{2}} \left(\frac{\mu_{vf}}{g(\rho_f - \rho_g)} \right)^{\frac{1}{3}} \quad (4-34)$$

Where,

h_{fg} = Latent heat of vaporization, Btu/lbm

ρ_f = Saturated liquid density, lbm/ft³

ρ_g = Saturated vapor density, lbf/ft³

σ = Surface tension, lbf/ft

ρ_{vf} = Vapor density at the film temperature, lbf/ft³

k_{vf} = Vapor thermal conductivity at the film temperature, Btu/s-ft-°F

μ_{vf} = Vapor viscosity at the film temperature, lbf/s-ft

g = Acceleration of gravity, 32.2 ft/s²

g_c = Force to mass conversion constant for EU, 32.2 lbf-ft/lbf-s²

The film temperature (T_{vf}) used for determining fluid properties near the rod surface is defined as the average of the rod surface temperature and the coolant saturation temperature, that is:

$$T_{vf} = \frac{T_s + T_{sat}}{2} \quad (4-35)$$

Where,

T_{vf} = Estimated temperature of vapor film near the heated surface, °F

T_s = Local rod surface temperature, °F

T_{sat} = Fluid saturation temperature, °F

Modified Condie-Bengston

The modified Condie-Bengston correlation [INEL, 1978] can be selected by user input for transition boiling heat transfer. This correlation is similar to the Tong-Young correlation, in that it defines the transition boiling heat flux in terms of the CHF and the stable film boiling heat flux. The relationship is formulated as:

$$q''_{TB} = C_1 \exp \left[0.5 (T_s - T_{sat})^{0.5} \right] (T_s - T_{sat}) \quad (4-36)$$

Where,

q''_{TB} = Transition boiling heat flux, Btu/hr-ft²

T_s = Local rod surface temperature, °F

T_{sat} = Fluid saturation temperature, °F

C_1 = Empirical coefficient

The empirical coefficient C_1 is defined in terms of the CHF, the CHF temperature, and the film boiling heat flux, as:

$$C_1 = \exp \left[\ln (q''_{CHF} - q'' (T_{CHF})_{FB}) + 0.5 (T_{CHF} - T_{sat})^{0.5} - \ln (T_{CHF} - T_{sat}) \right] \quad (4-37)$$

Where,

$$q''_{CHF} = \text{CHF, Btu/hr-ft}^2$$

$$q'' (T_{CHF})_{FB} = \text{Film boiling heat flux at the CHF temperature, Btu/hr-ft}^2$$

$$T_{CHF} = \text{CHF temperature, } ^\circ\text{F}$$

$$T_{sat} = \text{Fluid saturation temperature, } ^\circ\text{F}$$

The film boiling heat flux at the CHF temperature is defined using the film boiling correlation selected for Mode 5, such that:

$$q'' (T_{CHF})_{FB} = h_{FB} (T_{CHF} - T_{sat}) \quad (4-38)$$

Where,

$$h_{FB} = \text{Film boiling heat transfer coefficient evaluated at the CHF temperature, Btu/hr-ft}^2\text{-}^\circ\text{F}$$

$$T_{CHF} = \text{CHF temperature, } ^\circ\text{F}$$

$$T_{sat} = \text{Fluid saturation temperature, } ^\circ\text{F}$$

4.2.3.4 Mode 5 Post-CHF: Film Boiling

Groeneveld 5.7 and 5.9 Correlations

The Groeneveld 5.9 [Groeneveld, 1978] correlation is the default correlation for film boiling heat transfer (Mode 5). Both correlations use the same form, with different coefficients defined in Table 4-2. The correlation defines the film boiling heat flux as:

$$q''_{FB} = h_{FB} (T_s - T_{sat}) \quad (4-39)$$

Where,

$$q''_{FB} = \text{Film boiling heat flux, W/m}^2$$

$$h_{FB} = \text{Film boiling heat transfer coefficient, W/m}^2\text{-K (Equation 4-40)}$$

T_s = Local rod surface temperature, K

T_{sat} = Fluid saturation temperature, K

The general form of the film boiling heat transfer coefficient is defined as:

$$h_{FB} = a \left(\frac{k_g}{D_e} \right) (Re_{HOM})^b (Pr_w)^c Y^d \quad (4-40)$$

Where,

k_g = Thermal conductivity of saturated vapor, W/m-K

D_e = Channel hydraulic diameter, m

Re_{HOM} = Homogeneous two-phase Reynolds number (Equation 4-41)

Pr_w = Prandtl number, with fluid properties evaluated at the wall temperature

Y = Empirical parameter, unitless (Equation 4-42)

a, b, c, d = Empirical coefficients (see Table 4-2)

The homogeneous two-phase Reynolds number is defined as:

$$Re_{HOM} = Re_g \left(x + \left(\frac{\rho_g}{\rho_f} \right) (1 - x) \right) = \left(\frac{GD_e}{\mu_g} \right) \left(x + \left(\frac{\rho_g}{\rho_f} \right) (1 - x) \right) \quad (4-41)$$

Where,

x = Equilibrium quality, unitless

G = Homogeneous mass velocity of fluid, kg/m²-s

D_e = Hydraulic diameter of flow channel, m

α = Homogeneous void fraction, (Equation 4-46)

μ_g = Saturated vapor viscosity, kg/m-s

ρ_f = Saturated liquid density, kg/m³

ρ_g = Saturated vapor density, kg/m³

The empirical correction factor Y makes use of the quality and phase densities:

$$Y = 1.0 - 0.1 \left(\frac{\rho_g}{\rho_f} - 1 \right)^{0.4} (1 - x)^{0.4} \quad (4-42)$$

The empirical coefficients a, b, c and d of the Groeneveld correlation (Equation 4-40) were fitted for two different data sets. One data set consisted of film flow boiling in annular channels, and the fit to this data set was presented in Equation 5.7 in the original reference [Groeneveld, 1973]. The other data set consisted of film boiling in test sections consisting of rod clusters. The fit to this data set was presented in Equation 5.9 of the original reference. The two formulations of the Groeneveld correlation, therefore, are generally referred to as Groeneveld 5.7 [Groeneveld, 1973] and Groeneveld 5.9 [Groeneveld, 1978]. The formulation for rod clusters (Groeneveld 5.9) is the default selection for Mode 5. However, the formulation for annular channels (Groeneveld 5.7) can be selected by user input. The values of the fitted constants for the two forms of the correlation are listed in Table 4-2.

Table 4-2. Groeneveld fitting constants

Constant	Groeneveld 5.7	Groeneveld 5.9
a	0.052	0.00327
b	0.688	0.90100
c	1.260	1.32000
d	-1.060	-1.50000

Bishop-Sandberg-Tong Correlation

The Bishop-Sandberg-Tong correlation [Bishop et al., 1965] can be specified by user input for heat transfer in the film boiling region. This correlation defines the film boiling heat flux in the same manner as shown in Equation 4-39 for the Groeneveld correlation, that is:

$$q''_{FB} = h_{FB} (T_s - T_{sat}) \quad (4-43)$$

The film boiling heat transfer coefficient is defined primarily in terms of the properties of the vapor film at the wall, with the film temperature defined as in Equation 4-35. The heat transfer coefficient is of the form:

$$h_{FB} = C_1 \left(\frac{k_{vf}}{D_e} \right) (Re_{vf})^{0.8} (Pr_{vf})^{1.23} \quad (4-44)$$

$$C_1 = 0.0193 \left(\frac{\rho_g}{\rho_b} \right)^{0.68} \left(\frac{\rho_g}{\rho_f} \right)^{0.068}$$

Where,

k_{vf} = Coolant thermal conductivity at the film temperature, Btu/hr-ft-°F

D_e = Hydraulic diameter of flow channel, ft

Re_{vf} = Reynolds number, with fluid properties evaluated at the film temperature

Pr_{vf} = Prandtl number, with fluid properties evaluated at the film temperature

ρ_f = Saturated liquid density, lbm/ft³

ρ_g = Saturated vapor density, lbm/ft³

ρ_b = Bulk fluid density, lbm/ft³

The bulk fluid density (ρ_b) is defined in terms of the equilibrium void fraction as:

$$\rho_b = \rho_g \alpha + \rho_f (1 - \alpha) \quad (4-45)$$

The homogeneous void fraction (α) is defined as:

$$\alpha = \frac{x}{x + \left(\frac{\rho_g}{\rho_f}\right) (1 - x)} \quad (4-46)$$

Where,

x = Equilibrium quality, unitless

ρ_f = Saturated liquid density, kg/m³

ρ_g = Saturated vapor density, kg/m³

Groeneveld-Delorme Correlation

The Groeneveld-Delorme correlation [Groeneveld and Delorme, 1976] can be specified by user input for heat transfer in the film boiling region. This correlation defines the film boiling heat flux using the vapor temperature, rather than the saturation temperature, as the coolant sink temperature. That is:

$$q''_{FB} = h_{FB} (T_s - T_v) \quad (4-47)$$

Where,

h_{FB} = Film boiling heat transfer coefficient, Btu/hr-ft²-°F (Equation 4-48)

T_s = Local rod surface temperature, °F

T_v = Vapor temperature, °F corresponding to vapor enthalpy (h_v) calculated in Equation 4-52.

The heat transfer coefficient for film boiling is defined as:

$$h_{FB} = 8.348 \times 10^{-3} \left(\frac{k_{vf}}{D_e} \right) \left[\frac{GD_e}{\mu_{vf}} \left(x_a + \frac{\rho_v}{\rho_f} (1 - x_a) \right) \right]^{0.8774} Pr_{vf}^{0.6112} \quad (4-48)$$

Where,

k_{vf} = Vapor thermal conductivity at the film temperature, Btu/hr-ft-°F

D_e = Hydraulic diameter of flow channel, ft

G = Mass velocity of fluid, lbm/hr-ft²

μ_{vf} = Vapor viscosity at the film temperature, lbm/hr-ft

x_a = Modified equilibrium quality (see Equation 4-49) based on vapor enthalpy, unitless

ρ_v = Vapor density at vapor enthalpy (see Equation 4-52), lbm/ft³

ρ_f = Saturated liquid density, lbm/ft³

Pr_{vf} = Prandtl number, with fluid properties evaluated at the film temperature

The film temperature is the average of the rod surface temperature and the fluid saturation temperature, as defined in Equation 4-35.

The modified equilibrium quality (x_a) is included in the correlation to capture the effect of vapor superheat at the wall. The standard definition of the equilibrium quality is multiplied by a correction factor based on an approximation of the true enthalpy of the vapor phase, and is of the form:

$$x_a = x \left(\frac{h_{fg}}{h_v - h_f} \right) \quad (4-49)$$

Where,

x = Equilibrium quality (see Equation 4-50), unitless

h_{fg} = Latent heat of vaporization, Btu/lbm

h_f = Saturated liquid enthalpy, Btu/lbm

h_v = Enthalpy of the vapor phase (see Equation 4-52), Btu/lbm

The standard equilibrium quality is defined as:

$$x = \frac{h - h_f}{h_{fg}} \quad (4-50)$$

Where,

h = Local bulk fluid enthalpy, Btu/lbm

h_f = Saturated liquid enthalpy, Btu/lbm

h_{fg} = Latent heat of vaporization, Btu/lbm

Therefore, the equilibrium quality can be re-written as:

$$x_a = \frac{h - h_f}{h_v - h_f} \quad (4-51)$$

The enthalpy of the vapor phase (h_v) is estimated in terms of the vapor superheat at the wall, and is calculated as:

$$h_v = h_g + h_{fg} \exp\left(-\Psi - \frac{1}{(3\alpha)^4}\right) \quad (4-52)$$

Where,

h_g = Saturated vapor enthalpy, Btu/lbm

α = Homogeneous void fraction (see Equation 4-46)

Ψ = Empirical model parameter (see Equation 4-53)

The model parameter Ψ was determined from an empirical fit to the correlation's database, and has the functional form:

$$\Psi = \tan [C_1 (1.3072 - 1.0833x + 0.8455x^2)] \quad (4-53)$$

Where,

x = Equilibrium quality, unitless

C_1 = Empirical function of flow parameters (see Equation 4-54)

The coefficient C_1 is defined as:

$$C_1 \equiv \frac{0.13864 (Pr_g)^{0.2031} (Re_{HOM})^{0.20006}}{\left(\frac{q'' D_e C_{pg}}{k_g h_{fg}}\right)^{0.09232}} \quad (4-54)$$

Where,

k_g = Thermal conductivity of saturated vapor, Btu/hr-ft-°F

D_e = Channel hydraulic diameter, ft

Re_{HOM} = Homogeneous two-phase Reynolds number (see Equation 4-41)

Pr_g = Prandtl number, evaluated with saturated vapor properties

C_{pg} = Specific heat of saturated vapor, Btu/lbm-°F

h_{fg} = Latent heat of vaporization, Btu/lbm

q'' = Film boiling heat flux, calculated using Equation 4-47

4.2.3.5 Mode 7 Post-CHF Boiling for Low Flow Conditions

This mode is selected for post-CHF boiling heat transfer if the mass flux is below 2×10^3 lbm/hr-ft². No distinction is made between transition boiling and film boiling in this region. The surface heat flux is evaluated as:

$$q'' = h_{postCHF} (T_s - T_{sat}) \quad (4-55)$$

The default heat transfer coefficient in this region is the Bromley film boiling correlation [Bromley, 1949]. This correlation was developed from data obtained in round tubes at low flow rates and relatively low equilibrium quality, and is of the form:

$$h_{postCHF} = 0.62 \left(\frac{D_e}{2\pi \sqrt{\frac{g_c \sigma}{g (\rho_f - \rho_{vf})}}} \right)^{0.172} \left(\frac{k_{vf}^3 \rho_{vf} (\rho_f - \rho_{vf}) h_{fg} g}{D_e \mu_{vf} \Delta T_f} \right)^{0.25} \quad (4-56)$$

Where,

D_e = Hydraulic diameter of flow channel, ft

g = Acceleration of gravity, 32.2 ft/s²

g_c = Force to mass conversion constant for EU, 32.2 lbm-ft/lbf-s²

σ = Surface tension, lbf/ft

ρ_f = Saturated liquid density, lbm/ft³

ρ_{vf} = Vapor density at the film temperature, lbm/ft³

k_{vf} = Vapor thermal conductivity at the film temperature, Btu/hr-ft-°F

h_{fg} = Latent heat of vaporization, Btu/lbm

μ_{vf} = Vapor viscosity at the film temperature, lbm/hr-ft

ΔT_f = Wall superheat, $T_s - T_{sat}$ where T_s is the local rod surface temperature and T_{sat} is the saturation temperature, °F

The film temperature is the average of the rod surface temperature and the fluid saturation temperature, as defined in Equation 4-35.

4.2.3.6 Mode 8: Single-Phase Convection to Superheated Vapor

This mode is defined for conditions where the bulk fluid temperature is above the saturation temperature and the fluid can be treated as single-phase vapor. Heat transfer in this regime is calculated using the Dittus-Boelter correlation, with thermal properties defined at the vapor temperature; that is:

$$h_{spv} = 0.023 \left(\frac{k_v}{D_e} \right) \text{Re}^{0.8} \text{Pr}^{0.4} \quad (4-57)$$

Where,

h_{spv} = Heat transfer coefficient for single-phase vapor, W/m²-K

k_v = Thermal conductivity at the vapor temperature, W/m-K

D_e = Hydraulic diameter of flow channel, m

Re = Reynolds number (for characteristic length D_e)

Pr = Prandtl number

For conditions where the equilibrium quality is >1.0 , the heat transfer coefficient is defined as the minimum of the value for single-phase convection (obtained with Equation 4-57) and the value obtained with the user-specified film boiling correlation (in Mode 5 or 7). That is, in Mode 8, the heat transfer coefficient is defined as:

$$h_{Mode8} = \min(h_{FB}, h_{spv}) \quad (4-58)$$

Where,

h_{Mode8} = Heat transfer coefficient for single-phase vapor, W/m²-K

h_{FB} = Heat transfer coefficient for the fluid conditions, assuming Mode 5 or 7

h_{spv} = Heat transfer coefficient for the fluid conditions, assuming Mode 8

This approach avoids non-physical discontinuities in the transition between the film boiling and forced convection with single-phase vapor, which can occur due to the simplifications and approximations inherent in the homogeneous two-phase flow model used in FAST.

4.2.4 Critical Heat Flux Correlations

4.2.4.1 EPRI-1 CHF Correlation

The EPRI-1 correlation is the default CHF correlation in the FAST heat transfer package. This correlation was developed from a wide range of data obtained at Columbia University in BWR and PWR rod bundles, over the following range of parameters [Reddy and Fighetti, 1983]:

Table 4-3. Range of conditions for EPRI-1 CHF correlation

Parameter	Value or Range
Pressure	200–2400 psia
Mass Velocity	0.2–4.5 Mlbm/hr-ft ²
Equilibrium Quality	-0.25–0.75
Rod bundle geometry	3 × 3, 4 × 4, 5 × 5 rod arrays simulating commercial LWR fuel assemblies
Heated length	30, 48, 66, 72, 84, 96, 144, 150 and 168 in
Rod diameter	Typical PWR and BWR fuel rod diameters
Axial power profile	Uniform
Radial power distribution	Uniform and peaked (up to 1.3)

The pressure range of this database is extremely wide, and the form of this correlation is such that it can be extrapolated to pressures above 2450 psia and still produce reasonable predictions of CHF. Similarly, quality dependence can be extrapolated to subcooled conditions below -0.25 and still give reasonable predictions of CHF, and geometry dependence is relatively insensitive to rod diameter or channel hydraulic diameter. Extrapolation beyond the range of mass velocity, however, particularly into the lower range (below 0.2 Mlbm/hr-ft²), is inadvisable. For this range, the default in the code is the modified Zuber correlation [Zuber, 1961], regardless of the correlation selection specified by user input. When the EPRI-1 correlation is specified by user input, but the mass velocity is above 4.5 Mlbm/hr-ft², the code uses the Biasi correlation [Biasi et al., 1967] to determine CHF.

The general form of the EPRI-1 CHF correlation is:

$$q''_{CHF} = \frac{A - x_{in}}{C + \frac{x - x_{in}}{q''_L}} \quad (4-59)$$

Where,

q''_{CHF} = Critical heat flux, Btu/hr-ft²

x_{in} = Equilibrium quality at the beginning of the heated length, unitless

x = Local equilibrium quality, unitless

q''_L = Local heat flux at the rod surface, Btu/hr-ft²

A, C = Empirical parameters (see Equations 4-61 and 4-62).

The equilibrium quality is defined as:

$$x = \frac{h - h_f}{h_{fg}} \quad (4-60)$$

Where,

h = Bulk fluid enthalpy, Btu/lbm

h_f = Saturated liquid enthalpy, Btu/lbm

h_{fg} = Latent heat of vaporization, Btu/lbm

Parameters A and C are optimized statistical fits relating CHF to test conditions of pressure and mass velocity, and have the form:

$$A = c_1 P_r^{c_2} G^{c_5 + c_7 P_r} \quad (4-61)$$

$$C = c_3 P_r^{c_4} G^{c_6 + c_8 P_r} \quad (4-62)$$

Where,

P_r = Critical pressure ratio, $P_r = P/P_{crit}$

P = System pressure, psia

P_{crit} = Critical pressure, 3208.2 psia for water

G = Local mass velocity, Mlbm/hr-ft²

c_n = Optimized constants from statistical fit to data (see Table 4-4)

Table 4-4. Optimized constants for EPRI-1 CHF correlation

Constant	Value
c_1	0.5328
c_2	0.1212
c_3	1.6151
c_4	1.4066
c_5	-0.3040
c_6	0.4843
c_7	-0.3285
c_8	-2.0749

The base correlation (Equation 4-59) can be modified with three optional correction factors:

1. A two-part cold wall correction for corner-peaked bundles modeled with sub-channels (primarily applicable to BWR fuel assemblies)
2. A grid spacer correction factor for rod bundles with relatively high-loss grid designs (primarily applicable to fuel assemblies with mixing vane grids)
3. A non-uniform axial power correction factor

All of these options can be selected by user input. However, the default is to use only the base correlation.

The cold wall correction is applied by means of the following modifications to the critical heat flux defined in Equation 4-59:

$$q''_{CHF} = \frac{AF_a - x_{in}}{CF_c + \frac{x - x_{in}}{q''_L}} \quad (4-63)$$

The cold wall correction factors (F_A , F_C) are defined as:

$$F_A = 1.000G^{0.1} \quad (4-64a)$$

$$F_C = 1.183G^{0.1} \quad (4-64b)$$

The grid spacer correction is applied in a similar manner, as:

$$q''_{CHF} = \frac{A - x_{in}}{CF_g + \frac{x - x_{in}}{q''_L}} \quad (4-65)$$

The grid spacer correction factor (F_g) is defined as a function of the form loss coefficient for the grid (C_g , unitless) by the following equation:

$$F_g = 1.3 - 0.3C_g \quad (4-66)$$

The non-uniform axial power correction is applied identically as the grid spacer correction:

$$q''_{CHF} = \frac{A - x_{in}}{CF_{nu} + \frac{x - x_{in}}{q''_L}} \quad (4-67)$$

The non-uniform axial power correction factor (F_{nu}) is defined as:

$$F_{nu} = 1.0 + \frac{Y - 1}{1 + G} \quad (4-68)$$

Where Y is Bowring's non-uniform axial power factor (see Equation 4-77).

4.2.4.2 Bowring's Mixed Flow Cluster CHF Correlation

The CHF correlation developed by Bowring [Bowring, 1977] for mixed flow clusters can be specified by user input. This correlation was developed for application to thermal-hydraulic analysis of blowdown transients modeled with RELAP-UK, and is designed with the assumption that the local fuel assembly sub-channels are modeled as a single assembly-averaged flow channel. This correlation is not designed for detailed sub-channel analysis of the rod array. (For such applications, the EPRI-1 correlation is the recommended option.)

Bowring's correlation was developed from a very large database with test geometries representing rod clusters in pressure tube reactors, as well as test assemblies modeling BWR and PWR rod bundles. This correlation's database includes the following range of parameters:

Table 4-5. Range of conditions for Bowring's CHF correlation

Parameter	Range
Pressure	90–2250 psia
Mass Velocity	0.04–3.0 Mlbm/hr-ft ²
Hydraulic diameter	0.3–1.4 in (based on heated perimeter)
Heated length	60–180 in
Rod diameter	Typical PWR and BWR fuel rod diameters
Axial power profile	1.0–1.38 peak-to-average axial flux ratio
Radial power distribution	1.0–1.32 peak-to-average rod power ratio

The pressure range of this database is extremely wide, and dependence on this parameter is such that the correlation can generally be extrapolated to pressures above 2250 psia and still produces reasonable predictions of CHF. Similarly, geometry dependence is relatively insensitive to rod diameter or channel hydraulic diameter. Extrapolation beyond the range of mass velocity of the correlation's database, however, particularly into the lower range (below 0.04 Mlbm/hr-ft²), is inadvisable. For this range, the default in the code is the modified Zuber correlation, regardless of the correlation specified by user input.

The general form of Bowring's mixed cluster correlation is:

$$q''_{CHF} = \frac{A - Bh_{in}}{C + zY} \quad (4-69)$$

Where,

q''_{CHF} = Critical heat flux, Btu/hr-ft²

h_{in} = Enthalpy subcooling at inlet, Btu/lbm $h_{in} = h_f - h_{in}$

h_f = Saturated liquid enthalpy, Btu/lbm

h_{in} = Fluid enthalpy at inlet, Btu/lbm

z = Axial distance from beginning of heated length, in

Y = Non-uniform axial heat flux correction factor (see Equation 4-77)

A, B, C = Empirical parameters (see Equation 4-70 through Equation 4-74 for parameter A , Equation 4-75 for parameter B , and Equation 4-76 for parameter C), based on data obtained in pressure tube geometries with subcooled inlet conditions.

The empirical parameter A of this correlation is a function of the flow rate, the system pressure and the geometry (through the hydraulic diameter terms), and is defined as follows:

$$A = \frac{242.2F_1GD_e}{1 + \left(\frac{1.52(F_p D_e)^2 G}{F_2 D_h^{1.3} [1 + G(0.8F_p \frac{D_e}{D_h} - 1)]} \right)} \quad (4-70)$$

Where,

G = Mass velocity, lbm/hr-ft²

D_e = Channel hydraulic diameter based on wetted perimeter, ft

D_h = Channel hydraulic diameter based on heated perimeter, ft

F_p = Radial peaking (ratio of peak rod power to average rod power)

F_1, F_2 = Empirical parameters (see Equation 4-71 and Equation 4-72)

The parameters F_1 and F_2 in Equation 4-70 are statistically fitted functions of pressure, and have the form:

$$F_1 = \left(1 - 0.04P_T \sqrt{1 + 0.47P_T^2} \right)^2 \quad (4-71)$$

$$F_2 = \begin{cases} 0.45 + 1.25P_T & P \leq 415 \text{ psia} \\ 0.424 + 1.959P_T - 1.556P_T^2 & 415 \text{ psia} < P \leq 650 \text{ psia} \\ (3.2 - P_T)(0.32 + 0.135P_T) & P > 650 \text{ psia} \end{cases} \quad (4-72)$$

Where P_T is reduced pressure; $P_T = 0.001P$, where P is the system pressure in psia.

The formulation in Equation 4-70 for parameter A is applicable to pool test reactor, BWR, and PWR geometries when the pressure is below 1250 psia. When the system pressure is above 1250 psia, however, this parameter requires additional terms, as follows:

$$A = A_2 + (2.25 - 0.001P)(A_1 - A_2) \quad (4-73)$$

Where,

$A_1 = A$ from Equation 4-70, evaluated at $P = 1250$ psia

$A_2 =$ Correlation parameter (see Equation 4-74)

The high-pressure term for parameter A is a function of mass velocity and geometry, and is defined as:

$$A_2 = 18G + \frac{9.5GD_e}{0.1 + G} \quad (4-74)$$

Where,

G = Mass velocity, lbm/hr-ft²

D_e = Channel hydraulic diameter based on wetted perimeter, ft

Correlation parameter B is a function of the mass velocity and channel hydraulic diameter, and is defined as:

$$B = 0.25GD_e e^{-0.2G} \quad (4-75)$$

Where,

G = Mass velocity, lbm/hr-ft²

D_e = Channel hydraulic diameter based on wetted perimeter, ft

Correlation parameter C contains the axial power shape correction factor, and is of the form:

$$C = 60D_h^{0.57} G^{0.27} \left(1 + \frac{Y - 1}{G + 1} \right) \quad (4-76)$$

Where,

G = Mass velocity, lbm/hr-ft²

D_e = Channel hydraulic diameter based on wetted perimeter, ft

The parameter Y is the non-uniform axial heat flux correction factor for this correlation, and is defined as:

$$Y = \frac{\int_0^Z \bar{q}''(z) dz}{\bar{q}''(Z) Z} \quad (4-77)$$

Where,

$\bar{q}''(z)$ = Radially averaged axial heat flux at axial location z , Btu/hr-ft²

Z = Axial distance from beginning of heated length, in

The integral in Equation 4-77 is adapted to the discrete nodes of a computer model by converting the continuous integration function to a summation over the axial nodal steps, as shown by:

$$\frac{\int_0^Z \bar{q}''(z) dz}{\bar{q}''(Z) Z} \cong \frac{\sum_{j=2}^J \bar{q}''_j x_j}{\bar{q}''_J X_J} \quad (4-78)$$

Where,

\bar{q}''_j = Radially averaged axial heat flux at node j , Btu/hr-ft²

X_J = Axial distance from beginning of heated length to node J in

x_j = Length of axial node j , in

j = Axial node index counter

J = Index of axial node corresponding to axial distance Z

4.2.4.3 MacBeth's CHF Correlation

The CHF correlation developed by MacBeth and Thompson [Thompson and MacBeth, 1964] can be specified by user input. This correlation was developed using a database consisting of a compilation of a large amount of CHF data from a wide variety of sources. This data consisted entirely of uniformly heated round tubes with vertical up-flow. The database includes the following range of parameters:

Table 4-6. Range of conditions for MacBeth's CHF correlation

Parameter	Range
Pressure	15–2700 psia
Mass Velocity	0.0073–13.7 Mlbm/hr-ft ²
Hydraulic diameter	0.04–1.475 in
Heated length	1.0–144 in
Axial power profile	uniform

Although the database of this correlation consists entirely of burnout tests in round tubes, the correlation has been successfully extrapolated to CHF in annuli and rod bundles at low pressure. For pressure conditions outside the range of the database, or mass velocities above 13.7 Mlbm/hr-ft², the CHF correlation selection logic in FAST defaults to the Biasi correlation [Biasi et al., 1967]. For mass velocity values below the extremely low lower bound of the database, the code defaults to the modified Zuber correlation.

The MacBeth correlation is constructed with two essentially separate functions, one applicable to CHF for relatively low flow conditions, and one for high flow conditions. At low flow conditions, the

relationship between mass velocity and CHF is approximately linear, and is essentially independent of pressure. For these conditions, the correlation defines the CHF as:

$$q''_{CHF_{Low-Velocity}} = 6.33 \times 10^{-3} h_{fg} D_e^{-0.1} \left(\frac{G}{10^6} \right)^{0.51} (1 - x) \quad (4-79)$$

Where,

$q''_{CHF_{Low-Velocity}}$ = Critical heat flux in low velocity region, Btu/hr-ft²

D_e = Channel hydraulic diameter based on wetted perimeter, ft

h_{fg} = Latent heat of vaporization, Btu/lbm

G = Mass velocity, lbm/hr-ft²

x = Equilibrium quality, unitless

For high flow conditions, the correlation defines the CHF as a somewhat more complex function of mass velocity, equilibrium quality, and geometry, with a strong dependence on pressure. The form of the correlation in this region is:

$$q''_{CHF_{High-Velocity}} = \frac{A - 0.25 D_e \left(\frac{G}{10^6} \right) h_{fg} x}{C} \quad (4-80)$$

Where,

$q''_{CHF_{HighVelocity}}$ = Critical heat flux in high velocity region, Btu/hr-ft²

D_e = Channel hydraulic diameter based on wetted perimeter, ft

h_{fg} = Latent heat of vaporization, Btu/lbm

G = Mass velocity, lbm/hr-ft²

x = Equilibrium quality, unitless

A, C = Empirical parameters (see Equation 4-81 and Equation 4-82)

The empirical parameters A and C were defined using statistical optimization for two overlapping sets of data. The first data set consisted of 1344 test points, over the following ranges of conditions:

Table 4-7. Range of conditions for MacBeth's 6-coefficient correlation

Parameter	Range
Pressure	15–2700 psia
Mass Velocity	0.01–7.82 Mlbm/hr-ft ²
Hydraulic diameter	0.04–0.934 in
Heated length	1.0–123 in

The parameters A and C for this data set are formulated as:

$$A = y_0 D_e^{y_1} \left(\frac{G}{10^6} \right)^{y_2} \quad (4-81a)$$

$$C = y_3 D_e^{y_4} \left(\frac{G}{10^6} \right)^{y_5} \quad (4-81b)$$

Where,

D_e = Channel hydraulic diameter, based on wetted perimeter, ft

G = Mass velocity, lbm/hr-ft²

y_n = Empirical coefficients (see Table 4-8)

Table 4-8. Coefficients for MacBeth's 6-coefficient model for a given reference pressure (psia)

Coefficient	250	530	1000	1570	2000	2700
y_0	106.5	123.5	124.5	59.90	67.50	1.300
y_1	0.847	0.834	0.913	0.873	1.130	-0.050
y_2	0.677	0.408	0.376	0.120	0.535	1.020
y_3	60.30	78.80	118.0	82.70	108.0	103.0
y_4	1.400	1.400	1.400	1.400	1.400	1.400
y_5	0.937	0.737	0.555	0.096	0.343	0.529

The second data set expanded the number of test points by 232, to 1576, to create the complete database of the correlation. The additional tests expanded the database to encompass the following ranges of conditions:

Table 4-9. Range of conditions for MacBeth’s 12-coefficient model

Parameter	Range
Pressure	15–2700 psia
Mass Velocity	0.0073–13.7 Mlbm/hr-ft ²
Hydraulic diameter	0.04–1.475 in
Heated length	1.0–144 in

The parameters *A* and *C* for this data set are formulated as:

$$A = y_0 D_e^{y_1} \left(\frac{G}{10^6} \right)^{y_2} \left[1 + y_3 D_e + y_4 \left(\frac{G}{10^6} \right) + y_5 D_e \left(\frac{G}{10^6} \right) \right] \tag{4-82a}$$

$$C = y_6 D_e^{y_7} \left(\frac{G}{10^6} \right)^{y_8} \left[1 + y_9 D_e + y_{10} \left(\frac{G}{10^6} \right) + y_{11} D_e \left(\frac{G}{10^6} \right) \right] \tag{4-82b}$$

Where,

D_e = Channel hydraulic diameter based on wetted perimeter, ft

G = Mass velocity, lbm/hr-ft²

y_n = Empirical coefficients (see Table 4-10)

Table 4-10. Coefficients for MacBeth’s 12-coefficient model for a given reference pressure (psia)

Coefficient	560	1000	1550	2000
<i>y</i> ₀	237.00	114.00	36.000	65.50
<i>y</i> ₁	1.2000	0.8110	0.5090	1.190
<i>y</i> ₂	0.4250	0.2210	-0.1090	0.376
<i>y</i> ₃	-0.9400	-0.1280	-0.1900	0.577
<i>y</i> ₄	-0.0324	0.0274	0.0240	0.220
<i>y</i> ₅	0.1110	-0.0667	0.4630	-0.373
<i>y</i> ₆	19.300	127.00	41.700	17.10
<i>y</i> ₇	0.9590	1.3200	0.9530	1.180
<i>y</i> ₈	0.8310	0.4110	0.0191	-0.456
<i>y</i> ₉	2.6100	-0.2740	0.2310	-1.530
<i>y</i> ₁₀	-0.0578	-0.3970	0.0767	2.750
<i>y</i> ₁₁	0.1240	-0.0221	0.1170	2.240

4.2.4.4 Modified Zuber Correlation

The modified Zuber correlation [Zuber, 1961] [Smith and Griffith, 1976] is included in the CHF correlation selection option in FAST, and can be selected by user input. This correlation was developed for CHF calculations in LWRs in severe accident conditions and is applicable to very low flow conditions. The correlation is based on pool boiling CHF hydrodynamics, and is formulated in terms of local fluid conditions, which makes it essentially independent of pressure. It was originally formulated for very high void fraction (above 96%), but modifications have been developed⁴ that make the range of applicability essentially independent of void fraction. This was done to make the correlation applicable to inverted annular film boiling, which can include conditions where the bulk fluid is subcooled.

The modified Zuber correlation is the default selection in the code for all cases where the mass velocity is below 0.2 Mlbm/hr-ft² or the void fraction is above 80% . The general form of the correlation is as follows:

$$q''_{CHF} = 0.1309 F_G F_{subc} h_{fg} \sqrt{\rho_g} \left(\sigma g_c g (\rho_f - \rho_g) \right)^{0.25} \quad (4-83)$$

Where,

h_{fg} = Latent heat of vaporization, Btu/lbm

ρ_g = Saturated vapor density, lbm/ft³

ρ_f = Saturated liquid density, lbm/ft³

σ = Surface tension, lbf/ft

g = Acceleration of gravity, 32.2 ft/s²

g_c = Force to mass conversion constant for EU, 32.2 lbm-ft/lbf-s²

F_G = Correction factor for extended void fraction range (see Equation 4-84)

F_{subc} = Correction factor for bulk subcooled fluid conditions (see Equation 4-85)

The correction factor to generalize the void fraction range of the correlation is defined as

$$F_G = 0.9 (1 - \alpha) \quad (4-84)$$

Where,

α = Local void fraction, unitless

⁴Based on modifications to the Zuber correlation in the JAERI code NSR-77.

The correction factor for bulk subcooled conditions is

$$F_{subc} = 1 + 0.065 \left(\frac{\rho_f}{\rho_g} \right)^{0.8} \left(\frac{c_{pf}(T_{sat} - T_b)}{h_{fg}} \right) \quad (4-85)$$

Where,

ρ_g = Saturated vapor density, lbm/ft³

ρ_f = Saturated liquid density, lbm/ft³

c_{pf} = Specific heat of saturated liquid, Btu/lbm/°F

h_{fg} = Latent heat of vaporization, Btu/lbm

T_{sat} = Saturation temperature, °F

T_b = Bulk fluid temperature, °F

4.2.4.5 Biasi Correlation

The Biasi correlation [Biasi et al., 1967] is included in the CHF correlation selection option in FAST, and can be selected by user input. This correlation was developed for CHF calculations in LWRs in severe accident conditions and is applicable to very wide range of conditions. The Biasi correlation is the automatic default in the code for conditions where the system pressure is below the pressure range of the user-selected correlation, or the mass velocity is above the user-selected correlation's mass velocity range. However, if the void fraction is above 80% , the correlation selection defaults to the modified Zuber correlation, no matter what the flow rate or pressure, and regardless of which correlation has been selected by user input.

The Biasi correlation was derived in metric units, and has two separate formulations for the CHF:

$$q''_{CHF} = \max(q''_{CHF_1}, q''_{CHF_2}) \quad (4-86)$$

The first component is defined as:

$$q''_{CHF_1} = b_1 G^{b_2} \left(F_p G^{b_2} - x \right) D_e^{-n} \quad (4-87)$$

Where,

G = Mass velocity, g/s-cm²

F_p = Pressure-dependent empirical factor (see Equation 4-88)

x = Equilibrium quality, unitless

D_e = Channel hydraulic diameter based on wetted perimeter, cm

b_1, b_2, n = Empirical parameters

The pressure-dependent empirical factor F_p is defined as:

$$F_p = b_3 + b_4 P \exp(b_5 P) \quad (4-88)$$

Where,

P = Pressure, bar

b_3, b_4, b_5 = Empirical coefficients

The second component of the CHF is defined as

$$q''_{CHF_2} = c_1 G^{c_2} (F_H (1 - x)) D_e^{-n} \quad (4-89)$$

Where,

G = Mass velocity, g/s-cm²

F_H = Pressure-dependent empirical factor (see Equation 4-90)

x = Equilibrium quality, unitless

D_e = Channel hydraulic diameter, based on wetted perimeter, cm

c_1, c_2 = Empirical coefficients

n = Empirical coefficient on hydraulic diameter (see Equation 4-91)

The pressure-dependent empirical factor F_H is defined as:

$$F_H = c_3 + c_4 P e^{c_5 P} + \frac{c_6 P}{c_7 + P^2} \quad (4-90)$$

Where,

P = Pressure, bar

D_e = Channel hydraulic diameter based on wetted perimeter, cm

c_n = Empirical coefficients

The coefficient n on the hydraulic diameter in Equations 4-87 and 4-89 is defined as follows:

$$n = \begin{cases} 0.6, & D_e < 1.0 \\ 0.4, & D_e \geq 1.0 \end{cases} \quad (4-91)$$

4.2.5 Influence of Rod Bowing on Critical Heat Flux

The calculation of critical heat flux reduction due to fuel rod bowing is a user option in FAST. If this option is used, both CHF and fuel rod power are calculated according to the amount of fuel rod bowing. The reductions are calculated by empirical correlations. The correlations for CHF reduction are:

$$q_{CHFR}(Z) = 1 - f_{CHF}(Z)q_{CHF}(Z) \quad (4-92a)$$

$$f_{CHF}(Z) = \begin{cases} 0, & W(Z) \leq W_{Thr} \\ F_{BCHF} \frac{W(Z) - W_{Thr}}{1 - W_{Thr}}, & W(Z) > W_{Thr} \end{cases} \quad (4-92b)$$

Where,

$f_{CHF}(Z)$ = Fractional decrease in CHF due to fuel rod bowing at elevation Z

q_{CHFR} = Reduced critical heat flux

q_{CHF} = Critical heat flux in absence of fuel rod bowing

$W(Z)$ = Amount of fuel rod bowing (fraction of bowing required to contact adjacent fuel rod, 0 = no bowing, 1 = maximum possible bowing)

W_{Thr} = Maximum amount of bowing which can occur without an effect on CHF (fraction of maximum bowing possible) specified by user input.

F_{BCHF} = Multiplication factor specified by user input (see Section B.7)

The reduction in fuel rod power due to bowing is calculated by the equation:s

$$P_r = \begin{cases} P, & W(Z) \leq 0.3 \\ \left[1 + 0.01 \left(0.94W(Z) - 2.84W(Z)^2\right)\right] P, & W(Z) > 0.3 \end{cases} \quad (4-93)$$

Where,

P_r = Power reduced to account for fuel rod bowing

P = Power in absence of fuel rod bowing

4.3 Sodium

The correlations for the heat transfer coefficient are based on the assumption of a single phase liquid with incompressible flow. The correlations are expected to cover the range of conditions expected under normal and accident conditions for a sodium-cooled reactor, given the lower pressure and operating temperatures.

No correlation for CHF is implemented and will result in a value of 0.0.

4.3.1 Heat Transfer Coefficient Correlations

Heat transfer correlations are empirical models developed to quantify the rate of energy exchange between a solid surface and a fluid flowing over it. Heat transfer correlations are expressed as a coefficient relating the surface heat flux to the temperature difference between the surface and the fluid:

$$q'' = h (T_{wall} - T_{fluid}) \quad (4-94)$$

Where,

q'' = Surface heat flux, W/m²

T_{wall} = Wall surface temperature, K

T_{fluid} = Sodium temperature, K

h = Heat transfer coefficient, W/m²-K

4.3.1.1 Single-Phase Convection to Liquid

This mode is defined for conditions where the bulk fluid can be treated as single-phase liquid. Heat transfer in this regime is calculated using the Subbotin and Schad correlations [Ha et al., 2007], with thermal properties defined at the liquid temperature, as shown in Equation 4-95:

$$h = Nu \left(\frac{k_v}{D_e} \right) \quad (4-95)$$

Where,

h = Heat transfer coefficient for single-phase gas, W/m²-K

k_v = Thermal conductivity at the gas temperature, W/m-K

D_e = Hydraulic diameter of flow channel, m

Nu = Nusselt number (ratio of convective to conductive heat transfer)

The Nusselt number (Nu) is taken as the maximum of the values calculated using either the Schad (Nu_{schad}) or Subbotin (Nu_{sub}) correlation, as shown in Equations 4-96 and 4-97, respectively.

$$Nu_{schad} = \begin{cases} 5.0 + 0.25Pe^{0.8}, & Pe \leq 10.0 \\ 0.0, & Pe > 10.0 \end{cases} \quad (4-96)$$

$$Nu_{sub} = \begin{cases} 4.496 \left(-16.15 + 24.96 \left(\frac{Pitch}{Diameter} \right) - 8.55 \left(\frac{Pitch}{Diameter} \right)^2 \right), & Pe \leq 150.0 \\ \left(-16.15 + 24.96 \left(\frac{Pitch}{Diameter} \right) - 8.55 \left(\frac{Pitch}{Diameter} \right)^2 \right) Pe^{0.3}, & Pe > 150.0 \end{cases} \quad (4-97)$$

The Peclet number (Pe) is calculated using Equation 4-98:

$$Pe = Re \cdot Pr \quad (4-98)$$

Where,

Re = Reynolds number

Pr = Prandtl number

4.3.1.2 Range of applicability

These correlations are only valid for liquid sodium with a Peclet number up to 1000.0. Beyond this number, the Schad correlation is used but is not within the bounds of applicability.

4.4 Helium

The correlations for the heat transfer coefficient are based on the assumption of a single gas phase with incompressible flow. The correlations are expected to cover the range of conditions expected under normal and accident conditions for a gas-cooled reactor, such as those that were experienced in the Fort St. Vrain reactor.

This correlation only models the heat transfer due to convection. There is currently no correlation in FAST for heat transfer due to radiation; this will have a significant impact on overall heat transfer and fuel temperature. Additionally, due to the effects of radiative heat transfer, the approach in FAST to model a single pin in a closed fuel channel may not be applicable to gas reactors where heating from neighboring fuel elements is significant. This capability should be considered highly preliminary.

No correlation for CHF is implemented and will result in a value of 0.0.

4.4.1 Heat Transfer Coefficient Correlations

Heat transfer correlations are empirical models developed to quantify the rate of energy exchange between a solid surface and a fluid flowing over it. Heat transfer correlations are expressed as a

coefficient relating the surface heat flux to the temperature difference between the surface and the fluid:

$$q'' = h (T_{wall} - T_{fluid}) \quad (4-99)$$

Where,

q'' = Surface heat flux, W/m²

T_{wall} = Wall surface temperature, K

T_{fluid} = Gas temperature, K

h = Heat transfer coefficient, W/m²-K

4.4.1.1 Single-Phase Convection to Gas

This mode is defined for conditions where the bulk fluid can be treated as single-phase gas. Heat transfer in this regime is calculated using the Dittus-Boelter correlation, with thermal properties defined at the gas temperature; that is:

$$h = 0.024725 \left(\frac{k_v}{D_e} \right) Re^{0.8} Pr^{0.6} \quad (4-100)$$

Where,

h = Heat transfer coefficient for single-phase gas, W/m²-K

k_v = Thermal conductivity at the gas temperature, W/m-K

D_e = Hydraulic diameter of flow channel, m

Re = Reynolds number (for characteristic length D_e)

Pr = Prandtl number

4.4.1.2 Range of applicability

The correlations are only valid for a non-mixed helium gas. This correlation only includes the impact of gas convection and does not include radiative heat transfer, which is significant for gas-cooled reactors. The range of application based on flow rates and temperatures has not yet been derived.

5.0 External Code Interfaces

FAST is designed to be used as a stand-alone tool for current LWR licensing needs. However, there are circumstances that arise when the models within FAST are not sufficient to perform a new type of analysis, or the models within FAST are needed by another code. Some examples include:

- Rapid transients that require the full plant response and feedback between FAST and a systems code
- Alternate fuel forms where the models within FAST were developed for standard UO₂
- Analyses that require physics not modeled by FAST, such as I/Cs inventories for source term

In order to enhance the flexibility of the code and perform “multiphysics” calculations, FAST has been modified to support various interfaces. The following two interfaces are supported:

- ECI
- JSON

The codes that have been tested against include:

Table 5-1. Codes linked with FAST

Interface	Code(s) Supported
ECI	TRACE (NRC developed and maintained code)
JSON	EPIC (Developed by Oak Ridge National Laboratory)

This section describes the interfaces between FAST and external codes, the sync points, and what data can be transferred/received.

5.1 Communication Interfaces

5.1.1 File-based JSON Interface

The JavaScript Object Notation (JSON) input/output file interface is based on the ECMA-404 Standard [International, 2017]. This is an ASCII-based, user-readable simplistic file format with significant flexibility. To interface with the largely Fortran-written source code, FAST uses a modified version of the open source `json-fortran` code [Williams, 2018].

5.1.2 Exterior Communications Interface (ECI)

In addition to a file based communication interface, FAST utilizes the Exterior Communications Interface (ECI) [NRC, 2017] which transfers information between two or more codes via shared memory and a driver program (java based). The ECI was developed for the NRC's TRACE code and has been adopted by FAST to allow for FAST to couple with TRACE (and other external codes utilizing ECI). FAST can run as either the central or as a child process, meaning it can be the driver in progressing the calculation or it can be called by a driver ECI program. In short, the ECI works like this:

1. Startup of driver program, which enters an infinite loop doing the following:
 - Waits for connection
 - Transmits and receives necessary data
 - Starts necessary child processes
2. Start central program
3. Code(s) establish what information is available and/or requested
4. Central process drives the calculation
5. Each code provides/requests information at its internal sync points

5.1.3 FAST Driving External Codes

FAST has the ability to call other executable programs after it has started running, allowing the other program to be started normally without any additional modifications specific to FAST. There are two modes in which the external program can be run:

- Serial mode (the external code is called only once)
- Iterative mode (the external code is continually called)

5.2 FAST/EPIC Interface

EPIC is a code developed by Oak Ridge National Laboratory (ORNL) that uses the SCALE code packages for cross-section processing, transport and depletion to calculate the following parameters:

- Intra-pin power distribution
- Isotopics distribution

In order to calculate these parameters, EPIC needs the following types of information from FAST:

- Geometry definition
- Material definition (type, temperature, density, etc.)
- Time
- Power

5.2.1 Methodology for Single Rod Analysis

FAST can communicate with EPIC via a series of JSON formatted files, as described in Section 5.1.1.

A schematic of this information exchange can be seen in Figure 5-1.

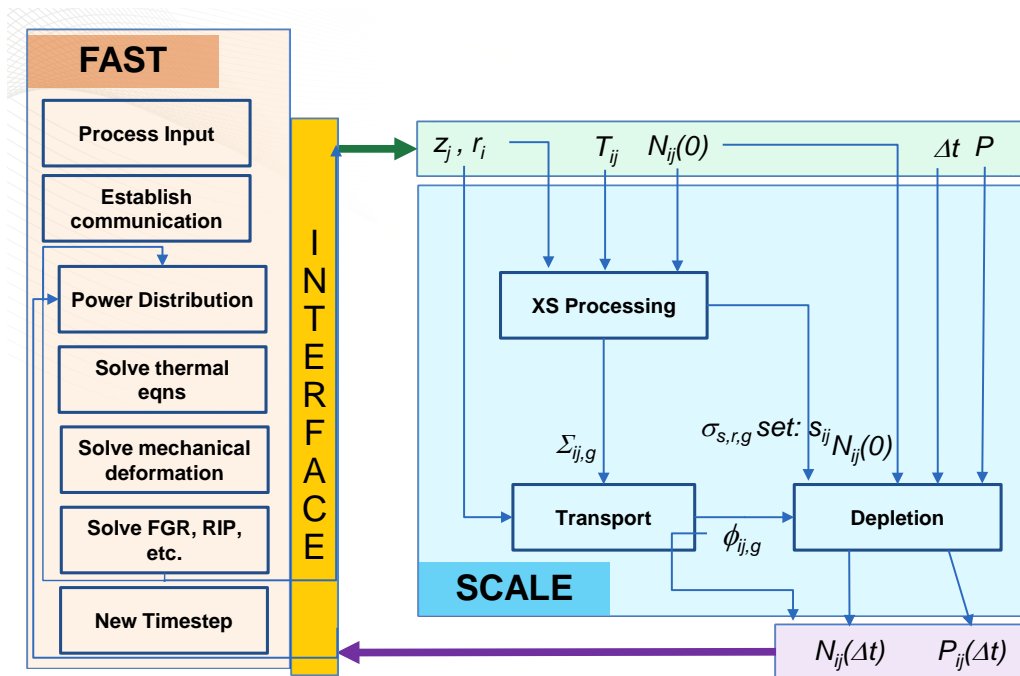


Figure 5-1. FAST-EPIC calculational scheme

5.2.2 FAST-to-EPIC File

The available definitions for the FAST-to-EPIC input file are shown in Table 5-2.

Table 5-2. FAST-to-EPIC file input definitions

Inputs	Description
geometryDefinition	Describes the geometry type
powerDefinition	Describes the power and time
meshDefinition	Describes the geometry nodalization and material placement
materialDefinition	Describes the material composition
stateDefinition	Describes the density and temperature

The following tables show the available inputs for each of the input definitions from Table 5-2. In JSON format, (S) stands for string, (N) stands for single number, and (A) stands for array of numbers.

Table 5-3. geometryDefinition options

Inputs	Description	Options/Units	Required
type (S)	Type of geometry	“FIXED”, “PIN”	Yes
latticeType (S)	Type of fuel assembly lattice	“SQUARE”, “HEXAGONAL”	Yes

Table 5-4. powerDefinition options

Inputs	Description	Options/Units	Required
type(S)	Type of geometry	“STEP CONSTANT”	Yes
dt (A)	Time step sizes	days	Yes
power (A)	Total power	W	Yes

Table 5-5. meshDefinition options

Inputs	Description	Options/Units	Required
type(S)	Type of geometry	“STRUCTURED AXIAL”	Yes
radialMaterialsByAxialZone (A)	Material IDs to match <user-defined id>	N/A	Yes
zoneRadii (A)	Distance to each radial boundary	m	Yes
zoneHeight (A)	Distance to each axial boundary	m	Yes

Table 5-6. materialDefinition options

Inputs	Description	Options/Units	Required
<user-defined id> (S)	User-defined ID for material	Must be ASCII a-z, A-Z, 0-9	Yes
type (A)	Material IDs for each zone	Must match IDs in materialDefinition	Yes
enrichment (N)	²³⁵ U enrichment	N/A	Yes

Within each material ID, there are several material options.

Table 5-7. stateDefinition options

Inputs	Description	Options/Units	Required
type (S)	Type of state definition	“ZONE CONSTANT”	Yes
density (A)	Material densities	kg/m ³	Yes
temperature (A)	Material temperatures	K	Yes

5.2.3 EPIC-to-FAST File

The file written by EPIC-to-FAST contains information related to power distribution, power uncertainty, and elemental composition (as determined using EPIC’s ORIGEN depletion module). In addition, the time is also provided as a consistency check between what FAST provided and what EPIC used in its calculation. The available inputs in this file are shown in Table 5-8.

Table 5-8. EPIC-to-FAST file input definitions

Inputs	Description	Options/Units	Required
timeList	Problem time (same as those provided by FAST)	days	Yes
powerList	Power	W	Yes
powerListStandardDeviation	Standard deviation of power	W	Yes
elementList	Describes the elemental compositions	at%	Yes

5.3 FAST/TRACE Interface

TRACE is the NRC’s code for system wide thermal hydraulic analysis [Division of Safety Analysis, 2017]. TRACE can be used by FAST in two modes: either FAST running TRACE in lieu of its own

coolant model, or TRACE running FAST as TRACE's fuel rod model code.

5.4 Output File for FAST-to-TRACE Data Transfer

For design basis accidents, the NRC uses the system-level thermal-hydraulics code TRACE for assessing the figures of merit for fuel behavior (which are typically burst, peak cladding temperature (PCT) and ECR. TRACE has simplified fuel performance models that are based on those found in fast (i.e., models that impact temperature distribution). However, TRACE is designed to work for short duration transients and therefore can not calculate the burnup of the fuel rod. FAST is used to provide the burnup-dependent information to TRACE to ensure that fuel temperatures and stored energy are not underestimated. In addition, this information is used to support the proposed new NRC LOCA regulations in 10 CFR 50.46(c) that require LOCA analyses to account for the pre-existing hydrogen in the cladding, which impacts how much transient oxidation can occur within the regulatory limits.

To perform this data transfer, the NRC uses the SNAP interface to transfer the data from FAST outputs into a TRACE input file to develop fuel rod inputs for both PWRs and BWRs, which are referred to in TRACE as heatstructures and CHANs, respectively. The NRC also uses a tool called MAKECHAN, developed under NRC contract by Energy Research, Inc., (ERI) which works with PARCS outputs to develop a TRACE/PARCS input deck.

This section outlines the file format that has been agreed upon by NRC, ERI and APT that contains all of the necessary information from a FAST calculation to populate a TRACE "fuel rod". To turn on the writing of this file, see Section B.3.

5.4.1 File Variables

The following burnup-dependent information calculated by FAST is needed to populate the fuel rod input parameters in TRACE:

- Gas composition - Total moles, mole fraction of each species, pressure
- Fuel composition - Axial Gadolinia content
- Burnup - Rod average, axial, and 2D (axial/radial)
- Deformations - Fuel swelling, densification and cladding inner radius permanent deformation
- Cladding data - Hydrogen content, oxide layer thickness, crud thickness
- Mesh data - Meshpoints, power and temperatures

Through sensitivity studies, the NRC has decided to use the number of moles of gas to calculate the rod internal pressure rather than the rod internal pressure input option. There are several reasons for this, with the most significant (as of TRACE V5P5) being that the rod internal pressure input for TRACE is assumed to be taken at room temperature, whereas the value produced by FAST is at operating conditions. It is not sufficient to assume a simple ideal gas law ($PV = nRT$) due to the changes in void volume associated with the change in fuel temperature.

5.4.2 File Units

The file is output entirely in SI, regardless of the FAST input file units (which can be SI or British). The units for each variable are shown in Table 5-9.

Table 5-9. Variables^(a) written in MAKECHAN file

Description	Units	File Syntax
Temperature	Kelvin	kelvin
Burnup	Mega-Watt days per Kilogram Uranium	MWd/kgU
Pressure	Pascals	pa
Moles	Moles	moles
Distance	Meters	meter
Time	Days	days
Weight Fraction	Weight Percent	wt%
Concentration	Parts per million	ppm
Unitless	-	na

^(a) All variables are rod average values.

5.4.3 File Header

The file header information printed to the file is shown in Tables 5-10 and 5-11. The header information is the generic information that describes information about the code version, when the file was produced, and descriptions of the variables being written to the file. This information is written before the start of the timestep dependent, FAST calculated data.

Table 5-10. File case-specific information

Line	Description
1	FAST Version ID
2	Date code was built
3	Date and time code was run
4	Case Description (as defined in input file)

The information for each FAST variable written to the file (ID, units, and description) shown in Table 5-11 is exactly as it appears in the file. This data starts on Line 5 and continues on a new line until the last variable in the table is written. The headings in the table (e.g., "Rod Average Data") also constitute a new line. These headings indicate changes to the format of the data written to the file, such as moving from a single value to an array of data.

Table 5-11. File variables written in MAKECHAN file

ID	Units	Description
Rod Average Data		
1	days	Problem time
2	MWd/kgU	Rod Average burnup
3	Pa	Rod internal pressure
10	mol	Moles of gas in rod
11	–	Mole fraction of Helium in gas
12	–	Mole fraction of Krypton in gas
13	–	Mole fraction of Xenon in gas
14	–	Mole fraction of Argon in gas
15	–	Mole fraction of Nitrogen in gas
16	–	Mole fraction of Hydrogen in gas
17	–	Mole fraction of Air in gas
18	–	Mole fraction of Steam in gas
Axial Data		
101	wt%	Gadolinia content
102	MWd/kgU	Nodal Burnup
110	m	Cladding Outer Oxide Thickness
111	m	Cladding Outer Crud Thickness
112	ppm	Cladding Hydrogen Concentration
120	m	Fuel Swelling
121	m	Fuel Densification
122	m	Fuel Relocation
123	m	Cladding Inner Radius Permanent Deformation
Axial x Radial Data		
200	m	Fuel Rod Mesh Radial Nodes
201	K	Fuel Rod Mesh Temperatures
202	–	Radial Power Profile
203	MWd/kgU	Fuel Rod Mesh Burnup

5.4.4 File Time-Dependent Data

The time-dependent data is written at every “plot” timestep (See Section B.3). Table 5-12 outlines the format of the time-dependent data as it is written to the file. This data follows the header information and is repeated for each timestep until the FAST code execution is terminated.

Table 5-12. Time-dependent information format

Description	File Syntax/Information
Start of new timestep	===next time step <timestep>
Example	===next time step 1
Rod average values	After ID, two spaces and array of real values
Example	1 1.15740741E-08
Axial values	After ID, two spaces and array of real values. The number of values is equal to the number of axial nodes, with the first value being axial node(1) at the bottom and the last value being at the top fueled axial node
Example	102 5.57881917E-11 1.27440309E-10
Axial by radial values	After ID, two spaces and an array of radial values (starting from the fuel centerline). The ID is repeated on the next line for each axial node, starting from the bottom (first row of values) to the top (last row of values for a given ID)
Example	201 6.40368328E+02 6.39045340E+02 201 7.39641329E+02 7.36258582E+02 201 1.16207667E+03 1.14673771E+03

FAST uses Fortran's Engineering Scientific notation (ES15.8), which contains one value before the period, eight values after the period, and two exponential placeholders. The format of each data value is [1.00000000E-03].

This page intentionally blank.

6.0 References

- [ANS, 1982] ANS. 1982. Method for Calculating the Fractional Release of Volatile Fission Products from Oxide Fuel. ANSI/ANS-5.4-1982, American Nuclear Society.
- [ANS, 2011] ANS. 2011. Method for Calculating the Fractional Release of Volatile Fission Products from Oxide Fuel. ANSI/ANS-5.4-2011, American Nuclear Society.
- [Baker and Just, 1962] Baker L and L Just. 1962. Studies of Metal Water Reactions at High Temperatures, III. Experimental and Theoretical Studies of the Zirconium-Water Reaction. ANL-6548, Argonne National Laboratory, Argonne, IL.
- [Beyer and Clifford, 2011] Beyer C and P Clifford. 2011. Update of Gap Release Fractions for Non-LOCA Events Utilizing the Revised ANS 5.4 Standard. Pacific Northwest National Laboratory, Richland, WA. PNNL-18212, Rev. 1.
- [Biasi et al., 1967] Biasi L, G Clerici, S Garribba, R Sala, and A Tozzi. 1967. "Studies on Burnout, Part 3: A New Correlation for Round Ducts and Uniform Heating and Its Comparison with World Data." *Energia Nucleare* 14:530–536.
- [Bishop et al., 1965] Bishop A, R Sandberg, and L Tong. 1965. Forced Convection Heat Transfer at High Pressure after the Critical Heat Flux. 65-HT-31.
- [Bjornard and Griffith, 1977] Bjornard T and P Griffith. 1977. "PWR Blowdown Heat Transfer." In *Symposium on the Thermal and Hydraulic Aspects of Nuclear Reactor Safety* Vol. 1, pp. 17-41, Vol. 1, pp. 17–41. Atlanta, GA. American Society of Mechanical Engineers.
- [Bohn, 1977] Bohn M. 1977. FRACAS: A Subcode for the Analysis of Fuel Pellet-Cladding Mechanical Interaction. TREE-NUREG-1028, EG&E Idaho, Inc., Idaho Falls, ID.
- [Booth, 1957] Booth A. 1957. A Method of Calculating Fission Gas Diffusion from UO_2 Fuel and Its Application to the X-2 Loop Test. AECL-496, CRDC-721, Atomic Energy of Canada, Ltd., Chalk River, ON.
- [Bowring, 1977] Bowring R. 1977. "A new mixed flow cluster dryout correlation for pressures in the range 0.6-15.5 MN/m² (90-2250 psia)-for use in a transient blowdown code." In *Heat and Fluid Flow in Water Reactor Safety*. Institution of Mechanical Engineers.
- [Bromley, 1949] Bromley L. 1949. Heat Transfer in Stable Film Boiling. Radiation Laboratory, University of California, Berkeley.
- [Cadek et al., 1972] Cadek F, D Dominicis, H Yeh, and R Leyse. 1972. PWR FLECHT Final Report Supplement. WCAP-7931, Westinghouse Electric Corporation, Pittsburgh, PA.
- [Cathcart et al., 1977] Cathcart J, R Pawel, R McKee, R Druschel, G Yurek, J Campbell, and S Jury. 1977. Zirconium metal–water oxidation kinetics, IV: reaction rate studies. ORNL/NUREG-17, Oak Ridge National Laboratory, Oak Ridge, TN.
- [Chen, 1963] Chen J. 1963. A Correlation for Boiling Heat Transfer to Saturated Fluids in Convective Flow. 63-HT-34, American Society of Mechanical Engineers.

- [Crank and Nicolson, 1974] Crank J and P Nicolson. 1974. "A practical method for numerical evaluation of solutions of partial differential equations of the heat-conduction type." *Mathematical Proceedings of the Cambridge Philosophical Society* 43(1):50–64.
- [Cunningham and Beyer, 1984] Cunningham M and C Beyer. 1984. GT2R2: An Updated Version of GAPCON THERMAL-2. NUREG/CR-3907, PNL-5178, Pacific Northwest Laboratory, Richland, WA.
- [Dittus and Boelter, 1930] Dittus F and L Boelter. 1930. "Heat Transfer in Automobile Radiators of the Tubular Type." *University of California Publications in Engineering* 2(13):443–461.
- [Division of Safety Analysis, 2017] Division of Safety Analysis. 2017. TRACE V5.0 Patch 5 Theory Manual. US Nuclear Regulatory Commission.
- [Ferrari, 1963] Ferrari H. 1963. "Nitrogen Release from UO₂ Pellets at Elevated Temperatures." *Nuclear Science and Engineering* 17(4):503–512.
- [Ferrari, 1964] Ferrari H. 1964. "Diffusion of nitrogen in uranium dioxide." *Journal of Nuclear Materials* 12(2):142–144.
- [Forsberg and Massih, 1985] Forsberg K and A Massih. 1985. "Diffusion theory of fission gas migration in irradiated nuclear fuel UO₂." *Journal of Nuclear Materials* 135(2–3):140–148.
- [Franklin et al., 1983] Franklin D, G Lucas, and A Bement. 1983. Creep of Zirconium Alloys in Nuclear Reactors. Number ASTM-STP-815. American Society for Testing and Materials, Philadelphia, PA.
- [Galbraith, 1973] Galbraith K. 1973. Pellet-Cladding Gap Closure from Pellet Cracking Data and Analysis. Exxon Nuclear Corporation, Richland, WA. XN-73-17.
- [Garzarolli et al., 1982] Garzarolli F, W Jung, H Shoenfeld, A Garde, G Parray, and P Smerd. 1982. Review of PWR fuel rod waterside corrosion behavior. EPRI NP-2789, Project 1250 Final Report, Electric Power Research Institute, Palo Alto, CA.
- [Geelhood, 2013] Geelhood K. 2013. "Implementing Primary Creep Calculations during Stress Changes and Reversals in the Fuel Performance Code FRAPCON-3." In TopFuel 2013. Charlotte, NC. American Nuclear Society.
- [Geelhood and Beyer, 2008] Geelhood K and C Beyer. 2008. "Corrosion and Hydrogen Pickup Modeling in Zirconium Based Alloys." In Water Reactor Fuel Performance Meeting. Seoul, Korea. Korean Nuclear Society.
- [Geelhood and Beyer, 2011] Geelhood K and C Beyer. 2011. "Hydrogen Pickup Models for Zircaloy-2, Zircaloy-4, M5™, and ZIRLO™." In Water Reactor Fuel Performance Meeting. Chengdu, China.
- [Geelhood et al., 2008] Geelhood K, W Luscher, and C Beyer. 2008. PNNL Stress/Strain Correlation for Zircaloy. PNNL-17700, Pacific Northwest National Laboratory, Richland, WA.

- [Geelhood et al., 2015a] Geelhood K, W Luscher, and J Cuta. 2015a. FRAPTRAN-2.0: A Computer Code for the Transient Analysis of Oxide Fuel Rods. PNNL-19400, Vol. 1, Rev. 2, Pacific Northwest National Laboratory, Richland, WA.
- [Geelhood et al., 2022a] Geelhood K, W Luscher, L Kyriazidis, C Goodson, and E Torres. 2022a. MatLib-1.1: Nuclear Material Properties Library. PNNL-32772, Pacific Northwest National Laboratory, Richland, WA.
- [Geelhood et al., 2015b] Geelhood K, W Luscher, P Raynaud, and I Porter. 2015b. FRAPCON-4.0: A Computer Code for the Calculation of Steady-State, Thermal-Mechanical Behavior of Oxide Fuel Rods for High Burnup. PNNL-19418, Vol. 1, Rev. 2, Pacific Northwest National Laboratory, Richland, WA.
- [Geelhood et al., 2022b] Geelhood K, D Richmond, D Colameco, W Luscher, L Kyriazidis, C Goodson, J Corson, and J Whitman. 2022b. FAST-1.1: A Computer Code for Thermal-Mechanical Nuclear Fuel Analysis under Steady-state and Transients. PNNL-32770, Pacific Northwest National Laboratory, Richland, WA.
- [Geelhood et al., 2022c] Geelhood K, D Richmond, D Colameco, T Zipperer, W Luscher, L Kyriazidis, C Goodson, and J Corson. 2022c. FAST-1.1: Integral Assessment. PNNL-32771, Pacific Northwest National Laboratory, Richland, WA.
- [Gilbon et al., 2000] Gilbon D, A Soniak, and aMJ Doriot S.. 2000. "Irradiation creep and growth behavior, and microstructural evolution of advanced Zr-base alloys." In Zirconium in the Nuclear Industry: Twelfth International Symposium, number ASTM-STP-1354, pp. 51–73. American Society of Testing and Materials.
- [Groeneveld, 1973] Groeneveld D. 1973. Post-Dryout Heat Transfer at Reactor Operating Conditions. AECL-4513, Atomic Energy of Canada, Ltd., Chalk River Project, Chalk River, ON.
- [Groeneveld, 1978] Groeneveld D. 1978. An Investigation of Heat Transfer in the Liquid Deficient Regime. Atomic Energy of Canada, Ltd., Chalk River Project, Chalk River, ON. AECL-3281, Revised 1979.
- [Groeneveld and Delorme, 1976] Groeneveld D and G Delorme. 1976. "Prediction of Thermal Non-equilibrium in the Post-Dryout Regime." Nuclear Engineering and Design 36(1):17–26.
- [Ha et al., 2007] Ha K, H Jeong, W Chang, Y Lee, and C Jo. 2007. Development of MARS-LMR and Steady-state Calculation for KALIMER-600. Korea Atomic Energy Research Institute, Korea. KAERI/TR-3418/2007.
- [Hagrman et al., 1981] Hagrman D, G Reymann, and G Mason. 1981. MATPRO-Version 11: A Handbook of Materials Properties for Use in the Analysis of Light Water Reactor Fuel Rod Behavior. NUREG/CR-0479 (TREE-1280), Rev. 2, EG&G Idaho, Inc., Idaho Falls, ID.
- [Iloeje et al., 1989] Iloeje O, W Rohsenow, and P Griffith. 1989. "Three-step model of dispersed flow heat transfer (post-CHF vertical flow)." Nigerian Journal of Technology 13(1):1–15.

- [INEL, 1978] INEL. 1978. RELAP5/MOD7 Blowdown Code, Version 2, Code Development and Analysis Program Report. CDAP-TR-78-036, Idaho National Engineering Laboratory, Idaho Falls, ID.
- [International, 2017] International E. 2017. The JSON Data Interchange Syntax. ECMA International. Standard ECMA-404.
- [Jens and Lottes, 1951] Jens W and P Lottes. 1951. Analysis of Heat Transfer, Burnout, Pressure Drop, and Density Data for High-Pressure Water. Argonne National Laboratory, Argonne, IL. ANL-4627.
- [Khorushii et al., 1999] Khorushii O, S Kourtchatov, and V Likhanskii. 1999. “New model of equiaxed grain growth in irradiated UO₂.” *Journal of Nuclear Materials* 265(1–2):112–116.
- [Knuutila, 2006] Knuutila A. 2006. Improvements on FRAPCON-3/FRAPTRAN Mechanical Modeling. VTT-R-11337-06, VTT Technical Research Centre of Finland, Espoo, Finland.
- [Kreith, 1964] Kreith F. 1964. Principles of Heat Transfer, 8th edition. International Book Company, Scranton, PA.
- [Lanning, 1982] Lanning D. 1982. “The Possible Impact of Fuel Pellet Cracking on Inferred Gap Conductance and Fuel Stored Energy.” *Nuclear Technology* 56(3):565–574.
- [Limbäck and Andersson, 1996] Limbäck M and T Andersson. 1996. “A model for analysis of the effect of final annealing on the in- and out-of-reactor creep behavior of zircaloy cladding.” In *Zirconium in the Nuclear Industry: Eleventh International Symposium*, number ASTM-STP-1295, pp. 448–468. American Society for Testing and Materials.
- [Luscher and Geelhood, 2014] Luscher W and K Geelhood. 2014. Material Property Correlations: Comparisons between FRAPCON-4.0, FRAPTRAN-2.0, and MATPRO. NUREG/CR-7024, Rev. 1, PNNL-19417, Rev. 1, Pacific Northwest National Laboratory, Richland, WA.
- [Manzel and Walker, 2000] Manzel R and C Walker. 2000. “High Burnup Fuel Microstructure and Its Effect on Fuel Rod Performance.” In *International Topical Meeting on Light Water Reactor Fuel Performance*. Park City, UT. American Nuclear Society.
- [Manzel and Walker, 2002] Manzel R and C Walker. 2002. “EPMA and SEM of fuel samples from PWR rods with an average burn-up of around 100 MWd/kgHM.” *Journal of Nuclear Materials* 301(2–3):170–182.
- [Matsuo, 1987] Matsuo Y. 1987. “Thermal Creep of Zircaloy-4 Cladding under Internal Pressure.” *Journal of Nuclear Science and Technology* 24(2):111–119.
- [McAdams, 1954] McAdams W. 1954. Heat Transmission, 3rd edition. McGraw-Hill Book Company, Inc., New York, NY.
- [Mendelson, 1968] Mendelson A. 1968. Plasticity: Theory and Applications. The MacMillan Company, New York, NY.

- [Meyer and Williams, 1962] Meyer J and JJ Williams. 1962. A Momentum Integral Model for the Treatment of Transient Fluid Flow, pp. 47–72. Bettis Atomic Power Laboratory, Pittsburgh, PA.
- [Mogensen et al., 1985] Mogensen M, C Walker, I Ray, and M Coquerelle. 1985. “Local fission gas release and swelling in water reactor fuel during slow power transients.” *Journal of Nuclear Materials* 131(2–3):162–171.
- [NRC, 2007] NRC. 2007. Standard Review Plan for the Review of Safety Analysis Reports for Nuclear Power Plants: LWR Edition: Section 4.2: Fuel System Design, Revision 3. NUREG-0800, U.S. Nuclear Regulatory Commission, Washington, D.C.
- [NRC, 2017] NRC. 2017. The Exterior Communications Interface. US Nuclear Regulatory Commission. Division of Safety Analysis.
- [Oguma, 1983] Oguma M. 1983. “Cracking and readdress behavior of nuclear fuel pellets during rise to power.” 76(1):35–45.
- [Pahl et al., 1992] Pahl R, D Porter, D Crawford, and L Walters. 1992. “Irradiation behavior of metallic fast reactor fuels.” *Journal of Nuclear Materials* 188:3–9.
- [Powers and Meyer, 1980] Powers D and R Meyer. 1980. Cladding Swelling and Rupture Models for LOCA Analysis. NUREG-0630, U.S. Nuclear Regulatory Commission, Washington, D.C.
- [Reddy and Fighetti, 1983] Reddy D and C Fighetti. 1983. Parametric Study of CHF data, Volume 2: A Generalized Subchannel CHF Correlation for PWR and BWR Fuel Assemblies. Final Report. Columbia University, New York, NY.
- [Sabol et al., 1994] Sabol G, R Comstock, R Weiner, P Larouere, and R Stanutz. 1994. “In-Reactor Corrosion Performance of ZIRLO™ and Zircaloy-4.” In *Zirconium in the Nuclear Industry: Tenth International Symposium*, number STP-1425, pp. 724–744. American Society for Testing and Materials.
- [Shestopalov et al., 1999] Shestopalov A, K Lioutov, L Yegorova, G Abyshov, and K Mikiotiouk. 1999. Modification of USNRC’s FRAP-T6 Fuel Rod Transient Code for High Burnup VVER Fuel. NUREG/IA-0164, U.S. Nuclear Regulatory Commission, Washington, D.C.
- [Smith and Griffith, 1976] Smith R and P Griffith. 1976. “A Simple Model for Estimating Time to CHF in a PWR LOCA.” In *National Heat Transfer Conference*.
- [Soniak et al., 2002] Soniak A, N L’Hullier, J Mardon, V Rebeyrolle, P Boffioux, and C Bernaudat. 2002. “Irradiation Creep Behavior of Zr-Base Alloys.” In *Zirconium in the Nuclear Industry: Thirteenth International Symposium*, number ASTM-STP-1423, pp. 837–862. West Conshohocken, PA. ASTM International.
- [Sontheimer and Nissen, 1994] Sontheimer F and K Nissen. 1994. “Evaluation of the Stress Reversal Creep Experiment IFA-585 in the HBWR and the Lift-Off Experiment ROPE-1 in the R2 Studsvik using the Siemens/KWU Clad Creep Model.” In *Enlarged HPG Meeting on High Burnup Fuel Performance, Safety and Reliability and Degradation of In-Core Materials and Water Chemistry Effect and Man-Machine Systems Research*, number HPR-345/28.

- [Sparrow et al., 1961] Sparrow E, A Loeffler Jr., and H Hubbard. 1961. "Heat Transfer to Longitudinal Laminar Flow between Cylinders." *Journal of Heat Transfer* 83(4):415–422.
- [Spino et al., 1996] Spino J, K Vennix, and M Coquerelle. 1996. "Detailed characterisation of the rim microstructure in PWR fuels in the burn-up range 40-67 GWd/tM." *Journal of Nuclear Materials* 231(3):179–190.
- [Thérache, 2005] Thérache B. 2005. *The High Initial Rating Test, IFA-677.1: Results after First Cycle of Irradiation*. HWR-819, OECD Halden Reactor Project, Halden, Norway.
- [Thom et al., 1965] Thom J, W Walker, T Fallon, and G Reising. 1965. "Boiling in Subcooled Water During Flow Up Heated Tubes and Annuli." In *Symposium on Boiling Heat Transfer in Steam Generating Units and Heat Exchangers*, number 7. London, United Kingdom. Institute of Mechanical Engineers.
- [Thompson and MacBeth, 1964] Thompson B and R MacBeth. 1964. *Boiling Water Heat Transfer Burnout in Uniformly Heated Round Tubes: a Compilation of World Data with Accurate Correlations*. United Kingdom Atomic Energy Authority.
- [Tong and Young, 1974] Tong L and J Young. 1974. "A Phenomenological Transition and Film Boiling Heat Transfer Correlation." In *Fifth International Heat Transfer Conference*, number 133.9. Tokyo, Japan.
- [Une et al., 2001] Une K, K Nogita, T Shiratori, and K Hayashi. 2001. "Rim structure formation of isothermally irradiated UO₂ fuel discs." *Journal of Nuclear Materials* 288(1):20–28.
- [Wagner, 1963] Wagner R. 1963. *HEAT-1: A One-Dimensional Time Dependent or Steady-State Heat Conduction Code*. IDO-16867, Philips Petroleum Co, Atomic Energy Division, Idaho Falls, ID.
- [Williams, 2018] Williams J. 2018. "JSON-Fortran: A Fortran 2008 JSON API." <https://github.com/jacobwilliams/json-fortran>.
- [Zuber, 1961] Zuber N. 1961. "The hydrodynamic crisis in pool boiling of saturated and subcooled liquids." *International Developments in Heat Transfer* 27:230–236.

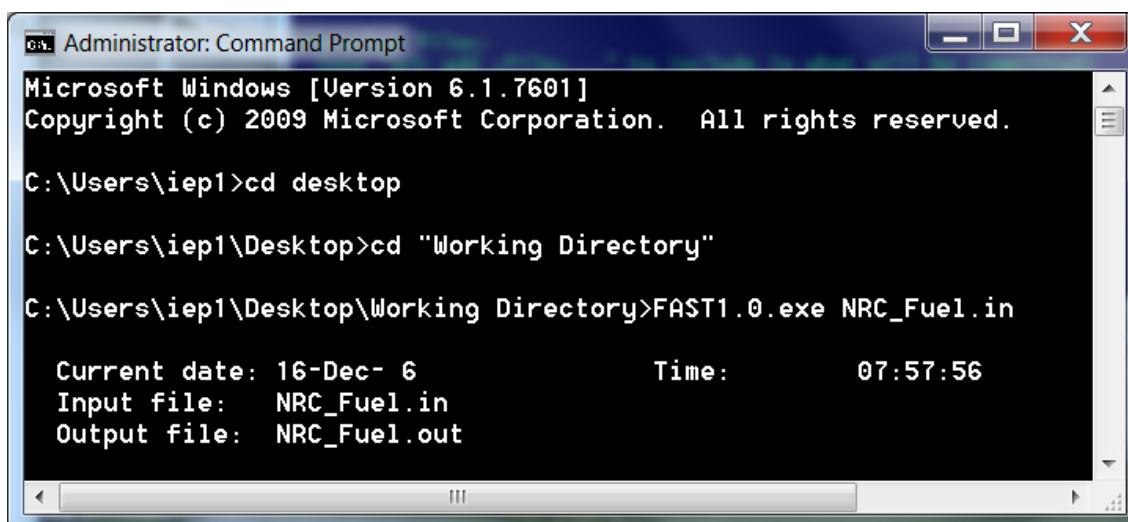
Appendix A – Running the Code

The FAST code is designed to be run using a command prompt on Windows and Linux based operating systems, but the code can also be run through a graphical user interface. The NRC currently uses and supports the Symbolic Nuclear Analysis Package (SNAP) that can serve as the GUI to create the input file, run the code, and visualize the results. SNAP can also be used to link FAST with other NRC supported codes, such as the thermal-hydraulics code TRACE, and for performing statistical analysis using DAKOTA. For more information about SNAP, visit <https://www.aptpilot.com>.

Using a command-line interface, the only (optional) argument that is allowed is the input file name. By default, the input file that the FAST executable looks for is `fast.in`.

A.1 Windows-Based OS

On a Windows based computer, by double clicking on the executable the code will automatically try to run using the file `fast.in`. If the file does not exist, the code will prompt the user to re-enter the file name, at which point the user can type in the file name they wish to use. It is important that the input file be in the same directory as the executable. When using a Windows command prompt, use the `cd` command to move into the working directory (the folder which contains the executable and the input file), type in the name of the executable followed by a space and the name of the input file (`fast.exe <FILENAME>`). An example is shown in Figure A.1.



```
Administrator: Command Prompt
Microsoft Windows [Version 6.1.7601]
Copyright (c) 2009 Microsoft Corporation. All rights reserved.

C:\Users\iep1>cd desktop

C:\Users\iep1\Desktop>cd "Working Directory"

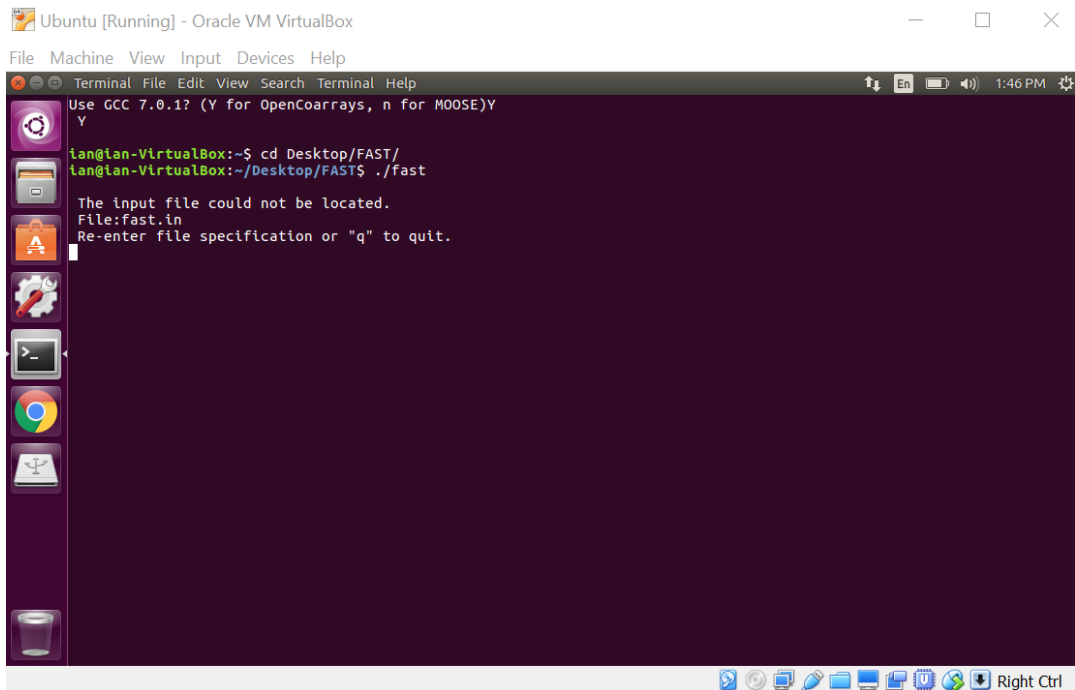
C:\Users\iep1\Desktop\Working Directory>FAST1.0.exe NRC_Fuel.in

Current date: 16-Dec- 6           Time:           07:57:56
Input file:   NRC_Fuel.in
Output file:  NRC_Fuel.out
```

Figure A.1. Running FAST using the Windows Command Prompt

A.2 Linux-Based OS

Running FAST on a Linux based OS is nearly identical to running on Windows OS. Rather than typing in the name of the program (`fast.exe`), type in `./` followed by the name of the program (`./fast <INPUT FILENAME>`). An example is shown in Figure A.2.



```
Ubuntu [Running] - Oracle VM VirtualBox
File Machine View Input Devices Help
Terminal File Edit View Search Terminal Help
Use GCC 7.0.1? (Y for OpenCoarrays, n for MOOSE)Y
Y
ian@lan-VirtualBox:~$ cd Desktop/FAST/
ian@lan-VirtualBox:~/Desktop/FAST$ ./fast

The input file could not be located.
File:fast.in
Re-enter file specification or "q" to quit.
```

Figure A.2. Running FAST using the Linux Command Line (OS=Ubuntu 16)

A.3 Using SNAP

Once a SNAP model has been created (or imported from an ASCII file), go to **Tools--> Submit Job...** and the job will be submitted to the working directory specified in the model.

Appendix B – Input Instructions for the FAST-1.1 Code

This appendix contains the requirements for the input file structure and the available input parameters for FAST-1.1.

B.1 File and Comment Structure

The input file contains the information for fuel rod design, model options, defining the mesh, reactor conditions, and code output options. The beginning of the file is designated for naming output files and adding any comments.

Any comments to be included at the top of the input file should start on Line 1 with a “*”. Up to 200 characters are allowed on these lines, and as many lines as needed are allowed. It is highly recommended that the version of FAST the input file was developed for be included in these comments.

After all comments are completed, the input and output file specification begins. The list of allowed input files and available output files is shown in Table B.1. Each input file requires the following information: `FILE#='FileName.Extension',STATUS='StatusType'`

Where # and `Extension` are shown in Table 5.1, `FileName` is defined by the user (recommended to be the same as the name of the input file) and `StatusType` is “UNKNOWN” for Output files and “OLD” for Input Files.

Table B.1. Available input and output files in FAST-1.1

Type	Description	Unit	Extension	Corresponding Input Variable
Input Files				
Restart	Reads an already created restart file for FAST-to-FAST restarts	13	.restart	nread
Output Files				
Output Summary	Provides a summary of important parameters at either each axial node or for the peak power axial node	06	.out	nopt/jdlpr
Plotting	Provides numerous calculated parameters of interest to be used by FRAPlot and APT Plot	66	.plot	nplot
Data Output	Provides the necessary FAST data to populate a TRACE fuel rod model with burnup dependent parameters	50	.ftt	nmakechan
VTK Format	Provides numerous calculated parameters of interest in vtk format, can be used by ParaView	20	.vtk	vtkplot

The end of the comment and input file section is designated by a line starting with “/*”. An example of the comment and file input structure is shown in Figure B.1.

```

1 *****
2 * Code Version: FAST-1.0 *
3 * Date Created: 5 December 2016 *
4 * Author: Ian Porter, NRC *
5 *-----*
6 * Input file description: *
7 * *
8 * This input file resembles a 17x17 PWR fuel rod irradiated for 3 cycles in a W4LP PWR *
9 * The data used to develop the rod design is from: *
10 * (N/A) *
11 * The data used to develop the power history and coolant conditions is from: *
12 * (N/A) *
13 * *
14 *****
15 * Output File *
16 FILE06='NRC_Fuel.out', STATUS='UNKNOWN' *
17 * Plot File *
18 FILE66='NRC_Fuel.plot', STATUS='UNKNOWN', FORM='FORMATTED' *
19 * Restart File *
20 FILE12='NRC_Fuel.restart', STATUS='OLD' *
21 /*****
22 NRC_Fuel
23 $frpcn
24 ! im: number of time steps, nr: number of fuel radial nodes
25 ! ngasr: number of gas radial nodes, na: number of axial nodes
26 ! mechan: option to select mechanical model (2=FRACAS-I, 1=FEA)
27 im=2, nr=17, ngasr=45, na=5, mechan=2, ncmesh=2, noxide=0, ncrud=0
28 $end
  
```

Figure B.1. Sample comment and file input structure for FAST input file

There are ten Fortran namelist input blocks. These blocks start with the syntax \$namelist and are terminated with a /, where namelist is defined in the following appendices. There is no order dependency of each namelist block. The available input blocks are shown in Table B.2.

Table B.2. Available namelist input blocks

Input Block	Description
frpcn	Defines the problem discretization
frpcon	Defines power information and steady-state modeling options
geometry	Geometry information
material	Material information
transient	Parameters defining the transient solution timestep size and model options
boundary	Cladding OD Boundary Conditions (Coolant conditions and imposed cladding conditions)
spentfuel	Spent fuel modeling options
refabrication	Refabrication options
uncertainty	Uncertainty options
developer	Developer modeling options to change numerous models

B.2 frpcn block

This block, Table B.3, is used for discretizing the mesh and array sizes.

Table B.3. frpcn input block

Variable Name (Type)	Description	Units		Limitations and Default Value
		British	SI	
im (I)	Number of time steps	N/A		> 1 (Required Input)
mechan (I)	Option to select cladding mechanical deformation model 1 = FEA model 2 = FRACAS-I model 3 = FRACAS-CT model	N/A		Default = 2
ncc (I)	Number of radial elements in the cladding for FEA model	N/A		Default = 5
na (I)	Number of equal-length axial regions along the rod, for which calculations are performed and output	N/A		Default = 9 Must be greater than 1
nr (I)	Number of radial boundaries in the pellet (for temperature calculations and temperature distribution output) These are spaced by the code with greater fraction in the outer region to optimize definition of the heat generation radial distribution.	N/A		Default = 17 Must be greater than 1, suggested minimum is 17
ngasr (I)	Number of equal-volume radial rings in the pellet for gas release calculations	N/A		Default = 45 Must be greater than 6, suggested is 45.
naxim (I)	Number of values in input arrays (if larger than na*im)	N/A		Default = na*im
ncmesh (I)	Number of evenly spaced radial boundaries in the cladding	N/A		Default = 1
noxide (I)	Number of evenly spaced radial boundaries in the OD oxide layer	N/A		Default = 1
ncrud (I)	Number of evenly spaced radial boundaries in the OD crud layer	N/A		Default = 1
nlayers (I)	Number of evenly spaced radial boundaries in the cladding OD coating	N/A		Default = 1
nlayersid (I)	Number of evenly spaced radial boundaries in the cladding ID coating	N/A		Default = 1

- (I) Integer
- (R) Real
- (L) Logical
- (C) Character

B.3 frpcon Block

This block, Table B.4, contains the bulk of the information related to geometry, fabrication, model options, and power. *Note: In moving from FRAPCON-4.0 to FAST, some of the input variables in this block have been moved to new input blocks (e.g., \$boundary, \$uncertainty). These options are no longer listed in this section but are still allowed in FAST-1.1 when using a FRAPCON-4.0 input file. However, in order to take advantage of the new features of FAST, the new input blocks must be used. Future versions of FAST will remove their ability to be input in this block entirely.*

Table B.4. frpcon input block

Variable Name (Type)	Description	Units		Limitations and Default Value
		British	SI	
Reactor Conditions				
iplant (I)	Flag for reactor type			
	-2 = PWR			Default = -2 (PWR)
	-3 = BWR			
	-4 = HBWR			
	-5 = HTGR			
-6 = SFR				
flux(j+1) (R)	Conversion between fuel specific power (W/g) and fast neutron flux, E> 1 MeV (n/m ² /s)	n/m ² /s of fuel	W/g of fuel	Default = 0.221 × 10 ¹⁷
icor (I)	Index for crud model			
	0 = Constant thickness 2 = Time-dependent crud growth rate (crdtr) starting from zero crud		N/A	Default = 0
crdt (R)	Initial thickness of crud layer on cladding outer surface	mils	m	Default = 0.0
crdtr (R)	Rate of crud accumulation (used if icor = 2)	mils/hr	m/s	Default = 0.0
crudmult(j) (R)	Axial array of multipliers on crud thickness or growth rate (if icor = 0 or 2, respectively)		N/A	Default = 1.0 <i>Must be input for all axial nodes if used</i>

Table B.4. *frpcon* input block (continued)

Variable Name (Type)	Description	Units		Limitations and Default Value
		British	SI	
Power History Specification				
ProblemTime (IT)(R)	Cumulative time or burnup (See TimeFormat) at the end of each time step <i>Note: Time steps greater than 50 days are not recommended. If steady-state operation is being modeled, use time steps greater than 1 day. Time steps less than 1 day should only be used when modeling a fast power ramp.</i>	Set by TimeFormat)		Required input
TimeFormat (I)	Type of units specified by ProblemTime, irrespective of units 0 = Days 1 = Hours 2 = Seconds 3 = MWd/mtU	N/A		Default = 0
qmpy (IT)(R)	The linear heat generation rate at each time step This equals the rod-average value if $i_q = 0$ and the peak value if $i_q = 1$.	kW/ft	kW/m	Required input
DecayModel (I)	Decay heat model; turned on when $qmpy < 0$ 1 = ANS-5.1 (2005) Standard 2 = ANS-1973 Model	N/A		Default = 1
fpcay (R)	Multiplicative factor applied to power given by decay heat model	N/A		Default = 1.0
Axial Power Profile				
i_q (I)	Indicator for axial power shape 0 = User-input power shapes 1 = Chopped-cosine shape	N/A		Default = 1.0
x (N)(R)	The elevations in each qf array defining a power shape <i>Note: the first value must be 0.0 and the last value must = totl</i>	ft	m	Required input if $i_q = 0$

Table B.4. frpcon input block (continued)

Variable Name (Type)	Description	Units		Limitations and Default Value
		British	SI	
qf (N)(R)	The ratio of the linear power at the x elevation to the axially-averaged value provided by qmpy for the M th power shape. The number of (qf, x) pairs for the M-th power shape is defined by jn(M). The code will normalize to an average value of 1.0.	N/A		Required input if iq = 0
jn (M)(I)	The number of (qf, x) pairs for each axial power shape. Input in the same sequence as the (qf, x) arrays	N/A		Required input if iq = 0
jst (IT)(I)	The sequential number of the power shape to be used for each timestep. One value is required per timestep (if iq = 0)	N/A		Required input if iq = 0
fa (R)	Peak-to-average power ratio for cosine-type axial power shape (used only if iq = 1)	N/A		Required input if iq = 1
Radial Power Options				
radialpowermodel (I)	Radial power profile model 0 = User-supplied 1 = TUBRNP 1993 model 2 = TUBRNP 2017 model	N/A		Default = 1 (TUBRNP 1993 model)
Radpowprofile [nt, nz, nr, times, ax_loc, rad_loc, powprof(time, ax_loc, rad_loc)] (R)	User-supplied array of sets of radial power profiles. To apply the same radial power profile at all axial nodes, enter nz = 1 and set ax _{loc} = 0.0. <i>Note: This will bypass FAST's calculation of radial power profile using the TUBRNP model</i>	s, m, m, relativefrac	s, ft, ft, relativefrac	Required input if radialpowermodel = 0
Code Output Options				
nopt (I)	Control on printout of Output file 0 = Printout each time step, controlled by jdlpr 1 = Case input and summary sheet only	N/A		Default = 0
jdlpr (I)	Output file print control for each time step -1 = Axial summary 0 = All axial nodes 1 = Peak-power axial node	N/A		Default = 0

Table B.4. *frpcon* input block (continued)

Variable Name (Type)	Description	Units		Limitations and Default Value
		British	SI	
<i>nplot</i> (I)	Control on printout of Plot file 0 = No plot file created 1 = Plot file with standard options 2 = Detailed plot file including fission gas distribution		N/A	Default = 1
Code Operation and Models				
<i>nunits</i> (I)	Flag for units system used in input file 0 = SI 1 = British		N/A	Required input
<i>ngasmod</i> (I)	Fission gas release model 1 = ANS5.4 (1982) 2 = Massih 3 = FRAPFGR 4 = ANS5.4 (2011) <i>Note: ANS5.4 (2011) uses Massih model for stable release.</i>		N/A	Default = 2 (Massih)
<i>igas</i> (I)	Time step to begin calculation of fission gas release For all time steps prior to <i>igas</i> , the calculated gas release will not be included in the void volume calculation.		N/A	Default = 0
<i>sgapf</i> (R)	Number of fission gas atoms produced per 100 fissions		N/A	Default = 31.0
<i>crephr</i> (R)	Subdivision for internal creep steps <i>Note: Should be set to a minimum of 10 creep steps per smallest time step</i>		N/A	Default = 10.0
<i>frcoef</i> (R)	Coulomb friction coefficient between cladding and fuel pellet (only used if <i>mechan</i> = 2)		N/A	Default = 0.015
<i>slim</i> (R)	Limit on fuel volumetric swelling		N/A	Default = 0.05
<i>qend</i> (R)	Fraction of end-node heat transfer transfers to the plenum gas		N/A	Default = 0.3
<i>igascal</i> (I)	Internal rod pressure calculation 0 = User-specified gas pressure vs. time 1 = Static rod pressure calculation 2 = Transient gas flow		N/A	Default = 1 (static)

Table B.4. *frpcon* input block (continued)

Variable Name (Type)	Description	Units		Limitations and Default Value
		British	SI	
p1 (IT)(R)	Rod internal pressure for each time step	psia	Pa	Required input only if <i>igasca1</i> = 0
nsp (I)	Signal for time-dependent input arrays for p2, <i>tw</i> , and <i>go</i> : 0 = single values for these three values will be used for all time steps 1 = a value for each variable for each time step must be input	N/A		Required input unless otherwise specified in boundary input block
p2 (IT)	Coolant system pressure Input for each time step if <i>nsp</i> = 1.	psia	Pa	Required input unless otherwise specified in boundary input block
<i>tw</i> (IT)	Coolant inlet temperature Input for each time step if <i>nsp</i> = 1.	°F	K	Required input unless otherwise specified in boundary input block
<i>go</i> (IT)	Mass flux of coolant around fuel rod Input for each time step if <i>nsp</i> = 1. Note that <i>go</i> input may have to be adjusted to yield both desired coolant and desired cladding surface temperatures. Concurrent adjustment of <i>pitch</i> may also be required.	lb/hr-ft ²	kg/s-m ²	Required input unless otherwise specified in boundary input block

(I) Integer

(R) Real

(L) Logical

(C) Character

(N) Axial Node Index for Input Power Profile

(M) Power Shape Number

(IT) Time Step Index

B.4 geometry block

This block, Table B.5, is used to define the geometry.

Table B.5. geometry input block

Variable Name (Type)	Description	Units		Limitations and Default Value
		British	SI	
Cylindrical Geometry Design				
dco (R) ⁽¹⁾	Cladding outer diameter	in	m	Required input
thkcld (R) ⁽¹⁾	Cladding wall thickness	in	m	Required input
thkcoatid (R) ⁽¹⁾	Cladding inner coating thickness	in	m	Default = 0.0
thkcoat (R) ⁽¹⁾	Cladding outer coating thickness	in	m	Default = 0.0
thkgap (R) ⁽¹⁾	Pellet-cladding as-fabricated radial gap thickness	in	m	Required input
totl (R)	The total (active) fuel column length	ft	m	Required input
cp1 (R) ²	Cold upper plenum length	in	m	Required input
extplenumV (R)	External plenum volume	in ³	m ³	Default = 0.0
User-Specified Geometry Options (overrides defaults)				
ivardm (I)	Option to use equal length axial nodes or variable length axial nodes 0 = Equal length 1 = Variable length		N/A	Default = 0
deltaz (NA)(R)	Array of axial node lengths for fuel region starting at the bottom of the rod <i>Note: The sum of all values must equal totl</i>	ft	m	Required input only if ivardm = 1
Spring Dimensions				
dspg (R) ⁽²⁾	Outer diameter of plenum spring	in	m	Required input (dspg should be less than the clad inner diameter + ID coating)
dspgw (R) ⁽²⁾	Diameter of the plenum spring wire	in	m	Required input
vs (R) ⁽²⁾	Number of turns in the plenum spring		N/A	Required input

Table B.5. geometry input block (continued)

Variable Name (Type)	Description	Units		Limitations and Default Value
		British	SI	
Pellet Design				
hplt (R)	Height (length) of each pellet	in	m	Required input
rc (R) ⁽¹⁾	The inner pellet radius	in	m	Default = 0.0
hdish (R)	Height (depth) of pellet dish, assumed to be a spherical indentation	in	m	Default = 0.0
dishsd (R)	Pellet end-dish shoulder width (outer radius of fuel pellet minus radius of dish)	in	m	Default = 0.0
chmfrh (R)	Chamfer height	in	m	Default = 0.0
chmfrw (R)	Chamfer width	in	m	Default = 0.0
zrb2thick (R) ⁽¹⁾	ZrB ₂ layer thickness on pellets	in	m	Default = 0.0

^(I) Integer

^(R) Real

^(L) Logical

^(C) Character

⁽¹⁾ May input one value for entire pellet stack or input values as an array for each axial node starting at the bottom

⁽²⁾ May input one value (for upper plenum only) or as 2 values (first value for upper plenum, second value for lower plenum)

B.5 material block

This block, Table B.6, is used to define the material and composition.

Table B.6. material Input Block

Variable Name (Type)	Description	Units		Limitations and Default Value
		British	SI	
Pellet Isotopics				
imox (I)	Fuel material indicator			
	0 = UO ₂			
	1 = MOX fuel using the Duriez/Ronchi/NFI Mod thermal conductivity correlation		N/A	Default = 0
	2 = MOX fuel using the Halden thermal conductivity correlation			
	3 = U ₃ Si ₂ 5 = U-Pu-Zr			
enrch (R) ⁽¹⁾	Fuel pellet ²³⁵ U enrichment	at% ²³⁵ U in total U		Required input
comp (R) ⁽¹⁾	Weight percent of plutonia in fuel (must specify if imox = 1 or 2)	wt%		Default = 0.0
comZr (R) ⁽¹⁾	Weight percent of zirconium in fuel (must specify only if imox = 5)	wt%		Default = 0.0
moxtype (I)	Type of Pu used in MOX fuel			Default = 1 (reactor grade)
	1 = Reactor grade 2 = Weapons grade		N/A	
enrpu39 (R)	Fuel pellet ²³⁹ Pu enrichment	at% ²³⁹ Pu in total Pu		Default = 0.0
enrpu40 (R)	Fuel pellet ²⁴⁰ Pu enrichment	at% ²⁴⁰ Pu in total Pu		Default = 0.0
enrpu41 (R)	Fuel pellet ²⁴¹ Pu enrichment	at% ²⁴¹ Pu in total Pu		Default = 0.0
enrpu42 (R)	Fuel pellet ²⁴² Pu enrichment	at% ²⁴² Pu in total Pu		Default = 0.0
totmt1 (R)	Oxygen-to-metal (O/M) atomic ratio in the oxide fuel pellet		N/A	Default = 2.0 (If MOX fuel is selected, totmt1 should be less than 2.0.)
gadoin (R) ⁽¹⁾	Weight fraction of gadolinia in urania-gadolinia fuel pellets		N/A	Default = 0.0
gdtype (I)	Type of gadolinium			Default = 1 (natural)
	1 = Natural		N/A	
	2 = Depleted			

Table B.6. material Input Block (continued)

Variable Name (Type)	Description	Units		Limitations and Default Value
		British	SI	
ppmh2o (R)	Parts per million by weight of moisture in the as-fabricated pellets	ppm		Default = 0.0
ppmn2 (R)	Parts per million by weight of nitrogen in the as-fabricated pellets	ppm		Default = 0.0
Pellet Fabrication				
den (R)	As-fabricated apparent fuel density	%TD		Required input
deng (R)	Open porosity fraction for fuel pellet	%TD		Default = 0.0
roughf (R)	Fuel pellet surface arithmetic mean roughness	in	m	Default = 2.0×10^{-6} m
rsntr (R)	The increase in pellet density expected during in-reactor operation (determined from a standard re-sintering test per NUREG-0085 and Regulatory Guide 1.126) <i>Note: For UO₂-Gd₂O₃ fuel, 0.1 kg/m³ is recommended.</i>	kg/m ³		Required input
tsint (R)	Temperature at which pellets were sintered	°F	K	Default = 2911 °F (1872.59 K)
grnsize (R)	Fuel grain size using MLI	microns		Default = 10.0 <i>(Note: Will force to 10 microns for FGR calculations)</i>
IFBA Coating				
ifba (R)	Percent of IFBA rods in the core	%		Default = 0.0
b10 (R)	¹⁰ B enrichment in ZrB ₂	at%		Default = 0.0
zrb2den (R)	Percent theoretical density of ZrB ₂ where TD = 6.08 g/cm ³	%TD		Default = 90.0

Table B.6. material Input Block (continued)

Variable Name (Type)	Description	Units		Limitations and Default Value
		British	SI	
Cladding Fabrication				
icm (I)	Cladding material indicator			
	2 = Zircaloy-2			
	4 = Zircaloy-4			
	5 = M5			
	6 = ZIRLO			
	7 = Opt. ZIRLO			
	9 = Zr1Nb			
	10 = E110			
	11 = SiC			
	12 = SiGA ⁵			
	20 = Kanthal APMT			
	21 = C35M			
	22 = C36M			
	31 = SS			
35 = HT-9				
zr2vintage (I)	Flag to select vintage of Zircaloy-2 0 = Prior to 1998 1 = Newer than 1998	N/A		Default = 1 (only used if icm = 2)
cldwks (R)	Cold-work of the cladding (fractional reduction in cross-section area due to processing) <i>Note: Recommend 0.5 for SRA; 0.0 for RXA</i>	N/A		Default = 0.2
roughc (R)	Cladding surface arithmetic mean roughness	in	m	Default = 5.0×10^{-7} m
catexf (R)	Cladding texture factor, defined as the fraction of cladding cells with basal poles parallel to the longitudinal axis of the cladding tube	N/A		Default = 0.05
chorg (R)	As-fabricated hydrogen in cladding	ppm		Default = 10.0
ictm (I)	OD coating material indicator			
	0 = Cr 1 = CrN			
ictmi (I)	ID coating material indicator; inputs are same as ictm above	N/A		Required input if thkcoatid > 0.0

⁵SiGA[®] is a registered trademark of General Atomics.

Table B.6. material Input Block (continued)

Variable Name (Type)	Description	Units		Limitations and Default Value
		British	SI	
Rod Fill Conditions				
fgpav (R)	Initial fill gas pressure (taken to be at temperature TGasFab)	psia	Pa	Required input
TGasFab (R)	Temperature at which the fill gas pressure is measured	°F	K	Default = 77.0 °F (298.15 K)
idxgas (I)	Initial fill type (space between fuel and clad) 1 = Helium 2 = Air 3 = Nitrogen 4 = Fission Gas 5 = Argon 6 = User-specified gas mix 10 = Sodium		N/A	Default = 1
amfair (R)	Mole fraction of air (use only if idxgas = 6)		N/A	Default = 0.0
amfarg (R)	Mole fraction of argon (use only if idxgas = 6)		N/A	Default = 0.0
amffg (R)	Mole fraction of fission gas (use only if idxgas = 6 AND both amfxe and amfkry = 0.0)		N/A	Default = 0.0
amfhe (R)	Mole fraction of helium (use only if idxgas = 6)		N/A	Default = 0.0
amfh2 (R)	Mole fraction of hydrogen (use only if idxgas = 6)		N/A	Default = 0.0
amfh2o (R)	Mole fraction of water vapor (use only if idxgas = 6)		N/A	Default = 0.0
amfn2 (R)	Mole fraction of nitrogen (use only if idxgas = 6)		N/A	Default = 0.0
amfkry (R)	Mole fraction of krypton (use only if idxgas = 6)		N/A	Default = 0.0
amfxe (R)	Mole fraction of xenon (use only if idxgas = 6)		N/A	Default = 0.0

Table B.6. material Input Block (continued)

Variable Name (Type)	Description	Units		Limitations and Default Value
		British	SI	
User Defined Material Properties				
swell_rate (R)	Fuel swelling rate for both open and closed gap regimes <i>Note: user may use either swell_rate or both swell_rate_open and swell_rate_closed</i>	m/m	at%	Default = -1.0 (off)
swell_rate_open (R)	Fuel swelling rate for open gap regime <i>Note: open gap is defined as gap before hard contact between fuel and cladding</i>	m/m	at%	Default = -1.0 (off)
swell_rate_closed (R)	Fuel swelling rate for closed gap regime <i>Note: closed gap is defined as gap after hard contact between fuel and cladding</i>	m/m	at%	Default = -1.0 (off)
cladelmod (R)	User-defined cladding elastic modulus		Pa	Default = -1.0 (not used). Must be > 0.0 to use.

(I) Integer

(R) Real

(L) Logical

(C) Character

(1) May input one value for entire pellet stack or input values as an array for each axial node starting at the bottom.

B.6 transient Block

This block contains the variables that control the transient correlations, including the time step size and printing options.

Table B.7. transient input block

Variable Name (Type)	Description	Units		Limitations and Default Value
		British	SI	
Problem Time and Output Options				
dtmaxa (R) ^(1,2)	<p>Specify the time step size as a function of problem time.</p> <p>dtmaxa(1) = time step size at problem time dtmaxa(2).</p> <p>A time step size of 0.0 will result in the steady-state solution being performed. See Table 2-16 for more information on suggested time step sizes for various transients.</p>		S	<p>Default = 0.0 (steady-state solution, steps determined by ProblemTime)</p> <p><i>Required if transient solution is to be used.</i></p>
dtpoa (R) ^(1,2)	<p>Specify the interval of problem time between output file prints.</p> <p>dtpoa(1) = time interval between printout at problem time of dtpoa(2).</p> <p>If not supplied, will print at intervals specified in ProblemTime.</p>		S	<p>Default = 0.0 (only prints at intervals defined by ProblemTime(1:im)).</p>
dtplta (R) ^(1,2)	<p>Specify the interval of problem time between plot file prints.</p> <p>dtplt(1) = time interval between plot output at problem time of dtplt(2).</p> <p>If not supplied, will print at intervals specified in ProblemTime.</p>		S	<p>Default = 0.0 (only prints at intervals defined by ProblemTime(1:im)).</p>

Table B.7. transient input block (continued)

Variable Name (Type)	Description	Units		Limitations and Default Value
		British	SI	
Thermal Expansion Options				
nthermex (I)	Option to specify fuel thermal expansion model			
	0 = Pellet radius change calculated by adding the radius change in each ring due to radial thermal expansion	N/A		Default value = 0
	1 = Pellet radius change calculated by taking the maximum of the sum of the radius changes from each node inside the current ring due to radial thermal expansion or the radius change due to circumferential thermal expansion for the current ring			
High-Temperature Oxidation Model Options				
modmw (I)	High-temperature zirconium/water reaction model for cladding OD and ID.			
	0 = Off (No high temperature oxidation) 1 = Cathcart-Pawel 2 = Baker-Just	N/A		Default = 1 (Cathcart-Pawel)
	For cladding OD and ID to use the high temperature oxidation models, the coolant must be water or user-supplied.			
	<i>Note: The energy term will be generated at the cladding ID only if the rod has ruptured.</i>			

Table B.7. transient input block (continued)

Variable Name (Type)	Description	Units		Limitations and Default Value
		British	SI	
iStoicGrad (I)	Option to choose between assuming perfectly stoichiometric oxide or a stoichiometry gradient in modeling the weight gain calculated by the Cathcart-Pawel model. 0 = Cathcart-Pawel model assuming perfect stoichiometry 1 = Cathcart-Pawel model assuming stoichiometry gradient	N/A		Default = 0 (perfect stoichiometry)
ProtectiveOxide (I)	Option to model initial oxide as protective or non-protective. .TRUE. = Initial oxide is protective .FALSE. = Initial oxide is non-protective	N/A		Default = .TRUE. (protective oxide)
Ballooning Model Options				
Balloon (L)	Turns the BALON2 model on or off.	N/A		Default = .TRUE. (BALON2 turned on)
rnbnt (R)	Ratio of balloonable rods to total rods in bundle; normally, this ratio is 0.92. Control rods and water rods are examples of rods which cannot balloon. <i>Note: Use default value if a 17x17 bundle.</i>	N/A		Default = 1.0 (all rods balloonable)
totnb (R)	Total number of rods in fuel bundle. <i>Note: Use default value if a 17x17 bundle.</i>	N/A		Default = 289 (17x17)

(I) Integer

(R) Real

(L) Logical

(C) Character

(1) By default, a maximum of 200 time step pairs is allowed. Use `defsize` to increase this.

(2) Each time step size is used until a new time step size is input for a later time.

B.7 boundary Block

This block contains the information related to the fuel rod boundary conditions. This includes the clad-to-coolant heat transfer correlations, coolant type, and coolant conditions (T,P).

Table B.8. boundary input block

Variable Name (Type)	Description	Units		Limitations and Default Value
		British	SI	
Coolant Definitions				
CoolantType (I)	Coolant type to be used. The available coolants are: 0 = user-defined 1 = Water (sth2xt package) 2 = Helium 3 = Sodium (liquid) 5 = Nitrogen	N/A		Default = 1 (water)
	The user-defined option allows for the modeling of different coolants.			
clad_bc (# pairs, (time, bc_type))	Cladding outer surface temperature and pressure boundary condition flag. Input boundary condition type as a function of time. The options for bc_type are: 0 = Coolant model (FAST calculates temperature, pressure, HTC) 1 = User-specified coolant temperature, pressure, HTC 2 = User-specified coolant temperature, pressure (HTC calculated by FAST) 3 = User-specified surface temperature and pressure	N/A		Default = 1, 0.0, 0 (1 pair, starting at time 0.0 using coolant model)
User-Specified Cladding Temperature				
clad_temp [nt, nz, times, elevs, temps(time, elev (R))	User-specified cladding temperatures as a function of time <i>See Note 1 for Temperature</i>	s, ft, °F	s, m, K	Required

Table B.8. boundary input block (continued)

Variable Name (Type)	Description	Units		Limitations and Default Value
		British	SI	
User-Specified Coolant HTC				
HTC [nt, nz, times, elevs, HTC(time, elev)] (R)	User-specified clad-to-coolant heat transfer coefficients as a function of time and elevation <i>See Note 1 for Temperature</i>	s, ft, Btu/ft ² -hr-°F	s, m, W/m ² -K	Required
Enthalpy Rise Model				
Coolant Geometry				
pitch (R)	Center-to-center spacing of fuel rods	ft	m	Required input
dhe (R)	Heated equivalent diameter of coolant flow channel	ft	m	Default = 0.0
dhy (R)	Hydraulic diameter of coolant flow channel	ft	m	Default = 0.0
achn (R)	Cross-sectional area of flow channel	ft ²	m ²	Default = 0.0
Coolant Conditions				
Temperature [nt, nz, times, elevs, temps(time, elev)] (R)	Coolant temperature as a function of time and elevation. <i>Note 1: To specify only inlet conditions, use 1 axial zone and set all elevations (elevs) to 0.0. To specify constant values at all axial zones, use 2 axial zones, one with elevation at 0.0 and the second with elevation at tot1+cpl.</i> <i>Note 2: For water, the input temperature must be the coolant sink temperature. For subcooled or super-heated forced convection heat transfer, the actual coolant temperature is input. For boiling heat transfer, the coolant saturation temperature is input.</i>	s, ft, °F	s, m, K	Required input (unless using the input Enthalpy)
Pressure [nt, nz, times, elevs, press(time, elev)] (R)	Coolant pressure as a function of time and elevation <i>Note: See Note 1 for Temperature</i>	s, ft, psia	s, m, Pa	Required input
MassFlux [nt, times, flux(time)] (R)	Coolant inlet mass flux as a function of time	s, lb/hr-ft ²	s, kg/s-m ²	Required input

Table B.8. boundary input block (continued)

Variable Name (Type)	Description	Units		Limitations and Default Value
		British	SI	
Enthalpy [nt, nz, times, elevs, H(time,elev)] (R)	Coolant enthalpy as a function of time <i>Note: See Note 1 for Temperature</i>	s, Btu/lbm	s, J/kg	Required input (<i>unless using the input Temperature</i>)
EnthalpyType (I)	Specifies location of enthalpy value provided when only 1 elevation provided 0 = Core inlet 1 = Core average 2 = Core outlet	N/A		Default = 0 (core inlet)
VoidFraction [nt, nz, times, elevs, vf(time,elev)] (R)	Void fraction	s, ft, N/A	s, m, N/A	Required input for water (<i>unless using the input Enthalpy</i>)
InterpMethod (I)	Method of interpolation for mapping user-supplied coolant conditions with the cladding mesh 0 = Linear 1 = Weighted	N/A		Default = 0 (linear)
Clad-to-Coolant Heat Transfer Models for Water				
Mode (I)	Option to allow the user to force a specific mode of heat transfer <i>Note: applied for entire calculation.</i> Enter a value > 0 to enable. See Section 4.0 for available heat transfer modes.	N/A		Default = -1 (Off)
nbhtc (I)	Indicator for nucleate boiling heat transfer correlation. 0 = Thom + Dittus Boelter 1 = Chen 2 = Jens-Lottes	N/A		Default = 2 (Jens-Lottes)

Table B.8. boundary input block (continued)

Variable Name (Type)	Description	Units		Limitations and Default Value
		British	SI	
jfb (I)	Indicator for film boiling heat transfer correlation 0 = Groeneveld 5.9 (cluster geometry form) 1 = Groeneveld 5.7 (open annulus form) 2 = Bishop-Sandburg-Tong 3 = Groeneveld-Delorme	N/A		Default = 0 (Groeneveld 5.9)
jtr (I)	Indicator for transition boiling heat transfer correlation 0 = Tong-Young 1 = Condie-Bengston 2 = Bjornard-Griffith	N/A		Default = 0 (Tong-Young)
jchf (I)	Indicator for CHF correlation to be used. 0 = EPRI-1 1 = Bowring mixed flow cluster 2 = MacBeth 3 = Modified Zuber 4 = Biasi	N/A		Default = 0 (EPRI-1)
coldwallcf (L)	Option to modify the EPRI-1 CHF correlation for cold wall effects	N/A		Default = .FALSE.
axpowcf (L)	Option to modify the EPRI-1 CHF correlation for the effect of axially varying power. <i>Note: If flow reverses, automatically turned off.</i>	N/A		Default = .FALSE.
Bowring effects on CHF				
bowing (I)	Option to modify the CHF to account for bowing. To turn on, enter a value equal to the number of axial nodes for bowing.	N/A		Default = 0 (off)
ffch (R)	User-specified multiplier in equation for CHF reduction due to bowing. See Section 4.2.5 for more details	N/A		Default = 0.0

Table B.8. boundary input block (continued)

Variable Name (Type)	Description	Units		Limitations and Default Value
		British	SI	
bowthr (R)	Maximum fractional amount of bowing that can occur without any effect on CHF. If any amount of bowing affects CHF, enter a value of 0.0. If rods must be in contact, enter a value of 1.0.	N/A		Default = 0.0
extentofbow (R)	Axial array of ratios of deflection due to bowing to maximum possible deflection. <i>Note: Maximum possible deflection is taken as the fuel rod spacing minus fuel rod diameter.</i>	N/A		Default = 0.0

(I) Integer

(R) Real

(L) Logical

(C) Character

B.8 spentfuel Block

This block contains the information related to the performing spent fuel calculations. These calculations are performed after the in-reactor analysis is completed.

Table B.9. *spentfuel* input block

Variable Name (Type)	Description	Units		Limitations and Default Value	
		British	SI		
idatingcreep (I)	DATING Modeling Options			N/A	Default = 0 (do not model dry cask storage)
	0 = Do not model creep in dry cask storage following reactor operation				
	1 = Model creep in spent fuel using conservative creep and conservative Monkman-Grant				
	2 = Model creep in spent fuel using conservative creep and best estimate Monkman-Grant				
ncreephist (I)	Temperature/pressure history for spent fuel storage			N/A	Default = 1 (helium decay curve) <i>Note: if ncreephist = 3 or 4, input ncreeptab, creeptabtime, creeptabtemp, and creeptabstress.</i>
	1 = Helium decay curve (good for 35 [GWd/MTU])				
	2 = Nitrogen decay curve (good for 35 [GWd/MTU])				
	3 = Input temperature history. Temperature profile will be normalized to start at FAST predicted EOL temperature.				
	4 = Input temperature and rod hoop stress history				
datingtstep (R)	Timestep size to be used for DATING creep calculations		s	Default = 1.0 <i>must be ≤ 1.0</i>	
creeptime (R)	Time in dry storage		y	Default = 0.0	

Table B.9. `spentfuel` input block (continued)

Variable Name (Type)	Description	Units		Limitations and Default Value
		British	SI	
<code>creepooltime</code> (R)	Time since discharge from reactor (time spent in fuel pool prior to dry storage)	y		Default = 5.0 <i>(Note: Should not be less than 5 years)</i>
<code>ncreepstep</code> (I)	Number of output time steps	N/A		Default = 1
<code>ncreeptab</code> (I)	Number of entries in user defined temperature and rod internal pressure histories	N/A		Default = 1 Required if <code>ncreephist</code> = 3 or 4
<code>creeptabtime</code> (IT)(R)	Time in storage from reactor discharge for user defined temperature and rod internal pressure histories	y		Default = 0.0 Required if <code>ncreephist</code> = 3 or 4
<code>creeptabtemp</code> (IT)(R)	User defined temperature history	°F	°C	Default = 0.0 Required if <code>ncreephist</code> = 3 or 4
<code>creeptabstress</code> (IT)(R)	User defined midwall hoop stress history	psia	Pa	Default = 0.0 Required if <code>ncreephist</code> = 4
<code>stopox</code> (R)	Indicator for when to stop the oxide calculation. This value should correspond to the <code>ProblemTime</code> value when the fuel is out of the pool. If it does not line up exactly with a <code>ProblemTime</code> value, the oxidation calculation will stop when the value for <code>stopox</code> > <code>ProblemTime(it)</code> . Values for oxidation layer thickness & hydrogen uptake from the coolant will remain the same value as the last time step before oxidation was turned off.	days		Default = 1×10^{10}
<code>addswell</code> (IT)(R)	Additional volumetric swelling. Enter as a volumetric strain value. Must enter one value for every time step specified in <code>ProblemTime</code> . Values will be used at current time step only and do not compound with previous time step's value.	N/A		Default = 0.0

Table B.9. *spentfuel* input block (continued)

Variable Name (Type)	Description	Units		Limitations and Default Value
		British	SI	
addgmles (IT)(R)	Additional gram moles of gas added to the rod internal gas pressure calculation. Must enter one value for every time step specified in <i>ProblemTime</i> . Values will be used at current time step only and do not compound with previous time step's value.		mol	Default = 0.0

- (I) Integer
- (R) Real
- (L) Logical
- (C) Character
- (IT) Time Step Index

B.9 refabrication block

This block is used to define the refabrication characteristics when a refabrication is performed during the analysis. An example of using this block would be when analyzing a full length rod in commercial operation and then analyzing a portion of the rod that was refabricated and placed in a test reactor, such as Halden.

Table B.10. *refabrication* input block

Variable Name (Type)	Description	Units		Limitations and Default Value
		British	SI	
Refabrication				
irefab (I)	Time step to start using refabricated values		N/A	Default = 10000 (no refabrication)
nrefab1 (I)	Lower axial node for refabrication		N/A	Required input (if modeling refabrication)
nrefab2 (I)	Upper axial node for refabrication		N/A	Required input (if modeling refabrication)
cplrefab (R) ⁽¹⁾	Refabricated plenum length	in	m	Required input (if modeling refabrication)
vsrefab (R) ⁽¹⁾	New plenum springs' number of turns in refabricated plenum		N/A	Required input (if modeling refabrication)

Table B.10. refabrication input block (continued)

Variable Name (Type)	Description	Units		Limitations and Default Value
		British	SI	
dspgrefab (R) ⁽¹⁾	New plenum spring coil diameter	in	m	Required Input (if modeling refabrication)
dspgwrefab (R) ⁽¹⁾	New plenum spring wire diameter	in	m	Required Input (if modeling refabrication)
extplenumVrefab (R)	New External plenum volume	in ³	m ³	Default = 0.0
fgpavrefab (R)	Fill gas pressure at time step of refabrication	psia	Pa	Default = 0.0
herrefab (R)	Fraction of helium in refabricated rod	N/A		Default = 1.0
airrefab (R)	Fraction of air in refabricated rod	N/A		Default = 0.0
n2refab (R)	Fraction of nitrogen in refabricated rod	N/A		Default = 0.0
arrefab (R)	Fraction of argon in refabricated rod	N/A		Default = 0.0
fgrefab (R)	Fraction of fission gas in refabricated rod	N/A		Default = 0.0
krrefab (R)	Fraction of krypton in refabricated rod	N/A		Default = 0.0
xerefab (R)	Fraction of xenon in refabricated rod	N/A		Default = 0.0

^(I) Integer

^(R) Real

^(L) Logical

^(C) Character

⁽¹⁾ May input one value (for upper plenum only) or as 2 values (first value for upper plenum, second value for lower plenum)

B.10 uncertainty Block

This block contains the information related to performing uncertainty treatment on the FAST models. The bias applied to the models can be performed using either a set number of standard deviations (assuming the standard deviation is known, see the MatLib documentation [Geelhood et al., 2022a] for more details) or a multiplier on the model's calculated value.

Table B.11. uncertainty input block

Variable Name (Type)	Description	Units		Limitations and Default Value
		British	SI	
Uncertainty Variables				
	Type of bias to apply			
	0 = Bias is based on number of standard deviations			
biastype (I)	1 = Bias is a multiplier on to the calculated value		N/A	Default = 0
	<i>Note: If biastype = 1, all defaults of 0.0 below become 1.0</i>			
Biases or Multipliers				
sigftc (R)	Bias on fuel thermal conductivity model		N/A	Default = 0.0
sigfcp (R)	Bias on fuel specific heat model		N/A	Default = 0.0
sigftex (R)	Bias on fuel thermal expansion model		N/A	Default = 0.0
sigfgr (R)	Bias on fission gas release model		N/A	Default = 0.0
sigswell (R)	Bias on fuel swelling model		N/A	Default = 0.0
sigctc (R)	Bias on cladding thermal conductivity model		N/A	Default = 0.0
sigccp (R)	Bias on cladding specific heat model		N/A	Default = 0.0
sigctex (R)	Bias on cladding thermal expansion model		N/A	Default = 0.0
sigcreep (R)	Bias on cladding creep model		N/A	Default = 0.0
sigcyield (R)	Bias on cladding yield strength model		N/A	Default = 0.0
siggro (R)	Bias on cladding axial growth model		N/A	Default = 0.0
sigcor (R)	Bias on cladding corrosion model		N/A	Default = 0.0
sigh2 (R)	Bias on cladding hydrogen pickup model		N/A	Default = 0.0

Table B.11. uncertainty input block (continued)

Variable Name (Type)	Description	Units		Limitations and Default Value
		British	SI	
Multipliers Only				
sightc (R)	Multiplier on clad-to-coolant heat transfer coefficient		N/A	Default = 1.0
gaphtcmult (R)	Multiplier on gap conductance model		N/A	Default = 1.0

^(I) Integer

^(R) Real

B.11 developer Block

This block contains parameters that were designed to be used by the code developers to perform targeted code assessments. These inputs can be used to make fundamental changes to the models in FAST, and therefore the results when using these options are NOT validated.

Table B.12. developer input block

Variable Name (Type)	Description	Units		Limitations and Default Value
		British	SI	
Calcoxide (L)	Flag to specify whether or not to calculate oxidation. If set to .FALSE., no cladding oxidation will occur and the hydrogen intake into the cladding will also be turned off.		N/A	Default value = .TRUE.
Modheat (R)	Moderator heating fraction. Specifies the fraction of input linear heat generation rate to be deposited directly into the coolant. To use default values based on plant type, set modheat = -1.		fraction	Default value = 0.0. Default values if modheat = -1 are: PWR: 0.026 BWR: 0.035 HWR: 0.084
Relocmodel (C)	Fuel relocation model options. 'FRAPCON-3.5' 'FRAPCON-3.4' 'OFF' 'USER'		N/A	Default = 'FRAPCON-3.5'
Fuelreloc (R)	Fuel relocation fraction of as-fabricated gap. Fuel relocation fraction will ramp from 0.0 to fuelreloc over 10 GWd/MTU burnup. This value is only used when relocmodel = 'USER'		fraction	Default = -1.0 (not used) Must be 0.0 to 1.0 to use

Table B.12. developer input block (continued)

Variable Name (Type)	Description	Units		Limitations and Default Value
		British	SI	
Gaprecov (R)	Fraction of relocated fuel allowed to recover before hard contact occurs. This fraction will be added to the fuel surface as permanent deformation.	fraction		Default = 0.5
nread (R)	Flag to start from a restart file. The value of nread is the time step to start from. <i>Note: User must switch the restart-write tape file number from 12 to 13 to make it a restart-read tape.</i>	N/A		Default = 0
restarttime (R)	Problem time to use for a restart calculation. Problem time of < 0 will default to the last calculation time	s		If < 0, will use last restart time.
nrestr (I)	Flag for writing a restart file 0 = No restart file 1 = Write restart file	N/A		Default = 0

(I) Integer

(R) Real

(L) Logical

(C) Character

B.12 lua Block

This block contains parameters that enable the use of lua functions in the input file to replace the pre-compiled material properties. These functions, written in the lua scripting language, must be added to the end of the input file following a line that reads #LUA. Enabling one or more of these options will result in FAST printing a commented template for the function that must be added to the scripted block at the end of the input file. For more information see Appendix E. These inputs can be used to make fundamental changes to the models in FAST, and therefore the results when using these options are NOT validated.

Table B.13. lua input block

Variable Name (Type)	Description	Units		Limitations and Default Value
		British	SI	
Fuel				
lua_fuel_thermcond (L)	Flag to specify whether or not to use the lua function for fuel thermal conductivity.	N/A		Default value = .FALSE.
lua_fuel_tdensity (L)	Flag to specify whether or not to use the lua function for fuel theoretical density.	N/A		Default value = .FALSE.
lua_fuel_density (L)	Flag to specify whether or not to use the lua function for fuel density.	N/A		Default value = .FALSE.
lua_fuel_tmelt (L)	Flag to specify whether or not to use the lua function for fuel melting temperature.	N/A		Default value = .FALSE.
lua_fuel_heat_fusion (L)	Flag to specify whether or not to use the lua function for fuel thermal conductivity.	N/A		Default value = .FALSE.
lua_fuel_specheat (L)	Flag to specify whether or not to use the lua function for fuel specific heat.	N/A		Default value = .FALSE.
lua_fuel_thexp (L)	Flag to specify whether or not to use the lua function for fuel thermal expansion.	N/A		Default value = .FALSE.
lua_fuel_swelling (L)	Flag to specify whether or not to use the lua function for fuel swelling.	N/A		Default value = .FALSE.
lua_fuel_emiss (L)	Flag to specify whether or not to use the lua function for fuel emissivity.	N/A		Default value = .FALSE.
lua_fuel_densification (L)	Flag to specify whether or not to use the lua function for fuel densification.	N/A		Default value = .FALSE.

Table B.13. lua input block (continued)

Variable Name (Type)	Description	Units		Limitations and Default Value
		British	SI	
lua_fuel_enthalpy (L)	Flag to specify whether or not to use the lua function for fuel enthalpy.	N/A		Default value = .FALSE.
lua_fuel_relocation (L)	Flag to specify whether or not to use the lua function for fuel relocation.	N/A		Default value = .FALSE.
lua_fuel_mwt_u_fraction (L)	Flag to specify whether or not to use the lua function for fuel heavy metal weight fraction.	N/A		Default value = .FALSE.
lua_fuel_mwt_u (L)	Flag to specify whether or not to use the lua function for fuel heavy metal molecular weight.	N/A		Default value = .FALSE.
Cladding				
lua_clad_thermcond (L)	Flag to specify whether or not to use the lua function for cladding thermal conductivity.	N/A		Default value = .FALSE.
lua_clad_density (L)	Flag to specify whether or not to use the lua function for cladding density.	N/A		Default value = .FALSE.
lua_clad_tmelt (L)	Flag to specify whether or not to use the lua function for cladding melting temperature.	N/A		Default value = .FALSE.
lua_clad_ttrans_start (L)	Flag to specify whether or not to use the lua function for cladding lower transition temperature.	N/A		Default value = .FALSE.
lua_clad_ttrans_end (L)	Flag to specify whether or not to use the lua function for cladding upper transition temperature.	N/A		Default value = .FALSE.
lua_clad_heat_fusion (L)	Flag to specify whether or not to use the lua function for cladding thermal conductivity.	N/A		Default value = .FALSE.
lua_clad_specheat (L)	Flag to specify whether or not to use the lua function for cladding specific heat.	N/A		Default value = .FALSE.
lua_clad_specheat_integral (L)	Flag to specify whether or not to use the lua function for cladding specific heat integral.	N/A		Default value = .FALSE.
lua_clad_thexp_axial (L)	Flag to specify whether or not to use the lua function for cladding thermal expansion in the axial direction.	N/A		Default value = .FALSE.

Table B.13. lua input block (continued)

Variable Name (Type)	Description	Units		Limitations and Default Value
		British	SI	
lua_clad_thexp_radial (L)	Flag to specify whether or not to use the lua function for cladding thermal expansion in the radial direction.	N/A		Default value = .FALSE.
lua_clad_thexp (L)	Flag to specify whether or not to use the lua function for cladding isotropic thermal expansion (acts as if the same function is used for previous two thexp variables).	N/A		Default value = .FALSE.
lua_clad_emiss (L)	Flag to specify whether or not to use the lua function for cladding emissivity.	N/A		Default value = .FALSE.
lua_clad_pois_ratio (L)	Flag to specify whether or not to use the lua function for cladding Poisson's ratio.	N/A		Default value = .FALSE.
lua_clad_young_mod (L)	Flag to specify whether or not to use the lua function for cladding Young's modulus.	N/A		Default value = .FALSE.
lua_clad_shear_mod (L)	Flag to specify whether or not to use the lua function for cladding shear modulus.	N/A		Default value = .FALSE.
lua_clad_yield_stress (L)	Flag to specify whether or not to use the lua function for cladding yield stress.	N/A		Default value = .FALSE.
lua_clad_axial_growth (L)	Flag to specify whether or not to use the lua function for cladding axial growth.	N/A		Default value = .FALSE.
lua_clad_meyer_hard (L)	Flag to specify whether or not to use the lua function for cladding Meyer hardness.	N/A		Default value = .FALSE.
lua_clad_ut_stress (L)	Flag to specify whether or not to use the lua function for cladding ultimate tensile stress.	N/A		Default value = .FALSE.
Clad Coating				
lua_coating_thermcond (L)	Flag to specify whether or not to use the lua function for clad coating thermal conductivity.	N/A		Default value = .FALSE.
lua_coating_density (L)	Flag to specify whether or not to use the lua function for clad coating density.	N/A		Default value = .FALSE.

Table B.13. lua input block (continued)

Variable Name (Type)	Description	Units		Limitations and Default Value
		British	SI	
lua_coating_tmelt (L)	Flag to specify whether or not to use the lua function for clad coating melting temperature.	N/A		Default value = .FALSE.
lua_coating_speheat (L)	Flag to specify whether or not to use the lua function for clad coating specific heat.	N/A		Default value = .FALSE.
Oxides				
lua_oxide_thermcond (L)	Flag to specify whether or not to use the lua function for clad oxide thermal conductivity.	N/A		Default value = .FALSE.
lua_oxide_density (L)	Flag to specify whether or not to use the lua function for clad oxide density.	N/A		Default value = .FALSE.
lua_oxide_tmelt (L)	Flag to specify whether or not to use the lua function for clad oxide melting temperature.	N/A		Default value = .FALSE.
lua_oxide_speheat (L)	Flag to specify whether or not to use the lua function for clad oxide specific heat.	N/A		Default value = .FALSE.
CRUD				
lua_crud_thermcond (L)	Flag to specify whether or not to use the lua function for CRUD thermal conductivity.	N/A		Default value = .FALSE.
lua_crud_density (L)	Flag to specify whether or not to use the lua function for CRUD density.	N/A		Default value = .FALSE.
lua_crud_tmelt (L)	Flag to specify whether or not to use the lua function for CRUD melting temperature.	N/A		Default value = .FALSE.
lua_crud_speheat (L)	Flag to specify whether or not to use the lua function for CRUD specific heat.	N/A		Default value = .FALSE.
Plenum Spring				
lua_spring_thexp (L)	Flag to specify whether or not to use the lua function for plenum spring thermal expansion.	N/A		Default value = .FALSE.

- (I) Integer
- (R) Real
- (L) Logical
- (C) Character

This page intentionally blank.

Appendix C – Output and Plotting Capabilities

This appendix contains the information relating to the output and plotting capabilities of FAST. As shown in Table B.1, FAST-1.1 can produce an ASCII text-based output file that summarizes the results in an easy to read format, as well as an ASCII numerical-only plot file that contains scalars and arrays of many important modeling parameters as a function of time. This file was designed to work with a Microsoft Excel based tool called FRAPlot as well as AptPlot, which is also designed to work with the SNAP tool previously mentioned. However, this file being written in a simple, ASCII format will allow it to be read using any text editor.

C.1 Output File

The output file is a text-based summary of the calculation results that is laid out in an easy to read format. The output file can be broken down into three main sections, as shown in Figure C.1. The input processing portion contains the code version used in the analysis, a re-write of the input file, and a summary report of the fuel rod design and user-supplied coolant conditions and power history. The time-dependent results contain important calculated parameters, such as temperature distributions, dimensional changes, contributions to rod internal pressure, and cladding corrosion. These values can be printed for every axial node, the peak power axial node or as an axial summary (`jd1pr`) at the end of every user-specified timestep or as a summary at the end of the calculation (`nopt` for steady-state calculations, `dtproa` for transient calculations). The level of detail in the output file is controlled by the input flags.

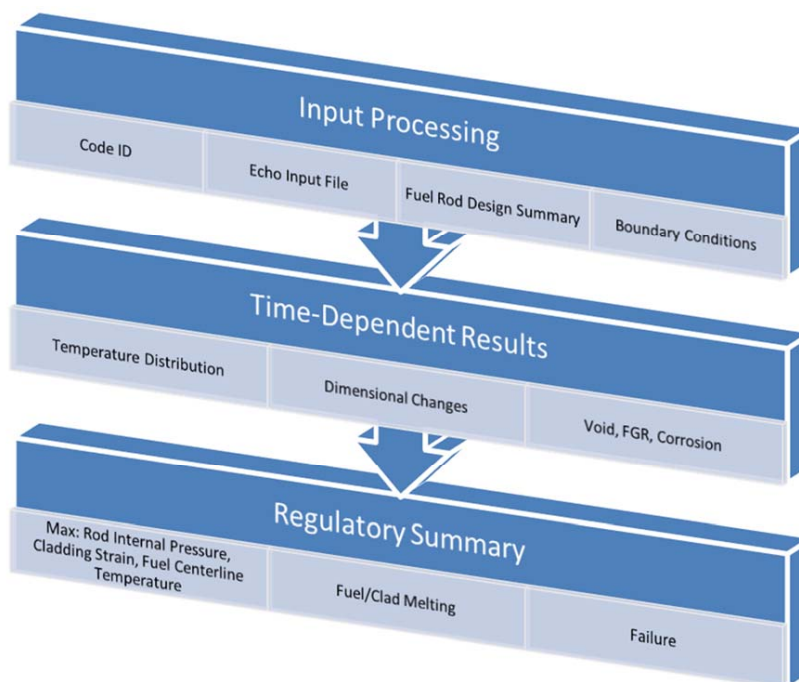


Figure C.1. Summary of output file layout

C.2 Plot File

The plot file is an ASCII-based file that contains both scalars and arrays of parameters typically assessed against experimental data or other codes. All of the parameters are printed at each timestep (as opposed to printing each variable as a function of time at the end of the calculation). For steady-state calculations, the print interval is equal to `nplot`, whereas for transient calculations it is controlled by `dtplot`. The level of detail contained in the plot file is controlled by `nplot`. The list of plot variables is shown in Table C.1.

Table C.1. Available parameters in plot file

Scalars	Axial Arrays	2-D(r,z) Arrays
<ul style="list-style-type: none"> • Time • Average and peak powers • Rod average burnup • Peak power axial node, burnup, centerline temperature, surface temperature, clad ID and OD temperature • Average fuel temperature • Fueled region stored energy • Plenum gas temperature and pressure • Total void volume • Fuel stack and cladding axial extension • Relative fuel stack and cladding axial extension • Fission gas release • Molar fraction of He, Xe, Kr, Ar, air • Free gas in rod • Moles of He released for IFBA fuel • Moles of fission gas released • Moles of gas in rod 	<ul style="list-style-type: none"> • Power (absolute and relative) • Surface heat flux • Burnup and fast fluence • Elevation • Fuel centerline, surface, and volume average temperature • Gap average temperature • Cladding ID, average, and OD temperature • Oxide surface temperature, CRUD temperature • Coolant temperature, pressure, density, and mass flux • Fuel duty index • Stored energy • Cladding axial, hoop, and effective stress • Cladding axial, hoop, and radial total, elastic, and plastic strains • Fuel and cladding deformations • Fuel thermal expansion, swelling, densification, relocation, and swelling rate • Nodal FGR • ¹⁰B enrichment for IFBA fuel • Fuel/clad interfacial pressure and rod internal pressure • Mechanical and thermal gap thickness • Gap conductance • Oxide thickness and hydrogen concentration • Fuel rim length if using FRAPFGR model 	<ul style="list-style-type: none"> • Mesh locations (distance) • Temperature • Burnup • Fuel porosity fraction • Plutonium concentration • Radial power profile • Radial fuel density <p style="text-align: center;">Gas Arrays</p> <ul style="list-style-type: none"> • Mesh locations (distance) • Produced, released, and retained fission gas concentrations • Grain boundary, intra-granular, and re-solved gas concentrations • Fuel restructuring and porosity

C.3 FRAPlot

The Microsoft Excel-based tool developed for use with the FAST codes is FRAPlot. FRAPlot has a series of Macros that enables it to read the plot file, create arrays, develop ListBoxes that contain

the information about each array, and create plots. There are four Tabs at the bottom of the workbook that contain plot-able data which corresponds to each of the boxes from Figure C.2: *Data* (Scalars), *1D Data* (Axial Arrays), *2D Data* (2-D (r,z) Arrays) and *Gas Data* (Gas Arrays).

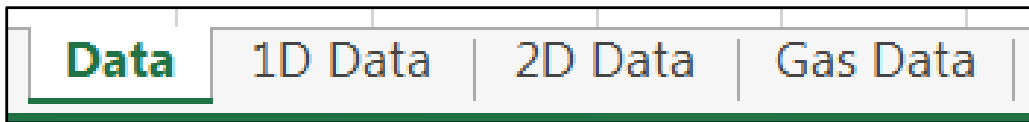


Figure C.2. FRAPlot's tabs containing plottable data

Note: in order to use FRAPlot, you must 1) have an activated version of Microsoft Excel and 2) enable macros when the workbook is opened.

FRAPlot has the ability to switch between British and SI units, regardless of the units printed in the plot file, using the same unit conversions as those contained in FAST. This option is available on all Tabs. As shown in Figure C.3, the units selection is in cell B5 and contains a dropdown selection of either *SI* or *British*.

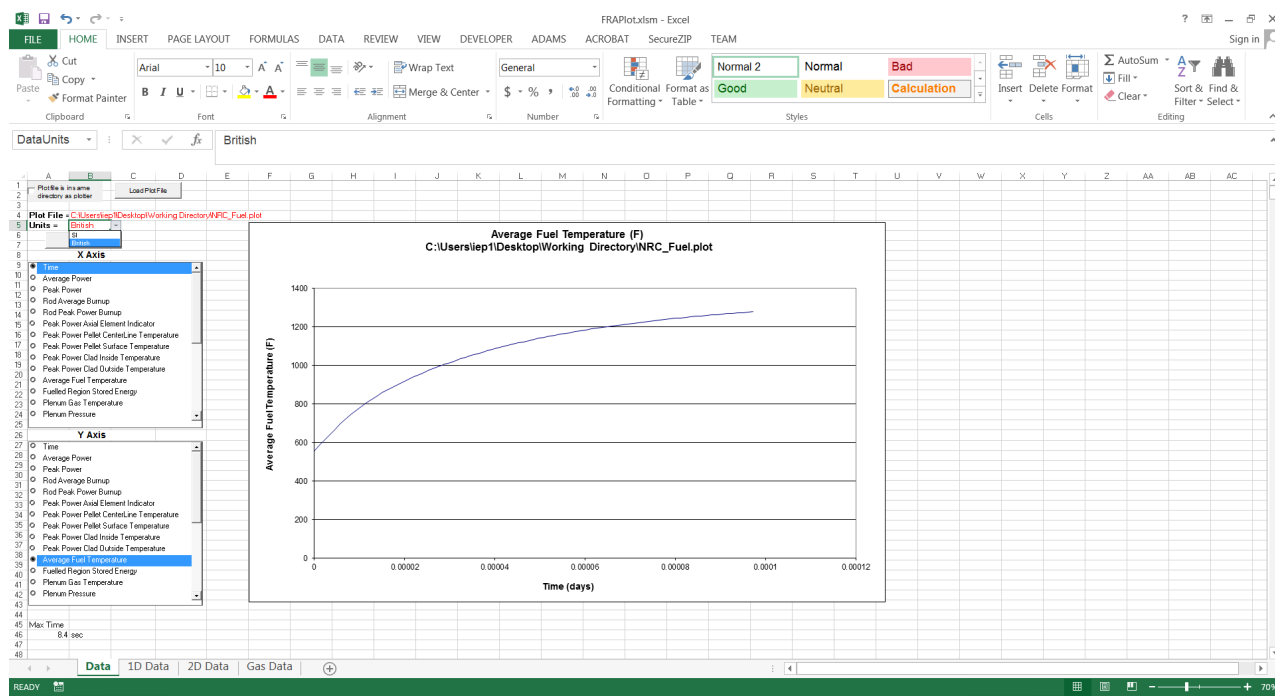


Figure C.3. Units selection

After opening FRAPlot, click the button labeled “Load Plot File”, as shown in Figure C.4. This button is available on all four of the Tabs; any of the tabs may be used. When switching from one tab to another, this step does not need to be repeated.

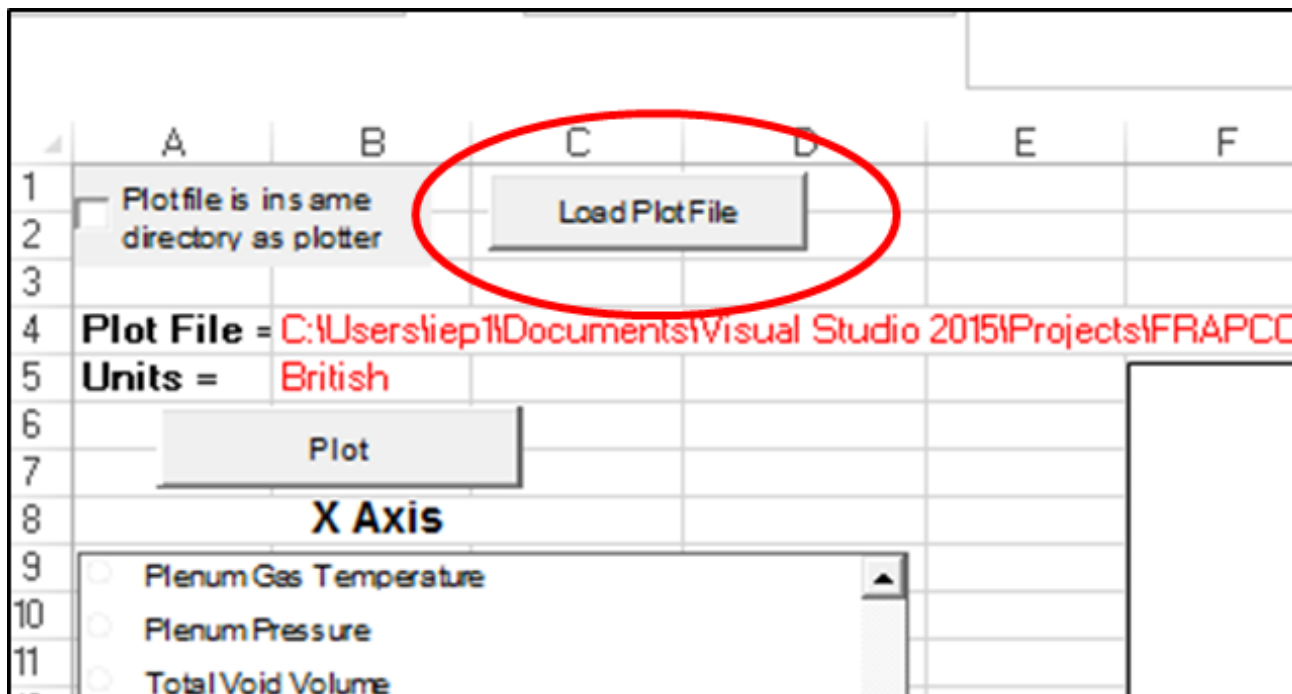


Figure C.4. "Load Plot File" selection

A pop-up window will appear that allows you to select the plot file. Click the "Browse" button and find your plot file on your computer. Note: This tool will only show files with the .plot extension. If your plot file was not named with the .plot extension, as recommended in Figure C.5, it must be renamed FileName.plot. Once you have selected your plot file, click the "Ok" button.

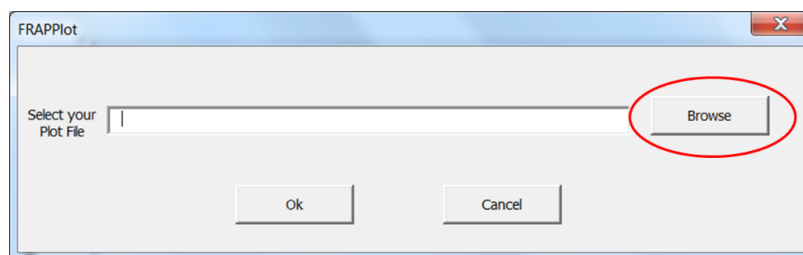


Figure C.5. "Load Plot File" pop-up window

Depending on the size of the plot file, it may take several seconds up to a minute for the file to load into Excel's memory. Once it is loaded, the ListBoxes will populate with the available plotting data.

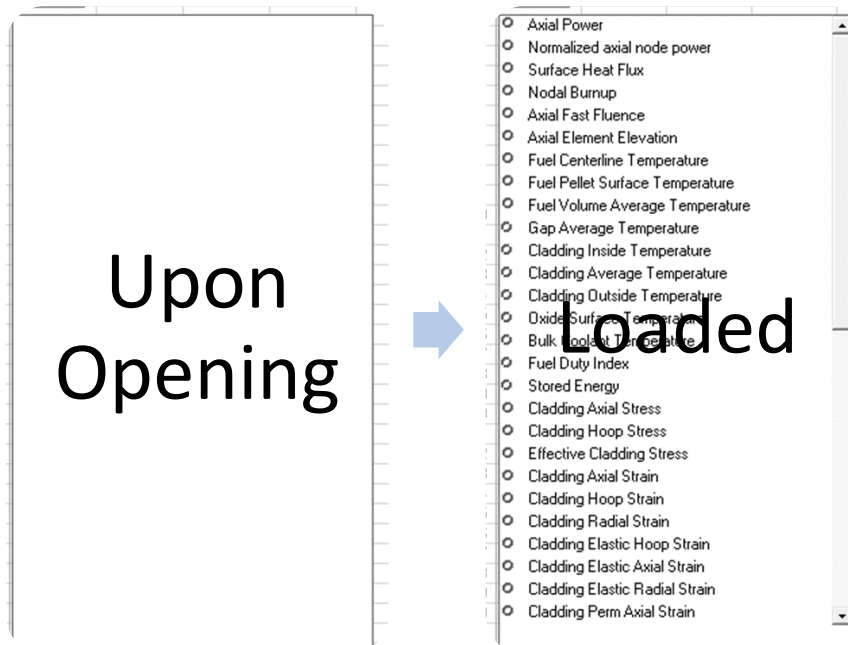


Figure C.6. View of Listboxes once Plot File is loaded into Memory

To plot the scalar data (*Data* tab), select a variable from both the X Axis and Y Axis ListBoxes, make sure that the proper Units are selected, and press the “Plot” button.

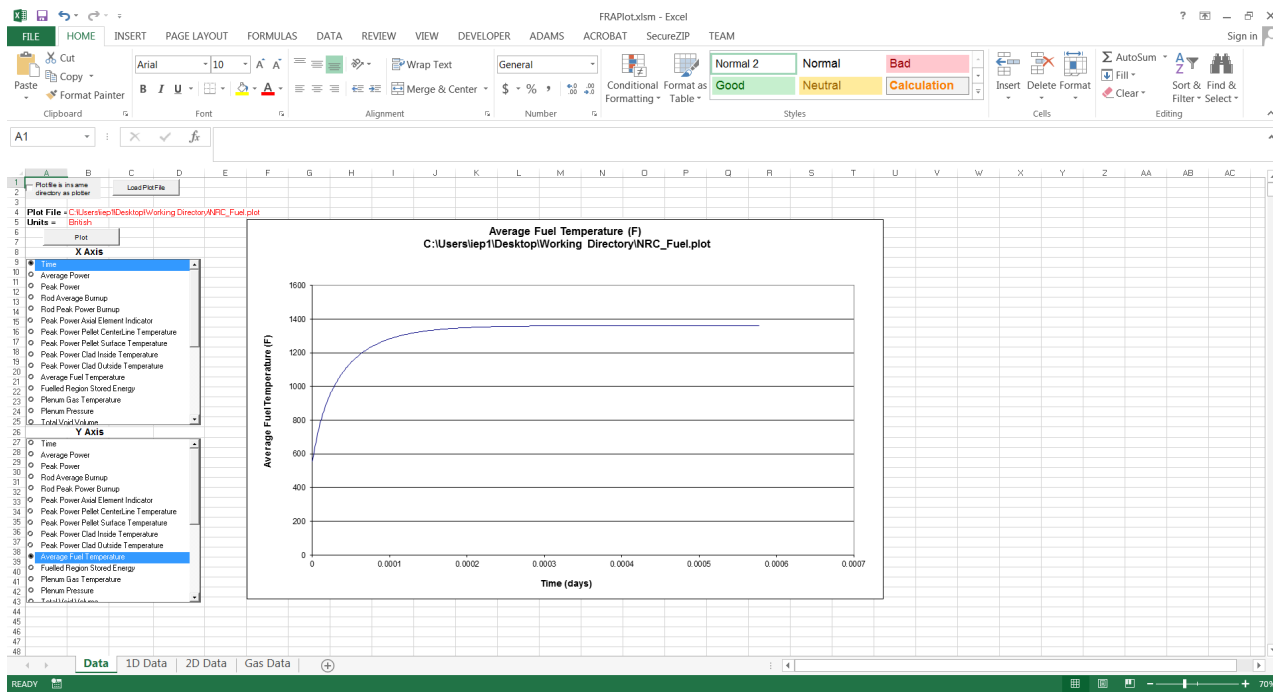


Figure C.7. Examples of “Data” plot using British units

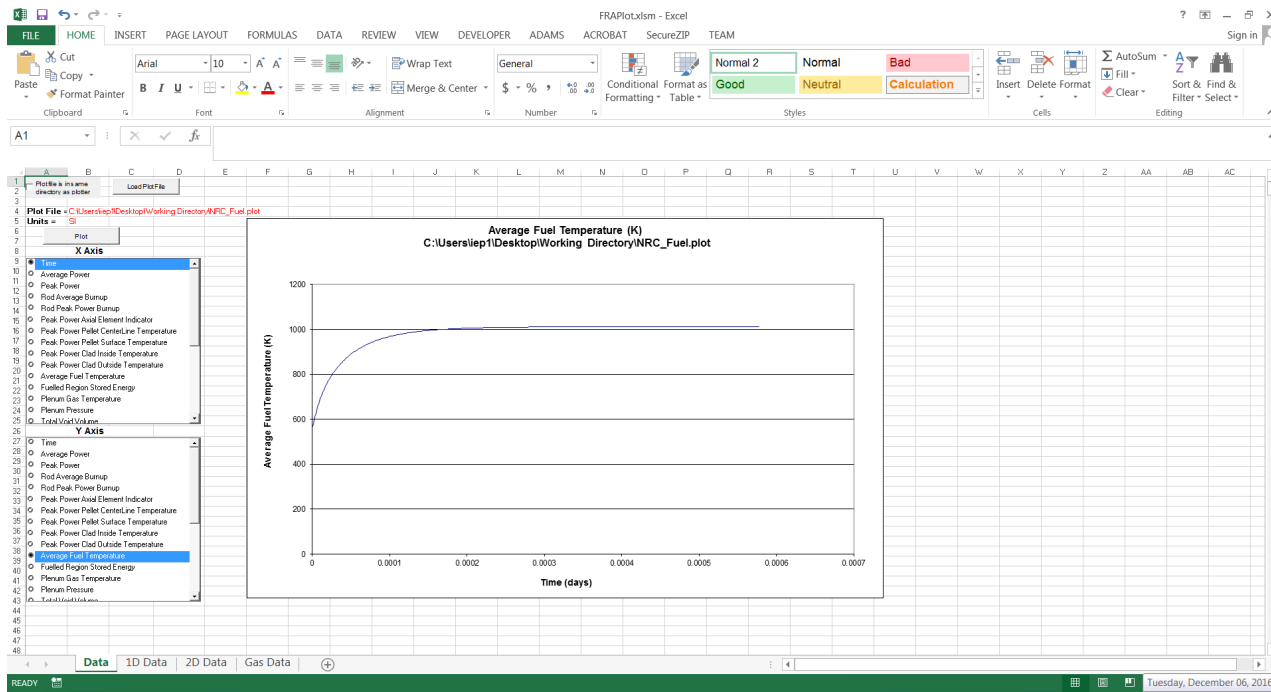


Figure C.8. Examples of “Data” plot using SI units (continued)

To plot the Axial Arrays, click on the *1D Data* tab. There are two plotting buttons on this tab: “Nodal Plot” and “Axial Plot”. The “Nodal Plot” button will produce a plot of the selected value for each axial node as a function of the X-axis variable selected. The X-axis for the graph in this tab can be selected as being either problem time days or rod-average burnup GWd/MTU.

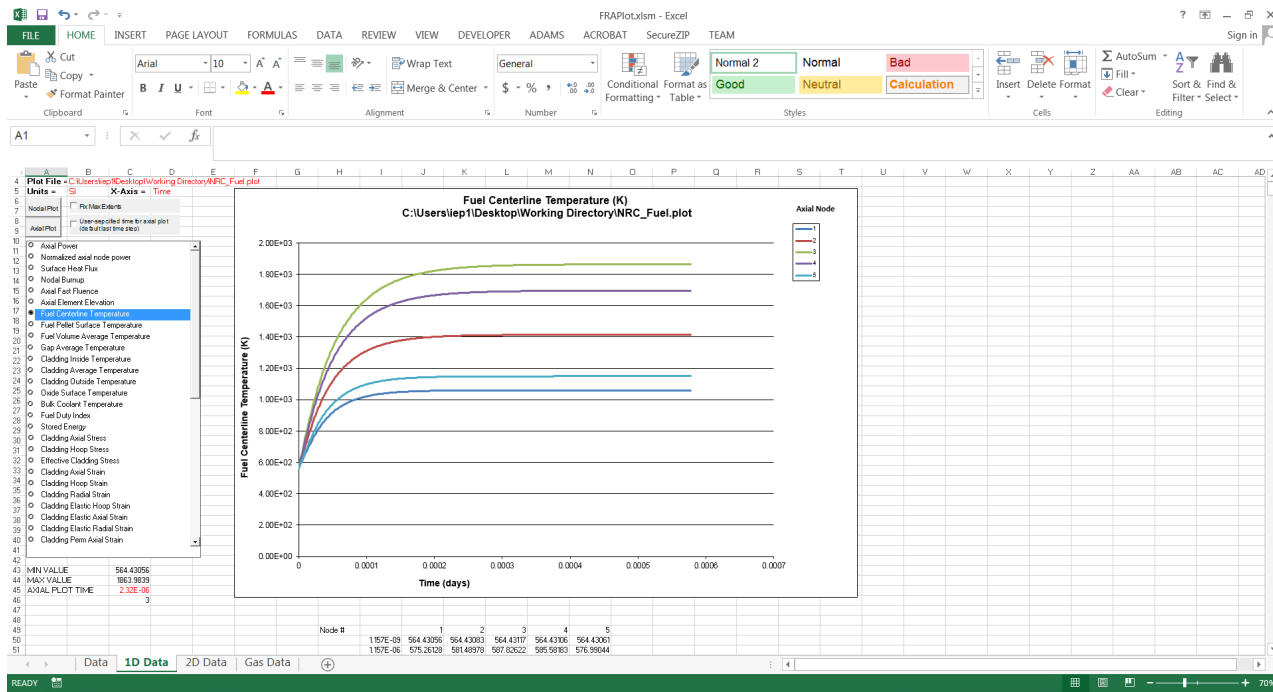


Figure C.9. Nodal plot using burnup for x-axis

The “Axial Plot” button will produce a graph of the selected array versus axial elevation at a certain point in time. If the checkbox is not checked where it says “User-specified time for axial plot (default last timestep)”, FRAPLOT will pull the data at the last timestep. If this checkbox is checked, then the code will use the closest timestep that is less than or equal to the value in cell C45, next to the words “AXIAL PLOT TIME”. If the value here is larger than the last timestep, it will default to using the last timestep. For both plotting options, the user can select the checkbox “Fix Max Extents” if they wish to set the minimum and maximum values on the Y-Axis to the minimum and maximum values being plotted. An example of the “Axial Plot” is shown in Figure C.10.

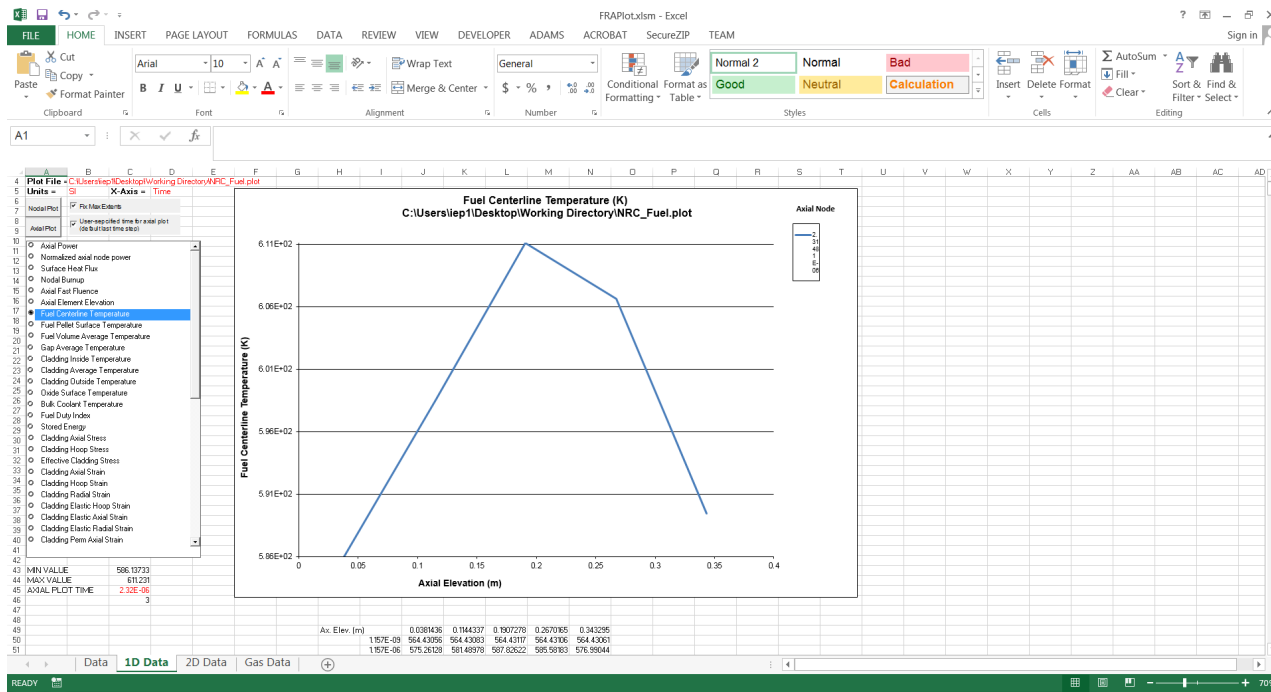


Figure C.10. Axial Plot with “Fix Max Extents” and “User-specified Time for Axial Plot”

The *2D Data* plotting options are similar to the *1D Data* options, without the ability to select the X-axis variables. Rather than having an X- and Y-axis, there is a Horizontal (similar to X-axis), Vertical (similar to Y-axis) and a Depth axis, as shown in Figure C.10. The Horizontal axis is for the radial nodes for the entire fuel rod (fuel, gap, clad, oxide, crud), where 1 represents the outermost (cladding OD crud) temperature and each incremental number increase moves inward by 1 mesh point towards the fuel centerline. The Depth axis is for the axial nodes, where 1 corresponds to the bottom-most segment of the fuel rod.

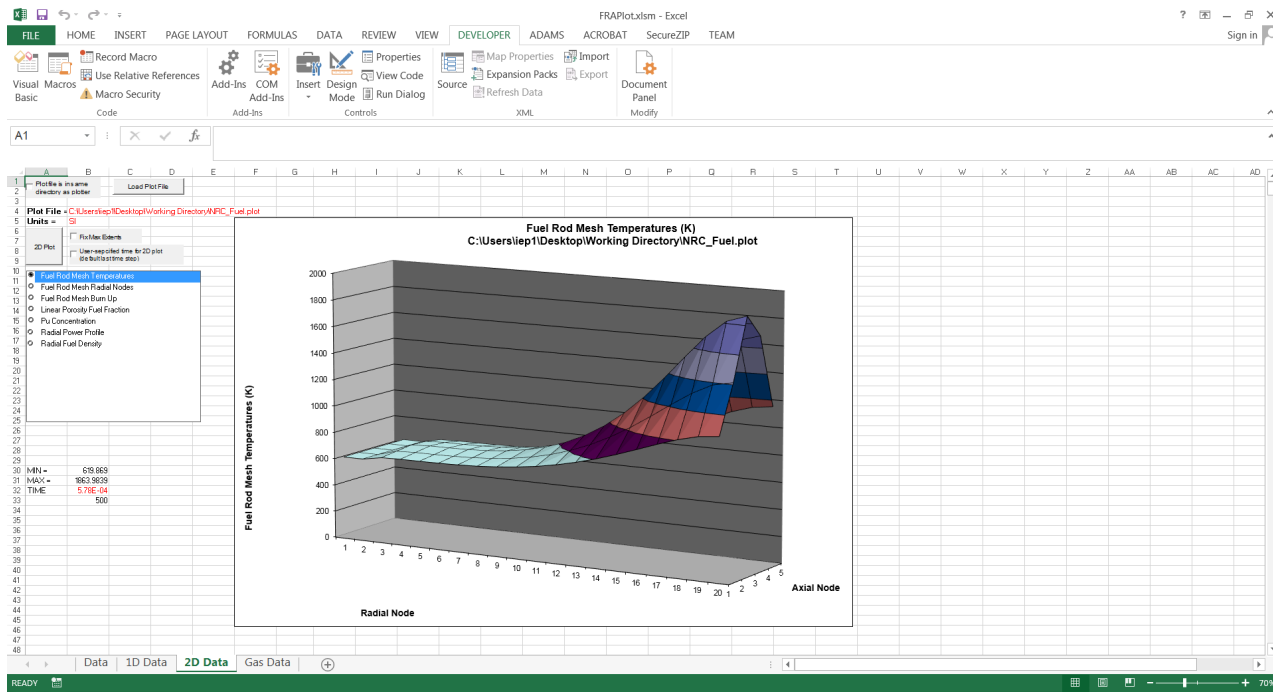


Figure C.11. Example of a 2D Data plot

The *Gas Data* tab will only contain data if the proper value is used in the input variable *np1ot*. This tab is very similar to the *2D Data* tab, with the plotting button labeled as “Gas Plot”. However, the radial gas nodes are for the fuel mesh only and use a reversed nodalization from the temperature calculation (where 1 corresponds to the fuel centerline).

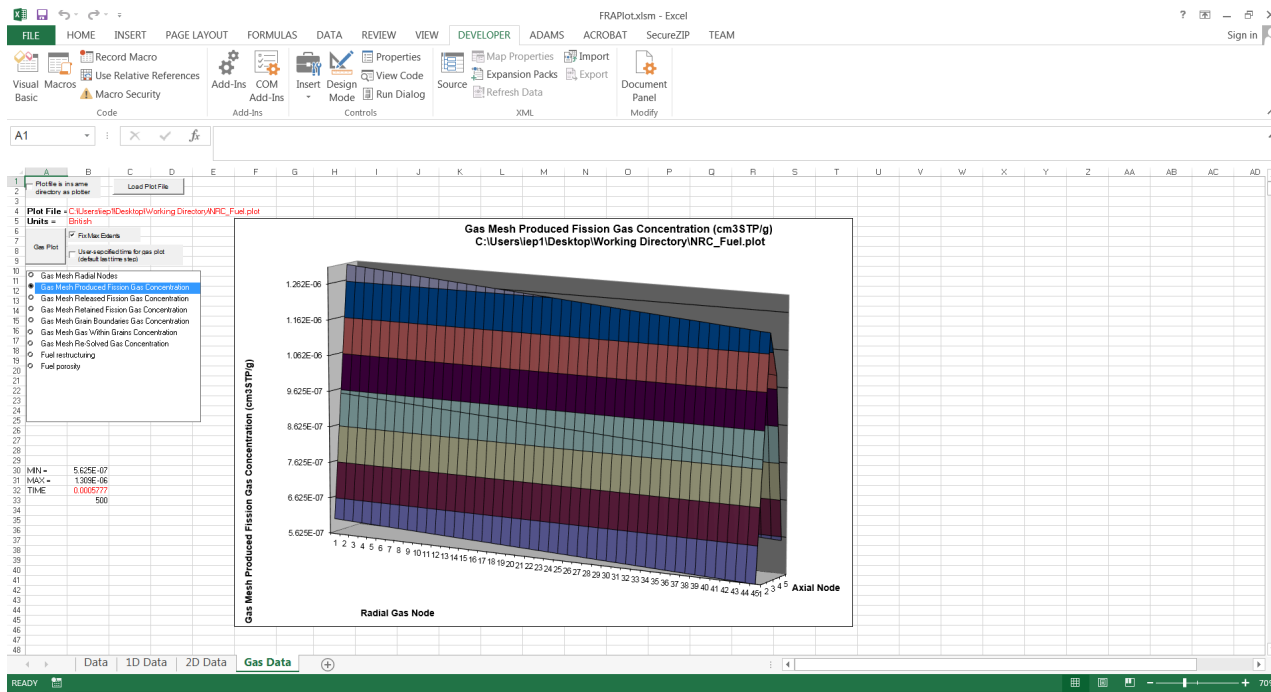


Figure C.12. Example of a Gas Data plot

C.4 AptPlot

The ACS plug-in has been updated for use with AptPlot that allows it to read the plot file generated by FAST. This section is a brief overview of how to load the FRAPCON file into AptPlot. For more detailed information regarding the capabilities of AptPlot, visit <https://www.aptpplot.com>. Additionally, AptPlot contains a “Help” feature that contains additional information regarding the ACS plug-in and creating FAST plots.

The same options that were outlined in Figure ?? are available for plotting. After opening up the AptPlot program, search for the FAST-generated plot file by selecting File -> Read -> FAST data. A pop-up window will appear that will allow for the selection of the FILENAME .plot file. After selecting it, press Open. These steps are shown in Figure C.13 and C.14.

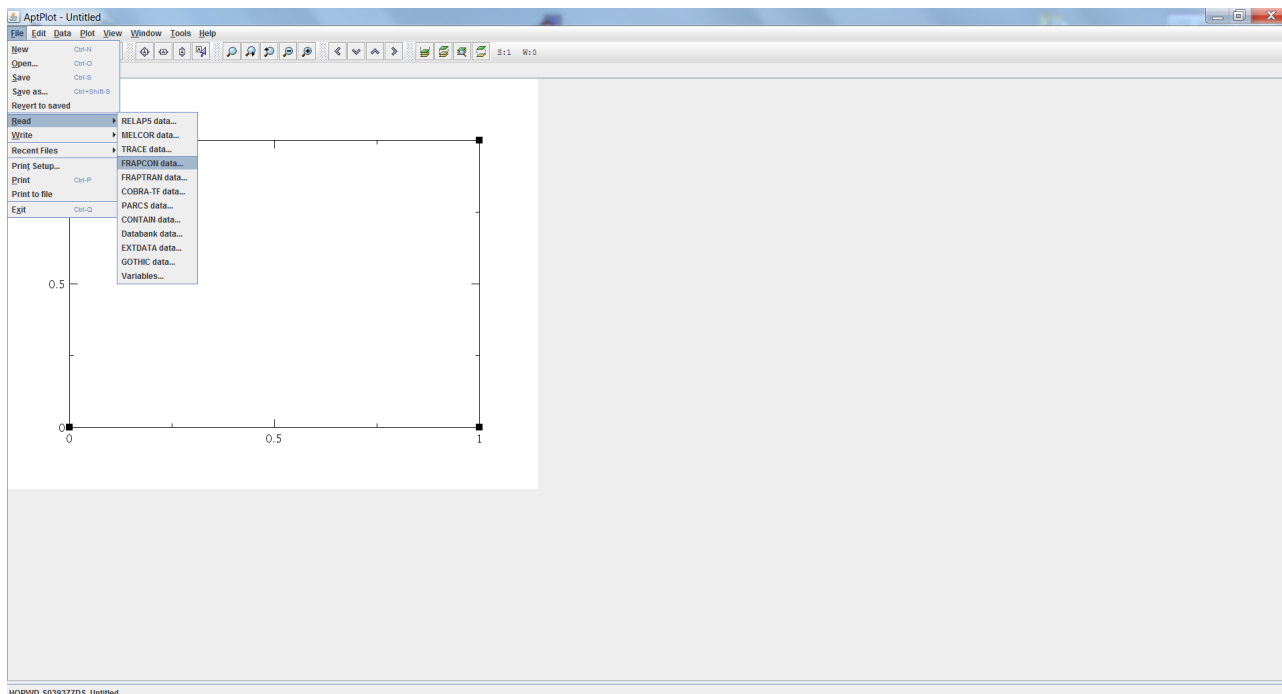


Figure C.13. How to load FAST plot file in AptPlot (a)

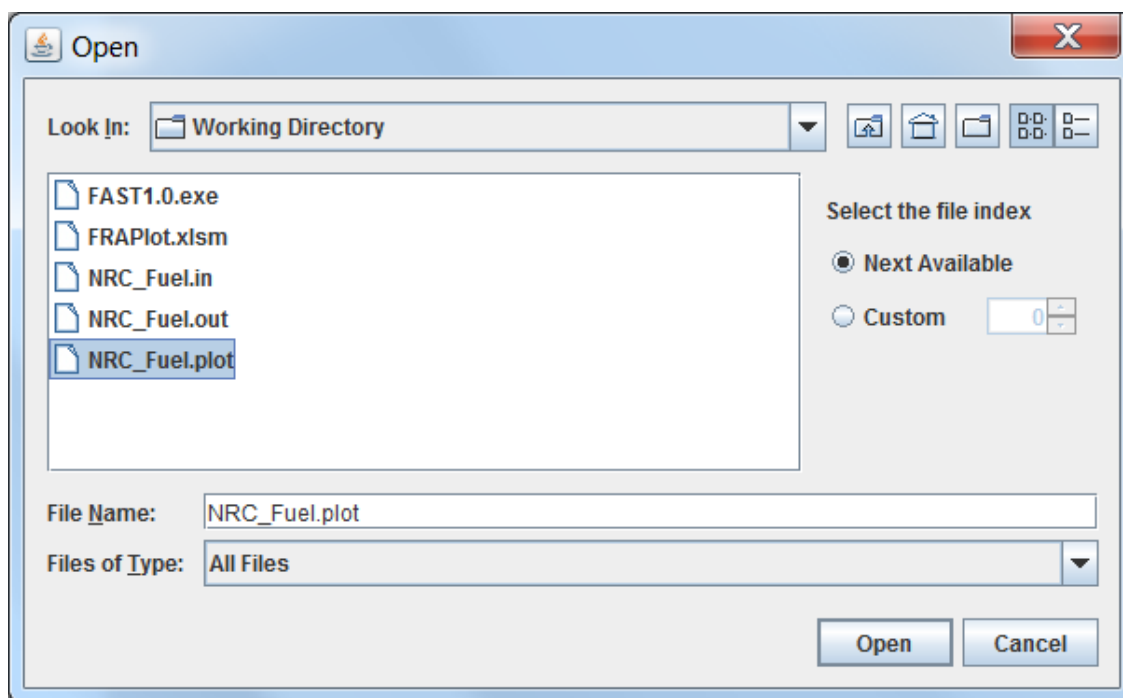


Figure C.14. How to load FAST plot file in AptPlot (b)

After pressing Open, a new window will appear (Figure C.15) that contains all of the selectable variables (these are referred to as data channels within AptPlot). In this window, there are several options similar to those available in the FRAPlot tool. The user can select the plotting units

(SI/British) and X-axis Time units. Rather than the multiple Tabs in the FRAPlot tool, a drop-down menu is available that allows for multiple Plot Types: Time Dependent, Axial and Radial plots. For the Axial and Radial plots, the plot time can be input; otherwise, it will default to the last time step.

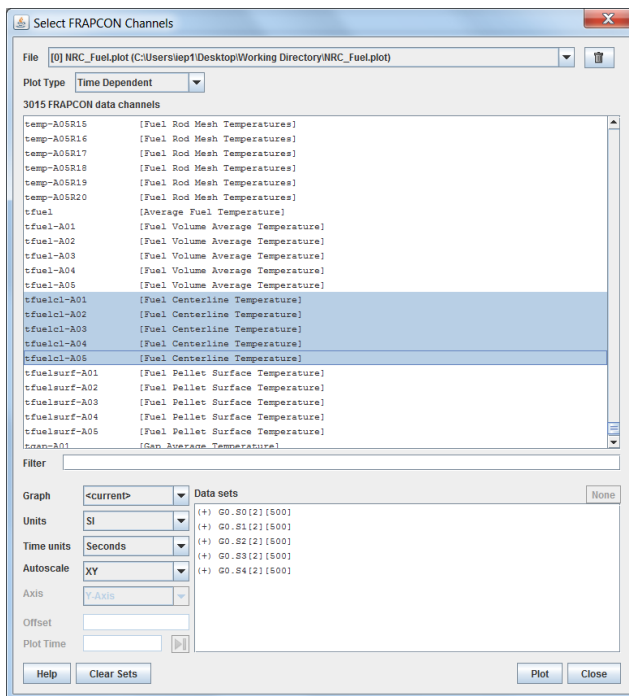


Figure C.15. Available data channels for the FAST plug-in in AptPlot

After selecting the data channel(s), the units, and plot time (if available), press plot. Examples of Time Dependent and Axial plots are shown in Figure C.16.

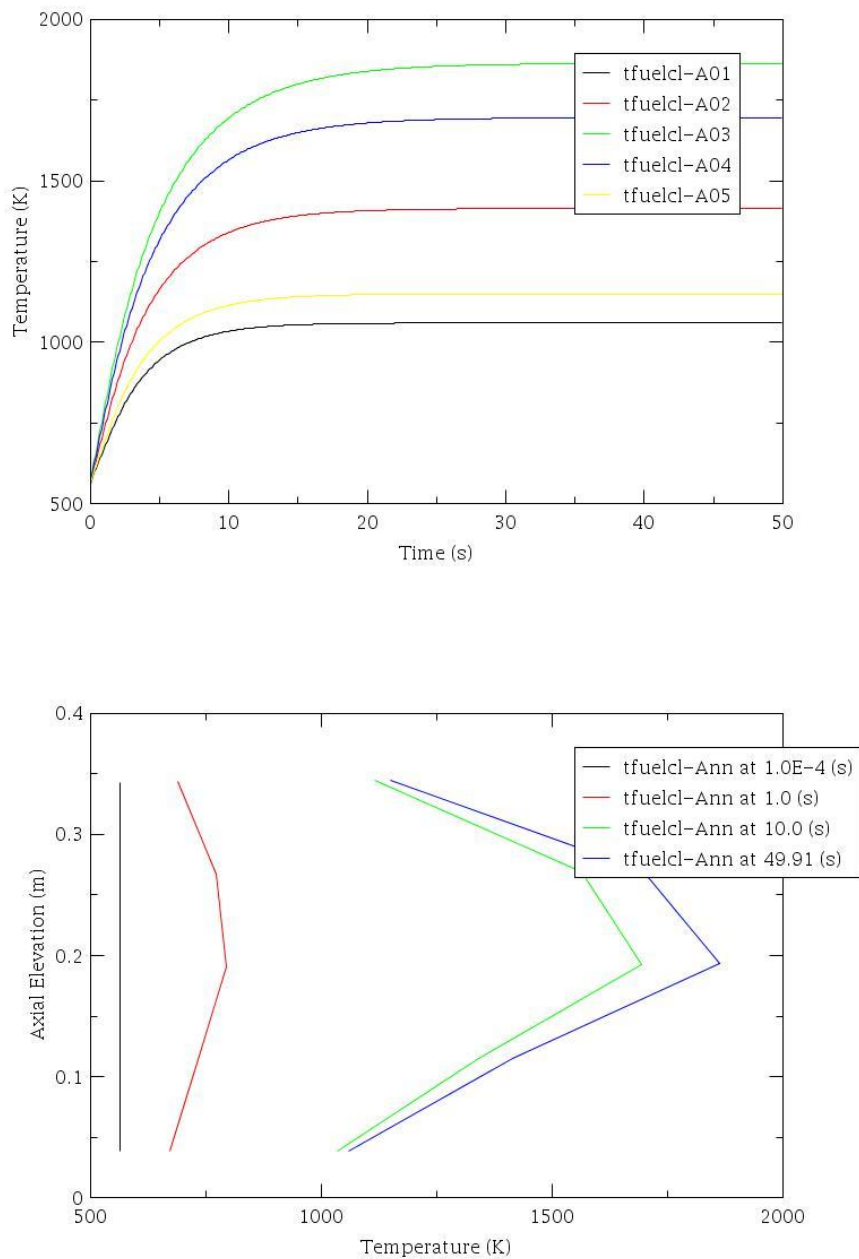


Figure C.16. Examples of fuel centerline temperature measurements using AptPlot's (a) time-dependent and (b) axial graphs.

Appendix D – Numerical Solution of the Plenum Energy Equations

The Crank-Nicolson finite difference form of the six energy equations presented in Section 2.4.1 is as follows.

- Plenum Gas

$$\rho_g V_g C_g \frac{T_g^{m+1} - T_g^m}{\tau} = \frac{A_{ep} h_{ep}}{2} (T_{ep}^m - T_g^m - T_g^{m+1} + T_{ip}^{m+1}) + \frac{A_{cl} h_{cl}}{2} (T_{cli}^m - T_g^m + T_{cli}^{m+1} - T_g^{m+1}) + \frac{A_{SS} h_{SS}}{2} (T_{SS}^m - T_g^m + T_{SS}^{m+1} - T_g^{m+1}) \quad (D.1)$$

- Spring Center Node

$$\rho_S V_{SC} C_S \frac{T_{SC}^{m+1} - T_{SC}^m}{\tau} = \bar{q}''' V_{SC} + \frac{A_{SC} K_S}{2 R_{SS}} (T_{SS}^m - T_{SC}^m + T_{SS}^{m+1} + T_{SC}^{m+1}) \quad (D.2)$$

- Spring Surface Node

$$\rho_S V_{SS} C_S \frac{T_{SC}^{m+1} - T_{SC}^m}{\tau} = \bar{q}''' V_{SS} + \frac{A_{SC} K_S}{2 R_{SS}} (T_{SC}^m - T_{SS}^m + T_{SC}^{m+1} - T_{SS}^{m+1}) + \frac{A_{SS} (h_{rads} + h_{conc})}{2} (T_{cli}^m - T_{SS}^m + T_{cli}^{m+1} - T_{SS}^{m+1}) + \frac{A_{SS} h_S}{2} (T_g^m - T_{SS}^m + T_g^{m+1} - T_{SS}^{m+1}) \quad (D.3)$$

- Cladding Interior Node

$$\rho_{cli} V_{cli} C_{cl} \frac{T_{cli}^{m+1} - T_{cli}^m}{\tau} = \bar{q}''' V_{cli} + \frac{A_{cl} h_{radc} + A_{SS} h_{conc}}{2} (T_{SS}^m - T_{cli}^m + T_{SS}^{m+1} - T_{cli}^{m+1}) + \frac{A_{cl} h_{cl}}{2} (T_g^m - T_{cli}^m + T_g^{m+1} - T_{cli}^{m+1}) + \frac{A_{cl} K_{cl}}{2 \Delta r / 2} (T_{clc}^m - T_{cli}^m + T_{clc}^{m+1} - T_{cli}^{m+1}) \quad (D.4)$$

- Cladding Center Node

$$\rho_{cl} V_{clc} C_{cl} \frac{T_{clc}^{m+1} - T_{clc}^m}{\tau} = \bar{q}''' V_{clc} + \frac{A_{cl} K_{cl}}{2 \Delta r / 2} (T_{cli}^m - T_{clc}^m + T_{cli}^{m+1} - T_{clc}^{m+1}) + \frac{A_{cl} K_{cl}}{2 \Delta r / 2} (T_{clo}^m - T_{clc}^m + T_{clo}^{m+1} - T_{clc}^{m+1}) \quad (D.5)$$

- Cladding Exterior Node

$$T_{clo}^{m+1} = T_{cool}^{m+1} \quad (D.6)$$

The superscripts m and $m+1$ represent the values of quantities at the old (m) and new ($m+1$) time. The steady-state finite difference equations are obtained by setting the left side of Equations D.1 through D.5 to zero and by dropping the superscripts m and $m+1$. Equations D.1 through D.5 can be written in the following simplified form by combining constant coefficients and known temperatures (T_{jm}).

- Plenum Gas

$$A_1 T_g^{m+1} + B_1 T_{cli}^{m+1} + C_1 T_{SS}^{m+1} = I_1 \quad (D.7)$$

- Spring Center Node

$$C_2 T_{SS}^{m+1} + D_2 T_{SC}^{m+1} = I_2 \quad (D.8)$$

- Spring Surface Node

$$A_3 T_g^{m+1} + B_3 T_{cli}^{m+1} + C_3 T_{SS}^{m+1} + D_3 T_{SC}^{m+1} = I_3 \quad (D.9)$$

Combining Equations D.8 and D.9:

$$A_3 T_g^{m+1} + B_3 T_{cli}^{m+1} + \bar{C}_3 T_{SS}^{m+1} = \bar{I}_3 \quad (D.10)$$

Where,

$$\bar{C}_3 = C_3 - \frac{D_3}{D_2} C_2 \quad (D.11)$$

$$\bar{I}_3 = I_3 - \frac{D_3}{D_2} I_2 \quad (D.12)$$

- Cladding Interior Node

$$A_4 T_g^{m+1} + B_4 T_{cli}^{m+1} + C_4 T_{SS}^{m+1} + E_4 T_{clc}^{m+1} = I_4 \quad (D.13)$$

- Cladding Center Node

$$B_5 T_{cli}^{m+1} + E_5 T_{clc}^{m+1} + F_3 T_{clo}^{m+1} = I_5 \quad (D.14)$$

Equations D.7 through D.14 represent a set of six equations having six unknowns.

In the above equations, all material properties and heat transfer coefficients (except convection to the coolant) are shown as constants. For the transient case, the temperature-dependent material properties and heat transfer coefficients are evaluated at the average of the temperatures (TBAR) at the start and end times of each time step. For the steady-state calculation, TBAR represents an estimate of the true steady-state temperature. Therefore, it is required that the steady-state and transient solutions to Equations D.7 through D.14 be iterated to convergence on TBAR.

Appendix E – Overriding Material Properties With Lua Scripts

Functionality has been added to FAST to allow the user to override certain material properties by adding custom scripts to the input file. Using this functionality invalidates the verification and validation testing that is performed on FAST; in other words: use at your own risk!

For information on the lua scripting language, visit lua.org. Lua version 5.1 is embedded in FAST.

For a demonstration of the lua input scripting features described below please see the lua examples included with the FAST executable distribution package.

E.1 Basic Operation

To use lua scripting the user must first add the `lua` input block and activate the flags for the desired material properties (see Appendix B). The user then must add `#LUA` at the very end of the input file; everything that follows will be read by the lua interpreter and must be valid lua. Comments are allowed and are denoted by double hyphens (`--this is a lua comment`).

For each material property flag set to `.TRUE.` in the `$lua` input block, an appropriately named function must be included in the lua scripting section. The required function name can be found by removing the leading `lua_` from the flag name. For example, to override the cladding thermal conductivity model, a user must set `lua_clad_thermcond = .TRUE.` in the `lua` input block. The user must then add the `#LUA` designator to the end of the input file; following this must be a function titled `clad_thermcond`.

Each property has a different set of inputs that will be passed from FAST when the function is called. The order of the inputs is important, as the interpreter cannot check the names of the variables. The easiest way to ensure that the scripted functions are in the correct format is to enable the desired `namelist` flag and run FAST. Whenever any lua flags are enabled a template for all enabled functions is printed to the console as well as the `.out` file. This template contains the framework for the function with the inputs in the expected order and also includes comments describing what units the return value should be, what the inputs represent, and in what units they will be passed from FAST.

E.2 Advanced Features

Additional helper functions can be added and called by any of the scripted properties.

Property functions can also be moved to a separate file. For example, the user could place a set of property functions in a file named `newFuelPelletProps.lua` located in the same folder in which FAST is run. Then they may set any property flags in the `$lua` input block to `.TRUE.` and add `#LUA require "newFuelPelletProps"` to the input file. The scripted functions will then override the built in material properties.

Pacific Northwest National Laboratory

902 Battelle Boulevard
P.O. Box 999
Richland, WA 99352
1-888-375-PNNL (7675)

www.pnnl.gov